Kelvin André Pacheco

Assessment of CO_2 Conversion Processes to Value-Added Products

São Paulo
2023

Kelvin André Pacheco

Assessment of CO_2 Conversion Processes to Value-Added Products

Revised Version

Thesis presented to the Graduate Program in Chemical Engineering at the Polytechnic School of the Universidade de São Paulo to obtain the degree in Doctor of Science.

Area of Concentration: Chemical Engineering.

Advisor: Profa. Dra. Rita M. de B. Alves

São Paulo
2023

Este exemplar foi revisado e corrigido em relação à versão original, sob responsabilidade única do autor e com a anuência de seu orientador.

São Paulo, 24 de agosto de 2023

Assinatura do autor: Kelvin André Pacheco

Assinatura do orientador: Rita Maria de Brito Alves

Catalogação-na-publicação

Pacheco, Kelvin André
Assessment of CO2 Conversion Processes to Value-Added Products / K. A. Pacheco -- versão corr. -- São Paulo, 2023.
288 p.

Tese (Doutorado) - Escola Politécnica da Universidade de São Paulo. Departamento de Engenharia Química.

1.Carbon Dioxide Utilization 2.CO2 Chemical Conversion 3.Multi-Criteria Decision Analysis 4.Artificial Neural Network 5.Flowsheet Optimization I.Universidade de São Paulo. Escola Politécnica. Departamento de Engenharia Química II.t.

Name: Kelvin André Pacheco

Title: Assessment of CO_2 Conversion Processes to Value-Added Products

PhD Thesis presented to the Graduate Program in Chemical Engineering at the Escola Politécnica da Universidade de São Paulo to obtain the degree in Doctor of Science.

Examining Board:

Profa. Dra. Rita Maria de Brito Alves

Departamento de Engenharia Química da Escola Politécnica/USP - Presidente

Evaluation: Approved

Prof. Dr. Christos Maravelias

Department of Chemical and Biological Engineering/Princeton University- Membro

Evaluation: Approved

Dr. Goutham Kotamreddy

Braskem - Membro

Evaluation: Approved

Dr. Adriano Ferreira de Mattos Silvares

Departamento de Engenharia Química da Escola Politécnica/USP - Membro

Evaluation: Approved

Dr. Alessandra de Carvalho Reis

Universidade Federal do Rio de Janeiro - Membro

Evaluation: Approved

Acknowledgments

I would like to thank my advisor Prof. Rita Maria de Brito Alves, and Dr. Antonio Esio Bresciani for their support. They generously shared their knowledge and expertise, guiding me with wisdom, patience, and dedication. Their critical and encouraging guidance has not only shaped my academic thinking but also empowered me to surpass the limits of my own knowledge.

I also acknowledge FAPESP, the State of São Paulo Research Foundation, for a PhD scholarship grant (FAPESP Proc. 2017/26683-8).

I dedicate this work to my family, whose constant support have been the foundation that sustained me throughout my academic life. You inspired me to pursue excellence in all areas of my life. This achievement is as much yours as it is mine.

A grateful thank to all friend who I made during my time at the University of São Paulo. There were many conversations and learning moments, often held over a cup of coffee. The intellectually stimulating discussions, idea exchanges, and debates have enriched my research journey and made this path so much more meaningful.

May this doctoral thesis be a tribute to all those who accompanied me on this journey and a valuable contribution to the field of research. My sincere gratitude to all of you.

"Não vá aonde o caminho pode levar,
vá onde não há caminho e deixe uma trilha."
(Ralph Waldo Emerson/ Muriel Strode)

Resumo

PACHECO, K. A. **Avaliação dos Processos de Conversão de CO_2 em Produtos de Alto Valor Agregado.** Tese (Doutorado em Engenharia Química) - Escola Politécnica, Universidade de São Paulo, 2023

A perspectiva do dióxido de carbono (CO_2) de ser considerado um resíduo para se tornar um recurso valioso com potencial como fonte de carbono e alternativa aos combustíveis fósseis é explorada nesse trabalho. A Utilização do Dióxido de Carbono (UDC) concentra-se em avançar além das tecnologias de captura e armazenamento de carbono, as estratégias para reciclar o CO_2 em vetores de energia e intermediários químicos, e avaliar o potencial de produtos derivados do CO_2. Ao utilizar o CO_2 como base de carbono, produtos químicos podem ser produzidos com custos competitivos e impacto ambiental reduzido. A adoção de matérias-primas alternativas, como CO_2, pode trazer mudanças disruptivas para a indústria. O CO_2 pode ser integrado à indústria química existente por meio de produtos químicos fundamentais, como metanol, ou como uma possível base de carbono C_1. Ao avaliar uma tecnologia de UDC, fatores como potencial de redução de emissões, restrições termodinâmicas e viabilidade comercial devem ser considerados. Para enfrentar o desafio de avaliar tecnologias de utilização de CO_2 e identificar produtos promissores, uma abordagem sistemática utilizando uma análise de decisão multicritério foi desenvolvida. Critérios específicos para a conversão do dióxido de carbono são estabelecidos, e uma avaliação em três níveis é aplicada para selecionar os produtos mais adequados com base na viabilidade econômica, maturidade tecnológica e relevância científica. Carbonato de dimetila, éter dimetílico e ácido acético são identificados como produtos favoráveis, com recomendação de estudos de projeto de processo. Um processo inovador para a produção de ácido acético a partir do CO_2 usando a rota de hidrocarboxilação do metanol foi desenvolvida, incorporando ajustes nas matérias-primas, faixas de temperatura, pressão e unidades de separação eficientes. O estudo contribui para o campo de síntese de processo para a conversão do CO_2 em produtos de alto valor agregado, abordando a escassez de dados literários sobre os processos de produção de ácido acético. Além disso, uma avaliação da conversão de CO_2 em metanol e éter dimetílico foi conduzida. É proposto um framework para otimizar as plantas químicas, considerando tanto o custo anualizado total quanto as emissões de CO_2 resultantes do uso de utilidades. Modelos simplificados, como redes neurais, representaram com precisão o comportamento da planta, possibilitando uma otimização eficiente. Os esforços de otimização de processos têm produzido resultados positivos tanto do ponto de vista econômico quanto ambiental. A redução no custo total anualizado demonstra maior eficiência financeira, enquanto a diminuição nas emissões de $CO_{2,eq}$ significa um passo em direção à sustentabilidade. No geral, este trabalho apresenta avaliações importantes sobre a utilização de CO_2 como um recurso, otimizando a planta química e direcionando a indústria para práticas mais sustentáveis e eficientes. Mais pesquisas nessas áreas contribuirão para uma economia mais sustentável e circular.

Palavras-Chaves: Utilização de Dióxido de Carbono; Conversão Química de CO_2; Análise de Decisão Multicritério; Redes Neurais Artificiais; Otimização de Processos

Abstract

PACHECO, K. A. **Assessment of CO_2 Conversion Processes to Value-Added Products.** Thesis (PhD in Chemical Engineering) - Escola Politécnica, Universidade de São Paulo, 2023

The perspective on carbon dioxide (CO_2) from being considered a waste product to a valuable resource with potential as a carbon source and alternative to fossil fuels is explored. Carbon Dioxide Utilization (CDU) focuses on advancing carbon capture and storage technologies, developing strategies for recycling CO_2 into energy vectors and chemical intermediates, and evaluating the potential of CO_2-derived products. By using CO_2 as a carbon building block, chemicals can be produced with competitive costs and reduced environmental impact. Adopting alternative feedstocks, such as CO_2, can bring disruptive changes to the industry. CO_2 can be integrated into the existing chemical industry through fundamental chemicals like methanol or as a potential C_1 building block. When evaluating a CDU technology, factors such as emission reduction potential, thermodynamic restrictions, and commercial viability should be considered. To address the challenge of evaluating CO_2 utilization technologies and identifying promising products, a systematic approach is developed using a Multi-criteria decision analysis. Specific criteria for carbon dioxide conversion are established, and a three-level assessment is applied to select the most suitable products based on economic viability, technological maturity, and scientific significance. Dimethyl carbonate, dimethyl ether, and acetic acid are identified as favorable products, with further process design studies recommended. An innovative process for acetic acid production from CO_2 using the methanol hydrocarboxylation route is developed, incorporating adjustments in feedstock, temperature, pressure ranges, and efficient separation units. The study contributes to the field of process synthesis for converting CO_2 into high-value products, addressing the scarcity of literature data on acetic acid production processes. Additionally, a comprehensive evaluation of CO_2 conversion into methanol and dimethyl ether is conducted. A framework for optimizing chemical plants is proposed, considering both the total annualized cost and resulting CO_2 emissions from utility usage. Simplified models, particularly neural networks, accurately represented plant behavior, enabling efficient optimization. Optimization efforts in the processes have yielded positive outcomes in terms of both economic and environmental perspectives. The reduction in total annualized cost demonstrates improved financial efficiency, while the decrease in CO_2 equivalent emissions signifies a commendable step towards environmental sustainability. Overall, this thesis provides valuable insights into utilizing CO_2 as a valuable resource, optimizing chemical plant operations, and driving the industry towards more sustainable and efficient practices. Further research and development in these areas will contribute to a more sustainable and circular economy.

Keywords: Carbon Dioxide Utilization; CO_2 Chemical Conversion; Multi-Criteria Decision Analysis; Artificial Neural Network; Flowsheet Optimization

List of Figures

List of Tables

List of Symbols

α Weight for multi-objective function

G Gibbs Free Energy

H Enthalpy

K_{eq} Equilibrium Constant - Kinetic Equation

NC Number of Components

NP Number of phases

NR Number of Reactions

n Number of moles

P Pressure

R Universal Gas Constant

S Entropy

T Temperature

hf_k Energy Contribution of the Group (see Joback group contribution)

μ Chemical Potential

List of Abbreviations

AdaGrad Adaptive Gradient Algorithm

AGR Acid Gas Removal

AHP Analytic Hierarchy Process

AM1 Austin Method 1

ANN Artificial Neural Network

ANP Analytic Network Process

ATR Autothermal Reforming

AWE Alkaline Water Electrolyzer

BB Black Box Model

BFGS Broyden-Fletcher-Goldfarb-Shanno

CAGR Compound Average Growth Rate

CCP Climate Change Potential

CCS Carbon Capture and Storage

CCU Carbon Capture and Utilization

CDU Carbon Dioxide Utilization

CPD Chemical Product Design

CRI Carbon Recycling International

CTL Coal-To-Liquid

DFT Density Functional Theory

DII Derwent Innovations Index

DME Dimethyl ether

DSTWU Shortcut Distillation Column Model - Aspen Plus

E1 Legates and McCabe's efficiency

ECBM Enhanced Coalbed Methane

EGR Enhanced Gas or Condensate Recovery

ELECTRE ELimination Et Choix Traduisant la REalité

EOR Enhanced Oil Recovery

ETL Emissions-to-Liquids

GB Gray Box Model

GTL Gas-To-Liquid

HEN Heat Exchanger Network

HOC Hayden-O'Connell equation

ISBL Inside Battery Limit Envelope

LCM Law of Conservation of Mass

LHHW Langmuir-Hinshelwood-Hougen-Watson

LPO Liquid-Phase Oxidation

MAE Mean Absolute Error

MAUT Multi-Attribute Utility Theory

MCDA Multiple Criteria Decision Analysis

MINLP Mixed-Integer Non-Linear Programs

MMFF94 Merck Molecular Force Field 94

NG Natural Gas

NGL Natural Gas Liquids

PCES Property Constant Estimation System

PFR Plug Flow Reactor

PM6 Parameterization Method 6

PM7 Parameterization Method 7

PROMETHEE Preference Ranking Organization Method for Enrichment Evaluations

PSA Pressure Swing Adsorption

RadFrac Rigorous Distillation Column Model - Aspen Plus

ReLU Rectified Linear Unit

RMAE Relative MAE

RMSE Root Mean Square Error

RMSProp Root Mean Square Propagation

RNN Recurrent Neural Network

RRMSE Relative RMSE

SEQC Semi-Empirical Quantum Chemistry

SGD Stochastic Gradient Descent

SOEC Solid Oxide Electrolyzer Cell

TanH Hyperbolic Tangent

TOPSIS Technique for Order Preference by Similarity to an Ideal Solution

TRL Technical Readiness Level

VEcv Variance explained by predictive models based on cross-validation

VLE Vapor-Liquid Equilibrium

WGS Water Gas Shift

WoS Web of Science

WP Willingness to Pay

Contents

Chapter 1

Introduction

Inside the history involving civilizations, the particular 20^{th} century is recognized beyond expectations growth in energy utilization and fast increase in the human population. According to the projections of World Energy Outlook 2016 [1], the world population is expected to grow from 7.3 billion in 2014 to 9.2 billion in 2040, representing an average growth of 0.9% per year. The population is one of the fundamental determinants of energy use, along with remarkable progress in technology creation and the intensifying business expansion of man-made materials.

Not only the population will increase but also the gross domestic product, which is assumed to grow at a compound average rate of 3.4% per year for the period to 2040, implies that the whole economy is considerably larger than double compared with the current year [1].

Over the decades, the use of fossil fuels, such as coal, oil and natural gas introduced an era of prosperity and progress. The transport revolution of the last century with the creation of cars, truck and engines generate a world susceptible to hydrocarbon fuels such as gasoline and diesel [2]. Additionally, the electrification of our daily basis boosts the use of carbon-based resources in power plants.

Figure 1.1 stratifies the energy consumption by fuel or by end-use. For the energy consumption by fuel (Figure 1.1a), the term oil comprehends crude, Natural Gas Liquids (NGL), Gas-To-Liquid (GTL), Coal-To-Liquid (CTL), condensate and refinery gains. The term "renewable" embodies a multitude of concepts. In the context of the report of World Energy Outlook 2016 [1], it includes wind, solar, geothermal, biomass, and biofuels and excludes large-scale hydro.

The contribution of renewable energy will increase up to 14% by the year 2040, although oil and natural gas still play important roles in energy consumption with a participation of 27% and 26%, respectively.

Regarding the primary energy consumption by end use, the industry will remain the main consumer, it is projected a consumption of 7207 Mtoe by the year 2030, with an increase of 8.45% by the year 2040 reaching 7843 Mtoe consumption.

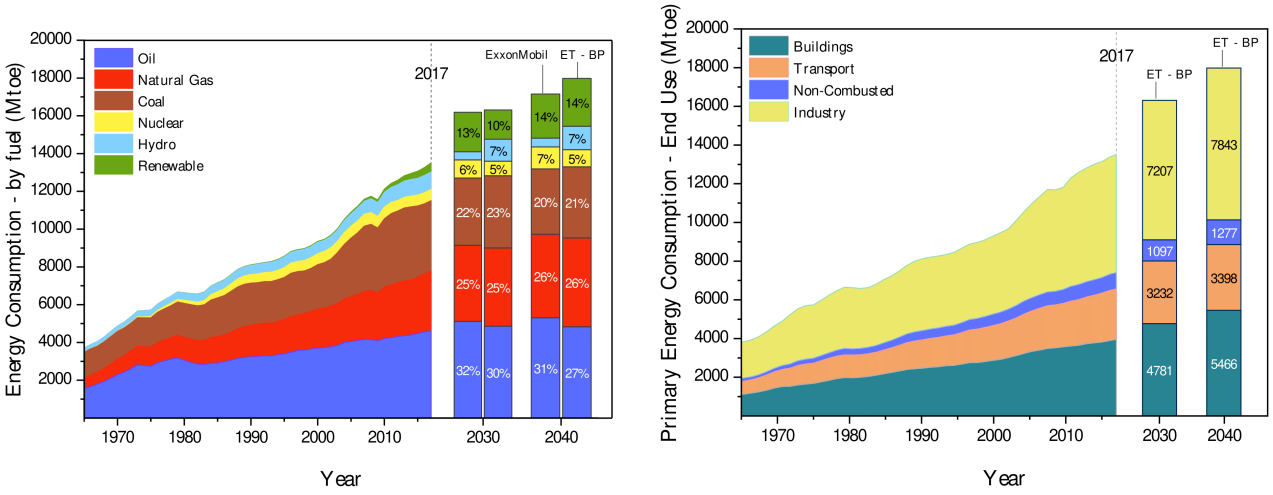

(a) by fuel (b) by end-use

Figure 1.1: Energy consumption stratified by fuel or end use. Data source obtain from ExxonMobil Report [3] and Evolving Transition - British Petroleum [3].

Given the carbon-based biology and environment, it is unsurprising a consumer culture has been developed, which is heavily reliant on carbon-based sources of energy and products. Coal, oil and natural gas are the primary sources of energy, while plastic, fabric and materials, personal care items, cleaning products, dyes and coatings are all derived from carbon-based organic chemicals [4].

Large-scale industries, such as those involving the production of inorganic chemicals and fertilizers, as well as construction materials, depend on the utilization of carbon, mainly in the form of an abundance of energy as presented in Figure 1.2.

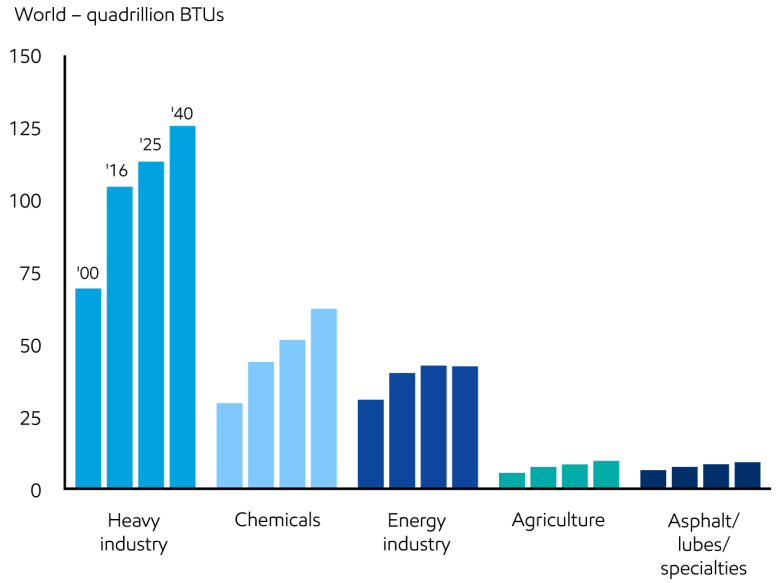

Figure 1.2: Industry undergirds global economic expansion (Source: ExxonMobil [5]).

Addressing the grand challenges of energy, water, environment, and food currently faced by modern society requires novel and more sustainable production systems [6].

It is important to develop significantly improved and/or novel processing techniques in order to convert available resources into useful products, recycle unused material, and reutilize used material without adversely affecting the sustainability of modern society.

In this context, CO_2 utilization technologies seek to mitigate carbon emissions and expand the energy supply while using CO_2 as a useful commodity [7, 8]. CO_2 can be used as a carbon building block to manufacture chemicals, which represents defiance to manufacture materials at a competitive cost with less environmental impact. The contribution of CO_2 conversion goes beyond lowering global warming, by means of reducing fossil resource depletion or even yielding more benign production pathways [9].

1.1 Carbon Dioxide Utilization

Since CO_2 is emitted from a generating source (power plants, industries) and therefore refueled at a rate faster than the current one is being used. CO_2 for utilization can be considered as a renewable alternative source of carbon, leading ideally to carbon neutral cycles in processes with sources of large amounts of CO_2 (such as a power plant) [10].

The Carbon Dioxide Utilization (CDU) introduces a new economic approach for CO_2, where captured CO2 can be utilized as a raw material for various processes. These processes include the creation of chemicals and materials (like methanol, formic acid, polyols for polyurethanes, and carbonates), fuels (such as gasoline, diesel, and sustainable aviation kerosene), as well as direct applications based on the physicochemical properties of CO_2 (like solvents and refrigeration) as depicted in Figure 1.3 [11].

In some cases, the capture of CO_2 is included in the definition, and it is referred to as Carbon Capture and Utilization (CCU) in analogy to the term often used Carbon Capture and Storage (CCS). The difference between the two concepts is that in CCS, carbon dioxide is stored (underground/marine reservoirs), while in the CDU/CCU is utilized within the economy through carbon dioxide valorization [12].

According to Aresta, Dibenedetto and Angelini [13] CDU technologies can be complementary to the CCS techniques. Currently, the existing CO_2 reuse represents 0.4% of the carbon emitted. The growth potential however can reach 10% of the carbon emitted today. The estimate is that 164 million tons of CO_2 are directly consumed in industrial processes per year, mainly for the production of urea. However, the total potential is estimated to be 23 times higher, totaling 3.7 billion tons per year. Worldwide, about 37 billion tons of CO_2 were issued in 2010 [14, 15].

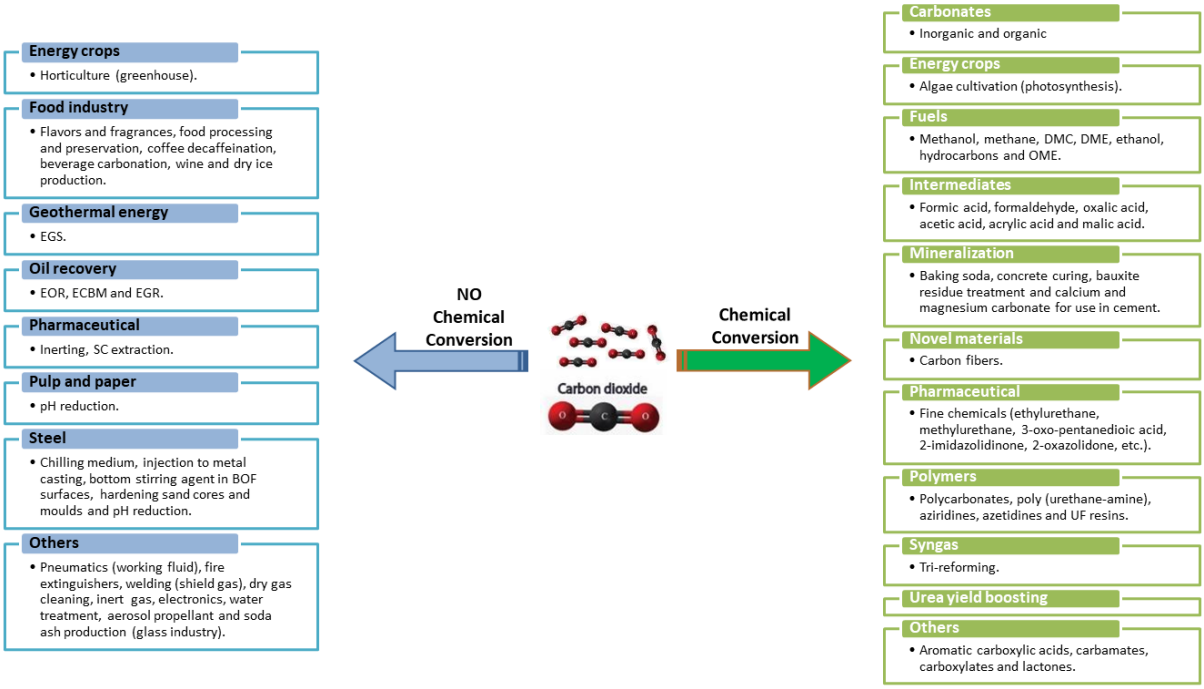

Figure 1.3: Potential uses of carbon dioxide.

The technological use (no chemical conversion) is related to its physical nature, including compression, recycling, phase transition, etc. Among practical uses are the Enhanced Oil Recovery (EOR) and Enhanced Gas or Condensate Recovery (EGR), the Enhanced Coalbed Methane (ECBM), the preservation of cereals (bactericidal), beverage additives, food packaging, dry cleaning, extraction, mechanical industries, fire extinguishers, air conditioning as well as water treatment [16].

The chemical conversion includes photocatalysis and chemical photocatalysis [17] as well as thermochemical processes [18], electrochemistry [19] and mineralization [20].

It's worth highlighting that the conversion of CO_2 can be classified into two reaction categories. The first category involves lower energy consumption and aims to convert CO_2 into organic compounds with a high carbon content (with oxidation states of +4 or +3). These reactions typically occur at lower temperatures (below 273 K). On the other hand, the second category requires higher energy input and aims to reduce CO_2 into fuel or chemical compounds with a low carbon content (reduced states of +2 or less) [21].

According to Zheng *et al.* [22] in terms of global market demand, fuels are larger than chemicals (12-14 times), and the production of fuels converts larger volumes of CO_2 (Gt/year) than chemicals (> 300 Mt/year). Technologies can be summarized based on the application based on a limit of 5 Mt/year of potential CO_2 use, where this threshold focuses on the study of technologies that will likely require the use of CO_2 on a scale compatible with the emissions

generated by thermal power plants [14].

In a short-to-medium-term, the chemical conversion of CO_2 will expand notably in more developed fields, for example, CO_2 hydrogenation, carboxylation and CO_2-containing polymers. Therefore, there is a need for research on catalysts, reactors, separations, processes, unconventional energy sources, and combinations of processes [23].

1.2 Framework for Flowsheet Optimization

Usually, CDU technologies are treated as single-end product, whereby the principal drawback is an economic unfeasibility (in some circumstances). Nevertheless, multiple fuels and chemicals integrated facilities contribute to synergies (more efficient energy and resource use), in analogy to the refinery concept [24].

Therefore, a configuration of a multi-product CDU can be advantageous in terms of economic feasibility besides being environmentally friendly. To guarantee that the configuration or structure is designed as efficiently as possible, process synthesis and process integration, among other techniques, are used.

Chemical process design and optimization is a complex scheme, which comprises process modeling and design and combinatorial defiance. There are two major approaches: the traditional sequential form and the optimization-based synthesis using superstructure models. In the former category, the problem is solved in sequential scheme, by decomposition where there is a hierarchy of elements that can be depicted by an Onion Diagram (reactor, separation, heat recovery and utility).

The latter category considers the full integration between decisions at the single step, *i.e.* determining the optimal structure and operating conditions simultaneously. Therefore, this approach contemplates all possible complex interactions between the engineering choices, including equipment (potentially selected in the optimized flowsheet), the interconnection and operating conditions formulated as an optimization problem in different fields as water network design [25], bio-separation networks [26] and process synthesis [27].

There is a diversity of proposed methodologies to represent a general process superstructure [28]. However, due to the inner complexity of the superstructure, the large-scale non-convex Mixed-Integer Non-Linear Programs (MINLP) suffer from effective approaches to solve them [29].

In order to circumvent the solution problem of a superstructure, Henao and Maravelias (2010) [30] proposed a framework to replace complex unit models (based on first principles) by surrogate models, developed through artificial neural networks.

The use of simplified models or surrogates at the unit operation level is advantageous because they are present in any process simulator. Additionally, surrogates can be used to represent an entire subsystem consisting of a definite number of units. Artificial Neural Network (ANN) may be used to generate the surrogate models, due to their fitting characteristics [31].

Subsequently, a reformulation of the superstructure model is introduced to keep the activation or deactivation through a function (for example the Hyperbolic Tangent Function) as the only source of non-linearity, contributing to the tractability of the problem.

The innovative research will propose a framework for process simulation and optimization. This work will adopt the combination of some techniques to solve the environmental impact of greenhouse gas emissions, among them integration of CO_2 conversion processes, rigorous modeling/simulation and optimization of certain parameters.

Research and development are crucial to move towards a competitive CDU technology, from the most fundamental level of research (e.g. Haunschild [32], focusing on catalyst research) to integrated studies at the conceptual design level as a complete plant in the work by Milani et al. [33]. Thus, there is a need for a detailed analysis regarding the impact that different CDU options/processes have on the energy of the system and under which conditions the obtained products can achieve a sustainable market [34].

In summary, the current CO_2 market has great potential for expansion with new CO_2 applications in different sectors. The optimization of CO_2 conversion processes, from the use of streams (steam/energy) to a conceptual configuration that can potentially reduce the CO_2 emitted into the atmosphere is crucial for CDU. In this way, the processes developed should help to face the problems related to the use of CO_2 as raw material to an optimized chemical plant.

1.3 Objectives

1.3.1 General Objective

The objective of the thesis is to present a framework that combines the exploration of the most attractive products derived from CO_2 with the optimization of a theoretical chemical plant, all while considering emissions and cost reductions.

1.3.2 Specific Objectives

The specific objectives are described as:

- To propose a multi criteria decision analysis framework to select potential products that use CO_2 (directly or indirectly) as raw material;

- To select the most promising process for the selected products from CO_2;
- To generate an appropriate surrogate model for the subsystem of the chemical plant, which contains processes for the production of high value-added products;
- To incorporate the surrogate in an optimization problem to reduce costs and CO_2 emissions due to utilities usage.
- To assess different scenarios, for example, cost of hydrogen and carbon tax, for understand the influence of these variables on economics and carbon emission.

1.4 Thesis Organization

The **Chapter 1** situates the reader about the topic, introduces the justification of the work and presents the objectives of the study.

In an effort to enhance and further complete the database of the products obtained from CO_2, **Chapter 2** deals with the investigation of different procedures to estimate the basic thermodynamic properties of the reactants and products of these reactions. To further develop and improve the database of products generated from CO_2 for the purpose of understanding and modeling the formation of species, basic thermodynamic data is necessary. The development of detailed reaction schemes in the field is also scarce. The chapter was published as an article entitled 'Assessment of property estimation methods for the thermodynamics of carbon dioxide-based products' in the Energy Conversion and Management journal, doi:10.1016/j.enconman.2020.112756 (see [35]).

The **Chapter 3** proposes a method to perform a local market analysis for potential products from CO_2 chemical conversion. The analysis was carried out for the Brazilian scenario. The forecast behavior of this market for 2030 was also calculated. The chapter was published as an article entitled 'Assessment of the Brazilian Market for Products by Carbon Dioxide Conversion' in the Frontiers in Energy Research journal, doi:10.3389/fenrg.2019.00075 (see [36]).

A multi-criteria decision analysis to select the most promising products derived from CO_2 conversion in a broader overview is discussed in **Chapter 4**. The findings and insights from Chapter 2 were utilized as crucial input for these assessments. The outcomes of this analysis subsequently guided the development of simulations in the subsequent chapters. This chapter was published as an article entitled 'Multi criteria decision analysis for screening carbon dioxide conversion products' in Journal of CO_2 utilization, doi:10.1016/j.jcou.2020.101391 (see [37]).

In **Chapter 5**, an assessment of acetic acid production routes is presented. The comparison of CO_2 innovative routes was performed and a multi-criteria decision analysis of CO_2 innovative

routes was carried out. The simulation of the acetic acid was performed with exergy analysis. A minor part of this chapter was published as a conference proceedings entitled 'CO_2-based Acetic Acid Production Assessment' in the proceeding of the 31^{st} European Symposium on Computer Aided Process Engineering, doi:10.1016/B978-0-12-823377-1.50172-5 (see [38]). The entire chapter is being prepared for submission to a publication.

Chapter 6 of the thesis focuses on the simulation of methanol and dimethyl ether production. The selected routes for these processes were hydrogenation of CO_2 for methanol and methanol dehydration for dimethyl ether. The chapter evaluates the technical feasibility of these production pathways and offers valuable insights into the behavior of the processes. It also identifies areas that can be optimized.

Chapter 7 proposes a framework for flowsheet optimization based on surrogate models. The artificial neural networks were selected as the algorithm to produce the surrogates, and the two chemical plants: (i) acetic acid (as described in Chapter 5) and (ii) methanol and dimethyl ether (as described in Chapter 6) were used as a case study. The chapter is being prepared for submission to a publication.

Finally, **Chapter 8** presents the conclusions, key insights and highlight the major findings of the study. They provide a concise summary of the research outcomes, emphasizing the significance and relevance of the conducted research. Additionally, suggestions for future works are presented, from the identified research gaps, limitations encountered during the study, and areas that require further exploration.

Chapter 2

Assessment of property estimation methods for the thermodynamics of carbon dioxide-based products

Carbon dioxide can be used as feedstock to produce chemicals. Albeit promising, the literature data regarding the quantity of energy needed to convert carbon dioxide into chemicals is limited and narrowed to the most studied processes and products. In order to understand and model the formation of species using carbon dioxide as raw material, some basic thermodynamic data are needed. To enhance and further complete the database of the products obtained from CO_2, this chapter investigates different procedures to estimate the basic thermodynamic properties. The results showed that semi empirical quantum-chemistry methods revealed to be more accurate and robust for the studied species. These results provide important insights into the thermodynamics of CO_2 related products.

Contents

2.1 Introduction

CDU technologies seek to mitigate carbon emissions and expand energy supply while using CO_2, considered a waste, as a useful commodity, diverging from conventional technologies of abatement [8]. The closed carbon cycle concept, then, arises, concerning processes to produce hydrogen (without the use of fossil fuels) and the CO_2 capture from a variety of sources, such as cement or steel industries, power plants or fermentation process [39].

A novel CO_2 based process is, usually, more material and energy intense than the traditional route, in which a better integration and process synthesis to minimize these issues are needed. Wiesberg, de Medeiros, Alves, Coutinho and Araújo [40] investigated two different routes to produce methanol from CO_2. Blumberg, Morosuk and Tsatsaronis [41] performed an exergy study to analyze the CO_2-integration potential and the constraints within the reforming and synthesis. Dabral and Schaub [42] reported a review of new CO_2-based compounds for industrial scale. Chauvy, Meunier, Thomas and Weireld [43] ranked emerging CO_2-based products for short- to mid-term deployment. Koytsoumpa, Bergins and Kakaras [44] assessed the potential of CO_2 for fuel and for combined heat and power production. Accordingly, CO_2 is a critical enabling element for the sustainable future of chemical production [7].

In a short-to-medium-term, the chemical conversion of CO_2 will expand, notably in more developed fields, for example CO_2 hydrogenation, carboxylation and CO_2-containing polymers. According to the projection of Exxon Mobil report [5], the energy for the industry will increase 20% from 2016 to 2040, whilst the growth of chemicals will be 40% at the same period. Similar behavior is predicted by the Shell report [45], in which a demand growth for chemicals in the medium term is due to economic growth.

In this context, Chemical Product Design (CPD) is an alternative for important changes in the chemical industry, including a split in the industry between manufacturers of commodity chemicals and developers of special chemicals. However, it is an expensive laborious routine restricted to a specified quantity of resources (budget, raw material, products and time) [46]. Other methodologies must be explored to solve the issue of produce new chemicals or new routes faced the growing demand.

Novel advances in the field of computational approaches, mainly on computer-aided molecular design, are one of the pillars for the study.

To perform CPD studies, several parameters and properties of the chemicals are necessary. One of the most fundamental thermodynamic property needed is the enthalpy of formation, which is

critical in many engineering areas, since energy balances depends on their accurate values [47].

In some cases, the properties must be estimated. One can relate chemical structures to properties at several levels of accuracy (group contribution, molecular mechanics, semi-empirical, *ab initio*). The most used methods are group contribution, which assumes the property of a molecule can be predicted by the number of molecular sub-structures appearances [48]. The Joback and Reid method [49] is the most popular. The Benson method is even more complex and considers the interaction of a group with its neighborhood [50].

However, group contribution methods cannot distinguish isomers and there is a lack of consistency in groups used to predict various properties [51]. In order to increase accuracy and avoid costly methods such as Hartree-Fock *ab initio* methods or Density Functional Theory (DFT), the quantum–chemical semiempirical methods, which are a variant of electronic structure theory, can be used [52].

The semiempirical methods depart from *ab initio* or first principles formalism, and after consider assumptions to accelerate the calculations, usually neglecting terms in the equations. To balance the errors, empirical parameters are taken into consideration and calibrated against experimental reference data. If the model is able to describe the properties, the parameterization may consider all other effects in an average sense [52]. Different approaches for the integral approximation or parameterization have been proposed, among them the Austin Method 1 (AM1) [53], Parameterization Method 6 (PM6) [54] and the Parameterization Method 7 (PM7) [55] are widely used. The last two cover almost the full periodic table and can compute molecular and solid-state properties.

In this work, the ability of five different methods of property estimation was evaluated to calculate the theoretical gas-phase enthalpy of formation ($\Delta_f H^o_{298,g}$). The methods encompass (i) two group contributions: Joback method and Property Constant Estimation System (PCES) built in Aspen Plus and (ii) three semi-empirical: AM1, PM6 and PM7 calculated in MOPAC Software. The main objectives of this research is to determine which is the best method for estimation the properties of selected compounds. The reason for testing various methods is to study the products from CO_2 conversions using a less demanding method than *ab initio* methods resulting in important properties to perform CPD studies.

2.2 Methods

The steps for the estimation of thermodynamic properties employed in this work are depicted in Figure 2.1. A database of 122 compounds is selected from the literature as products from CO_2 conversion [56]. Complete details of the compounds are presented in the Appendix A. A test dataset is a subgroup of the complete dataset and is composed of 30 chemical species, since was

possible to retrieve their values of enthalpy of formation values from the literature.

Enthalpy of formation calculations were carried out for every species on the test database using one of the methods group contributions (Joback and PCES) or semi-empirical (AM1, PM6 and PM7) methods. The routine for the group contribution methods is introduced in Section 2.2.1, while for semi-empirical in Section 2.2.2.

A statistical analysis was performed in order to select the best method (for the group of chemical species in study) and, then, the selected method was used to estimate the thermodynamic properties (enthalpy of formation, Gibbs free energy) for the remaining 92 chemical species.

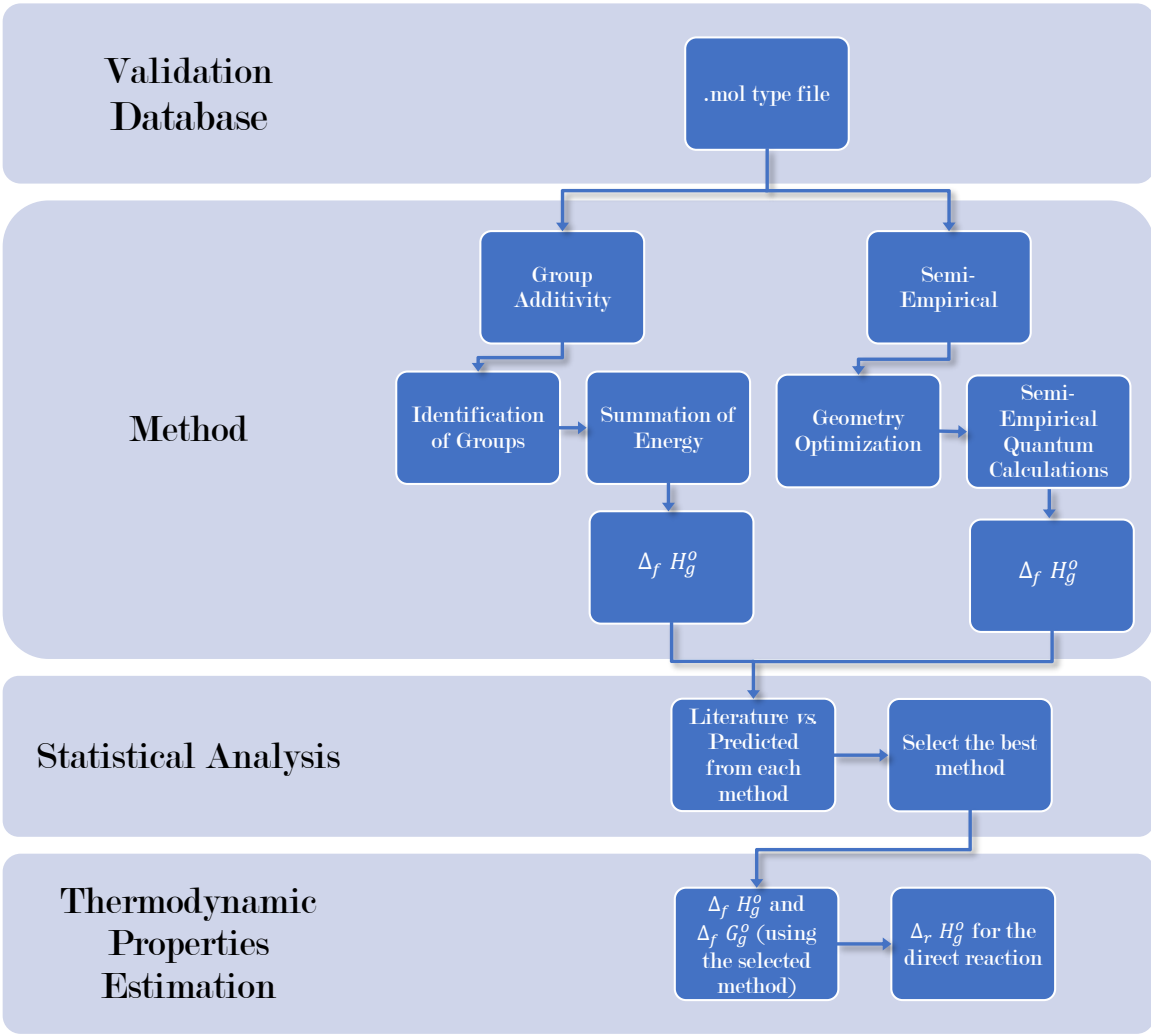

Figure 2.1: Methodology used in this study for the estimation of thermodynamic properties.

2.2.1 Group Contribution

The first order group contribution method of Joback and Reid [49] was used. The Equation 2.2.1 was used to calculate the enthalpy of formation and was implemented in spreadsheets

using the values of energy for the group hf_k reported in Joback *et al.* [49].

$$\Delta_f H^o_{298,g} = 68.29 + \sum_k N_k \cdot hf_k \tag{2.2.1}$$

where N_k stands for the number of groups k existing in a specific molecule and hf_k is the energy contribution of the group.

In order to generalize and avoid the limitations of the original Joback and Reid method, a second-order group contribution method (Benson Method) presented in the commercial software Aspen Plus was also used through Property Constant Estimation System [57].

In this method there are two types of functional groups:

- Group increments: for example $-CH_3$ or $-COO-$
- Corrections: for example the correction for the presence of a benzene ring

The molecular 2D structure is supplied and, subsequently, the PCES automatically generates the functional groups, provided the selected method is able to model that molecule. In case there are missing groups, *e.g.* a correction for a specific second order group contribution, the PCES will use the Joback and Reid method instead.

2.2.2 Semi-Empirical Quantum Chemistry

The methods of Semi-Empirical Quantum Chemistry (SEQC) theory have been employed. They neglect or approximate in an empirical way the integrals used for solving the time-independent electronic Schrödinger equation.

The first step is to obtain a stable structure and for the geometry optimization, a minimization of the binding energy of the molecule was performed. Energy minimization alters the molecular geometry (bonds, angles, dihedrals) to lower energy levels, and yields a more stable conformation. As the minimization progresses, it searches for a molecular structure in which the energy does not change with infinitesimal changes in geometry.

Initial geometries were supplied in internal coordinates, placing symmetry constraints on the appropriate bond lengths, bond angles and dihedrals in Avogadro software, version 1.2.0 [58].

The 3D representation of a molecule was exported and a routine employing an openbabel python binding (pybel version 1.7 [59]) was used, following the steps:

1. Steepest descent geometry optimization with the Merck Molecular Force Field 94 (MMFF94) [60, 61]. The method provides good accuracy across a range of organic and drug-like molecules;

2. Weighted Rotor conformational search. It uses an iterative procedure to find a more stable conformation, choosing from the allowed torsion angles, but the choice is re-weighted based on the energy of the generated conformer;

3. Conjugate gradient geometry optimization

A second geometry optimization without restriction of any symmetry of the molecules in its ground state was performed using AM1, PM6 or PM7 level with the Broyden-Fletcher-Goldfarb-Shanno (BFGS) algorithm as energy minimization routine as incorporated in Molecular Orbital PACkage 2016 (MOPAC2016) [62]. All semi-empirical calculations (AM1, PM6 and PM7) were performed using the original parameter set of the MOPAC2016 [62].

2.2.3 Statistical Analysis

Statistical analysis was carried out for a test subset due to the literature data available to compare experimental heats of formation with the estimation of the methods under evaluation.

The performance of a model can be measured using a number of statistics, such as: the Pearson's product-moment correlation coefficient (r) and its square, the coefficient of determination (r^2), which describes the degree of collinearity between the observed and model-simulated variates. They are essentially by determining the error sum of squares ($\sum(y - \hat{y}_b)^2$). However, the coefficient of determination is limited, because it standardizes for differences between observed and calculated means and variances, being insensitive to additive and proportional differences between datasets [63].

To compare and further evaluate the ability of the methods, other statistics were also calculated. Chai *et al.* [64] stated that multiple metrics are required to provide a complete picture of error distribution.

Root Mean Square Error (RMSE) (Equation 2.2.2) is more suitable than Mean Absolute Error (MAE) (Equation 2.2.3), when the type of error is normal distributed and unbiased [64].

$$\mathrm{RMSE} = \sqrt{\frac{\sum_1^n \left(y_i - \hat{y}_i\right)^2}{n}} \tag{2.2.2}$$

$$\mathrm{MAE} = \frac{\sum_1^n |y_i - \hat{y}_i|}{n} \tag{2.2.3}$$

Relative RMSE (RRMSE) (Equation 2.2.4) and Relative MAE (RMAE) (Equation 2.2.5) are independent of unit/scale and not sensitive to data means according to their definitions. Even though they enable comparison of different datasets with different data means, they are linearly

correlated with data variance [65].

$$\mathrm{RRMSE} = \frac{\mathrm{RMSE}}{\overline{y}} \cdot 100 \tag{2.2.4}$$

$$\mathrm{RMAE} = \frac{\mathrm{MAE}}{\overline{y}} \cdot 100 \tag{2.2.5}$$

In order to avoid such problems two other statistics were calculated. Variance explained by predictive models based on cross-validation (VEcv) (Equation 2.2.6) does not show the limitations and it is an accuracy measure. Moreover VEcv avoids the problems associated with Nash and Sutcliffe's efficiency [66].

$$\mathrm{VEcv} = \left(1 - \frac{\sum_i^n \left(y_i - \hat{y}_i\right)^2}{\sum_i^n \left(y_i - \overline{y}\right)^2}\right) \cdot 100 \tag{2.2.6}$$

Legates and McCabe's efficiency (E1) (Equation 2.2.7) is also an alternative accuracy measure [67].

$$\mathrm{E}_1 = \left(1 - \frac{\sum_i^n \left|y_i - \hat{y}_i\right|}{\sum_i^n \left|y_i - \overline{y}\right|}\right) \cdot 100 \tag{2.2.7}$$

A combination of the aforementioned metrics was used to define the most suitable method to predict the enthalpy of formation. The calculations of normality and homogeneity were performed using PASW Statistics 17.0.2.

2.2.4 Generation of Properties

After the selection of the most suitable method for property estimation, considering the statistical analysis, the thermodynamic properties calculations of the remaining species in database were carried out.

With the enthalpies of formation available, one can calculate the enthalpy of reaction executing basic algebraic operations according to Equation 2.2.8 [68].

$$\Delta H^o_{rxn} = \sum_{products} \nu \left(\Delta_f H^o_{298,g}\right) - \sum_{reactants} \nu \left(\Delta_f H^o_{298,g}\right) \tag{2.2.8}$$

The enthalpy of reaction can be determined by scaling each species enthalpy of formation by its stoichiometric coefficient. In this study only direct conversion routes to the products were

considered, *i.e.* the CO_2 reacts with one or more reactants to form directly in one step the products under assessment.

2.3 Results and Discussion

The first part of this section introduces the statistical analysis and error distribution, which lead to the selection of the most applicable method for property estimation. Comparison with other studies from the literature and lastly the evaluation of CO_2-based products and reactions are shown.

2.3.1 Statistical Results

For the statistical analysis, the requirements for parametric tests were tested. The ensemble of indicators was also computed (literature *vs.* estimated values.

The first set of analyses examined the hypotheses of normality of data (H_0 - null hypothesis, indicating that data is normal, H_1 - alternative hypothesis, rejecting the normality of data). H_0 is required for parametric tests.

A Shapiro-Wilk's test (p>0.05) [69] performed on the datasets is presented in 2.1. The test demonstrates the normal distribution with a significance level greater than 5% (p-value > 0.05).

Table 2.1: Shapiro-Wilk's Test for the test dataset.

Dataset	**p-value**
Literature	0.885
Joback	0.358
PCES Aspen	0.734
PM7	0.938
PM6	0.866
AM1	0.930

The evaluation of the symmetry and kurtosis estimators, which represent aspects related to the shape of the histogram, were also calculated. The value for the skewness or kurtosis divided by its standard error must lie between -1.96 and 1.96 to be considered a normal distribution. A skewness of 0.151, 0.088, 0.135, 0.173, 0.154 and 0.196 (std error = 0.427) was obtained for the Literature, Joback, PCES, PM7, PM6 and AM1 dataset, respectively. In respect of kurtosis [70] the values of -0.471, 0451, -0.212, -0.290, -0.363 and -0.324 (std error = 0.833) were obtained for for the Literature, Joback, PCES, PM7, PM6 and AM1 dataset, respectively. Therefore, the data corroborate the normality of the test dataset, which ratifies the possibility of using parametric analysis.

Additionally to the normality tests, the test of levene (p-value = 0.988) validated the homogeneity of the data.

2.3.2 Test Subset Values

Estimation of enthalpy of formation by the different methods (group contribution or semi-empirical quantum chemistry) were carried out for the test dataset. This data was used in Section 2.3.1 to perform the statistical analysis. Table 2.2 presents the results obtained and their comparison with available literature data.

Table 2.2: Comparison of the results for the test dataset with literature data. The values represent entalphy of formation (kcal/mol).

ID	Name	CAS	Lit.	Ref.	Group Contrib.		SEQC		
					Joback	PCES	PM7	PM6	AM1
			kcal/mol		kcal/mol		kcal/mol		
1	Formic acid	64-18-6	-90.49	[71]	-85.67	-90.26[a]	-80.80	-79.51	-89.99
2	Acetic acid	64-19-7	-103.35	[72]	-103.94	-103.37[a]	-95.44	-95.31	-97.19
3	Propionic Acid	79-09-4	-109.92	[72]	-108.87	-108.55[a]	-99.81	-99.08	-103.57
4	Acrylic acid	79-10-7	-77.61	[73]	-78.89	-75.39[a]	-75.17	-73.67	-76.36
6	Methacrylic Acid	79-41-4	-87.21	[74]	-86.17	-84.57[a]	-84.38	-82.72	-83.33
7	Oxalic Acid	144-62-7	-170.86	[73]	-187.66	-180.32[a]	-159.55	-156.25	-169.78
8	Benzoic Acid	65-85-0	-70.17	[73]	-72.07	-70.44[a]	-59.26	-58.46	-62.55
9	p-Salicylic acid	99-96-7	-114.16	[75]	-114.45	-112.57[a]	-105.17	-104.48	-107.16
10	Salicylic acid	69-72-7	-116.87	[73]	-114.45	-112.00[a]	-106.62	-105.35	-109.84
12	9H-Fluorene-9-carboxylic acid	1989-33-9	-43.25	[73]	-35.21	-35.21[b]	-36.21	-36.94	-30.46
36	Acetaldehyde	75-07-0	-40.01	[72]	-40.68	-39.23[a]	-41.13	-38.19	-41.60
37	Formaldehyde	50-00-0	-25.98	[73]	-22.40	-26.02[a]	-25.54	-20.70	-31.51
38	Methanol	67-56-1	-48.10	[73]	-51.67	-48.03[a]	-48.94	-48.35	-57.05
39	Propanol	71-23-8	-60.95	[72]	-61.54	-60.88[a]	-62.74	-62.02	-71.19
41	Styrol	100-42-5	35.35	[72]	36.69	35.25[a]	36.65	37.91	38.63
42	Dimethyl ether	115-10-6	-43.99	[73]	-51.82	-43.43[a]	-45.00	-45.78	-53.21
43	Ethylene Oxide	75-21-8	-12.57	[72]	-29.51	-12.51[a]	-11.26	-10.06	-8.99
44	Acetone	67-64-1	-51.82	[72]	-52.06	-51.64[a]	-54.99	-53.83	-48.50
45	Ethylene carbonate	96-49-1	-121.74	[73]	-101.85	-110.27[a]	-118.03	-123.36	-127.64
46	Propylene carbonate	108-32-7	-132.68	[73]	-111.64	-120.07[a]	-127.10	-132.57	-132.76
47	Dimethyl Carbonate	616-38-6	-136.55	[73]	-115.27	-132.59[a]	-135.00	-128.97	-137.10
48	Diethyl Carbonate	105-58-8	-152.43	[73]	-125.13	-142.45[a]	-142.57	-146.20	-149.65
49	Methyl Carbamate	598-55-0	-101.65	[76]	-70.65	-87.98[a]	-92.27	-92.21	-91.29
50	Urethane	51-79-6	-107.24	[76]	-75.59	-92.91[a]	-100.74	-100.74	-97.24
68	4-Ethyl-1,3-dioxolan-2-one	4437-85-8	-137.70	[73]	-116.58	-125.00[a]	-132.25	-137.48	-139.24
83	Methyl isocyanate	624-83-9	-14.36	[74]	-21.52	-21.52[b]	-24.32	-22.17	-14.02
105	Urea	57-13-6	-56.29	[77]	-26.04	-26.04[b]	-51.27	-48.82	-44.52
115	1,3-Diphenylurea	102-07-8	7.62	[73]	37.23	37.23[b]	7.68	6.50	28.52
118	Tetrahydro-2-pyrimidone	1852-17-1	-48.06	[78]	-27.08	-27.08[b]	-46.85	-48.89	-40.14
120	2-Imidazolidinone	120-93-4	-42.86	[73]	-20.68	-20.68[b]	-38.62	-39.68	-25.21

[a]Aspen Plus PCES selected automatically the Benson Method.

[b]Aspen Plus PCES selected automatically the Joback Method.

The ultimate objective of such computational strategy designed to estimate values for $\Delta_f H^o_{298,g}$ is to reduce deviations from calculated (estimated) to experimental (literature) values. A reason is that small errors in $\Delta_f H^o_{298,g}$ growth, in some cases exponentially, when generate other values dependent of such variable, for example Gibbs energy of reaction or even the equilibrium constant.

The group contribution method of Joback and PCES Aspen yielded calculated results in

which 47% (14/30) and 57% (17/30) of the predicted values, respectively, were within ± 5.0 kcal/mol of values in the reference literature set. Once the tolerance are setted within ± 15.0 kcal/mol the method Joback yielded 57% (17/30) while PCES Aspen yielded 87% (26/30). The maximum deviation of 31.7 kcal/mol and 30.2 kcal/mol for the Joback and PCES Aspen methods, respectively.

In reference to semi empirical quantum chemistry, the PM7, PM6 and AM1 method generated results whereby 50% (15/30), 50% (15/30) and 43% (13/30), respectively, are within ± 5.0 kcal/mol compared with literature reported data. By increasing the amplitude to ± 15.0 kcal/mol, the results were 100% (30/30), 100% (30/30) and 93% (28/30) enclosed in the selected range for PM7, PM6 and AM1. The deviation, in this case, was smaller for all the methods (PM7 = 11.3, PM6 = 14.6 and AM1 20.9 kcal/mol maximum deviation) when compared to group additivity methods.

The uncertainty associated with each estimation method has been published by the authors. The absolute average error for the heat of formation claimed for the Joback Method [49], Benson Method [50], PM7 [62], PM6 [62] and AM1 [62] are, respectively, 8.4 kJ/mol (std = 18 kJ/mol), 8.36 to 16.73 kJ/mol (according to the chemical class), 18.69 kJ/mol (std = 19.68 kJ/mol), 19.27 kJ/mol (std = 20.38 kJ/mol) and 52.14 kJ/mol (std = 41.53 kJ/mol).

Elioff *et al.* [79] compared different methods to estimate $\Delta_f H^o_{298,g}$ for a test set and their results were similar with the current study. The semi-empirical models (RM1 and PM7) displayed deviation ca. 14 kcal/mol, however, they were very rapid and with an acceptable accuracy compared with the *ab initio* methods tested in their study.

A fault of group additivity theory is that $\Delta_f H^o_{298,g}$ or other thermodynamic property is occasionally affected by structural features not properly addressed by the theory. Albeit more complex and with more corrections, one disadvantage of Benson method, implemented inside PCES Aspen Plus, is that group contribution value is missing for some of the substructures of several compounds in the test set.

Figure 2.2 presents the scatter plot comparing literature values with the values obtained for each method.

The scatter plot for Joback method showed the most disperse behavior, representing that the calculated value can diverge from the actual value. If the complexity of the method is considered, for example in the Benson method, the calculated values lie more on a diagonal line in the scatter plot.

The good representation of some molecules is due the fact that many of the compounds in the original experimental reference set were used to parameterize and develop the group additivity

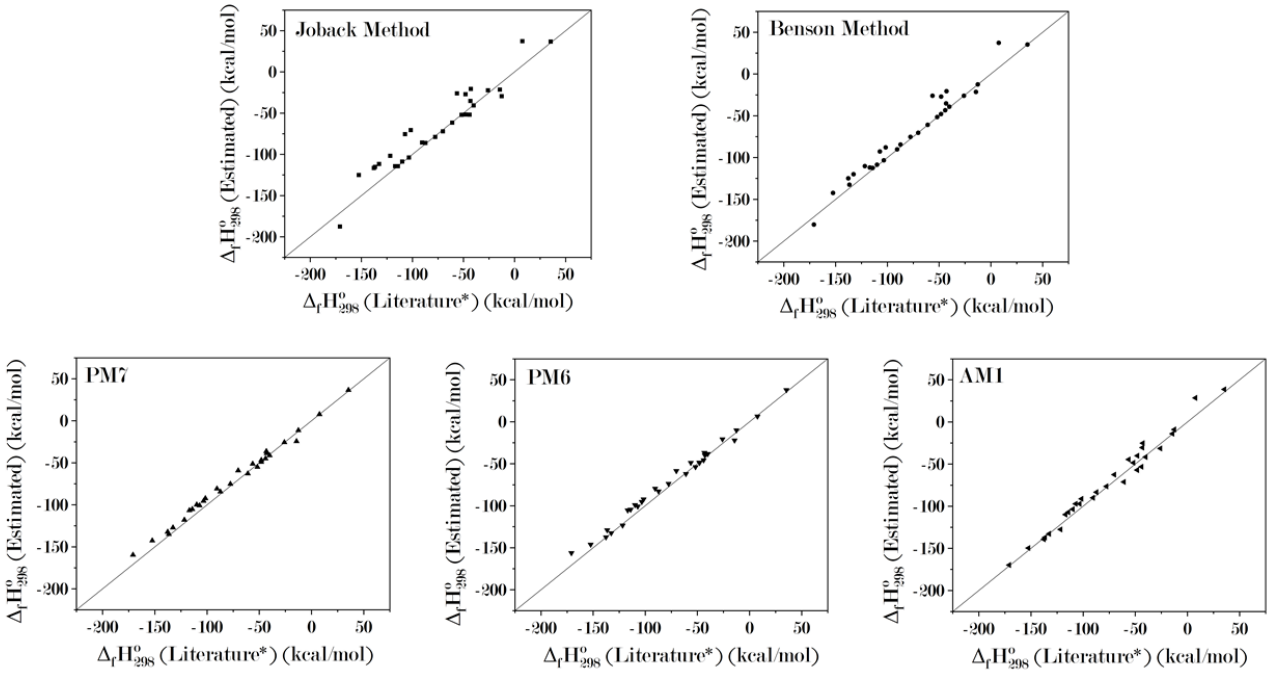

Figure 2.2: Scatter plot of calculated gas-phase enthalpy of formation *vs.* literature values. *According to data in Table 2.2.

computational approach/method. Pertinent methods such as Benson are often accurate, but one must carefully evaluate their application.

Semi empirical methods behaved similarly, although AM1 method was sufficient accurate, PM7 data were distributed closer to the literature values (diagonal).

2.3.3 Statistical Indicators of Performace Results

Predictive accuracy should be measured based on the difference between the observed values and predicted values. Assessing the accuracy of the methodologies is critical because it determines the quality of resultant predictions [80].

In order to compare pearson product-moment correlation coefficient (r) and the coefficient of determination (r^2) six other indicators were used to determine the most suitable method to calculate the enthalpy of formation of the full set of compounds.

Table2.3 shows the statistical indicators used to compare literature and calculated values for the enthalpy of formation.

Among all methods tested, PM7 showed the best result (closer to 1), with values of 0.996 and 0.993 for r and r^2, respectively.

To complement the assessment another six indicators were used. Relative MAE (RMAE), Relative RMSE (RRMSE), variance explained by predictive models based on cross-validation

Table 2.3: Statistical indicators used as comparison of literature and calculated values for gas-phase enthalpy of formation.

Estimation Method	**Indicator**							
	r	**r^2**	**RMSE**	**MAE**	**RMAE**	**RRMSE**	**VEcv**	**E_1**
Joback	0.957	0.916	16.310	11.883	-15.663	-21.500	88.856	71.367
PCES Aspen	0.982	0.964	11.445	7.382	-9.730	-15.086	94.513	82.213
PM7	0.996	0.993	6.384	5.166	-6.809	-8.415	98.293	87.553
PM6	0.995	0.991	6.750	5.384	-7.097	-8.897	98.092	87.026
AM1	0.990	0.979	8.075	6.305	-8.311	-10.644	97.268	84.808

(VEcv) and Legates and McCabe's (E1) [67, 81]. Regarding the results for RMSE and MAE, the best situation is to reduce the errors, then the smaller the value the better. In this case, Joback exhibited the highest errors (16.310 and 11.883 for RMSE and MAE, respectively). The method with the smallest error indicator was PM7.

In this situation, the method with the value closest to zero, shows the smallest relative error. PM7 demonstrates the best case scenario (RRMSE of -8.415 and RMAE of -6.809).

VEcv and E1 were presented in percentage to make their resultant values comparable. The higher the value the better the method/model is. In this case, the semi empirical methods achieved high scores ($> 97\%$ for VEcv and $> 84\%$ for E1). Group contribution methods attained high scores, however lower than SEQC methods. Comparing the values for VEcv and E1, the best method was PM7, with values of 98.293 and 87.553, respectively.

According to Li *et al.* [81] the VEcv and E1 should be used as complementary measures, they may be able to represent the difference between methods/models.

Overall, these results of the statistical analysis indicate that the most suitable method for this study is the semi-empirical PM7. Therefore, this method was used to calculate the enthalpy of formation for the whole dataset.

2.3.4 *Ab Initio* Comparison

The results obtained in this study using the PM7 level of theory were compared with values obtained using a more complex quantum chemistry level of theory calculations reported in the work of Ghahremanpour *et al.* [82].

Ghahremanpour *et al.* [82] used the standard G2 [83], G3 [84], G4 [85] and CBS-QB3 [86] methods for about 2000 molecules up to 47 atoms, and W1U and W1BD [87] were used for about 650 molecules up to 16 atoms. Computational cost is an important issue in evaluating computational methods apart from accuracy and reliability, G4 method is 8 and 24 times slower

than the G3 and CBS-QB3 methods, respectively, for calculations of $\Delta_f H^o_{298,g}$ and it is 28 times faster than the W1BD method.

Table 2.4 presents the enthalpy of formation for ten different chemical species using *ab initio* calculation (retrieved from [82]) or semi empirical calculation (results of the current study).

Table 2.4: Enthalpy of formation (kcal/mol) calculated using ab initio and semi-empirical quantum chemistry methods.

ID	**Name**	***Ab initio* Calculations**[a]						**SEQC**
		CBS-QB3	**G2**	**G3**	**G4**	**W1BD**	**W1U**	**PM7**
6	Methacrylic Acid	-86.69	-87.36	-86.66	-85.97	-87.83	-88.15	-84.38
36	Acetaldehyde	-39.65	-41.63	-40.46	-39.29	-40.08	-40.32	-41.13
37	Formaldehyde	-27.34	-28.01	-26.60	-26.79	-26.65	-26.89	-25.54
38	Methanol	-48.90	-49.47	-48.18	-48.09	-49.24	-49.35	-48.94
39	Propanol	-61.16	-62.14	-61.33	-60.76	-63.12	-63.26	-62.74
41	Styrol	37.36	39.58	35.49	35.18	–	–	36.65
42	Dimethyl ether	-45.39	-46.18	-44.55	-44.29	-45.46	-45.60	-45.00
43	Ethylene Oxide	-13.55	-13.98	-12.67	-13.00	-13.67	-13.86	-11.26
44	Acetone	-51.91	-53.20	-52.15	-51.77	-53.30	-53.54	-54.99
83	Methyl isocyanate	-26.48	-27.01	-26.20	-25.93	-26.12	-26.39	-24.32

[a]The results presented are retrieved from Ghahremanpour *et al.* [82].

One can see the small deviation from the *ab initio* calculations, considering all levels of theory the maximum deviation was less than 4 kcal/mol (3.77 kcal/mol for methacrylic acid using W1U compared with PM7).

The percentual difference remained limited to 10% (exception of ethylene oxide), the PM7 value from methanol was within 0.01% difference from CBS-QB3.

These results are consistent with those reported in Ghahremanpour *et al.* [82] and suggest that semi-empirical methods can be used to estimate enthalpy of formation with a reasonable accuracy and reliability with less computational effort. It is important to bear in mind a possible bias in these responses for different chemical species not in the studied group.

Table 2.5 displays the standard entropy for ten different chemical species using *ab initio* calculation (retrieved from [82]) or semi empirical calculation (results of the current study). The values were compared with literature/ experimental data.

The results, as shown in Table 2.5, indicate that the entropy is well estimated using either *ab initio* or semi-empirical methods for the compounds studied. The values of formaldehyde and ethylene oxide are within 0.48 cal/(mol.K), when compared calculated and literature/experimental data, which represents less than 1% of difference for all the methods.

Formaldehyde is a very small molecule, therefore is expected a considerable accuracy in the

Table 2.5: Standard Entropy - S^o - (cal/(mol·K)) - experimental and calculated by *ab initio* and semi empirical methods.

ID	Name	***Ab initio* Calculation**[c]						**SEQC**	**Lit.**
		CBS-QB3	**G2**	**G3**	**G4**	**W1BD**	**W1U**	**PM7**	
6	Methacrylic Acid	79.11	77.68	77.68	79.11	79.11	79.11	82.91	83.89[a]
36	Acetaldehyde	60.23	59.75	59.75	60.23	59.99	59.99	63.80	63.10[a]
37	Formaldehyde	52.10	52.10	52.10	52.10	52.10	52.10	52.26	52.34[a]
38	Methanol	56.88	56.64	56.64	56.88	56.88	56.88	57.46	57.36[a]
39	Propanol	72.18	71.22	71.22	72.42	72.42	72.42	73.89	77.20[a]
41	Styrol	83.17	80.54	80.54	82.70	–	–	82.75	82.46[b]
42	Dimethyl ether	63.10	62.62	62.62	63.10	63.34	63.34	64.32	63.81[a]
43	Ethylene Oxide	57.84	57.60	57.60	57.84	57.84	57.84	57.99	58.08[a]
44	Acetone	74.09	70.98	70.98	71.22	71.94	71.94	72.58	70.51[a]
83	Methyl isocyanate	69.31	70.27	70.27	70.03	69.79	69.79	68.33	64.77[b]

[a]The results presented are retrieved from [72].
[b]The results presented are retrieved from [74] .
[c]The results presented are retrieved from Ghahremanpour *et al.* [82].

estimation, probably due to the use of this chemical specie in the parameterization of PM7 method. The deviation was 0.087 cal/(mol.K) (-0.17%). Some other small molecules behaved similarly (e.g. methanol, styrene and dimethyl ether).

Propanol and methyl isocyanate showed the highest deviations from literature reported values. The latter exhibited a deviation c.a. 3.5 cal/(mol.K) (5.5%) using PM7 level of theory, while the former deviated 3.3 cal/(mol.K) (-4.3%), however it is still an adequate estimate for this thermodynamic property.

Regarding the differences between the two calculation using *ab initio* and semi-empirical methods, the deviation are within 5.23 cal/(mol.K). Maximum deviation was observed from methacrylic acid values of G2 and G3 level of theory (6.7%), while the minimum value deviation was observed from styrene, 0.05 cal/(mol.K) (0.06%).

Therefore, it can be assumed, when compared this study results with previous works, that the semi-empirical method could be used to estimate with a reasonable level of accuracy and reliability the enthalpy of formation and entropy for the studied group of chemical species.

2.3.5 Thermodynamic Properties Results

Once PM7 was selected as the most suitable method for estimating the studied thermodynamic properties, it was used for the whole dataset calculation, containing 122 chemical species.

The results for enthalpy of formation ($\Delta_f H^o_{298,g}$ - kcal/mol), entropy ($S^o_{298,g}$ - cal/(mol.K)) and Gibbs energy of formation ($\Delta_f G^o_{298,g}$ - kcal/mol) are described in the Supplementary Material. The latter thermodynamic property can be calculated using the Equation 2.3.1.

$$\Delta_f G^o_{298,g} = \Delta_f H^o_{298,g} - T \cdot S^o_{298,g} \quad (2.3.1)$$

One of the reasons to accurately estimate properties like enthalpy of formation and entropy is owing to error propagation when calculating other properties dependent on them. For example, for the purpose of calculating the equilibrium constant (K_{eq}) of a reaction, which depends exponentially upon Gibbs energy of reaction, small errors in the enthalpy of reaction and, consequently, in the enthalpy of formation can result in greatly different values of K_{eq}.

2.3.5.1 Energy of Reaction - Direct Route

For the characterization of CO_2 utilization reactions, the work of Otto *et al.* [56] was used as database of all reactions because they considered the possible synthesis products as a basic requirement, and gave an overview of important substance groups that can be synthesized with CO_2 as a feedstock, depending on the nature of the reactants.

The reactions were presented considering that a particular reactant when combined with CO_2 lead to the chemical species described in the database (see Supplementary Material for the full description of molecules).

Reaction enthalpies can be calculated as described in Section 2.2.4. It can also evaluate heat release, if the enthalpy change is negative ($\Delta H^o_{rxn} < 0$), the reaction is exothermic, while positive values ($\Delta H^o_{rxn} > 0$) indicate endothermic reactions. The values of enthalpy of formation for all the species studied are computed using PM7 level of theory, unless literature or experimental data are available.

Taking the reaction of the formation of dimethyl carbonate from CO_2 and methanol, the results showed a value of -4.10 kcal/mol. This value indicates that the gas phase reaction is exothermic at 298 K. Similar results were obtained by Bustamante *et al.* [88], who performed a study of dimethyl carbonate production from CO_2 and methanol, nevertheless the enthalpy of formation for chemical species were calculated using group additivity. The complete set of enthalpy of reaction is described in the Supplementary Material.

Figure 2.3 stratifies the reactions according to their chemical classification (see Supplementary Material).

The results indicate that 59% of the reactions are endothermic and 41% are exothermic. As Figure 2.3 shows, there is a significant difference among the chemical groups, for example all alcohol and ether reactions studied were exothermic, while all aldehyde and epoxides were endothermic.

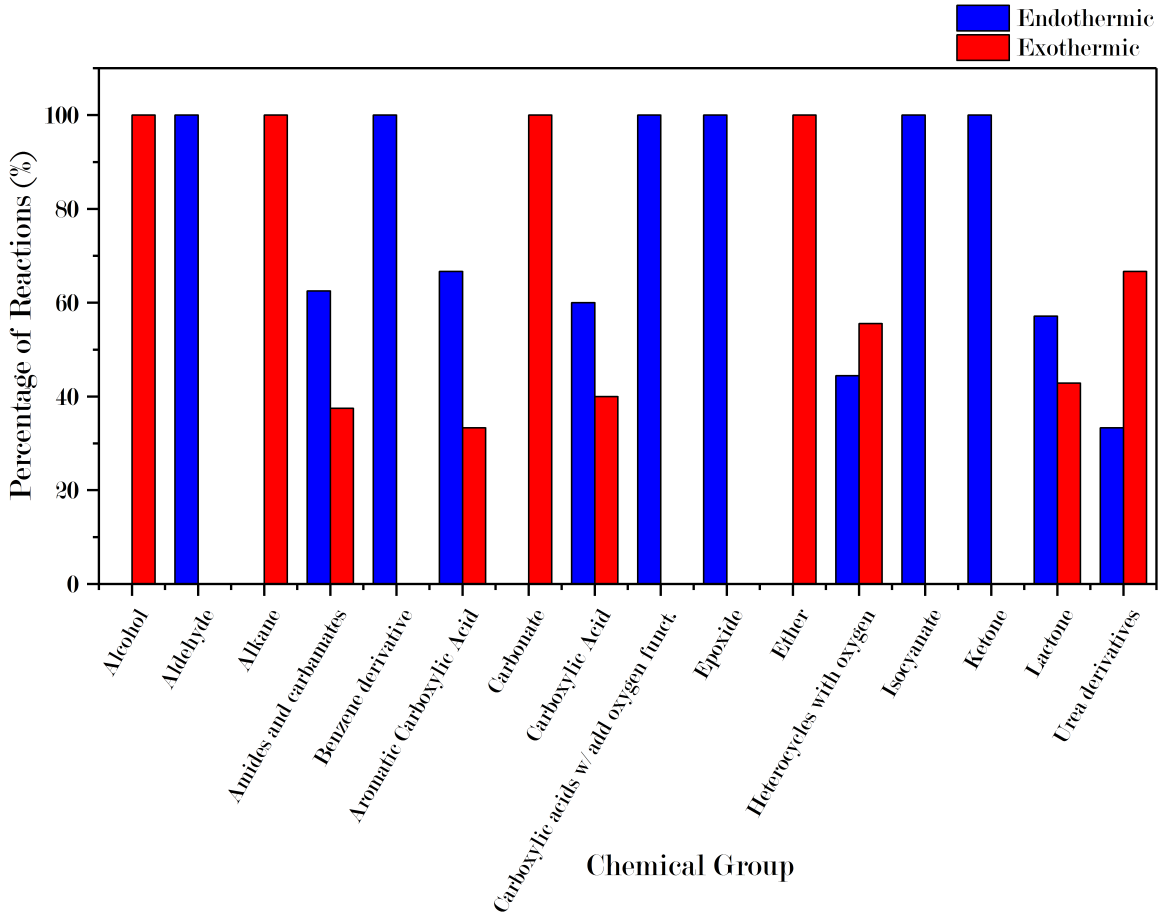

Figure 2.3: Stratification of reaction according to their chemical class.

2.4 Conclusion

In this chapter, different thermodynamic property estimation methods for chemicals produced from CO_2 were assessed. The estimations of enthalpy of formation for CO_2 products were evaluated and the most suitable method to perform the task was PM7, since it demonstrated to be statistically the most applicable within the chemical species studied. The method also showed good accuracy, robustness and efficiency compared with the other methods tested. PM7 was used to calculate properties such as entropy and Gibbs energy for all the chemical species under study.

Experimental thermochemistry data are limited, primarily because the measurements (calorimetry) usually require and destroy significant amounts of material. In this sense, computational chemistry methods are promising for the modelling of physiochemical properties and accessing the optimal structure of molecules. Most studies in CO_2 utilization have only been carried out in a small number of compounds, so, this work fills the gap of energy related content regarding CO_2 products, helping to address chemical product design study issues. The study also categorized the carbon dioxide derived products in sixteen chemical classes and the reaction enthalpy for the

direct route to manufacture the products were assessed and indicate a large difference among the classes.

This study can also lead to a more robust approach to not only characterize the chemical but also select, within the chemicals studied, the most promising for a detailed process synthesis design, as presented in Chapter 4.

Chapter 3

Assessment of the Brazilian Market for Products by CO2 Conversion

The carbon dioxide (CO_2) emissions account for more than 70% of the total greenhouse gases emissions; among the CO_2 emitting sectors, electricity generation accounts for 25% of the global emissions. CO_2 emissions from Brazilian power plants motivated their mapping, a method was proposed to performance a local market analysis for potential products from CO_2 chemical conversion. The forecast behavior of this market for 2030 was also calculated. Among the studied products, methanol, polycarbonates, formic acid and acetaldehyde are the most promising for local manufacture. The States of São Paulo, Paraná, Amazonas, Bahia, Rio Grande do Sul and Santa Catarina are the most promising regions in terms of potential of CO_2 utilization.

Contents

3.1 Introduction

The increasing concern about the environmental impact generated by global warming has stimulated a series of international agreements aimed at regulating greenhouse gases (GHG) emissions in the atmosphere. The UNCHE (United Nations Conference on the Human Environment) in

Stockholm (1972) is considered the first discussion about the global human influence on the environment. More recently, in 2005, the Kyoto Protocol entered into force, committing its Parties by setting internationally binding GHG emission reduction targets at least 18% below 1990 levels until 2020 [89, 90]. The Paris Agreement (the last one signed) goal is to enhance the global response to the threat of climate change by ensuring the average global temperature increase, in this century, below 2°C above pre-industrial levels and to continue efforts to limit temperature rise to up to 1.5°C above pre-industrial levels [90].

In 2016, total global GHG emissions continued to increase steadly by about 0.5% (±1%), to about 53.4 Gt $CO_{2\text{-eq}}$ (including land use, land-use change and forestry emissions, estimated at about 4.1 Gt), the slowest since the early 1990s, except for global recession years, according to Olivier *et al.* [91]. This result is justified by the partial replacement of coal consumption from fuel to natural gas and the increasing renewable power generation (wind and solar power, mostly).

GHG are basically composed of carbon dioxide (CO_2), methane (CH_4), nitrous oxide (N_2O) and fluorinated gases (F-gases). Although CO_2 is not the worse gas, its emissions account for more than 70% of the total GHG emissions, according with Figure 3.1a. Emphasizing CO_2, Figure 3.1b shows the CO_2 emitting sectors. Among them, electricity generation stands out, accounting for 25% of the global emissions [92].

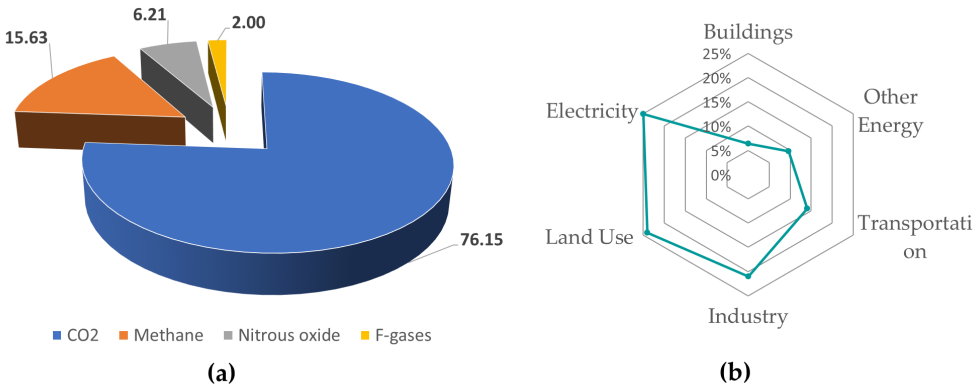

Figure 3.1: GHG and CO_2 emissions: (a) GHG emission composition [91] and (b) CO_2 emissions (%) per sector [92].

Since thermoelectric plants represent large, capital-intensive facilities with a 40-year technical (and economic) lifetime, there must be a link between profit maximization and concern for the environment and GHG emissions [93].

According to Azevedo and Angelo[94], in 2016, Brazil emitted about 1.7 billion tons of carbon dioxide equivalent ($GtCO_2$). This represents nearly 3% of global emissions (around 56 $GtCO_2$), placing Brazil as the sixth largest emitter of the globe. Natural gas has increased its share in electricity generation since 2000, with the third source in the matrix accounting for 8% of total

capacity. In 2014, 81 TWh of electricity from natural gas were produced, representing a growth of twenty times compared to the year 2000 [95]. According to the Energy Research Company [95], installed capacity in the 2016-2026 expansion program forecasts an increase of more than 38%, from 12,532 MW in 2016 to 17,339 MW in 2026 for natural gas. Due in part to the increase in the supply of natural gas being estimated with pre-salt production and unconventional gas sources expanding from 55 million m^3 in 2014 to 180 million m^3 in 2050 [96]. These data show the importance and necessity of the country adopting low carbon policies.

In 2015, at COP-21, the Paris Agreement was drafted, involving commitments to reduce GHG emissions. Brazil proposed to reduce its emissions by 37% in 2025, based on the 2005 emissions [95].

To this end, several treatment systems to reduce CO_2 have been proposed by researchers and industries. Among them are : (**i**) more efficient energy production, (**ii**) changing the fuel matrix, (**iii**) Carbon Capture, Use and Storage (CCUS) [97].

The term Carbon Dioxide Utilization (CDU), a subcategory of CCUS, describes a number of technologies that consume CO_2 to provide services or to manufacture products aiming at an economic benefit. In some cases, the capture of CO_2 is included in the definition, and the term is also referred to as Carbon Capture and Utilization (CCU) in an analogy to the term often used, CCS. The difference between the two concepts is that in CCS, carbon dioxide is stored (underground/marine reservoirs), while in the CDU/CCU, it is used in the economy [12]. According to Aresta *et al.* [13], CDU technologies, due to their inherent potential, can be complementary to the CCS techniques.

Research and development is, therefore, crucial to move towards a competitive CCUS technology, from the most fundamental level of research (e.g. Haunschild [32], focusing on catalyst research) to integrated studies at the conceptual design level as a complete plant in the work by Milani *et al.* [33]. Thus, there is a need for a detailed analysis regarding the impact that different CDU options / processes have on the energy of the system and under which conditions the products obtained can have a sustainable market [34].

The CDU represents a new economy for CO_2, since captured CO_2 could be used as a feedstock for other processes, including the synthesis of chemicals and materials (such as methanol, formic acid, polyols for polyurethanes, carbonates), fuels (such as methane or kerosene) and direct use in applications based on the physicochemical properties of CO_2 (as the supercritical state) [11].

Since CO_2 is emitted from a source and, therefore, supplied at a rate faster than its current consumption, CO_2 for utilization can be considered a renewable alternative source of carbon, ideally leading to carbon neutral cycles in processes with sources of large amounts of CO_2 (such as power plants) [10].

The use of CO_2 can reduce emissions through two main effects: first, -directly, - through CO_2 consumption, thus preventing its release into the atmosphere and second, - indirectly, - by replacing inputs in intensive emission of GHG. According to von der Assen, Jung and Bardow [98], the indirect effect may have a greater impact than the direct effect, but its quantification requires substantial simulation efforts and is the object of future research studies.

Worldwide, about 37 billion tons of CO_2 were issued in 2010 [14, 15]. According to Pérez-Fortes *et al.* [99] and Inagendo [100], 0.4 - 0.5% of the emitted carbon is used, it represents 144 - 185 Mton of CO_2 used in the industry. According to Aresta,Dibenedetto and Angelini [13] the estimate is that 172 million tons of CO_2 are directly consumed in industrial processes per year (2013 base year):, urea accounts for 114 Mton/year, methanol 8 Mton/year, inorganic carbonates ca 50 Mton/year and the group of organic carbonates and salicylic acid together represent less than 1 Mton/year. The growth potential, however, can reach 10% of the carbon emitted today, totalling 3.7 billion tons per year [14, 15].

CDU technologies can be divided into two main categories: technological use (physical processes) and chemical/catalytic conversion (chemical processes or biological/biochemical processes). Figure 3.2a displays CO_2 utilization alternatives.

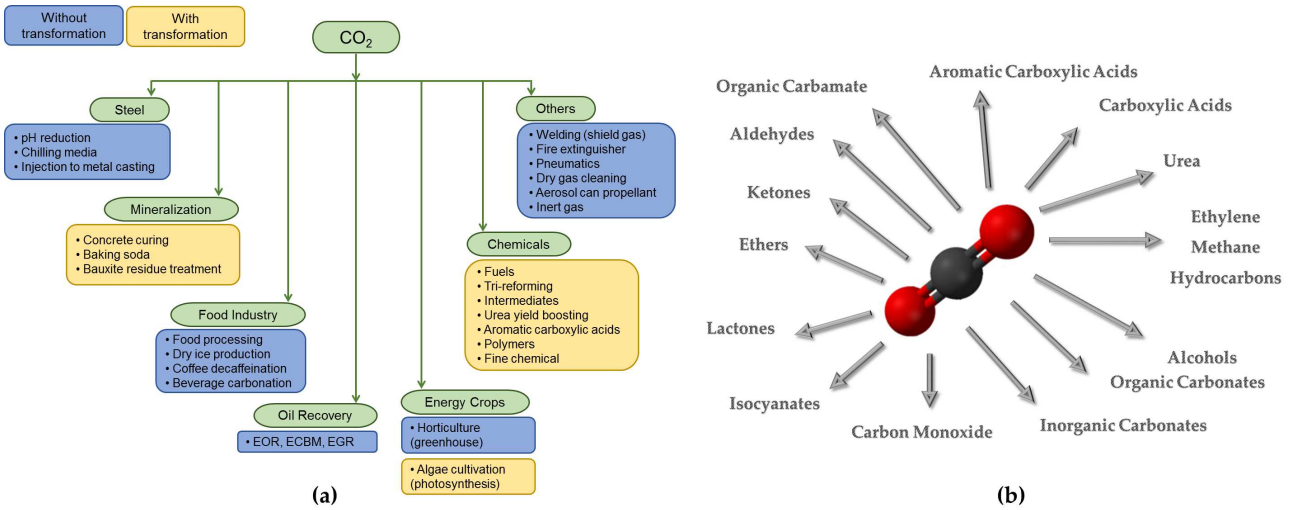

Figure 3.2: (a) CO_2 utilization alternatives. (b) Synthetic processes for some products obtained from CO_2 , divided into categories.

The technological use is related to the physical nature, including compression, recycle, phase transition, etc. Among practical uses are the preservation of cereals (bactericidal), beverage additives, food packaging, dry cleaning, extraction, mechanical industries, fire extinguishers, air conditioning, as well as water treatment [16].

Concerning CO_2 conversion, three main groups may be considered: chemical, mineralization, and bio-based routes [43]. The first category is focused on organic synthesis (including photocatalysis and chemical photocatalysis [101], thermochemical processes [18] and electrochemistry [19]).

The second category is inorganic mineralization (building materials [20]) and the last category uses microorganism to consume CO_2 and produce high added-value products [16].

So, based on important factors, such as distribution cost of energy, resources and implementation time, conversion of CO_2 into fuels or chemicals is an attractive solution, which, in addition to reducing greenhouse gases, provides alternative sources of profit from the sale of manufactured products. In the manuscript, the focus was on organic synthesis of chemicals from CO_2, a more embracing study is important, however is out of the scope of this study.

Many products and processes can use CO_2 as raw material to synthesize different chemicals (Figure 3.2b). Each product or production process brings some advantages and some penalties, making important to define some criteria to evaluate and to choose the most attractive products and processes.

Markewitz et al. [102] show two environmental criteria and one commercial criterion. The amount of CO_2 is computed by energy and carbon balances and represents how much carbon is fixed and the weight of the contribution to minimize global warming. The duration of fixation is evaluated by life-cycle assessment and represents how long this carbon will be out of the atmosphere. Value generation represents the commercial attractiveness and how the product or process is self-sustainable.

Dairanieh et al. [103] shows two environmental and three commercial criteria. CO_2 potential and permanence of capture are similar to the first two criteria of Markewitz *et al.* [102]. Willingness to pay is a criterion based on the product market price and represents how much the CO_2 is valued. Ease of implementation is a commercial criterion and represents the difficulties in entering in a market. Side effects and co-benefits evaluates other effects as either positives (or negatives), such as reduced air pollution or increase in fossil fuels consumption. This study recommends investments in eight products of four clusters: (**i**) Building materials (concrete and carbonate aggregates), (**ii**) Chemical intermediates (methanol, syngas and formic acid), (**iii**) Fuels (liquid fuels, methane) and (**iv**) Polymers (polyols and polycarbonates).

Otto et al. [56] studied 123 CO_2 utilization reactions, 23 to produce bulk chemicals (more than 10 kt/y) and 100 to produce fine chemicals (less than 10 kt/y). For bulk chemicals, the criteria were: specific mass of CO_2 as a feedstock (mass of CO_2 necessary to produce one kg of a product), CO_2 avoidance potential (mass of CO_2 necessary to produce one kg of a product multiplied by the global production), relative added value (difference between the value of the product and the prices of the reagents), independence from fossil reactants (if no carbon from fossil is used). Using these criteria, 6 bulk chemicals were chosen (formic acid, oxalic acid, formaldehyde, methanol, urea and DME). For fine chemicals, with similar criteria, the products selected were methylurethane, 3-oxo-pentanedioic acid, 2-imidazolidinone, ethylurethane, 2-oxazolidone and

isopropyl isocyanate.

This work propose a method that aims to analyze the Brazilian market for potential products from CO_2 chemical conversion, as well as to predict the behavior of this market in 2030. The selected products are used in a methodological framework for a region prioritization at a national level. This method may be easily applied for other countries through market analysis.

3.2 Methods

The proposed method comprises four steps. 1- Defining criteria to evaluate the products, grouped into technological, environmental and economical criteria; 2- Collecting data for each product; 3- Generating the decision matrix and carrying out a sensitivity analysis; 4- Carring out a top-down approach methodology including opportunity identification, resulting in cluster identification and region prioritization for Brazil.

3.2.1 Multiple criteria decision analysis assessment

Multiple criteria decision analysis (MCDA) refers to making preference decisions (**e.g.** evaluation and selection) over the available alternatives characterized by multiple, usually conflicting, attributes.

MCDA is a branch of operations research and deals with planning scientific and computational apparatuses to address a limited number of choices under a limited number of criteria by a unique or a group of decision makers.

There is a wide variety of approaches, for example analytic hierarchy process (AHP) [104], Preference Ranking Organization Method for Enrichment Evaluations (PROMETHEE) [105], Technique for Order Preference by Similarity to an Ideal Solution (TOPSIS) [106, 107] and the simple additive weighted (SAW) method [108] which have been successfully utilized in dealing with MCDA problems.

The latter two approaches were used in different case studies to select the most promising products for further/deeper study. The TOPSIS method designates alternatives that simultaneously have the shortest distance from the positive ideal solution (maximization of benefit criteria) and the farthest distance from the negative-ideal solution (maximization of cost criteria). More details about the method can be found in the work by Hwang and Yoon [107]. The SAW method is simpler as compared to TOPSIS, performing only the summation of the products of weight and the normalized value of each alternative.

The calculations of the TOPSIS method was performed using the python module Scikit-Criteria

(Scikit-Criteria, RRID:SCR_017084) v0.2.10 [109] running on python v2.7.15; for the SAW method, simple spreadsheets and MATLAB R2015a were used.

3.2.2 Criteria Description

The option of using CO_2 for chemical conversion has thermodynamic and intrinsic kinetic restrictions. Estimating their real potential will require a thorough comparative analysis of proposed and existing processes to determine whether or not the proposed conceptual plant reduces CO_2 emissions (directly or indirectly), and whether there is a sale of the obtained chemicals [11].

The evaluation of rejection or acceptance of the proposal will produce reliable results only if significant number of parameters is used; for this situation, ten criteria were employed. The criteria were grouped into technical, environmental and economic.

3.2.2.1 Technical Group

For the technical group, the standard enthalpy of reaction (ΔH^o_{rxn}) and the Technical Readiness Level (TRL) were evaluated.

Equation 3.2.1 was used to calculate the enthalpy of reaction. This was done by executing basic algebraic operations based on chemical equations of reactions taking into account the values of enthalpies of formation of the gas phase

$$\Delta H^o_{rxn} = \sum_{products} \nu_i \left(\Delta_f H^o_{298,g}\right)_i - \sum_{reactants} \nu_i \left(\Delta_f H^o_{298,g}\right)_i \tag{3.2.1}$$

The enthalpy of reaction can be determined by scaling each species enthalpy of formation (obtained from the literature - [73] or NIST-TDE inside Aspen Plus commercial simulator) by its stoichiometric coefficient ν_i. In this study, only direct conversion routes to the products were considered, **i.e.** the CO_2 reacts with one or more reactants to directly form the products under assessment.

TRL is a systematic metric/measurement system that determines the maturity of a specific technology. The methodology was proposed by NASA and, due to its simplicity and versatility, it expanded to other domains as well [110].

In this case, the TRL scale measures the development of technology from its basic concept (TRL 1) to being available at commercial/industrial scale (TRL 9), reaching the physical scale of deployment or its maximum technical maturity. Each step in between represents the increase in the level of maturity of the technology.

The TRL assessment refers to the innovative route for each product, not the conventional one. The TRL applied to this study ranges from basic and applied research, proof of concept and laboratory testing (stages 1-5), to prototyping, piloting and final development (stages 6-8), to full- scale deployment/market introduction (9).

Several products manufactured using CO_2 as a feedstock have been studied and produced. An overview of the set of compounds and their technological path can be found in international reports [14, 111–114], which are used to assign TRL to the chemicals described in Section 3.2.3.

3.2.2.2 Environmental Group

For the environmental group, the willingness to pay (WP), scientific relevance, side effects and benefits and utilization ratio were evaluated.

The side effects and benefits and WP were proposed by [103] to evaluate CO_2 products. The first criterion of this group (side effects and benefits) is related to the increased production of fossil fuels and the avoidance of a hazard route. The second criterion, despite being based on the economics of the target market, it is set in the environmental group because it represents the unit cost/price point of CO_2 supply at which the product is competitive for that use ($/tonne of CO_2).

The scientific relevance is a criterion proposed by Otto *et al.* [56], defined as the number of related references of a certain chemical (SCI-Finder database). According to the author, this criterion discerns rare application chemicals from diverse application chemicals. The former belong either to basic research or speciality chemicals; the latter can be use of a wide variety of applications as a feedstock, which are more attractive from an ecological and economic point of view. The number of citations was gathered in October and November 2018.

The utilization ratio is the amount fixed, which takes into consideration the mass of carbon dioxide, the mass of product and their respective stoichiometric coefficient (CO_2 and reference product) as shown in Eq. 3.2.2.

$$\frac{m_{CO_2}}{m_p} = \frac{|\nu_{CO_2}| \cdot M_{CO_2}}{|\nu_p| \cdot M_p} \tag{3.2.2}$$

Where m_{CO_2} is the mass of CO_2, m_P is the mass of product, ν_{CO_2} is the stoichiometric coefficient for CO_2, while ν_p is for product, M_{CO_2} is the molecular weight of CO_2 and M_p is the molecular weight of the product.

3.2.2.3 Economic Group

The economic group represents the market-related criteria (demand and price). The imports and exports (amount and price) of the compounds were taken into account. The data for the value (in millions of US$) were stated in *Free On Board* (FOB) value, which means that the exporter is responsible for the merchandise until it is inside the ship, for transportation, at the port indicated by the buyer.

The values of imports and exports for 2030 were forecast and the harmonized mean of values from 2015 - 2018 and 2030 for each chemical were used in the decision matrix.

The annual data were collected from the official website of foreign trade statistics of the Brazilian government [115].

3.2.2.4 Forecast Method

Time series analysis is a tool for forecasting future values, based on past and present events [116]. There are several forecasting alternative methodologies classified in automatic and non-automatic approach. While the latter required prior exploratory data analysis for each case, the former does it automatically.

Papacharalampous, Tyralis and Koutsoyiannis [117] explore the capability of seven different forecast methods used to predict monthly temperature and precipitation. The methods are a naïve, random walk (with drift), ARFIMA (AutoRegressive Fractionally Integrated Moving Average), BATS (Box–Cox transform, ARMA errors, Trend, and Seasonal components), simple exponential smoothing, Theta and Prophet. Their results indicate that the last five models performed better than the first two and the Prophet method is competitive.

In this work, the facebook prophet model [118] was used. It was introduced in 2017, inspired by a nature of time series forecast by the company. The package is available at an R library named 'prophet' [119]. The procedure used by prophet is additive regression model with the main components: a linear growth curve trend, yearly seasonal components modelled using the Fourier series.

The 2030 values were forecast for each product using the data available from 2000 to 2018. The time series analysis was based on its past values using prophet package (Prophet, RRID : SCR _017083) version 0.5 on R (version 3.6.0 (2019-04-26)).

3.2.3 Data Collection

A database of 13 chemicals was selected from the open literature as products from CO_2 conversion [2, 7, 13, 56, 120–123], for which was possible to retrieve their data related to Brazilian Statistics.

The chemical compounds used in this assessment are listed: 1- Acetaldehyde; 2- Acetic Acid; 3- Acetone; 4- Benzoic Acid; 5- Formaldehyde; 6- Formic Acid; 7- Methacrylic Acid; 8- Methanol; 9- Oxalic Acid; 10- Polycarbonates; 11- Propanol; 12- Salicylic Acid; and 13- Urea.

3.2.4 Weighting Method

The weight for each criterion can be assigned to two group categories: subjective and objective weights. Subjective weights are determined based on the preference of the decision maker (e.g. AHP method [104], weighted least squares method [124], Delphi method [125] and equal weights). Objective methods determine weights by solving mathematical models and do not account for the decision maker preference (**e.g.** Shannon entropy method [126, 127] and multiple objective programming [128]).

For solving problems, the expertise of a decision maker ought to be calculated; in this case, subjective weighting is preferable. However, when reliable subjective weights are difficult, objective weighting must be selected.

The Shannon information entropy measures the predicted value of the information contained in a message, usually in units of bits, nats or bans. The value is the average unpredictability in a random variable, equivalent to its information essence. In the MCDA context, the entropy method is an objective method to assign weights depending on the decision matrix [126, 127]. The relative weight of criterion j is calculated in relation to the amount of information supplied by the intrinsic set of alternatives.

The concept of entropy in an information channel was proposed by [126] and the procedure defines a series of steps:

1. Normalization of data.

   In order to remove anomalies with different measurements units and scales, the normalization procedure is carried out. Considering $p_{ij} = \frac{x_{ij}}{\sum_{j=1}^{m} x_{ij}}$, $j = 1, \cdots, m$, $i = 1, \cdots, n$, where p_{ij} is the normalized data and x_{ij} is the raw data (i alternative on j criterion).

2. Calculation of the entropy

   Entropy E_j for criterion j is calculated according to Eq. 3.2.3

$$E_i = -E_0 \cdot \sum_{j=1} (p_{ij} \cdot \ln(p_{ij})) \qquad i = 1, \cdot, n \tag{3.2.3}$$

The entropy constant E_0 was calculated as $\ln(m)^{-1}$.

3. Calculation of Diversity Criterion

   The diversity criterion is then calculated using Eq. 3.2.4, which represents the degree of diversification.

$$D_j = 1 - E_j \tag{3.2.4}$$

4. Computation of normalized weight

   Finally, the degree of importance is calculated according to Eq. 3.2.5

$$w_j = \frac{D_j}{\sum D_j} \tag{3.2.5}$$

The closer the entropy of a criterion is to 1, the less important the criterion is. Shannon entropy measures the amount of uncertainty with a probability distribution in terms of entropy taking into account the complete set of information available.

Along with Shannon entropy, subjective weighting was also employed in the case studies described in Section 3.2.5.

3.2.5 Sensitivity Analysis

In order to evaluate the use of a MCDA method (either TOPSIS or SAW) and the weighting system (either objective or subjective), a sensitivity analysis was carried out.

Table 3.1 shows the case studies involved in the sensitivity analysis.

Table 3.1: Different case studies involved in the sensitivity analysis.

Case	**Weight**	**Method**
Case 1	Shannon Entropy	TOPSIS
Case 2	Equal Weight[a]	TOPSIS
Case 3	Technical Criteria[b]	TOPSIS
Case 4	Economical Criteria[b]	TOPSIS
Case 5	Environmental Criteria[b]	TOPSIS
Case 6	Shannon Entropy	SAW
Case 7	Equal Weight[a]	SAW
Case 8	Technical Criteria[b]	SAW
Case 9	Economical Criteria[b]	SAW
Case 10	Environmental Criteria[b]	SAW

[a]All criteria received the same weight.

[b]Weights for the criterion that belongs to this group were the double when compared to the other groups

As a result, the most promising products will appear more often in the first places.

3.2.6 Opportunity Identification Approach

A top-down methodology approach developed by [129, 130] consisting of three consecutive steps was adapted and used to identify opportunities for CCU at national level. In the first step, technologies that use CO_2 in Brazil were identified. The second step is the geographical location of thermoelectric power plant (Natural Gas-based). The third step is matching the sources with the potential receiver, based only on geographic parameters.

3.2.6.1 Emission Calculations

In order to evaluate the CO_2 emissions of a Power Plant, the net capacity factor and the power capacity are used to calculate the energy generated in a year, according to Eq. 3.2.6 [131, 132].

$$E_a = F_c \cdot C \cdot 8760 \tag{3.2.6}$$

Where E_a is the annually produced energy, F_c is the capacity factor and C is the power plant installed capacity.

The capacity factor is the ratio of the actual output over a period. The data used in these calculations was based on a statistics of the Brazilian Government [133] for the year 2016, for the public generation of energy based on natural gas. The average F_C of 2016 was 0.43, a much lower indicator than in 2015 (0.72), but still higher than in 2011 (0.26). According to [134], the installed capacity of a power plant is directly proportional to its CO_2 emission (517 g CO_2/kWe-h), these values are then used.

3.3 Results and Discussions

3.3.1 Forecast Results

A time series forecasting model is designed to handle the common features of the business time series of imports and exports. The investigation of the predictability of imports and exports of 13 chemical products was performed from 2000 to 2018 to forecast 2030 values.

Figure 3.3a and Figure 3.3b present statistical data on the Brazilian trade balance of the last 4 years, in terms of imports absolute volume and value in US dollars, respectively, as well as the projection of these values for 2030. It is worth mentioning that no more CO_2 conversion products were analyzed, due to the difficulty in finding theirs NCM in the Brazilian trade system.

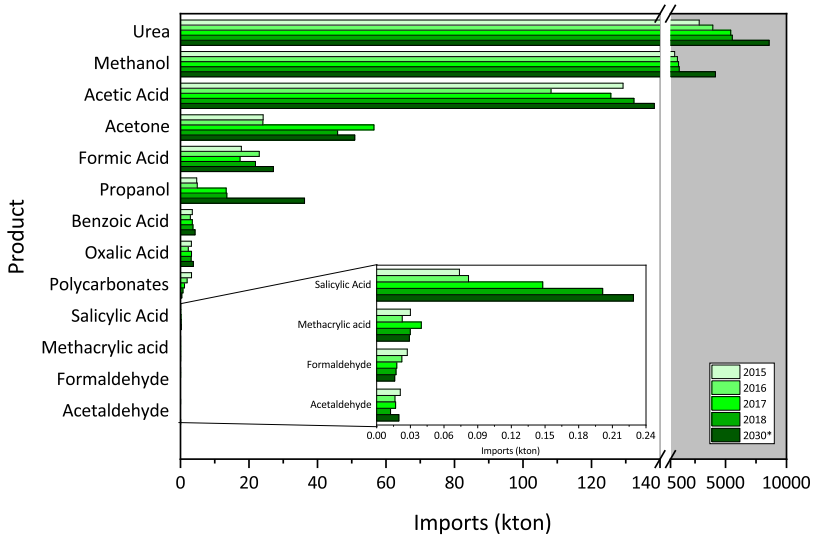

(a)

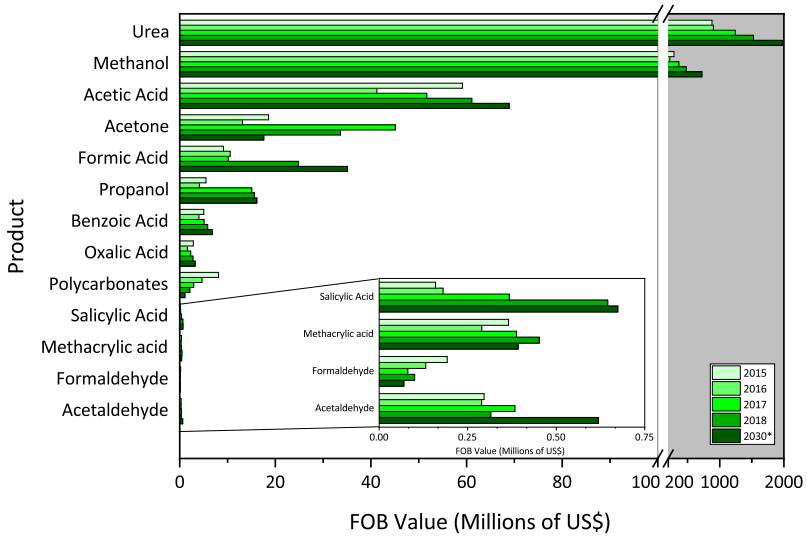

(b)

Figure 3.3: Brazilian importation data (a) absolute volume and (b) FOB value.

The annual absolute quantity imported (kton) is highlighted by the large average amount of urea, methanol and acetic acid imported (8574, 4168.7, 1383.4 kton, respectively for 2030) in this period, with tendency to increase in the evaluated period.

Next, come acetone and formic acid, showing forecast tendency to increase. Acetone was forecast to increase the imported absolute amount (from 45.9 kton in 2018 to 50.9 kton in 2030) and formic acid was forecast to increase 23.93% from 2018 to 2030. The other products exhibited imports smaller than 5 kton/year each (except for propanol in 2018 with 13.5 kton).

Regarding the value generated in the transactions, Figure 3b depicts the imports in millions of US$. Urea, methanol and acetic acid were the products with the highest value. However, the values for acetic acid are followed more closely by acetone, formic acid and acrylic acid, which have higher added value. Comparing 2030 to 2018, there is an increasing trend of import costs for methanol, acetic acid and urea, while a decrease for acetone.

It is possible to calculate the prices for imports and exports, taking into account the FOB value divided by the absolute amount for each chemical product (see Table 3.2 for details).

The situation changes when the prices are taken into account; the most expensive imported product is acetaldehyde, followed by methacrylic acid. Formaldehyde presented an oscillation during the evaluated period from 7.03 US$/kg in 2015 to 5.83 US$/kg in 2018. Polycarbonates were imported for an average price of 2.60 US$/kg, similar to salicylic acid (2.51 US$/kg).

Figure 3.4a reveals the annual absolute exported quantity (kton), while Figure 3.4b shows the involved costs.

Figure 3.4a points out the high average amount of methacrylic acid, salycilic acid and urea exported, followed by acetone, acetic acid and formaldehyde, all tending to increase exports in 2030, as compared with 2018, except for methacrylic acid.

Figure 3.4b displays the expected behavior of the exportation costs involved for products. Due to the higher market value, the export profit of methacrylic acid exceed that of urea. In 2030, as compared with 2018, profits appear to be higher for methacrylic acid and urea, and smaller for salicylic acid and acetone.

Anomalous data did not have a great impact on the forecast, due to the robustness of the time series analysis method. According to Papacharalampous, Tyralis and Koutsoyiannis [117], comparing different forecast methods, prophet exhibited the smallest median RMSE for the temperature forecasts, while offering 13-32% (depending on the examined set of time series) more accurate results than naive. In their case, the model is competitive to the ARFIMA, BATS, simple exponential smoothing and Theta models.

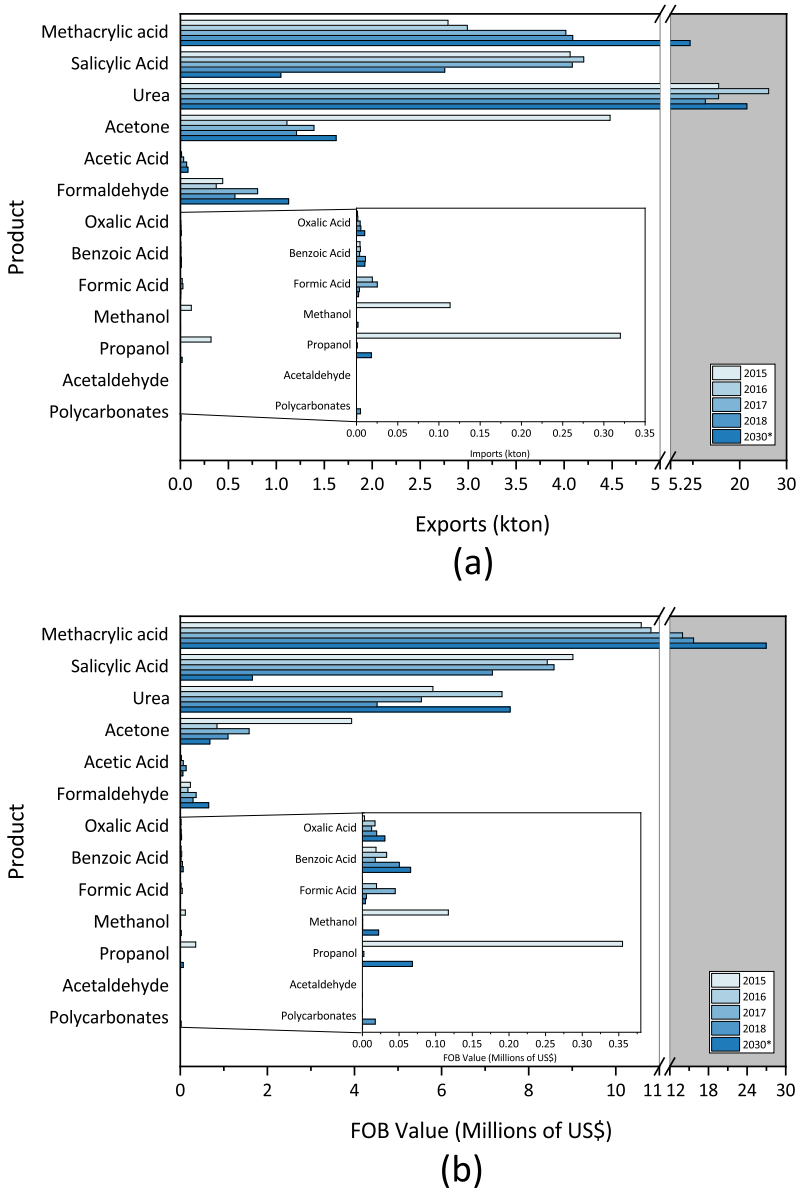

Figure 3.4: Brazilian exportation data (a) absolute volume and (b) FOB value

3.3.2 Multi-Criteria Performance Matrix

Estimating the use of CO_2 for chemical conversion by their real potential will require a full comparative analysis of the proposed processes to determine whether or not the process is feasible, and whether there is a market for the given products. In order to select the most promising products for further study, a multi-criteria performance table (Table 3.2) was constructed encompassing the criteria and alternatives.

Table 3.2 presents the performance of the alternatives (chemical compounds) in each criterion. Regarding the technical criteria, enthalpy of the direct reaction, acetone and formaldehyde are the most endothermic, while propanol and methanol the most exothermic. The maturity of urea and salicylic acid reflect the commercial production of this chemicals, on the other hand oxalic acid, methacrylic acid and acetic acid are in the early stages of research and development.

In the environmental group, the utilization ratio criteria that represents the amount of CO_2 fixed in the molecule, showed higher values for formaldehyde and methanol and lower values for salicylic acid and benzoic acid. There is no wide amplitude in scientific relevance and in effects, and two broad group of chemicals were identified through the criterion willingness to pay (represented by the numbers 225 or 28).

The economic group (imports and exports) showed a similar behavior compared with described in the forecast predictions.

3.3.3 Sensitivity Results

The 10 cases described in Section 3.2.5 used either the TOPSIS or SAW method for evaluation. Regarding the weighting method, either a subjective method or an objective method was employed.

The Shannon Entropy equation was used for the objective weighting method in order to express the relative intensities of criterion importance and to determine the objective weights. Table 3.3 presents the results of the proposed approach for weight elicitation.

Table 3.3 describes the criteria used and their relative importance. The exports amount, exports price and enthalpy of the reaction are cost-type criteria, indicating that the performance of every alternative must be as minimum as possible.

The enthalpy of a reaction and the willingness to pay showed the highest values for entropy indicating a minor importance when compared with other criterion. Scientific relevance and imports price showed higher relative importance.

Figure 3.5 presents the results of the sensitivity analysis. The classification in every case is

Table 3.2: Multi-criteria performance matrix for assessing CO_2 products.

Products	Economic Criterium				Technical Criterium		Environmental Criterium			
	Imports[a] (kg/y)	Imports Price[a] (US$/kg)	Exports[a] (kg/y)	Exports Price[a] (US$/kg)	ΔH^o_{rxn} [b] (kcal/mol)	TRL (–)	WP (US$/$t_{CO_2}$)	Sci. Rel. (%)	Effects[c] (–)	Utilization ratio ($kg_{CO_2}/kg_{prod.}$)
Acetaldehyde	16680	20.62	21	2.09	14.14	2	225	90	0	0.999
Acetic Acid	125856438	0.44	483	1.74	8.60	1	225	100	0	0.733
Acetone	35168454	0.58	1522373	0.73	20.23	2	225	100	0	0.758
Benzoic Acid	3484402	1.50	5539	5.24	4.08	2	225	90	0	0.360
Formaldehyde	19425	5.34	565624	0.50	10.28	1	225	100	1	1.465
Formic Acid	20856261	0.67	241	1.62	3.57	5	225	90	1	0.956
Methacrylic acid	29398	12.38	3867793	3.48	2.39	1	225	90	0	0.511
Methanol	1229493061	0.26	63	3.63	-11.84	5	28	100	1	1.374
Oxalic Acid	3020134	0.80	2516	3.41	17.25	1	225	90	1	0.978
Polycarbonates	873880	2.63	43	0.96	-4.10[d]	3	225	90	2	0.489
Propanol	8422607	0.83	2856	1.80	-37.24	2	225	90	0	0.732
Salicylic Acid	119416	2.54	2442643	2.05	-0.22	7	225	90	0	0.319
Urea	4609107497	0.25	17087027	0.34	1.91	7	28	100	1	0.733

[a] The values correspond to the harmonized average of the period 2015 - 2018 and 2030 (the latter year was estimated in this study - see Section 3.2.2.4), without outliers.

[b] The enthalpy of reaction is for the direct route only.

[c] The criteria named Effects refers to side effects and benefits summation for each product (avoid hazard route - 1, avoid use of fossil fuels - 1).

[d] The functional group ROC(O)OR' is a key constituent of organic products comprising molecules with one carbonate unit and polycarbonates with numerous carbonate moieties. Important representatives with one carbonate unit are dimethyl carbonate: its captive consumption for using in the production of polycarbonates is 46 kt/y, approximately 50% of the world production [135]. Therefore, the direct route was estimated for dimethyl carbonate.

Table 3.3: Shannon Entropy Weights (used in cases 1 and 6).

Criteria (i)	**Type**	**Min/Max**	**Entropy** (E_i)	**Diversity** (D_i)	**Normalized Weight** (w_i)
Imports (kg/y)	Benefit	max	0.875	0.125	0.066
Imports Price (US$/kg)	Benefit	max	0.613	0.387	0.203
Exports (kg/y)	Cost	min	0.875	0.125	0.065
Exports Price (US$/kg)	Cost	min	0.872	0.128	0.067
ΔH^o_{rxn} (kcal/mol)	Cost	min	0.960	0.040	0.021
TRL (–)	Benefit	max	0.761	0.239	0.125
WP (US$/tonne$_{CO_2}$)	Benefit	max	0.935	0.065	0.034
Sci. Relevance (Benefits (–)	Benefit	max	0.681	0.319	0.167
Utilization ratio (kg$_{CO_2}$/kg$_{\text{prod.}}$)	Benefit	max	0.891	0.109	0.057

assigned in the horizontal axis. The weighting method affects the final classification, and a sensitivity analysis could thus potentially incorporate this influence.

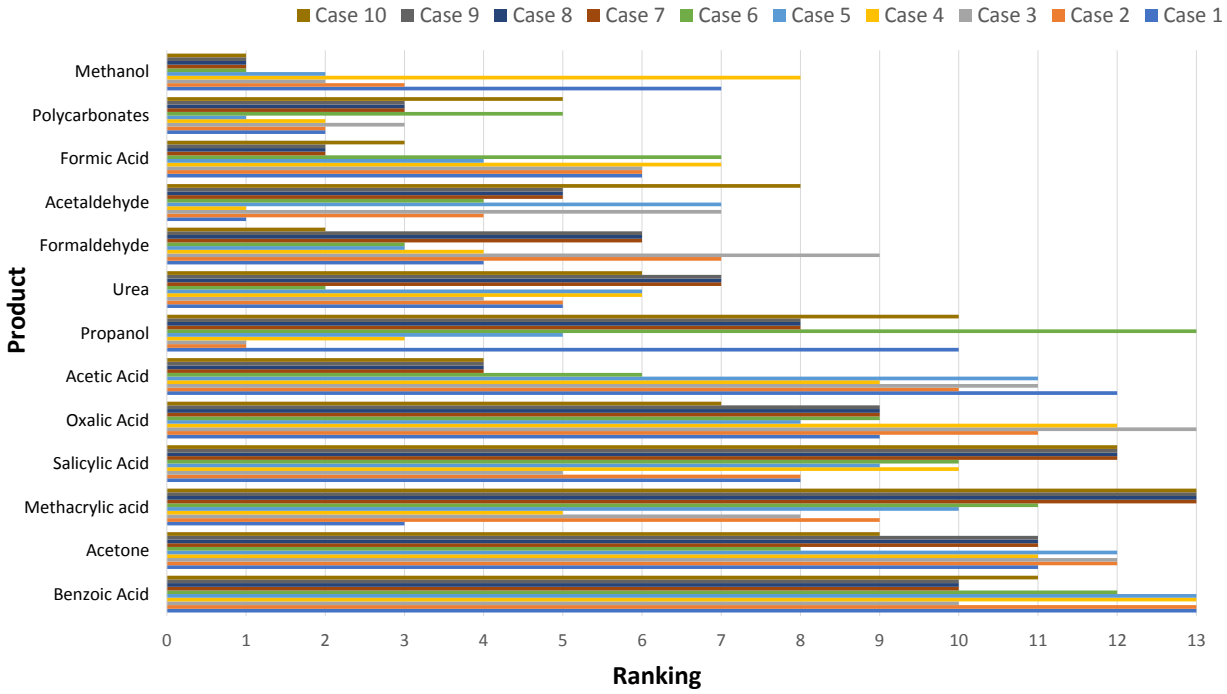

Figure 3.5: Sensitivity Study Results.

Methanol, polycarbonates, formic acid and acetaldehyde appear more often in the top positions. Therefore, their further study and implementation in Brazil is recommended, considering the evaluated criteria and the range of chemical products assessed.

The method proposed was robust for selecting the most promising products; the weights assigned or calculated were taken into consideration, however it was specific designed for the Brazilian context. The implementation of the method in other countries can assessed easly, it only required a detailed study of the local market and appropriate weight elicitation.

3.3.4 Opportunity Identification Results

Based on Eq. 3.2.6, the CO_2 amount emitted annually by the 20 Brazilian Power Plants with the highest installed capacity was calculated. Figure 3.6 shows the more emitters power plants in Brazil, as well as their respective locations.

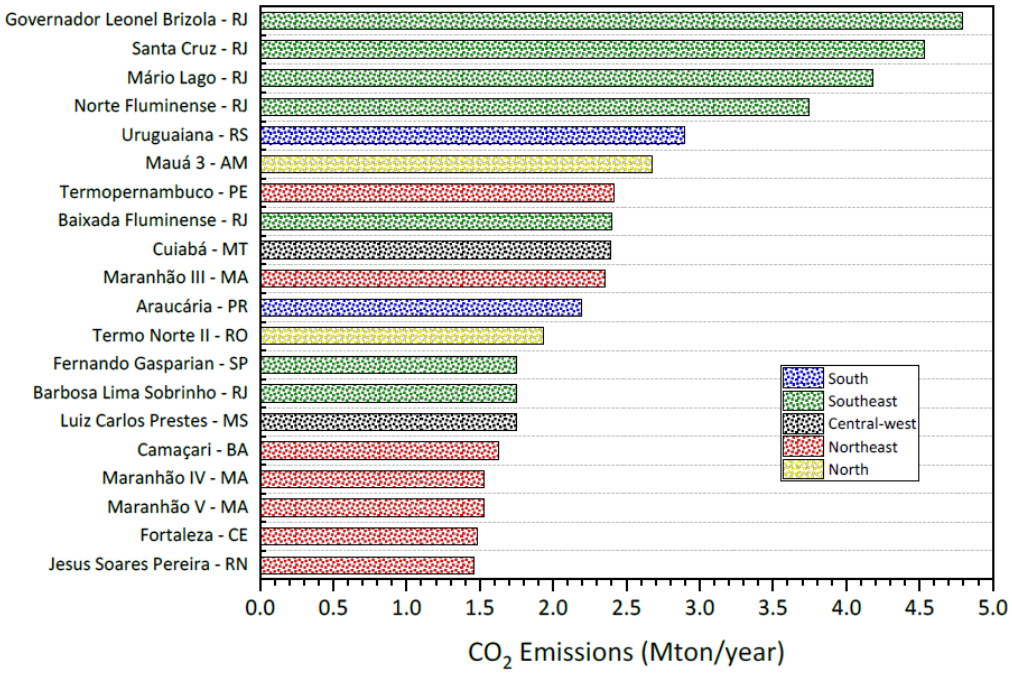

Figure 3.6: Annual emissions of 20 Brazilian Power Plant (natural gas) with higher installed capacity (RJ - Rio de Janeiro, RS - Rio Grande do Sul, AM - Amazonas, PE - Pernambuco, MT - Mato Grosso, MA - Maranhão, PR - Paraná, RO - Rondônia, SP - São Paulo, MS - Mato Grosso do Sul, BA - Bahia, CE - Ceará, RN - Rio Grande do Norte).

The power plants with the highest CO_2 emissions are present in the southeast region. Therefore, there is a greater supply of CO_2 in this region, which could support the installation of new plants of CO_2 conversion processes

Figure 3.7 presents the location and capacity of the Brazilian Natural gas based Power Plants.

São Paulo and Rio de Janeiro are the most promising regions in terms of CO_2 availability and infrastructure identified as clusters in Figure 3.7 were the most interesting spots. However, the third step of the methodology is the match with the local needs.

The final step is to identify the need in a specific State for a specific product. According to the sensitivity analysis, the most promising products were considered.

The stratification based on States rather than cities is due to the fiscal confidentiality, therefore it is not possible to access individual company data. It is important to emphasize that the exportation by State definition consider the producer of the chemical, independently the headquarters cities of the producer. The data can be also related to the entry port.

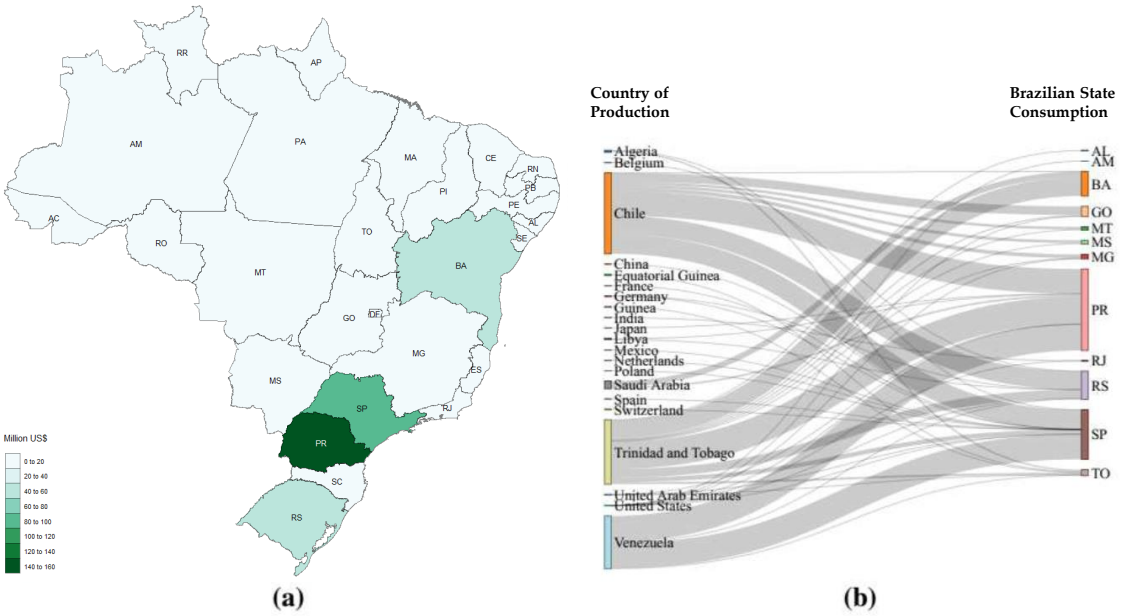

Figure 3.7: Location and capacity of Power Plant (Natural Gas-based).

The data contained in Figures 8b - 11b concern about the imports, separated by country of production and Brazilian state of consumption. The country refers to the location of the last registry of the product before enter in Brazil, not necessarily the producer location. The State refers to the Brazil entry location, not necessarily the final destination of the chemical's consumption. The valuation of the potential utilization per State is helpful for guiding decision makers and policy makers to invest in CDU. Figure 3.8 to Figure 3.11 depict the imports in 2017 for methanol, polycarbonates, formic acid and acetaldehyde, respectively.

From Figure 3.8 Paraná is the State that most imported methanol in 2017, followed by São Paulo, Rio Grande do Sul and Bahia. Paraná imported almost 40% more than São Paulo; moreover, Rio Grande do Sul and Bahia imported similar values of methanol (48.7 and 42.3 million US$, respectively).

According to Figure 3.9 São Paulo and Amazonas are the States with the highest imports, 1.73 and 1.03 million US$, respectively. Polycarbonates were imported mainly from the United States and Germany.

Regarding formic acid, São Paulo leads the importation with 3.57 million US$, followed by Rio Grande do Sul (1.64 million US$), Santa Catarina (1.44 million US$) and Paraná (1.03 million US$) (Figure 3.10).

For acetaldehyde, São Paulo heads the imports followed by Amazonas. Paraná, Goiás, Rio Grande do Sul and Santa Catarina also import the product, yet less than 0.003 million US$ (2800 US$) in 2017 (Figure 3.11).

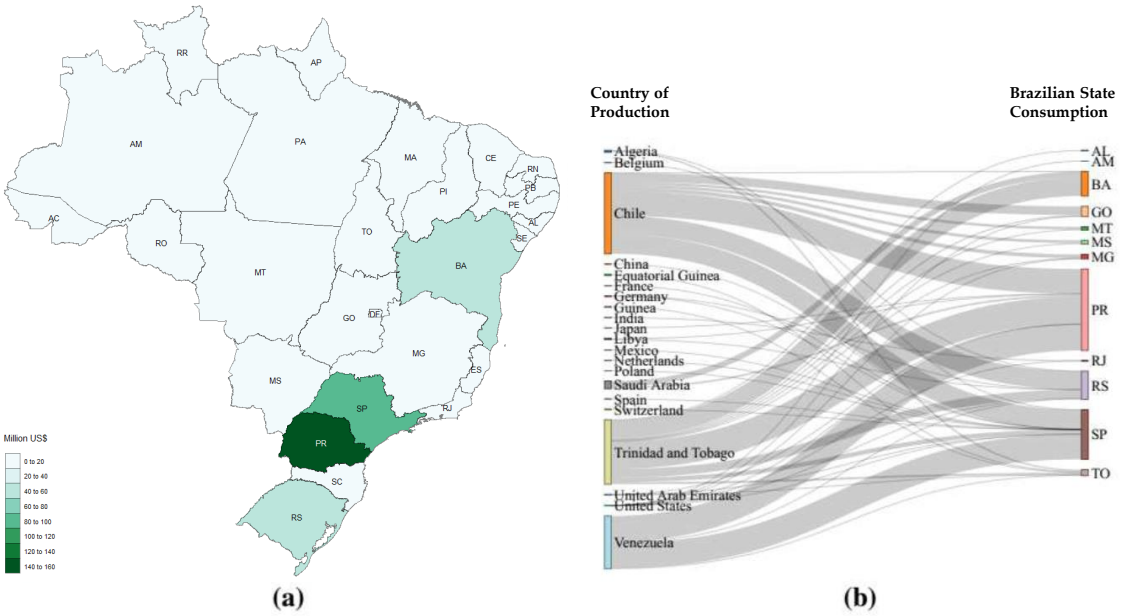

Figure 3.8: Methanol imports. (a) Local needs considering 2017; (b) Stratification for 2017, countries on the left represent the origin of the product studied and the states on the right represent the destination (AL - Alagoas, AM - Amazonas, BA - Bahia, GO - Goiás, MT - Mato Grosso, MS - Mato Grosso do Sul, MG - Minas Gerais, PR - Paraná, RJ - Rio de Janeiro, RS - Rio Grande do Sul, SP - São Paulo, TO - Tocantins).

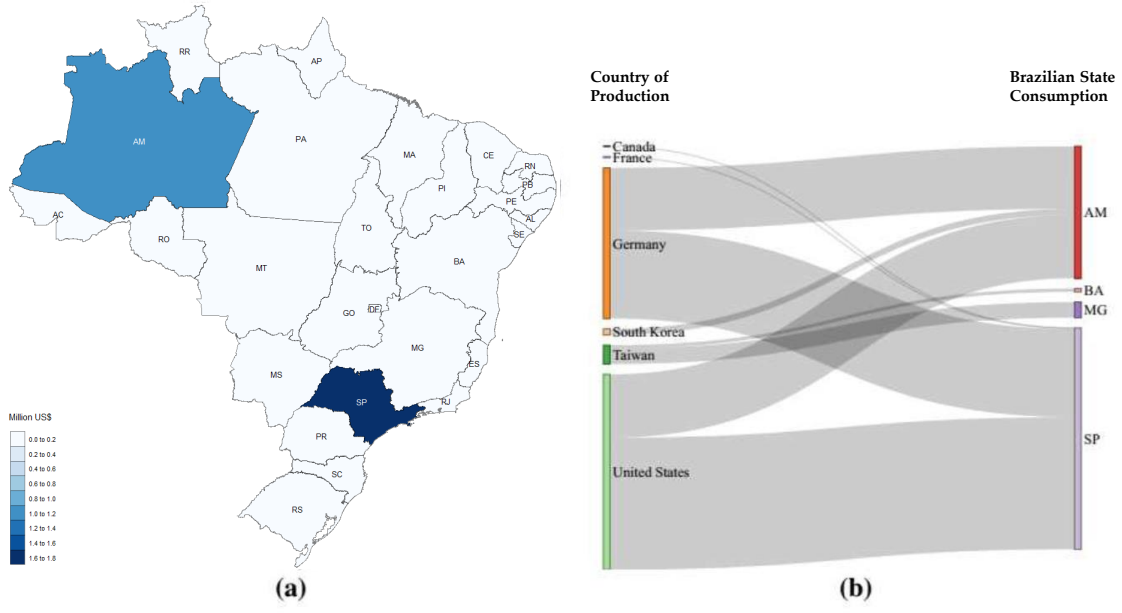

Figure 3.9: Polycarbonate imports. (a) Local needs considering 2017; (b) Stratification for 2017, countries on the left represent the origin of the product studied and the states on the right represent the destination (AM - Amazonas, BA - Bahia, MG - Minas Gerais, SP - São Paulo).

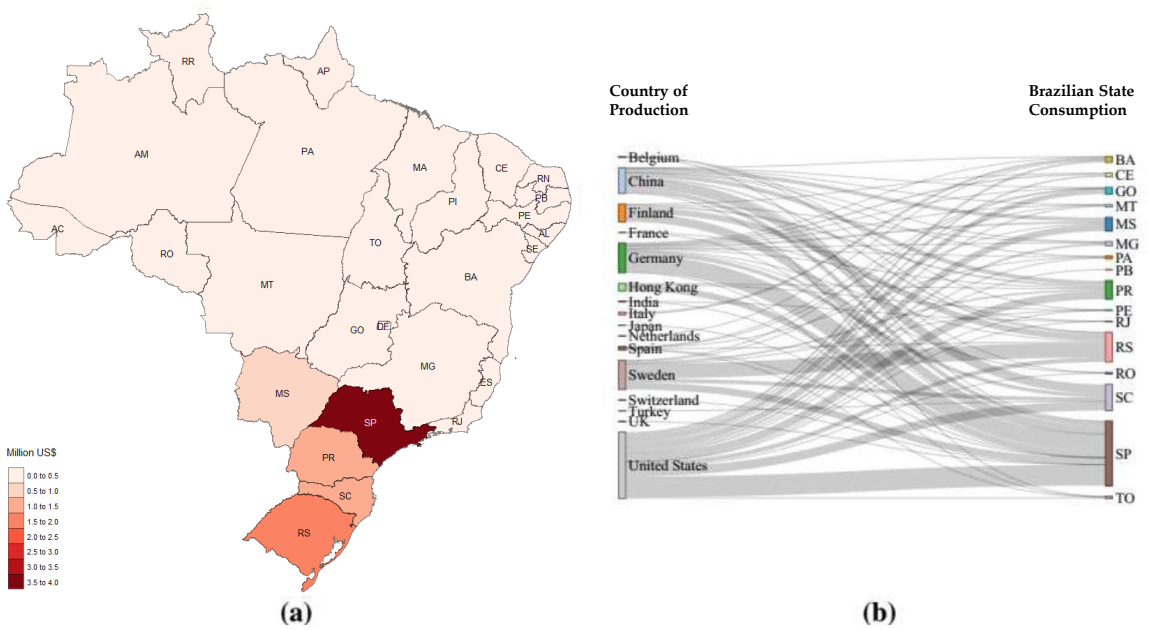

Figure 3.10: Formic Acid imports. (a) Local needs considering 2017; (b) Stratification for 2017, countries on the left represent the origin of the product studied and the states on the right represent the destination (BA - Bahia, CE - Ceará, GO - Goiás, MT - Mato Grosso, MS - Mato Grosso do Sul, MG - Minas Gerais, PA - Pará, PB - Paraíba, PR - Paraná, PE - Pernambuco, RJ - Rio de Janeiro, RS - Rio Grande do Sul, RO - Rondônia, SC - Santa Catarina, SP - São Paulo, TO - Tocantins).

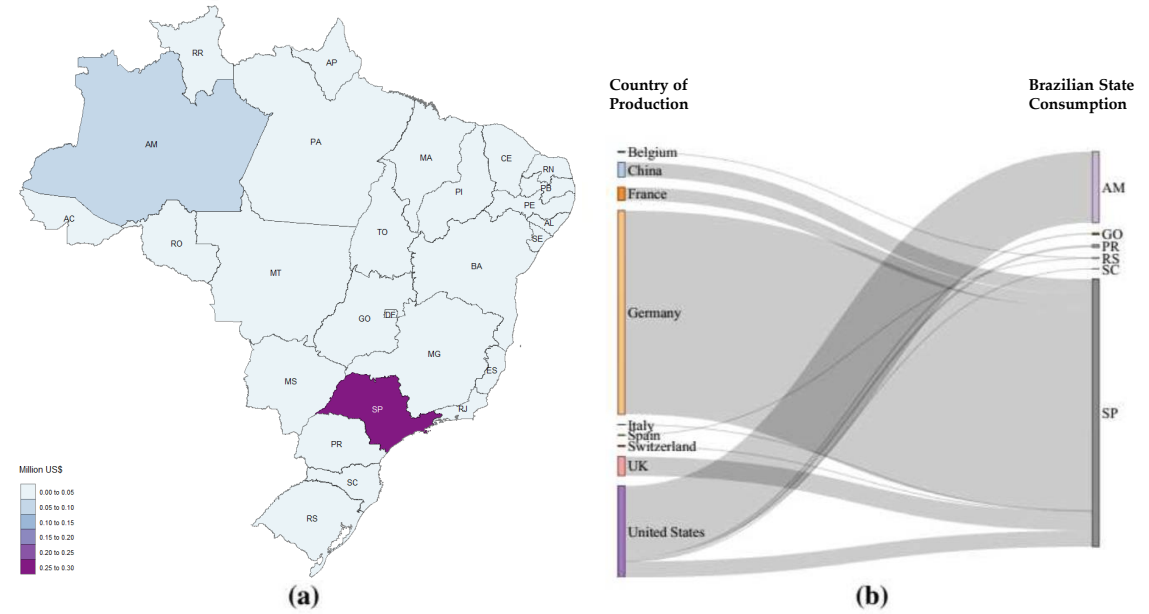

Figure 3.11: Acetaldehyde imports. (a) Local needs considering 2017; (b) Stratification for 2017, countries on the left represent the origin of the product studied and the states on the right represent the destination (AM - Amazonas, GO - Goiás, PR - Paraná, RS - Rio Grande do Sul, SC - Santa Catarina, SP - São Paulo).

Lastly, potential technologies can be assessed in São Paulo, Paraná, Rio Grande do Sul, Bahia and Santa Catarina States, where the demand is high and they are identified as favorable regions for developing CCU schemes. It also portrays and evaluates the commercial movement of Brazil with the other nations of the world, encompassing sales and purchases made externally

São Paulo showed high availability and demand, therefore it is indicated as location for implementation of CDU schemes.

3.4 Conclusion

The proposed method was robust for selecting the most promising products for CO_2 conversion. The concern regarding CO_2 emissions from Brazilian power plants motivated their mapping, as well the performance of a local market analysis for potential products from CO_2 chemical conversion.

Methanol, polycarbonates, formic acid and acetaldehyde were the most promising products for implementation in Brazil. The research pointed out that the power plants of higher capacity and, consequently, the greatest CO_2 emitters, are present in São Paulo and Rio de Janeiro. São Paulo showed higher demand of the assessed products and also CO_2 availability, indicating the location where a new CDU plant could potentially be installed.

Most of the current CO_2 technologies are in the research and development phase and there are already several collaborative works among researchers, startups and corporations in Europe and North America indicating a great potential for similar activities in Brazil. This work will contribute to this development.

Chapter 4

Selection of Carbon Dioxide Utilization Technologies

The production of chemicals and fuels from carbon dioxide can lead to a sustainable low carbon pathway for the chemical industry. The use of carbon dioxide as feedstock poses a commercially challenge, which is to develop alternative raw materials at lower cost and also to lower manufacturing impacts. Many products can be developed from carbon dioxide as raw material through carboxylation or hydrogenation reactions. In CCU, a particular carbon dioxide utilization technology shows specific aspects for emission reduction potential, intrinsic thermodynamic restrictions and commercial maturity level. Each product brings some advantages and penalties, making it therefore important to define some criteria to evaluate and to choose the most attractive products. This chapter proposes an exploratory screening procedure to identify promising chemical targets to be produced from carbon dioxide conversion among a large number of candidates. The results of the evaluation demonstrate that dimethyl carbonate, acetic acid and dimethyl ether are promising products for further study. Such a procedure would accelerate the development into the chemical design process of novel CCU technologies.

Contents

4.1 Introduction

The 20^{th} century has witnessed growth beyond expectations in energy use along with remarkable progress in technology creation, besides intensifying business expansion of man-made materials. Figure 4.1 shows the world primary energy consumption (in Mtoe) during the period between 1965-2017 (historical data gathered from BP [136]). Furthermore, projections of energy consumption of five different studies were incorporated for the comparison level; all the projection trends demonstrate an increase in the primary consumption worldwide. However, due to the recent health and economic crisis, the consumption behavior can be severely affected, taking years to return to the previous numbers.

According to Bertran et al. [6], the issues of energy, environment, food and water can be faced with novel and more sustainable production systems. In this context, CO_2 utilization technologies seek to mitigate carbon emissions and to expand energy supply while using CO_2 as a useful commodity [7, 8]. In this way, CO_2 can be used as a carbon building block to manufacture chemicals, which represents a challenge to manufacture materials at a competitive cost with lower environmental impact.

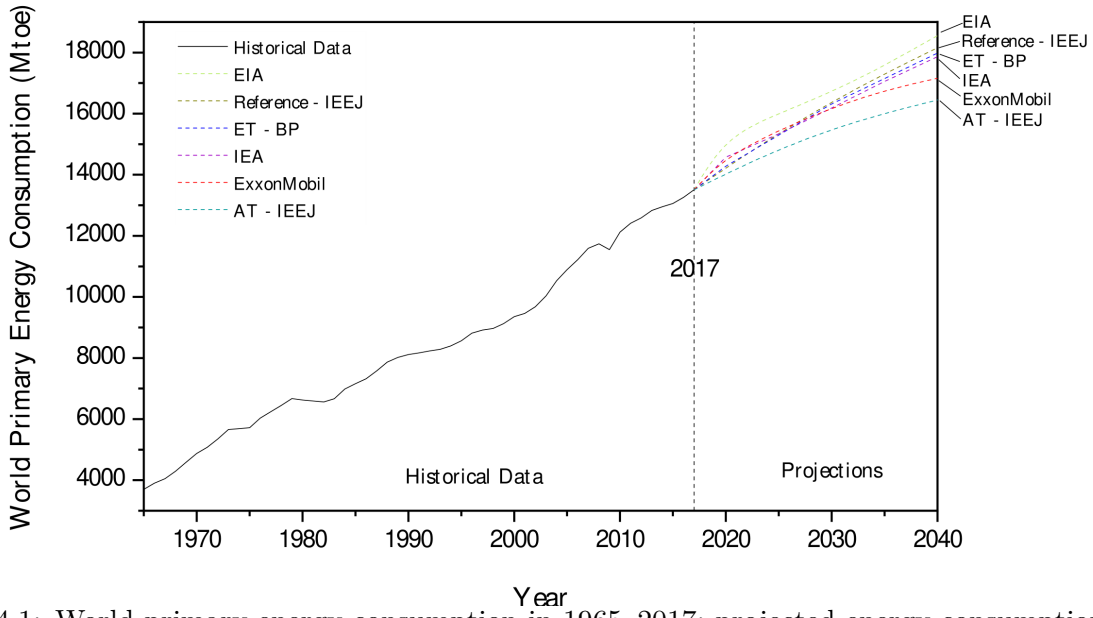

Figure 4.1: World primary energy consumption in 1965–2017; projected energy consumption up to 2040 (Source: Sections of [3, 5, 136–139]) EIA represents the Administration [137], IEEJ represents of Energy Economics Japan [139] where AT - IEEJ stands for Advanced Technologies Scenario, while Reference - IEEJ is the reference case, ET - BP is the abbreviation for Evolving Transition - British Petroleum from Economics [3], IEA represents the Agency [138] and ExxonMobil represents the report of ExxonMobil [5].

Groundbreaking changes will arise when using alternative feedstocks, for example, CO_2 or biomass. In the case of CO_2, it can be transferred to the existing chemical industry by means of basic chemicals (methanol, methane, carboxylic acids, etc.) or even as a potential C_1 building block. The contribution of CO_2 conversion goes beyond lowering global warming, since it also reduces fossil resource depletion, even yielding more benign production pathways [9].

A carbon-neutral chemical industry case analysis was conducted by Gabrielli et al. [140]. The authors found that the defossilization of the chemical industry can be achieved in a net-zero-CO_2 emission worldwide.

In a short-to-medium-term, the chemical conversion of CO_2 will expand notably in more developed fields, for example CO_2 hydrogenation, carboxylation and CO_2-containing polymers. Therefore, there is a need of researches on catalysts (carbon nanotubes based catalyst for tri-reforming [141] and dry reforming [142]), reactors (membrane reactors for tri-reforming [143]), separation processes (use of carbon nanoscrolls for CO2 filtering [144, 145]), unconventional energy sources (impacts of unconventional energy resources on the LNG sector [146]), and combinations of processes (resource- and energy-efficient chemical and fuel production [23]).

Moreover, the current CO_2 market has great potential for expansion with new CO_2 applications in different sectors. One set of the alternatives for CO_2 conversion was studied by Chauvy et al. [43], who ranked CO_2 conversion products using a multistep method to select products from

mid-term deployment.

In this context, the problem of selecting alternatives emerges. Ranking, choice or sorting problems are convoluted decision problems that, associate with a large set of criteria, make the decision process more assertive. Frequently, there is a need of multiple criteria consideration [147].

According to Ishizaka and Nemery [148] the perfect or ideal option which fits the whole set of criteria usually does not occur. It is important, then, to compromise, where the Multiple Criteria Decision Analysis (MCDA) can potentially provide guidance and techniques for reaching a compromise solution.

MCDA deals with decision-making (**e.g.** evaluation and selection) over a range of alternatives and attributes. The broad application of MCDA, in areas such as economics, management, engineering and information technology, presents robustness (even when applied to different conditions or scenarios it is able to produce good quality and assertive results) [149].

In the environmental field, Taylan, Kaya and Demirbas [150] used MCDA to select a compressor, taking into account the type of compressor, carbon emission, waste heat recovery and their capacities. Zhang, Peng, Tian, Wang and Xie [151] selected the optimal green material for sustainability using MCDA techniques.

The evaluation of clean power generation in the Pacific Northwest was performed by Daim, Yates, Peng and Jimenez [152]. Wind and clean burning coal are the two technologies assessed. Akber, Thaheem and Arshad [153] conducted a life cycle sustainability assessment for electricity generation, including 20 sustainability indicators of seven electricity generation sources.

In the carbon dioxide utilization field, Dairanieh [103] proposed a method to assess CO_2-based products, with both economic and environmental criteria. Otto et al. [56] performed an initial assessment of 123 CO_2 conversion reactions identifying potential products for future technical exploration. Pacheco, Bresciani, Nascimento and Alves [154] employed two different MCDA methods for assessing CO_2-derived chemicals. In the study 10 indicators of 13 chemicals were evaluated specifically for the Brazilian market scenario.

Resting on the powerful aspects of the MCDA, this work aims to propose a methodological framework procedure for selecting the most promising CO_2-derived products, expanding the scope of previous articles [154], including more chemicals and more indicators or criteria for a more robust and assertive assessment.

4.2 Methods

The proposed procedure structure, as depicted in Figure 4.2, involves three major parts for selecting the most promising products for CO_2 chemical conversion. **Part I** is related to criteria availability and definitions (Section 4.2.1), **Part II** refers to the multi-criteria decision analysis tools (Section 4.2.2) and **Part III** is the application of the three-level assessment for CO_2-derived products selection (Section 4.2.3).

4.2.1 Part I - Definition of Criteria

The set of criteria to evaluate chemical products, which could be potentially produced from CO_2, were built after a systematic search in the literature, mainly in the Web of Science [155] and Scopus [156] databases.

The procedure was based on the approach proposed by Zimmermann *et al.* [113], which was used as a chronological baseline for the current study. The authors focused on techno-economic assessments, seeing that they are indicators treated as a starting point for industrial scale implementation. Additionally, environmental and social indicators were also covered.The investigation reported herein was carried out in September 2018, including all the records by that date.

Thus, the search was split into two periods, in order to better evaluate the evolution of studies concerning CO_2 utilization. They were refered to before November 2015 (1997 - 2015), which takes into account the chronological baseline paper [113], and after November 2015.

The investigation was carried out in September 2018, including all the records showed by that date. The search was split into periods, refered to *before November 2015* (1997 - 2015) and *after November 2015* (2015 - 2018).

All the articles were screened using the R package metagear ver. 0.4 (metagear, RRID: SCR_017085) [157]. Based on the definition of CO_2 utilization presented by Zimmermann *et al.* [113]:

> "A range of technologies that consume CO_2 chemically or non-chemically to provide products or services with the main objective of an economic benefit, ideally with additional environmental and social benefits."

4.2.2 Part II - Multi-Criteria Decision Analysis Tools

To make decisions (evaluation or selection) over a list of alternatives characterized by multiple, usually conflicting, attributes one can use MCDA techniques. The literature concerning MCDA contemplates an extensive number of methods with different schools of thought [158]. In

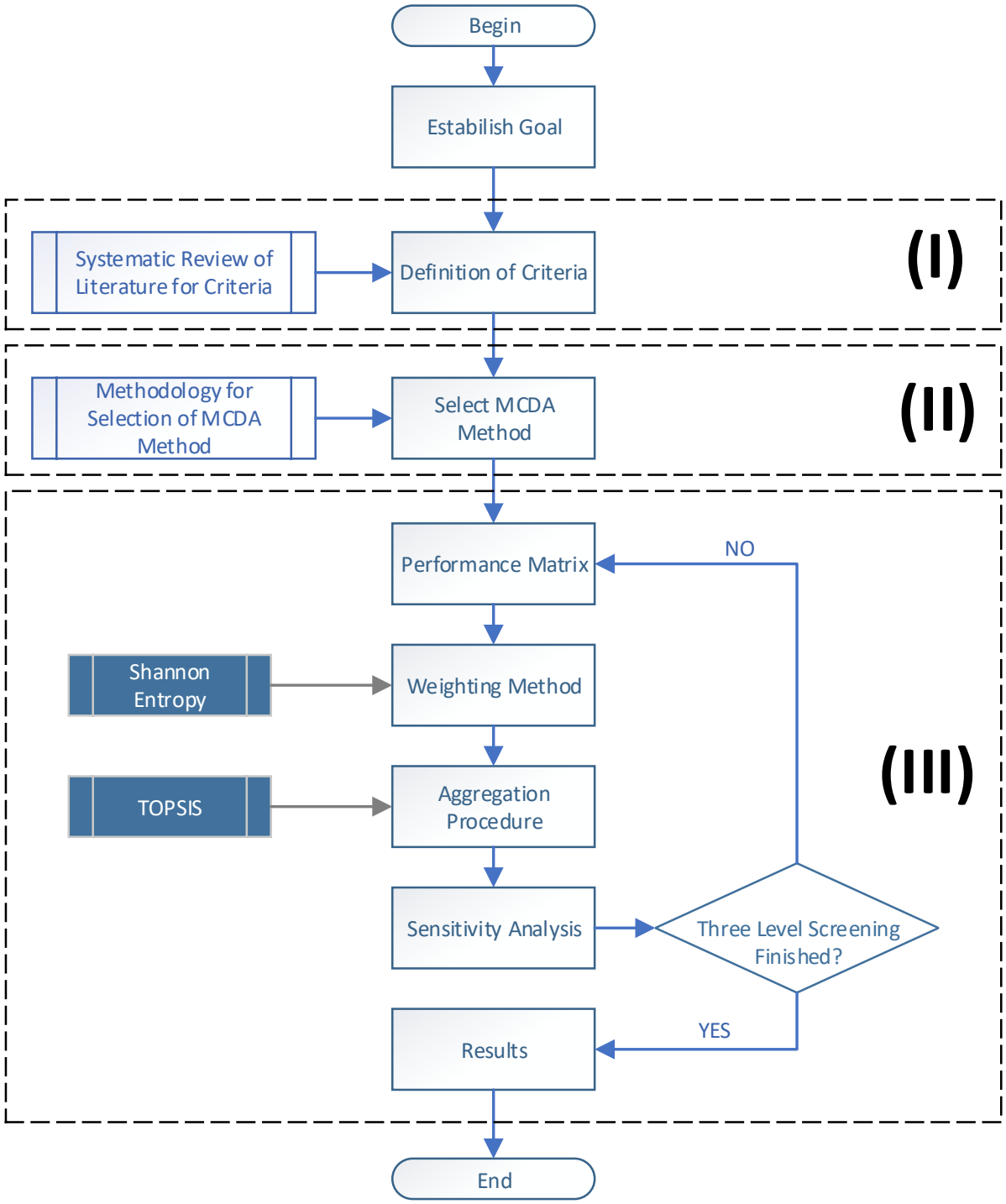

Figure 4.2: Methodology Structure used in the study. Part I is related with the available criteria, Part II refers to the MCDA tools and Part III is the three-level assessment for CO_2 derived products.

accordance with Saaty [159], there are more than 100 methods, among which the most commonly implemented are Analytic Hierarchy Process (AHP) [104], Preference Ranking Organization Method for Enrichment Evaluations (PROMETHEE)) [105], Technique for Order Preference by Similarity to an Ideal Solution (TOPSIS) [106], ELimination Et Choix Traduisant la REalité (ELECTRE) [160], Multi-Attribute Utility Theory (MAUT) [161], Analytic Network Process (ANP) [159].

Guarini, Battisti and Chiovitti [162] pointed out that no multi-criteria decision analysis method or tool can be considered perfect or applied to every situation. Thus, they proposed a theoretical-methodological approach to select the most appropriate MCDA method.

The approach formulates a taxonomy of the exogenous and endogenous variables, the exogenous variables are strictly related to the decision problem and the context from which they arise named: the number of evaluation alternatives, the typology of the criteria and expected solution, and the presence of technical support for computer aided tool implementation. The endogenous variables are related to the properties of MCDA methods, named: the type of decision-making problem, the solution approach and the implementation procedure.

The use of the theoretical-methodological approach from Guarini *et al.* [162] results in the indication of the MCDA method that best corresponds to the issues of the decision-making problem under assessment (**i.e.** in this case the screening carbon dioxide conversion products). Therefore, the theoretical-methodological approach was used.

4.2.3 Part III - Three-level screening

The MCDA method selected in Part II was used throughout the study in Part III. Typically, the MCDA method itself is divided into two phases. The first is the performance matrix construction, containing alternatives and criteria, accompanied by their weightings. In the second phase process, data, based on the objective previously defined, is aggregated. The procedure for aggregation depends on which method is under use [163].

4.2.3.1 Weighting Measure

To select an appropriate weighting method, the characteristics and the type of problem must be taken into account. The variance degree and the Independence of criteria and the preference of the decision maker are the factors considered to attain the weights [164].

The importance of the criteria is a major concept in MCDA. There are many methods for eliciting weights, which can be bisected into two group categories: subjective and objective weights. Subjective weights are determined based on the preference of the decision-maker or experts in the field (**e.g.** AHP method [104], weighted least squares method [124], Delphi

method [125] and equal weights). Objective methods, on the other hand, determine weights by solving mathematical models and do not account for the decision-maker preference (**e.g.** Shannon entropy method [126, 127] and multiple objective programming [128]).

In this work, the elicitation of criteria weights were obtained by objective weighting of Shannon entropy. It measures the predicted value of the information contained in a message, usually in units of bits, nats or bans. The value is the average unpredictability in a random variable, equivalent to its information essence. In the MCDA context, the entropy method is an objective method to assign weights depending on the decision matrix [127]. The relative weight of criterion j is calculated in relation to the amount of information supplied by the intrinsic set of alternatives.

The closer the entropy of a criterion is to 1, the less important the criterion is. Shannon entropy measures the amount of uncertainty with a probability distribution in terms of entropy taking into account the complete set of information available.

4.2.3.2 Sensitivity Analysis

The complex nature of the decision making, specially for the selection of carbon dioxide conversion products, is inevitably associated with a variety of uncertainties. They can be, mainly, caused by the criteria, the weights and priorities. These uncertainties can be evaluated through a sensitivity analysis

According to Broekhuizen et al. [165], evaluating the sources of uncertainty, their magnitude and how they eventually lead to a different result is needed to account for the uncertainty.

Chen et al. [166] reported that several factors affect the output of a MCDA, being the weights of criteria a notable one. Multiple weighting schemes can be exploited to verify if changes in weight vector lead to distinctive results. Moreover, the number of criteria and alternatives could influence the stability of the analysis; the Monte Carlo procedure was hence used to test the robustness of the MCDA. It was assumed that criteria weights aggregates are obtained from variables randomly drawn from a uniform distribution.

The sensitivity analysis was carried out using Monte Carlo Simulation to simulate a 15% variability in weights. The base value of a given criterion (calculated from Shannon Entropy) was, then, aggregate (using the Equation 4.2.1) with an aggregator, λ, whose value was obtained from a random uniform distribution sampling).

$$w_i^{'} = \frac{\lambda_i \cdot w_i}{\sum_i^N \lambda_i \cdot w_i} \tag{4.2.1}$$

This procedure is applied to each criterion and the aggregate weights were used in the TOPSIS

calculation. The results for 5000 runs were displayed as a score distribution for every chemical product. For the Monte Carlo Sensitivity Analysis, the software MATLAB R2015a was used.

4.3 Results and Discussion

4.3.1 Systematic Search and Criteria Selection

The search was split into periods, refered as *before November 2015* (1997 - 2015) and *after November 2015* (2015 - 2018). The former resulted in 140 unique publications (excluding 39 duplicates), while the latter resulted in 139 unique publications (excluding 52 duplicates) from the Web of Science database. The Scopus database showed 153 unique publications (excluding 9 duplicates) for the whole period (from 1978, the first publication, to 2018).

After a thorough scanning of the publication, 27 articles were selected (14 from the Web of Science, 4 from Scopus, non-duplicated, and 9 other publications included due to their similarity with the topic, which fulfilled the definition). Table 4.1 presents the final literature set used for selecting the criteria for further study.

Table 4.1: Literature set of publications under assessment (search from November 2018).

Nr.	Ref.	WoS	Scopus	Other	Nr.	Ref.	WoS	Scopus	Other
1	[167]	x			15	[168]	x		
2	[169]	x			17	[170]			x
3	[24]	x	x		16	[171]		x	
4	[172]			x	18	[173]	x	x	
5	[174]	x			19	[175]	x		
6	[176]	x	x		20	[177]		x	
7	[178]		x		21	[103]			x
8	[179]			x	22	[180]	x	x	
9	[181]	x	x		23	[99]	x	x	
10	[182]			x	24	[34]	x		
11	[183]			x	25	[184]			x
12	[185]		x		26	[186]	x		
13	[187]	x	x		27	[188]			x
14	[189]			x					

In order to compare the development of the studies concerning CO_2 utilization, the results were compared with the literature selected by Zimmermann *et al.* [113].

The authors selected 29 different articles to study which criteria to include. Figure 4.3 depicts

the evolution of criteria in literature, comparing the criteria found in articles from Table 4.1 (2015-2018) with criteria found in articles from Zimmermann *et al.* [113] (1997-2015). Four broad themes emerged from the analysis: technical, economic,environmental and social.

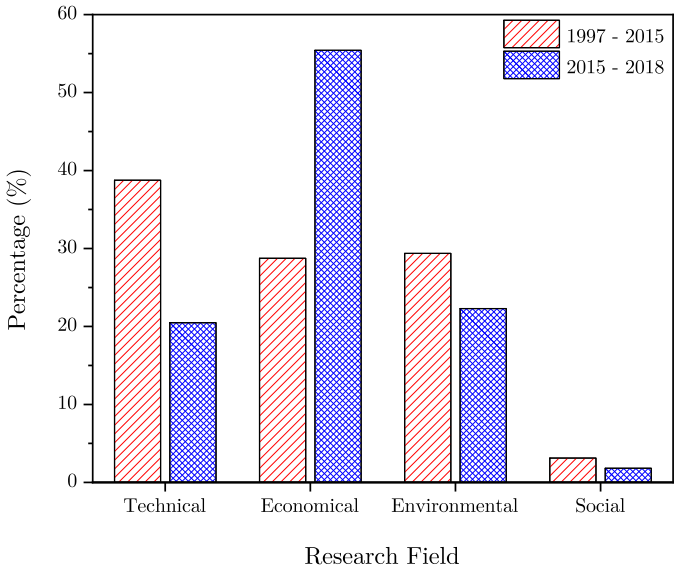

Figure 4.3: Evolution of Criteria in Literature.

Just over half the sample criteria (55%) fit in the economic criteria in the period from 2015 to 2018, compared with 29% from 1997 - 2015. The social criteria remained at low levels (below 3%).

A variety of perspectives were expressed within the articles published, many of the articles study the conversion process in detail; however, for early stage selections this approach was not suitable due to the lack of information. A number of issues were identified, among which ambiguous criteria, which could potentially be allocated in the economic or environmental research field, leading to a reduction or increment in the importance of the economic or environmental aspects.

These data must be interpreted with caution because the evaluation performed herein may differ from the study by Zimmermann *et al.* [113].

Reliability, appropriateness, practicality and limitations of measurement are parameters used to select the criteria, according to Wang *et al.* [164].

Usually, there are principles that must be met to select the 'major' criteria [164]. Systemic, consistency, independency, measurability and comparability principles guide the criteria selection. The authors pointed out that some 'minor' criteria could be chosen to construct a reasonable criteria system. The eligibility criteria required criterion candidates that met the aforementioned principles. After the application of the principles, the final criteria system contains seven major topics, as presented in Table 4.2.

Table 4.2: Final criteria system for CO_2 conversion selection based on the methodological framework.

Major Topic	**Description**
Thermodynamic-related	Basic thermodynamic properties of the reactants and products, Gibbs energy of formation and enthalpy of reaction. They can estimate the amount of energy inputs required
Scientific Relevance	It can differentiate rare application chemicals from diverse application chemicals
Economic-related	Product market (price, demand, value, growth). Price of the reactants can also be taken into account
Technical Readiness Level	It is a measurement system that determines the maturity of a specific technology
Utilization of CO_2 or CO_2 Ratio	It measures the amount of CO_2 fixed in a molecule on mass basis.
Affordability to produce a unique chemical	It represents the unit cost/price point of CO_2 supply at which the product is competitive
Innovation and novelty	It takes into account the novelty of process and products

The thermodynamic-related criteria were described in detail in Chapter 2. Scientific relevance was introduced by Otto et al. [56], defined as the number of related references of a certain chemical (SCI-Finder database). In the economic-related criteria, the estimation of price (either for product or reactant) is described in detail in the Appendix. The method used for the estimation was proposed by Hart and Sommerfeld [190]. The compound annual growth rate and the market size data were collected from the literature (see Appendix).

Technical Readiness Level (TRL) (proposed by NASA [110]) assessment refers to the innovative route for each product, not the conventional one, ranges from basic and applied research, proof of concept and laboratory testing (stages 1-3, receiving score 1), to prototyping, piloting and final development (stages 4-7, receiving score 2), to full- scale deployment/market introduction (stages 8-9, receiving score 3). An overview of the set of compounds and their technological path can be found in international reports [14, 111], which are used to assign TRL to each chemical.

Utilization of CO_2 or CO_2 ratio takes into consideration the mass of carbon dioxide, the mass of product and their respective stoichiometric coefficient (CO_2 and reference product). Affordability to produce a unique chemical or the willingness to pay was proposed by Dairanieh [103] to evaluate CO_2 products. Despite based on the economics of the target market, willingness to pay is set in the environmental group because it represents the unit cost/price point of CO_2 supply at which the product is competitive for that use (\$/tonne of CO_2).

Lastly, the innovation and novelty criteria contemplate literature, patent and reaction-related aspects. A Boolean search was executed in the online Web of Science database [155] for the first criterion. The investigation was carried out in March 2019, including all the records shown by that date.

The criteria system was accordingly used in the three-level assessment to screen the most promising products. Data availability was used to set which criteria could be used in each level.

4.3.2 Electing the MCDA method

The theoretical-methodological approach by Guarini *et al.* [162] was used to select the MCDA Tool as described in **Part II** of the methodological framework proposed herein. The approach takes into consideration the endogenous and exogenous variables, which sum up to 38 variables. The procedure was applied in the three-level assessment and the results are shown in Figure 4.4.

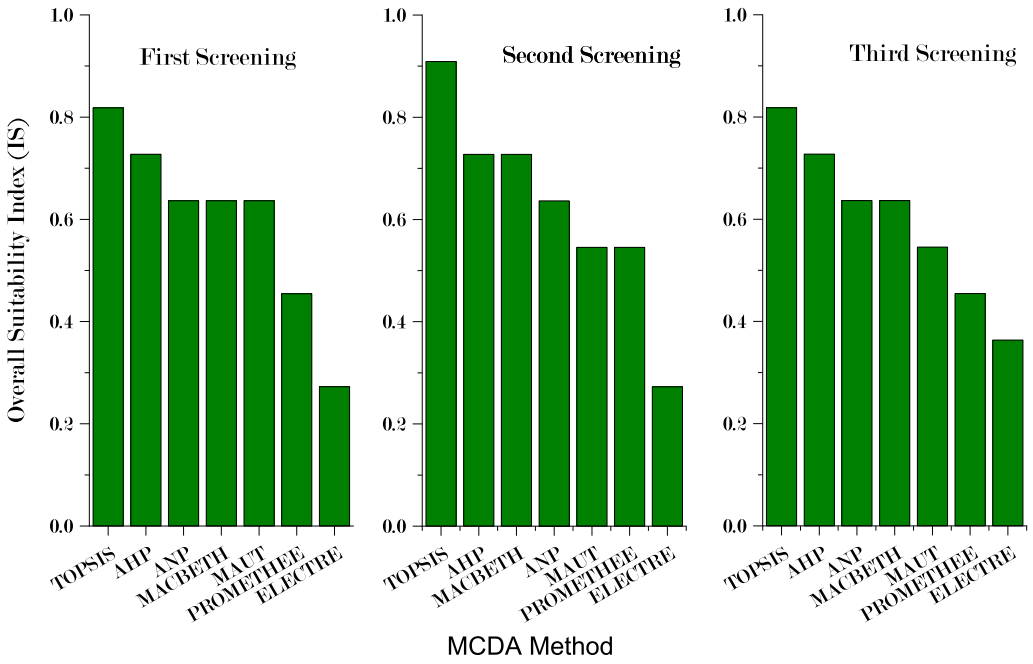

Figure 4.4: The order of potential MCDA methods to select the most promising chemical products from CO_2 conversion.

After the application of the procedure, TOPSIS was identified as the best adapted to the selection of chemicals from CO_2 conversion.

The order for the overall suitability index obtained for each MCDA identifies TOPSIS as best performing tool. For the first screening, TOPSIS obtained 0.818 for overall suitability index, AHP, the value of 0.727 and ANP, the value of 0.636. This represents 8 out of 10 properties consistent with the expected qualification. For the second screening and third screening, TOPSIS achieved a value of 0.909 and 0.818, respectively.

The result can be partially explained by the selection of qualifications for the exogenous variables (**e.g.** mixed indicators, no technical support for a specialist and the number of evaluation elements) and for the endogenous variables (**e.g.** the type of decision-making problem is a rank and implementation procedure).

The TOPSIS method designates alternatives that simultaneously have the shortest distance from the positive ideal solution (maximization of benefit criteria) and the farthest distance from the negative-ideal solution (maximization of cost criteria). More details about the method can be found in the work by Hwang *et al.* [107].

4.3.3 Three Level Assessment

In the context of selecting the most promising products for CO_2, the three-level assessment has been proposed. The first screening evaluates only thermodynamic properties and, consequently, the economic aspect of such reactions, along with their respective scientific relevance. The second screening evaluates economic, technical and environmental aspects. Lastly, the third screening takes into account the innovation and novelty of the products and processes. The distribution of these specific criteria at each level takes into account the data available for the chemical compounds under evaluation.

The option of using CO_2 for chemical conversion has thermodynamic and intrinsic kinetic restrictions. Estimating their real potential will require a thorough comparative analysis of proposed and existing processes to determine whether or not the proposed conceptual plant reduces CO_2 emissions (directly or indirectly), and whether the chemicals obtained are tradable [11].

4.3.3.1 First Screening Results

A dataset of 122 chemical compounds was selected based on the work by Otto et al. [56]. The criteria evaluated in the first screening include the Gibbs energy of formation, the enthalpy of reaction and scientific relevance (gathered in October and November 2018).

The results from the preliminary analysis of the scientific relevance raw data showed several outliers, with a median value of 392 and an amplitude of 421305. A clear benefit of normalizing the values is avoiding the influence of extreme values in the final result of MCDA. Therefore, the data were normalized, the median was 50 and an amplitude of 90 was obtained. The normalization procedure also correct kurtosis (value of -1.041, std error = 0.435) and skewness (value of 0.173, std error = 0.219).

A standard feature of multi-criteria analysis is a performance matrix, in which each row describes an alternative and each column describes one criterion. The performance matrix for the first

assessment is presented in the Supplementary Material. Table 4.3 presents the results of the Shannon Entropy applied to the first screening performance matrix.

Table 4.3: Shannon Entropy Weights results for the First Screening.

Criteria (i)	**Type**	**Min/Max**	**Entropy** (E_i)	**Weight** (w_i)
ΔG_f^o (kcal/mol)	cost	MIN	0.993	0.087
ΔH_{rxn}^o (kcal/mol)	cost	MIN	0.985	0.179
Scientific Rel. (–)	benefit	MAX	0.940	0.733

The results values for Entropy (E) closer to 1 for the ΔG_f^o and ΔH_{rxn}^o indicate minor importance compared with Scientific Relevance. The weights for the three criteria are also indicated in Table 4.3; the first two criteria showed similar weights, while the last presented significant importance.

The TOPSIS method was employed to evaluate the alternatives, Shannon Entropy was used as a weighting method. The results are introduced in Figure 4.5a, which depicts the 30 first places. In order to assess the influence of weights in the final outcome, a Monte Carlo analysis was performed (Figure 4.5b).

With respect to the first screening, it was found that methane, propanol and propionic acid achieved the highest scores, followed by propylene carbonate, ethylene carbonate and methanol. These results may partly be explained by the favorable products in terms of thermodynamics and also a sufficient amount of related scientific research.

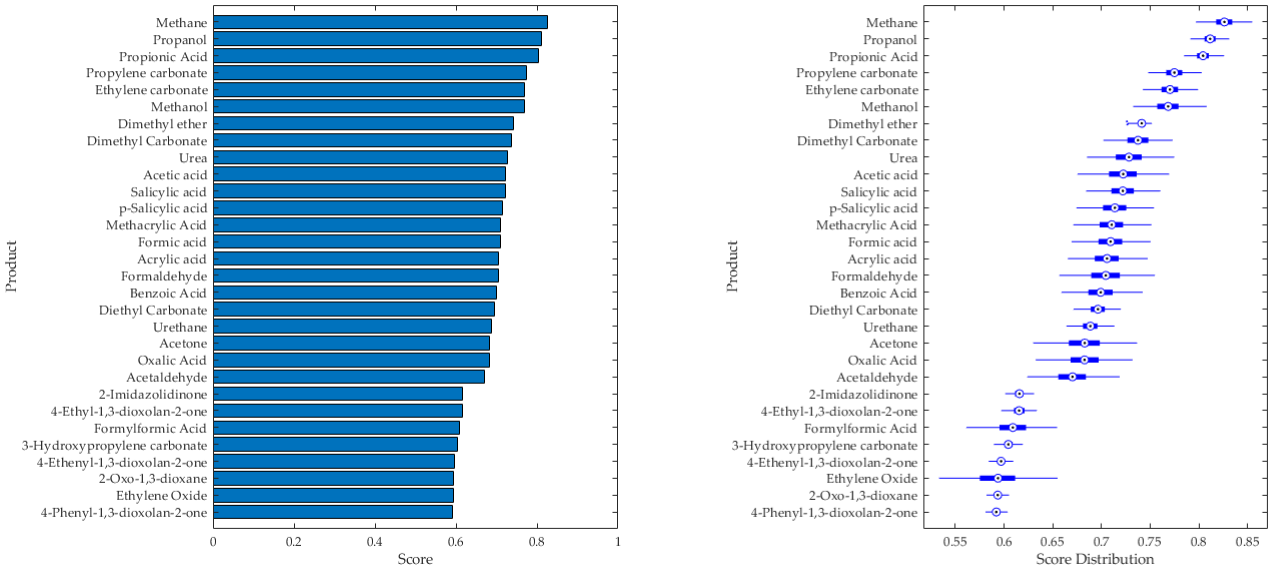

(a) (b)

Figure 4.5: Results for the first screening (30 first places). (a) Score and (b) Distribution.

The first block of 22 chemicals was selected for the second screening since the mean of the groups are significantly different (ANOVA test F=36553.7 and p-value=0). Additionally, there is a 8.10% difference between the mean of acetaldehyde compared with 2-Imidazolidinone.

4.3.3.2 Second Screening Results

The chemical compounds selected in the first screening were further assessed based on technical, economic and environmental aspects as presented in Figure 4.6. They represent investment for decision-makers (**e.g.** government, investors), but they can also be used as a base for innovative research.

For the economic group, four criteria were selected: Product Price, Reactant Price, Market Size and Compound Average Growth Rate (CAGR). For the technical group, the TRL was selected. The environmental group contains the utilization ratio and the willingness to pay criteria.

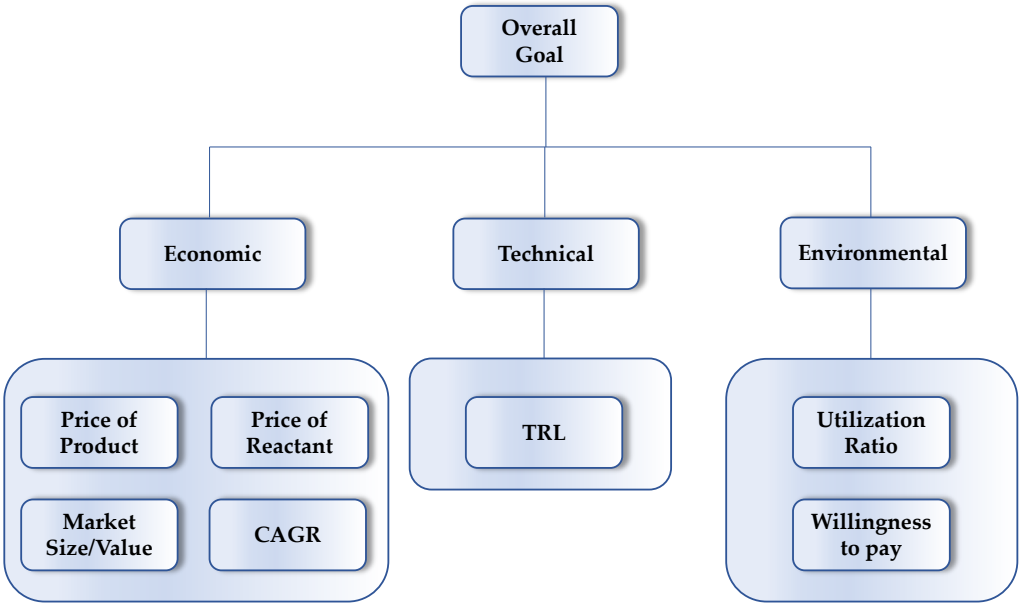

Figure 4.6: Criteria evaluated for the second screening analysis.

The final performance matrix for the second screening is presented in Table 4.4. The results indicate that dimethyl carbonate, dimethyl ether and p-salycilic acid are the most expensive products, whereas urea, methane and methanol are the cheapest products. However, methanol, urea and acetic acid showed the highest values for market value. The CAGR for methanol, dimethyl ether and acetic acid are the most expressive in the evaluated period.

The maturity level of most of CO_2 products are low, due to the early stages of research and development. Some products reached higher levels (for example, methanol and urea). Regarding

the utilization ratio, methane, dimethyl ether and formaldehyde presented the highest values. Lastly, in the criterion Willingness to Pay (WP), it is possible to identify two groups of chemicals.

Table 4.4: Decision matrix for the second assessment for CO_2 products.

Products	Economic Criteria				Technical Criteria	Environmental Criteria	
	Product Price (US$/kg)	Reactant Price (US$/kg)	Market Value (0-100)	CAGR (%)	TRL (–)	Utilization Ratio ($kg_{CO_2}/kg_{prod.}$)	WP (US$/tonne$_{CO_2}$)
Propionic Acid	3.51	6.65	60	3.0	1	0.594	225
Propanol	1.45	6.65	60	2.2	1	0.732	225
Methane	0.34	6.00	80	1.6	2	2.743	10
Propylene carbonate	0.68	1.02	70	6.2	1	0.431	225
Ethylene carbonate	4.76	0.80	30	5.2	1	0.500	225
Methanol	0.48	6.00	100	11.0	3	1.374	28
Dimethyl Carbonate	6.52	0.48	40	6.6	3	0.489	225
Dimethyl ether	6.43	6.00	30	9.9	1	1.911	225
Salicylic acid	4.69	3.04	30	5.5	2	0.319	225
Urea	0.30	0.33	90	2.0	3	0.733	10
Acetic acid	0.95	0.34	80	9.0	1	0.733	225
p-Salicylic acid	5.99	2.68	1	5.2	1	0.319	225
Methacrylic Acid	1.77	0.71	1	3.4	1	0.511	225
Diethyl Carbonate	2.80	0.67	20	2.4	1	0.373	225
Formic acid	0.74	6.00	30	2.5	2	0.956	225
Acrylic acid	2.25	0.65	80	7.6	1	0.611	225
Benzoic Acid	3.48	0.76	60	3.6	1	0.360	225
Formaldehyde	1.35	6.00	80	4.8	1	1.466	225
Urethane	5.71	1.00	1	2.0	1	0.494	225
Oxalic Acid	2.67	6.00	50	4.6	1	0.978	225
Acetone	1.23	0.34	70	3.6	1	0.758	225
Acetaldehyde	2.70	6.34	60	6.0	1	0.999	225

The calculation of weights for the criteria using Shannon Entropy was performed and the results are presented in Table 4.5.

Table 4.5: Shannon Entropy Weights results for the Second Screening.

Criteria (i)	**Type**	**Min/Max**	**Entropy** (E_i)	**Weight** (w_i)
Price Product (US$/kg)	benefit	MAX	0.879	0.113
Price Reactant (US$/kg)	cost	MIN	0.883	0.110
Market Value (–)	benefit	MAX	0.925	0.070
CAGR (%)	benefit	MAX	0.896	0.098
TRL	benefit	MAX	0.561	0.413
Utilization Ratio	benefit	MAX	0.834	0.156
WP	benefit	MAX	0.958	0.040

The relative importance of a criterion is defined by its entropy and, consequently, its weight. The criterion with less relative importance was WP ($E = 0.958$, $w = 0.04$), followed by Market value and CAGR. The TRL achieved the highest importance ($E = 0.561$, $w = 0.413$). These differences can partly be explained by the diversity of the data, which is inherently considered in the weighting method used. The only criterion that must be minimized is the price of reactants.

Price of product, price of reactant market size and CAGR showed similar ranges. TRL showed a broad distribution, due to the possible values for this criterion (1, 2 or 3). Most of the technologies are in their early stage of development (1) and just a few are commercially mature (3).

The weights calculated in Table 4.5, together with the data in Table 4.4, were used to assess the products. The TOPSIS method was used and the results are displayed in Figure 4.7a. To test how the weights could potentially influence the results, a sensitivity analysis was performed (Figure 4.7b).

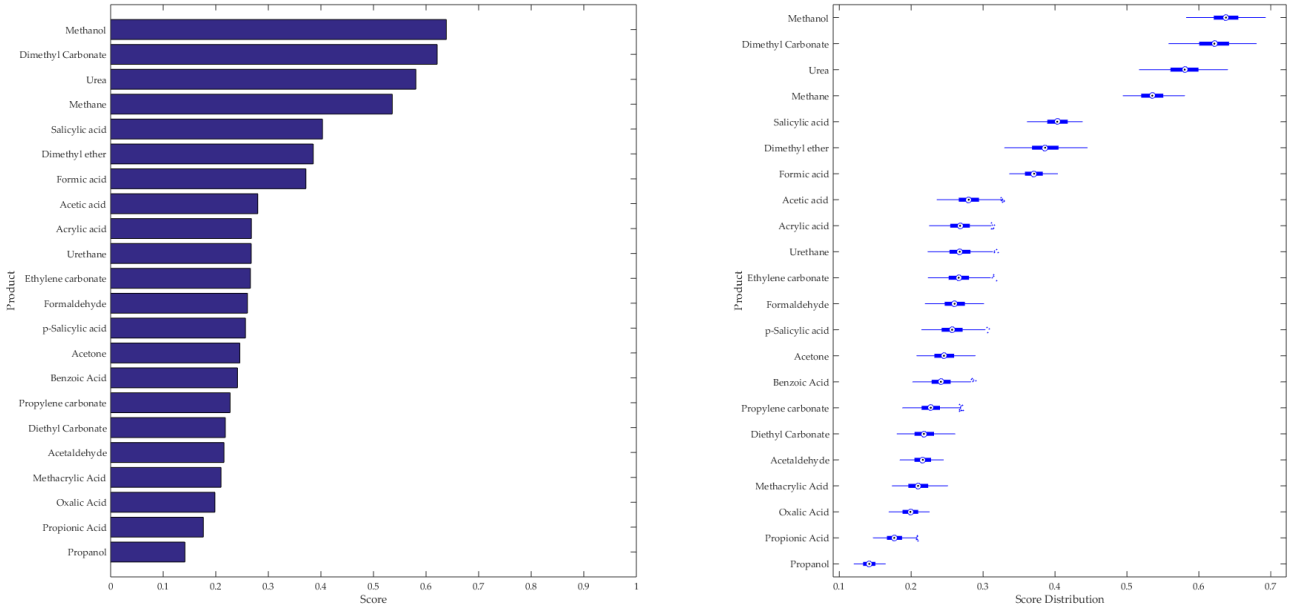

(a) (b)

Figure 4.7: Results for the second screening. (a) Score and (b) Distribution.

The TOPSIS method was applied to determine the rank of the most promising products for CO_2 conversion. It calculates the 'alternative' relative closeness to the ideal solution, ending with the Rank Preference Order for the alternative.

As can be seen from Figure 4.7a, the evaluation ranks methanol (score = 0.6386), dimethyl carbonate (score = 0.6212) and urea (score = 0.5807) in the first three positions. Followed by methane, salicylic acid, dimethyl ether, formic acid and acetic acid.

The comparison of these findings with those from of other studies [56, 184, 191] confirms methanol, urea and dimethyl ether as promising products.

The ANOVA-one way was carried out to evaluate the score distribution and to select the products included in the next screening. At the moment, a chemical product presents a score distribution with no difference in means, that is, the cut-off.

Using the data from Figure 4.7b, the chemicals in the positions 1 to 8 presented significant different means and the chemical in position 8 is included. Comparing the chemicals in positions 8 and 9, they are significantly different (F=1497.08, 380 p-value=0); however, the chemical in position 9 compared to 10 presents significant equal means (F=3.0823, p-value=0.0792). Therefore, the cut-off is the chemical in position 8 and, the chemicals from positions 9 to 22 are out of the third screening.

4.3.3.3 Third Screening Results

The final screening takes into account the novelty of the processes and products. It comprises eight chemicals, selected in the second screening, namely methanol, dimethyl carbonate, urea, methane, salicylic acid, dimethyl ether, formic acid and acetic acid.

The innovation and novelty topic (see Table 4.2) is investigated in the third screening. To contemplate different aspects, three criteria were analyzed: (i) Web of Science (WoS) Boolean Search (Literature-related), (ii) Derwent Innovations Index (DII) Boolean Search (Patent-related) and (iii) SciFinder Reaction Search.

The results for the WoS were normalized, using the natural logarithm function. The SciFinder web application allows the user to create a reaction and search for entries. Therefore, the number of entries for the reaction (not the CAS number) was retrieved and normalized using the natural logarithm function. The results are in the performance matrix presented in Table 4.6.

Table 4.6: Decision Matrix for the Third Assessment for CO_2 products.

Chemical Name	Literature - WoS	Patent - DII	Reaction - Scifinder
Methane	9.21	781	6.54
Dimethyl Carbonate	6.72	19	6.35
Methanol	8.85	683	7.18
Salicylic acid	6.48	31	8.19
Acetic acid	7.19	75	5.89
Urea	7.82	236	5.05
Dimethyl ether	6.75	117	5.27
Formic acid	7.13	46	11.19

It is possible to verify that concerning the literature, methane leads by number of related publications. The second place belongs to methanol, with more than 3000 publications, fewer than the first position, representing almost 45%. Following the list, urea comes up with 2490 publications.

Nonetheless, the smaller the number of publications, the better, because more room for innovation and novelty is possible. In this sense, salicylic acid and dimethyl carbonate showed the smallest number.

Regarding patents, dimethyl carbonate, salicylic acid, formic acid and acetic acid represent the alternatives with the fewest patents. Finally, the reaction database criterion is favorable for urea, dimethyl ether, acetic acid and dimethyl carbonate.

The relative weights for all the three criteria were calculated using the Shannon Entropy, presented in Table 4.7.

Table 4.7: Shannon Entropy Weights results for the Third Screening.

Criteria (i)	**Type**	**Min/Max**	**Entropy** (E_i)	**Weight** (w_i)
ln(WoSA)	cost	MIN	0.888	0.378
DII	cost	MIN	0.892	0.367
ln(Scifinder)	cost	MIN	0.925	0.255

The normalized weight for literature-related (WoS) was the highest; consequently, entropy is the smallest. Moreover, the relative importance of patent-related (DII) is similar to literature-related. The range of distribution regarding the literature-related and reaction-related are similar, while the patent-related showed a broader range of distribution.

TOPSIS was used to calculate the rank preference for the ideal solution. The results are presented in Figure 4.8a. To address the influence of weights in the final result, a sensitivity analysis was carried out. Figure 4.8b demonstrates the results.

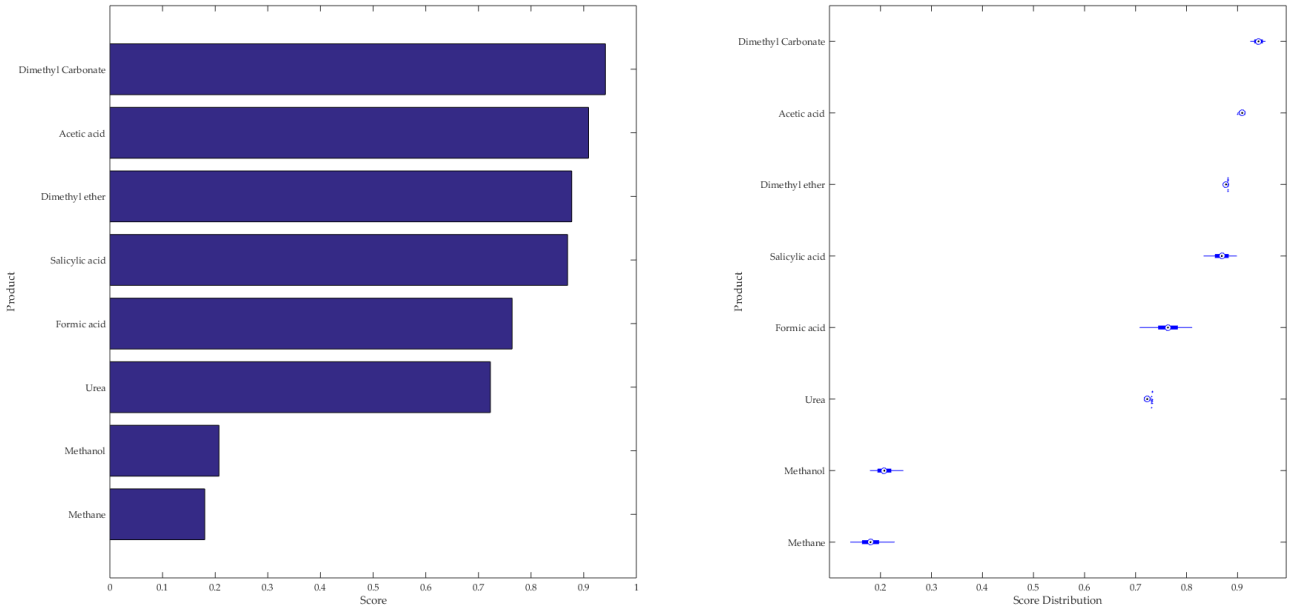

(a) (b)

Figure 4.8: Results for the third screening. (a) Score and (b) Distribution.

The first three products were dimethyl carbonate, acetic acid and dimethyl ether, which are the most promising products for further studies on chemical process synthesis and design.

Salicylic acid and formic acid showed the broader distribution compared with the other chemicals. Note that the final products ranking were the same, compared with the single value score.

One point must be highlighted; different multi-criteria methods, when applied to the same problem, can lead to different scenario results, even using similar data for analysis. The CO_2 conversion schemes require great investment and they are also attached with uncertainties (**e.g.** scaled up for commercialization), therefore, these results should be taken with caution.

4.4 Conclusion

The evaluation of CCU technologies to identify promising products among a broad number of candidates is a recurrent issue. In this sense, this study performed a systematic search to define suitable criteria in the context of carbon dioxide conversion and applied them to a three-level assessment for selecting CO_2 conversion products. The TOPSIS method was selected as the most adequate MCDA tool based on the objective.

The proposed methodological framework is an important tool for selecting the most promising products for CO_2 conversion by the three-level assessment. A multi-criteria decision analysis method was used jointly with an objective elicitation of weights. Dimethyl carbonate, dimethyl ether and acetic acid were the most favorable products for rigorous process design studies. This study can also accommodate variation in prices, maturity level or scientific relevance of the evaluated products.

This study may serve as guidance for further researches in chemicals synthesis, from the catalyst development point of view, new products should be created in order to overcome the limitations imposed by the CO_2 system. From the process modeling (see Chapter 5) and reactor calculation perspective, new design configurations studies can be proposed based on the current study.

Chapter 5

Process Design and Simulation of Acetic Acid Production from Carbon Dioxide

The outcomes of Chapter 4 pointed out several products for further investigation and studies. This chapter presents an assessment of one of that products, the acetic acid process. Efforts have been focused on exploring new methods to produce acetic acid using carbon dioxide as a raw material, aiming is to replace fossil-based raw materials with CO_2, offering a sustainable and low-carbon pathway for the chemical industry. The objective is to assess routes using MCDA. Viable CO_2 routes was identified, compared based on criteria like chemical utilization, energy consumption, and Gibbs energy, and a conceptual plant design was proposed. The methanol hydrocarboxylation route was found to be the most suitable option, and a hierarchical approach was employed in designing the process, demonstrating its feasibility and similarities to conventional production.

Contents

5.1 Introduction

Acetic acid is an important industrial chemical used in a wide range of applications, including food production, pharmaceuticals, and biorefining. In glacial form (less than 1.0% of water content), it can be used to manufacture vinyl acetate, with a market share of 34% in 2016, as well as acetic anhydride (13%) and chloroacetic acid, and be applied as a solvent for terephthalic acid (24%) [192]. The main producers, responsible for over 70% of the world's production capacity, are installed in Asia, where China accounts for 54% of this total, and North America, mainly the United States, with 18%. This economic performance projects a future revenue for this commodity of USD 12.8 billion [193].

Vinyl acetate has been employed in latex emulsion resins in a variety of applications (**e.g.** paper coating, adhesives, textile treatment and paints), accounting for more than 30% of the total market in terms of volume [194]. Acetic anhydride is a acetylation agent, which is used to synthesize cellulose acetate and cellulose plastics [195]. Acetic acid is, therefore, an important industrial chemical.

According to the Mordor Intelligence Report [196], the global market is expected to reach 18.29 Mton by 2023. Figure 5.1 presents the global demand for acetic acid and the projections for this market.

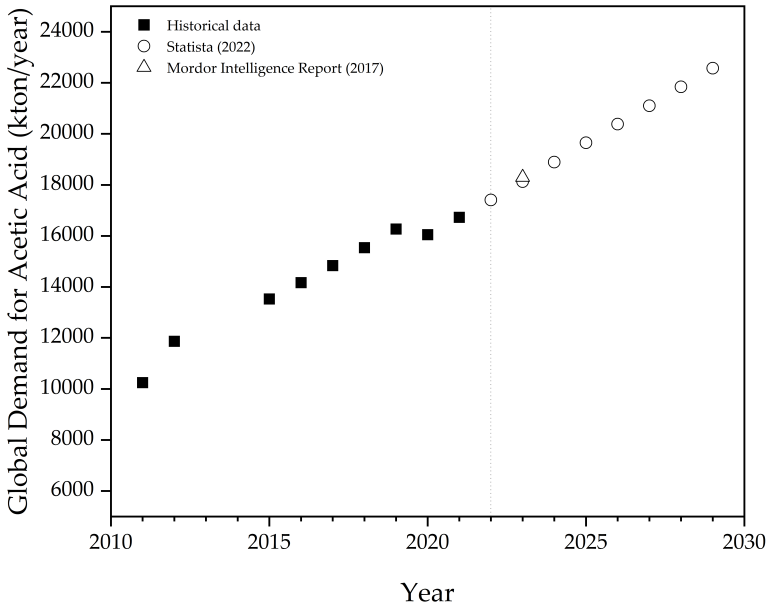

Figure 5.1: Global demand for Acetic Acid. Historical data from [197–199] . Projections: (open triangle) from Mordor Intelligence Report [196], (open circle) from Statista [199].

There are multiple routes to producing acetic acid. The most common and commercially significant route is methanol carbonylation. In this process, acetic acid is produced by the reaction of methanol with carbon monoxide in the presence of a catalyst, typically rhodium or iodide compounds. Another method is acetaldehyde oxidation, which involves oxidizing acetaldehyde with oxygen. A third route is the liquid-phase oxidation of hydrocarbons, where acetic acid is produced by partially oxidizing hydrocarbons like butane or naphtha in the presence of a catalyst and air [200].

Recent researches have focused on new synthetic routes for acetic acid production using CO_2. These alternative routes include the reaction of methane with CO_2 [201], hydrocarboxylation of methanol [202], lignin with CO_2 [203], and the hydrogenation of CO_2 [204]. However, the manufacture of acetic acid from CO_2 presents commercial and innovative challenges, such as reducing production impact, utilizing cost-effective raw materials, and designing efficient industrial processes.

Although there are other published articles discussing acetic acid production processes, such as the Cativa process [205, 206] and the Monsanto process [207, 208], no published articles specifically address the assessment of CO_2 routes and the design of a conceptual plant.

The assessment of innovative routes using CO_2 can be conducted using Multi-criteria decision analysis (MCDA) techniques. MCDA is employed as a structured approach to evaluate and compare multiple alternatives based on a set of criteria or factors. The primary objective of MCDA is to provide a systematic framework for evaluating alternatives and ranking them based on their performance against multiple criteria [159].

The evaluation of chemical process routes for acetic acid production involves several metrics and criteria. One of the criteria can be defined by the assessment of a chemical utilization scheme's suitability, which considers available information and builds upon previous work by Audus and Oonk [209]. Another criterion is focused on comparing energy consumption, as proposed by Muller and Arlt [210], which takes into account the exergy demand of the chemical reaction, resembling Gibbs energy. Since the use of CO_2 for chemical conversion faces thermodynamic and kinetic limitations, the final criterion is the Gibbs energy of the reaction. These criteria play a vital role in evaluating and selecting the most efficient and feasible process routes for acetic acid production from CO_2.

When it comes to process design, there are multiple approaches available, each with its own advantages and considerations. One notable approach is the hierarchical approach, which offers a systematic and structured framework for designing chemical processes. The hierarchical approach involves breaking down the overall process into smaller, interconnected stages or units. This hierarchical structure allows for better understanding and control of the process and

improved efficiency [211].

The objective of this study is to assess and evaluate innovative routes for acetic acid production using carbon dioxide through MCDA analysis. The study aims to identify the best CO_2 route, compare them based on criteria such chemical utilization, energy consumption, and Gibbs energy, and propose a conceptual plant design. By achieving these objectives, the research aims to contribute to the development of sustainable and efficient processes for acetic acid production from CO_2, offering insights for industrial aspects in chemical process design and green chemistry.

5.2 Production Routes

The industrial production of acetic acid is by bacterial fermentation and via synthetic route. The former accounts for only 10%, but is important for the production of vinegar, due to law regulations (food grade vinegar must be from biological origin) [212]. The latter is the preferential route for the glacial acetic acid production, includes traditional production routes, such as methanol carbonylation, acetaldehyde process, Liquid-Phase Oxidation (LPO), ethylene and ethane gas-phase, isomerization of methyl formate and methane carbonylation, and CO_2 innovative route, such as CO_2 and methane reaction, methanol hydrocarboxylation, lignin oxidation and CO_2 hydrogenation as depicted in Figure 5.2.

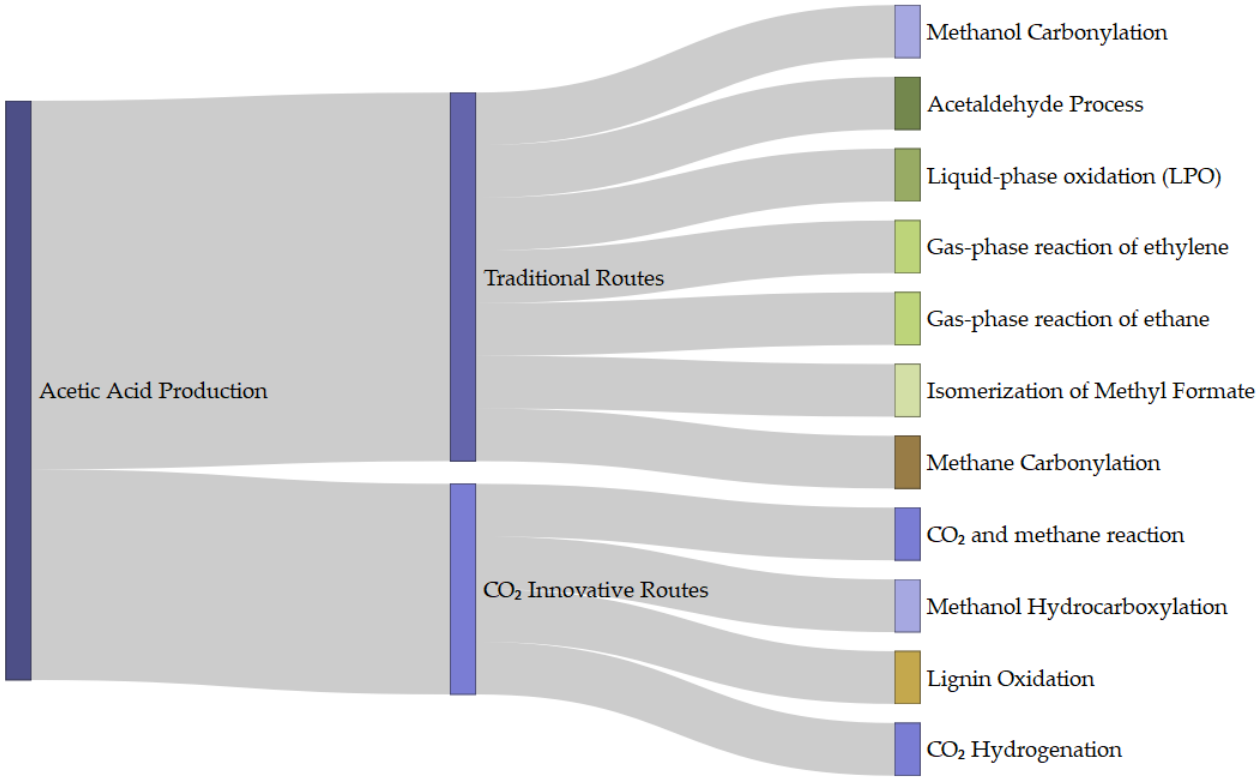

Figure 5.2: Synthetic acetic acid production routes, divided into traditional and CO_2 innovative.

The major producers of acetic acid include BP Chemicals, Celanese, Eastman Chemical, PetroChina, Daicel, LyondellBasell, SABIC, Jiangsu Sopo [213] as shown in Table 5.1.

Table 5.1: Acetic Acid Plant and location.

Company	**Location**	**Capacity ton/year**	**Technology**
Celanese	Pampa, Texas, USA	250,000	Butane LPO
	Edmonton, Alberta, Canada	75,000	Butane LPO
BP	Hull, UK	210,000	Butane LPO
Akzo Zout Chemie	Europoort, Netherlands	110,000	Butane LPO
Celanese	Clear Lake, Texas	1,350,000	Methanol Carbonylation
DuPont de Nemours	La Porte, Texas, USA	80,000	Methanol Carbonylation
Eastman Chamical Co	Kingsport, Tenn, USA	277,000	Methanol Carbonylation
	Texas City, Texas, USA	590,000	Methanol Carbonylation
LyondellBasell	La Porte, Texas, USA	544,000	Methanol Carbonylation

5.2.1 Traditional Production Routes

The large-scale production route to acetic acid is the methanol carbonylation, which represents over 65% of global capacity [214]. The liquid-phase oxidation of alkanes plants have been reduced their production gradually because of the competition with the methanol carbonylation route. Other technologies are in commercialization stage of maturity, among them the gas-phase reaction of ethylene and ethane, direct ethanol oxidation or synthesis gas [215].

5.2.1.1 Carbonylation of Methanol

The production of acetic acid by the carbonylation of methanol typically involves a catalytic reaction. This process involves several steps and requires specific conditions and catalysts. The overall chemical equation for the carbonylation of methanol to produce acetic acid is described in Eq. 5.2.1 [193].

$$CH_3OH + CO \longrightarrow CH_3COOH \tag{5.2.1}$$

In mid-1960s BASF commercialized the first industrial process to produce acetic acid using a cobalt catalyst methanol carbonylation reaction (in Ludwigshafen, Germany, with initial capacity of 3.6 kt/k). The high-pressure, high-temperature process (700 bar, 250 °C) with a cobalt iodide catalyst presented several advantages, such as the favorable raw material and energy costs [216].

In 1968, a rhodium based system under mild conditions was published by Monsanto [217]. The industrial utilization of the cobalt-catalysed technology was rapidly replaced by the Monsanto process, due to higher selectivity, less severe conditions and a faster reaction.

In the Monsanto process, methanol is carbonylated under pressures from 1 to 3 MPa, yielding 99% of acetic acid [217]. The technology was used at Texas City, Texas, with a initial capacity of 135,000 ton per year (expanded to 270,000 ton per year in 1975) [200].

Later modifications at the catalyst system level improved the capacity of a plant at Clear Lake, Texas, more than three times the initial capacity, reaching 900,000 tons per year [200].

Additional investigations into the process revealed that the use of an iridium catalyst is also successful in the conversion of methanol and carbon monoxide into acetic acid. In the mid-1990s, BP introduced a commercially viable iridium-catalyzed technology, known as the Cativa Process. This innovative approach offers improved economic efficiency by minimizing water usage, achieving an approximate 85% yield of acetic acid, enhancing catalyst durability, and reducing the formation of liquid byproducts. [218, 219].

According to Berre *et al.* [200] the low-reaction-water rhodium and iridium-based methanol carbonylation processes are economic competitive over all other acetic acid production processes.

The process comprises four-stages: (**i**) steam reforming to produce syngas, (**ii**) syngas into methanol, (**iii**) carbonylation of the methanol into acetic acid, where carbon monoxide and methanol are feed the reactor and (**iv**) acetic acid purification. The purification involves venting noncondensable byproducts (CO_2, H_2, and CH_4) from the reactor to regulate the carbon monoxide partial pressure. The light ends are recycled back to the reactor. The reactor solution is separated in a flash, with the catalyst recycled and crude acetic acid sent to a light-ends column. Methyl iodide, methyl acetate, and water are recycled as a two-phase stream, while wet acetic acid goes to a dehydration column. Aqueous acetic acid is recycled, and dry acetic acid is obtained as the final product. Propionic acid and other higher boiling carboxylic acids are removed as residue, and product acetic acid is recycled for purification [200].

Table 5.2 provides comprehensive information regarding the reaction conditions, catalysts, and by-products associated with the primary conventional routes for acetic acid production by methanol carbonylation. The data was retrieved from Martín-Espejo *et al.* [220].

Table 5.2: Characteristics of Methanol Carbonylation routes. The data was retrieved from Martín-Espejo *et al.* [220].

Process	Catalyst	T (^{o}C)	P (bar)	Yield (%)
BASF	Homogeneous Co-based iodide promoted	230-250	60-80	90
Monsanto	Homogeneous Rh-based iodide promoted	150-200	30-60	99
Cativa	Homogeneous Ir-based iodide promoted	190	28	>99
Acetica	Heterogenized homogeneous Rh-based	160-200	30-60	99

5.2.1.2 Acetaldehyde oxidation

Acetic acid production by acetaldehyde oxidation, which originally used petroleum feedstock, was the dominant method, accounting for over 45% of production [221]. However, due to economic considerations, the methanol carbonylation and LPO routes have replaced acetaldehyde oxidation. Acetaldehyde still accounts for 18% of global acetic acid capacity, as reported by Kent [222].

The commercial production of acetic acid via batch processes began in Germany in 1911, followed by the United States nine years later. In this method, oxygen is introduced into an acetaldehyde and manganese catalyst solution. The resulting mixture is separated in a distillation column, yielding 88-95% acetic acid [221].

Newer plants have adopted continuous processes to enhance safety. These processes involve the oxidation of acetaldehyde with oxygen by a radical mechanism, with peracetic acid serving as an intermediate. Notably, companies like UCC (US), Daicel (Japan), and British Celanese (UK) employ this technology in their commercial plants [223].

5.2.1.3 LPO of hydrocarbons

The worldwide usage of the LPO process for acetic acid production has decreased due to competition from the methanol carboxylation process. The choice of raw materials varies depending on availability. For example, butane is used in the US and Canada, while light naphtha is used in the UK [200].

Celanese was the first company to produce acetic acid from LPO using butane at their Pampa, Texas plant in 1952. Union Carbide Chemische Huls and Russian Refinery started production a decade later. By 1973, LPO technology accounted for 40% of the global acetic acid capacity. However, according to Weissermel *et al.* [223], the US participation decreased to 31% by 1982, with UCC and Celanese as the main players. In 2010, LPO-based production of acetic acid accounted for approximately 8% [222].

The LPO process utilizes cobalt catalysts, although other catalysts such as manganese, chromium, bismuth, and nickel are also employed. The choice of operating conditions and catalysts affects the product distribution. For instance, bismuth catalysts exhibit 97% selectivity for acetic acid with low formic acid production, while cobalt catalysts show 79% selectivity for acetic acid.

The separation of the product mixture, which includes acetic acid, formic acid, propionic acid, acrylic acid, methyl ethyl ketone, ethyl acetate, methyl vinyl ketone, and gammabutyrolactone, is an expensive process. It involves a combination of extraction, distillation, and extractive distillation techniques [221].

5.2.1.4 Other minor contribution routes

The conversion of ethylene directly to acetic acid was developed by Showa Denko [224], where a reaction of ethylene and oxygen over a palladium catalyst and a heteropolyacid or salt takes place in gas-phase. Commercial operation started in 1997, however is idle since 2008 [200].

The conversion of ethane to acetic acid has been investigated by several groups. Union Carbide developed the coproduction of ethylene and acetic acid with a catalyst (molybdenum, vanadium, niobium, calcium, and antimony) enhanced by water addition [225]. Hoechst Research and Technology [226, 227] employed molybdenum, palladium, and rhenium catalyst in a process to oxidize ethane to acetic acid, claiming selectivity of 90% and conversion of ethane of 10%.

The isomerization of methyl formate under heterogeneous catalyst to produce acetic acid was studied by Kawako and co-workers [228]. The authors claimed a 90% conversion and 99% acetic acid selectivity.

The methane can be carbonylated to acetic acid under strong acid conditions or high pressures to overcome thermodynamics. The raw materials include methane, carbon monoxide and oxygen. Volkov *et al.* [229] used molecular oxygen over silica materials (including rhodium chlorides) to produce acetic acid. The productivity depend on rhodium composition and the type of silica used for catalyst the preparation.

5.2.2 CO_2 Innovative Production Routes

New synthetic routes for acetic acid production using CO_2 have been studied. Alternative routes are reaction of methane with CO_2 [201], hydrocarboxylation of methanol [202, 230], ligning with CO_2 [203] and the hydrogenation of CO_2 [204].

However, manufacture of C_{2+} carboxylic acids, among them acetic acid, from CO_2 poses a commercial and innovative challenge: to reduce the production impact, raw materials with lower cost and industrial design and engineering are some of the defiance [231].

5.2.2.1 Methane and CO_2

The conversion of methane and CO_2 to acetic acid received much attention recently, because of the improvement potential (atom economy and avoid CO production step) [232]. The patent US6960682 [233] describes the production of acetyl anhydrides and acetic acid from CO_2 and methane using a catalyst based on $VO(acac)_2$ and $K_2S_2O_8$ as initiator dissolved in anhydrous acid and corresponding anhydride. The patent WO9605163 [234] claimed high selectivities (70-95%) when the catalyst used contained metals from VIA, VIIA, and/or VIIIA group.

The direct conversion, however, presents thermodynamic restrictions. According to Aresta *et al.*

[7], the carboxylation of CH_4 is considered a formal insertion of CO_2 into C-H bond. While the enthalpy change is favourable, the entropy change demonstrate severe influence on the free energy change. A decisive process is the C-H splitting with high kinetic barrier (either homolytic (R+H) or heterolytic (R^- + H^+)).

Wilcox et al. [235] synthesized acetic acid using heterogeneous catalyst (Pd/carbon and Pt/alumina). The authors used temperature programmed reaction and the formation of acetic acid occured above 623 K (Pd/carbon) and 473 K (Pt/alumina) reaching low yields.

To overcome thermodynamics, a periodic operation or a coupling reaction is required [236]. Ding, Huang and Wang [237] used Pd/SiO_2 and Rh/SiO_2 catalysts for carboxylation of methane in a step-wise isothermal process. The limiting steps are the methyl radical formation and CO_2 inserting on the intermediate.

A different approach to overcome thermodynamics is to use an additional reactant. Huang *et al.* [238] introduced oxygen as a oxidant through V_2O_5-$PdCl_2/Al_2O_3$-2 as a catalyst. The results showed low formation rates, with maximum of 30.79 µg/(g · h) at 723 K.

The shift of the equilibrium to the product, acetic acid, can be achieved by coupling with a second reaction. Spivey, Wilcox and Roberts [239] added acetylene as a reactant, favouring the production of vinyl acetate.

More efforts on a catalyst system to simultaneously activate both methane and CO_2 have been done. Rabie, Betiha and Park [240] employed a zeolite catalytic system (Cu^-M^+ZSM-5) to synthesize acetic acid and the results pointed out the Cu nanoparticles over ZSM-5 activate both methane and CO_2, yielding 395 umol(gcat)h for 10 h.

The mechanism over MFI zeolite exchanged with Cu was studied using density functional theory by Montejo-Valencia et al. [241]. The first step is the formation of (-Cu-CH_3), followed by CO_2 insertion producing surface acetate (-Cu- $OOCCH_3$), which abstracted the proton to form acetic acid.

So far, however, there has not been an efficient catalyst for acetic acid production from CH_4 and CO_2 [241].

5.2.2.2 Hydrocarboxylation of Methanol

The second route to produce acetic acid from CO_2 is the hydrocarboxylation of methanol proposed by [202, 230].

Qian *et al.* [230] proposed the reaction of methanol, carbon dioxide and hydrogen over bimetallic Ru-Rh homogeneous catalyst,using imidazole as ligant, LiI as promoter and 1,3 dimethyl-2-imidazolidinoe as solvent. The reported yield was 77%, and the TON exceeded 1000 after five

cycles.

A further study on the system, Cui *et al.* [202] used $Rh_2(CO)_4Cl_2$ as catalyst with 4-methylimidazole (4-MI) as ligand, LiCl as cocatalyst and LiI was used as promoter. The reported yield was 81.8% with a TOF of 26.2 h^{-1}.

A recent pre print study of Ahmad et al. [242] presents a Fe-based thermally transformed metal organic framework catalyst (MIL-88B) for hydrocarboxylation of methanol to produced acetic acid, and the results indicated a yield of 590.1 mmol/gcat.L, with 81.7% of selectivity for acetic acid.

The proposed mechanism indicates that the reaction did not proceed via the CO route (as compared with carboxylation of methanol). CH_3I is formed when LiI reacts with methanol, then the oxidative addition, in the Rh active sites, takes place. The CO_2 is inserted into the adsorbed specie to form CH_3COORh^*I, which form acetic acid by reductive elimination with H_2. LiI and H_2O were formed by the reaction of LiOH and HI.

Cheap and easily available feedstock are used in this promising route. It is composed by a simple catalytic system, less corrosive and more efficient than the previous one reported.

5.2.2.3 Other Routes

Within the context of biomass conversion and to valorize lignin as a renewable source of aromatics [243], Wang *et al.* [203] proposed a synthesis of acetic acid from ligning, CO_2 and H_2 over ionic liquid (e.g., [BMIm][Cl])-based catalytic system containing Ru–Rh bimetal catalyst ($Ru_3(CO)_{12}$ and RhI_3) and LiI. The achieved yield was 94% at relative mild conditions (180^{o}C and 6 MPa).

The hydrogenation of CO_2 to yield acetic acid was studied by Ikehara *et al.* [204] using Ag-modified Rh/SiO_2 catalyst. The major formed product was CO (selectivity was more than 90%), while the hydrogenated compounds, acetic acid is the most abundant one at 463 K, however with low yields. Jia et al. [244] studied the thermodynamics of CO_2 hydrogenation to carboxylic acids, the results showed a favourable production of higher-carbon acids (acetic acid, propionic acid) over formic acid, nonetheless kinetic constraints in C-C coupling is difficult in practice.

5.3 Problem Definition

CO_2 is revealed as a valuable environmental-friendly input for carbon dioxide utilization technology in the chemical industry [245]. Although recent studies have presented innovative routes and catalysts with more efficient kinetics, such as plasma catalysis [246] or MOF catalyst [242], the process route assessment and flowsheet design is still scarce.

In this scenario the current study aims to assess different CO_2-based routes to produce acetic acid in terms of energy and process requirements using multicriteria analysis.

The selected production route was further evaluated. In order to design and synthesize a given process, a process synthesis by hierarchical approach leads to a detailed flowsheet.

Additionally an exergy analysis was performed in the final flowsheet to reveal the exergy inefficiencies locations.

5.4 Methods

This section presents the criteria for multicriteria analysis and the definitions for the flowsheet design and exergy analysis.

The proposed procedure involves selecting the most promising route for CO_2 chemical conversion to acetic acid (Section 5.4.1), definitions for the flowsheet design of the selected route (Section 5.4.2) and simplified exergy analysis to address some inefficiencies of the final production process simulation (Section 5.4.3).

5.4.1 Route Selection through multi-criteria decision analysis

Table 5.3 shows the reactions involved in each system for acetic acid production. Although other chemicals can also be produced (**e.g.** formic acid in hydrogenation) they are not considered here due to the sake of simplicity to compare the systems.

Table 5.3: Reactions involved in acetic acid manufacture.

Process	**Reaction**	**Nr**
CO_2 and Methane	$CH_4 + CO_2 \longrightarrow CH_3COOH$	R1
Methanol Hydrocarboxylation	$CH_3OH + CO_2 + H_2 \longrightarrow CH_3COOH + H_2O$	R2
Lignin Oxidation	$C_7H_8O + CO_2 + H_2 \longrightarrow CH_3COOH + C_6H_5OH$	R3
CO_2 Hydrogenation	$CO_2 + 2\,H_2 \longrightarrow \frac{1}{2}\,CH_3COOH + H_2O$	R4

To compare the different routes to produce acetic acid (CO_2 innovative) a multi-criteria decision analysis using TOPSIS method was performed [106]. Details of the technique can be found on previous studies [36, 37].

The elicitation of criteria weights was obtained by Shannon Entropy method [126]. The sensitivity analysis was carried out using Monte Carlo Simulation to simulate a 20% variability in weights [166]. The base value was the one calculated from Shannon Entropy.

Three criteria were used: (**i**) the procedure proposed by Audus and Oonk (1997) [209]; (**ii**) short-cut exergy demand of the chemical reaction proposed by Müller and Arlt (2014)[210]; and (**iii**) Gibbs energy of the reaction.

The first criterion is a preliminary evaluation of processing routes for acetic acid manufacture from CO_2 based on the work of Audus and Oonk [209] with additional characteristics. The procedure is claimed to assess the suitability of a chemical utilisation scheme, by the use of simple information.

Table 5.4 introduces the process characteristics used in this work (from Audus and Oonk [209]), with additional information about the catalytic system.

Table 5.4: Process characteristics definitions of general processes and their respective values. Adapted from Audus and Oonk [209].

Characteristic	**Value**	
	1	**2**
Number of processes	React/Sep	React/H2/Sep
Operating Conditions	Mild	Mild/Medium
Disontinuities in the process	No	Yes
Change of phase	No	Yes
Possibility for process integration	Yes	No
Catalytic System	Adequate	Limited

The second indicator is based on a comparison of energy consumption. Müller *et al.* [210] proposed a criterion based on the the exergy demand of the chemical reaction, where the loss of chemical exergy is similar to Gibbs energy. The process exergy is usually assigned in terms of heat (Eq. 5.4.1) and depends on temperature T and the surrounding temperature T^{∞}.

$$Ex = Q\left(1 - \frac{T^{\infty}}{T}\right) \tag{5.4.1}$$

According to Müller *et al.* [210], the heating demand Q can be approximated by the enthalpy of reaction $\Delta_r H$, for in-advance evaluation.

The option of using CO_2 for chemical conversion has thermodynamic and intrinsic kinetic restrictions, therefore the final criterion is the Gibbs energy of the reaction. The equilibrium composition of a reaction system was calculated using equilibrium constants, and the calculation was conducted based on the gaseous phase. A complete and detailed study of thermodynamics of those reactions can be found on previous article of the group [247].

The most promising production route was then selected for further study.

5.4.2 Process Synthesis by Hierarchical Approach

Chemical process synthesis is a complex scheme, which comprises process modeling and design and combinatorial defiance. There are two major approaches: the traditional sequential form and the optimization-based synthesis using superstructure models. In the former category, the problem is solved in sequential scheme, by decomposition where there is a hierarchy of elements that can be depicted by an Onion Diagram (reactor, separation, heat recovery and utility) as illustrated in Figure 5.3. The use of heuristic rules defines adjustments in the flowsheet leading to an enhanced solution, but eventually sub-optimal solutions are found [248, 249].

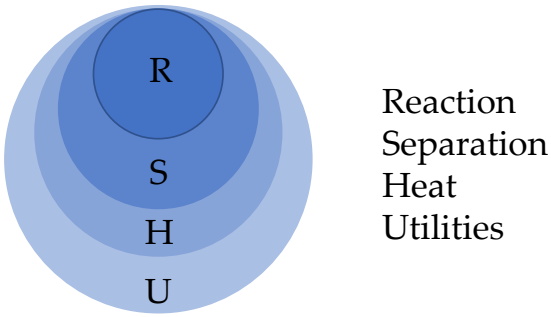

Figure 5.3: Process design approach.

The latter category considers the full integration between decisions at the single step, *i.e.* determine the optimal structure and operating conditions simultaneously. Therefore, this approach contemplates all possible complex interactions between the engineering choices, including equipment (potentially selected in the optimized flowsheet), the interconnection and operating conditions formulated as an optimization problem [25, 27, 250].

Dimian *et al.* [211] proposed an improved hierarchical approach, the reduced interactions between levels leads to a more efficient design methodology. The essential feature of the approach is the *reactor/separation/recycle* emphasis. The methodology can be employed in any chemical process industry, not only for new processes but also for revamping and retrofitting of existing processes.

The improved hierarchical approach proposed by Dimian *et al.* [211] was used to the process synthesis of the acetic acid manufacture from CO_2. The levels of the approach are depicted in Figure 5.4.

At level 0, known as Basis of Design, data encompassing technical and economical aspects is gathered to facilitate the conceptual design. Moving on to level 1, Chemistry and Thermodynamics, an intricate description of the chemical reactions occurring in the chemical reactor is provided, alongside an analysis of key mixtures regarding their nonideal behavior during separation. Level 2, titled Input/Output Analysis, establishes the foundation for the material

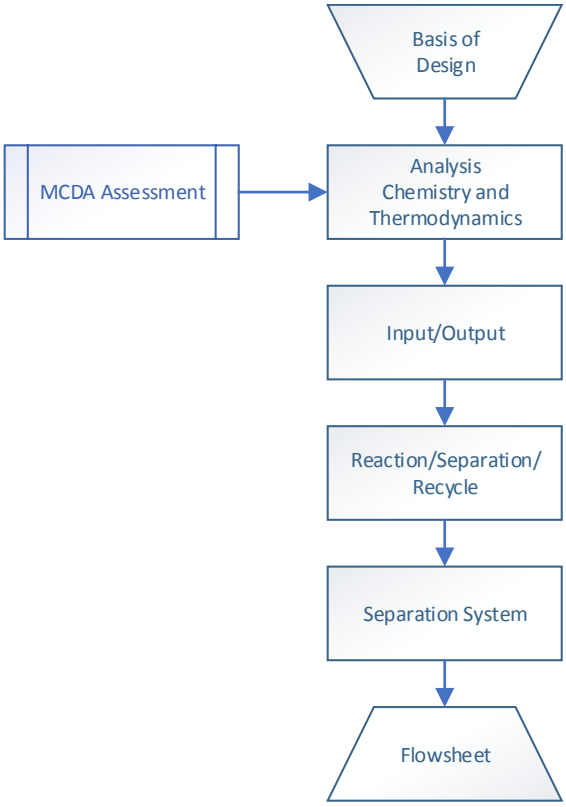

Figure 5.4: Process Synthesis by Hierarchical Approach for the acetic acid case study. Adapted from: Dimian *et al.* [211].

balance, where raw materials serve as inputs and products, byproducts, and waste form the outputs. Level 3, Reactor/Separation/Recycle, plays a crucial role in defining the process architecture by elucidating the interactions, particularly recycles, between the reactor and separation units. Finally, level 4 centers around the separation system, which employs a task-oriented methodology to address the treatment of homogeneous fluids by breaking down the problem into manageable subproblems.

5.4.3 Exergy Analysis

An exergy analysis based on the simulation results was carried out. Exergy refers to the maximum capacity of a system to produce useful work when balanced with its surroundings [251]. The standard chemical exergy table defined by Szargut, Morris and Steward (1987) [251] was used, and for non-reference components the method proposed by Haghbakhsh and Raeissi (2019) [251] was used.

The methodology described in Szargut, Morris and Steward (1987) [251] was used to calculate the chemical exergy, work and heat for a given unit operation.

5.5 Results and Discussion

This section presents the results of the multi-criteria decision analysis results for route selection, the proposed flowsheet and the exergy anaylsis.

5.5.1 Multi-Criteria Decision Analysis Results

In the context of selecting the most favourable route for producing acetic acid from CO_2, the current assessment has been proposed. The screening evaluates the suitability of a chemical utilisation scheme and a simplified energy consumption estimate.

5.5.1.1 Suitability of a Chemical Utilisation Scheme Results

The shortcut evaluation of utilisation schemes of CO_2 proposed by Audus *et al.* [209] was employed in this work. Table 5.5 present the results for the process production routes studied.

Table 5.5: Process Characteristics for Selected Process Production Routes.

Characteristic	**Production Process**	
	R1	**R2**
Number of processes	React/Sep	React/H2/Sep
Operating Conditions	Mild (1 atm)	Mild/ Medium (10 Mpa)
Discontinuities in the process	Yes (stepwise reaction process)	No
Change of phase	No	Yes
Possibility for process integration	Yes	Yes
Catalytic System	Limited	Adequate
Characteristic	**Production Process**	
	R3	**R4**
Number of processes	React/H2/Sep	React/H2/Sep
Operating Conditions	Mild/Medium (6 MPa)	Mild/Medium (2 Mpa)
Discontinuities in the process	No	No
Change of phase	Yes	No
Possibility for process integration	Yes	Yes
Catalytic System	Adequate	Limited

The process characteristics criterion demonstrated similar values for all the production processes evaluated (to be in mind that the small the value the better). Reaction $R1$ achieved a sum of 8, while Reaction $R2$, $R3$ and $R4$ achieved a sum of 9.

The attractiveness of converting two greenhouse gases (CH_4 and CO_2) into CH_3COOH, from a practical perspective, faces the low process efficiencies and no clear path for the process intensification was apparent.

5.5.1.2 Simplified Energy Consumption Estimate

Another shortcut method to evaluate different process proposed by Müller *et al.* [210] was used in this work. The exergy demand for the CO_2 innovative routes to acetic acid production are depicted in Figure 5.5.

The reaction temperature as function of the heating demand is represented in Figure 5.5, and for in-advance evaluation the heating demand was approximated by the enthalpy of reaction [210].

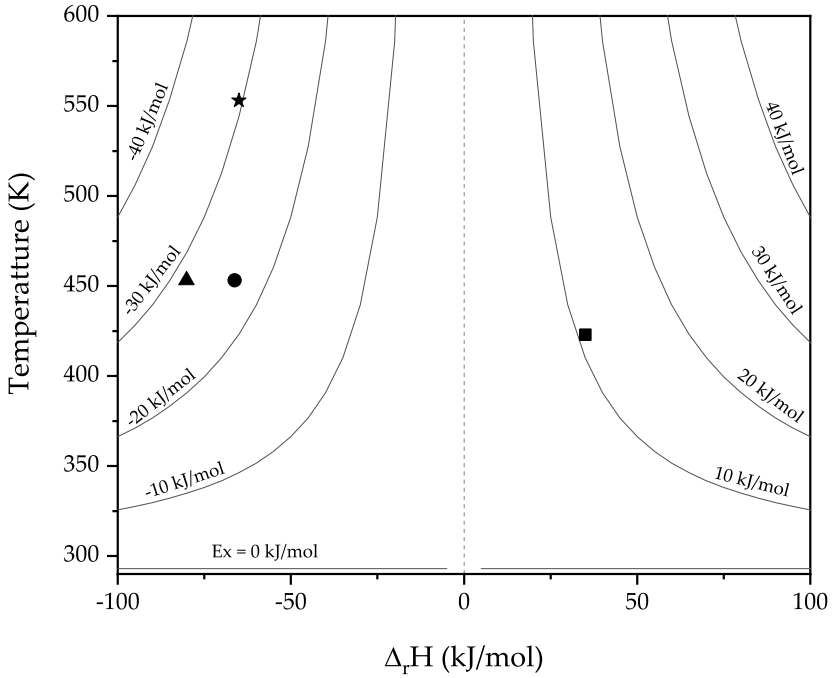

Figure 5.5: Reaction temperature as a function of the enthalpy of reaction. Lines of constant exergy are shown as solid lines for T^{∞}=293 K. Square represents CO_2 and Methane, triangle represents methanol hydrocarboxylation, circle represents lignin oxidation and star represents CO_2 hydrogenation.

The *isoexergetic* lines are shown for comparison, the values in the left upper corner represent low exergy, while right upper corner represent high exergy content. The thermal exergy demand can be compared, methanol hydrocarboxylation and CO_2 hydrogenation shown similar exergy, with a difference of 7.3%, and both reactions exhibited negative values in addition of the lignin reaction. On the other side, the reaction of CO_2 and methane has a positive exergy value (10.77 kJ/mol).

5.5.1.3 Gibbs Energy of Reaction

Table 5.6 presents the results from the equilibrium calculations for the selected reaction systems. The properties enthalpy of reaction and Gibbs energy of reaction from the literature are also shown.

Table 5.6: Thermodynamic Properties of Selected Reactions.

Reaction Nr	$\Delta_r H^o$ (kJ/mol)			$\Delta_r G^o$ (kJ/mol)		
	This Work	**Lit.**	**Ref.**	**This Work**	**Lit.**	**Ref.**
R1	35.04	36.07	[252]	70.19	71.04	[252]
R2	-80,10 (-171.1)	-137.60	[230]	-46,54 (-65.7)	-66.40	[230]
R3	-66.29			-35.92		
R4	-64.94	-64.80	[244]	-21.54	-21.60	[244]

The results from this study are in agreement with the available literature data. The results for reaction $R1$, for example, are within 3% of error.

The value in parenthesis for $R2$ represent the calculations for liquid product rather than in gaseous phase.

All reactions are exothermic, except from $R1$, which exhibited a enthalpy of reaction of 35.04 kJ/mol, classified as endothermic. Regarding the spontaneity of the reactions, there is the same pattern, only $R1$ is non spontaneous ($\Delta_r G^o > 0$). It is important to highlight that the calculations were performed at a specified pressure of 1 atm.

It is important to mind that a spontaneous process may take place quickly or slowly, because this property is not related to kinetics or reaction rate.

5.5.1.4 Route Selection Results

The four CO_2 innovative routes were compared through a MCDA based on the results from Section 5.5.1.1 to 5.5.1.3.

The three criterion assessed were organized and summarized in the performance matrix, Table 5.7.

Table 5.7: Performance matrix for the acetic acid production route.

Production Process	**Process Characteristics**	**Exergy (kJ/mol)**	$\Delta_r G^o$ **(kJ/mol)**
CO_2 and Methane	8	10.77	70.19
Methanol Hydrocarboxylation	9	-28.31	-46.54
Lignin Oxidation	9	-23.43	-35.92
CO_2 Hydrogenation	9	-30.53	-21.54

The criterion Gibbs energy of reaction exhibited negative values for three out of four of the production processes alternatives evaluated. The same behaviour was observed for exergy demand, and only the production process using methane and CO_2 displayed positive value.

The Shannon Entropy method was used to obtain the relative weights. It is capable to express the relative intensities of criterion importance and to determine the weights using the data from

the performance matrix. Table 5.8 presents the results of the approach.

Table 5.8: Shannon Entropy Weights results for the acetic acid production process.

Criteria	Max/Min	Entropy	Diversity	Normalized Weight
Process Characteristics	min	0.000	1.000	0.704
Exergy (kJ/mol)	min	0.790	0.210	0.148
$\Delta_r G^o$ (kJ/mol)	min	0.789	0.211	0.149

The criterion with highest relative importance was Process Characteristics ($E = 0.00$, $w = 0.704$). Gibbs energy and exergy displayed comparable values for normalized weight.

The weight calculated in Table 5.8 together with data in Table 5.7 were used to assess the production process. TOPSIS method was used, the results are displayed in Figure 5.6a.

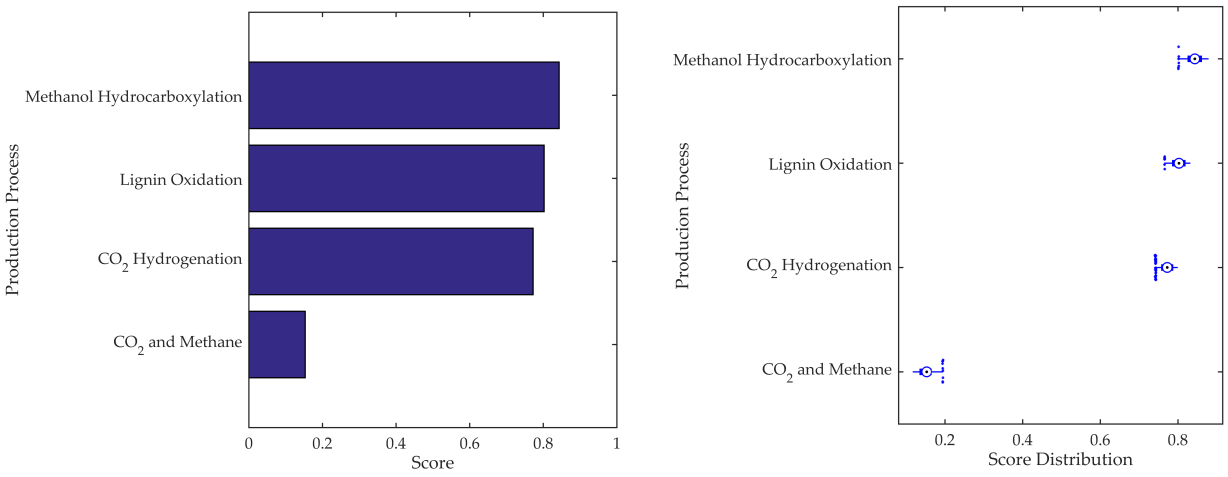

(a) Score (b) Distribution

Figure 5.6: Final Results for the acetic acid production process. (a) Score and (b) Distribution.

The most promising production route is methanol hydrocarboxylation (score = 0.843, std deviation = 0.007), followed by lignin oxidation (score = 0.802, std deviation = 0.008), CO_2 hydrogenation (score = 0.772, std deviation = 0.009) and lastly CO_2 and methane (score = 0.153, std deviation = 0.009). The selected route (methanol Hydrocarboxylation) is then used throughout the study.

5.5.2 Process Design

The methodology proposed by Dimian [211] was used to design the process and generate a close-to-optimal flowsheet. It is important to note that the route selected from the literature is still in consolidation phase and it does not achieve high technological maturity level.

The thermodynamic analysis in detail for this reaction was deeply studied by Alcantara et al. [247]. The study explores different inlet composition, temperature in the conversion of CO_2 and the results were used as basis for the flowsheet design.

5.5.2.1 Basis of Design

Considering the chemical plants in operation (Table 5.1), the proposed plant considers 200 kton/year as target production. For most chemical and petrochemical processes, the plant attainment will typically be between 90 to 95% of the total hours in a year (8760). Unless the process is known to require longer shut-down periods, a value of 8000 hours per year can be used for flowsheet preparation [253].

Methanol hydrocarboxylation route was studied in terms of catalyst availability and literature data. The chosen route is still undergoing studies and has not yet reached an advanced stage of technological development. Two studies reported experimental data (Table 5.9): the first study employed Ru-Rh bimetallic catalyst, while the second used Rh-based catalyst, both using the solvent 1,3-dimethyl- 2-imidazolidinone (DMI). The catalyst reported in Cui *et al.* [202] was selected for use in simulation because the amount of corrosive LiI used was reduced by 1/3. The noble Ru compound was removed and effectively yield acetic acid under mild conditions was achieved.

Table 5.9: Catalytic performance of selected experimental studies.

	1	2
Catalyst	$Ru_3(CO)_{12}/Rh_2(OAc)_4$	$Rh_2(CO)_4Cl_2$
Ligand	imidazole	4-methylimidazole (4-MI)
Cocatalyst	–	LiCl
Promoter	LiI	LiI
Solvent	DMI	DMI
TOF (h^{-1})	30.8	26.2
Yield (%)	70.3	81.8
Ref.	Qian *et al.* [230]	Cui *et al.* [202]

The proposed mechanism developed by Cui *et al.* [202] is introduced in Figure 5.7.

In order to simulate the process in a commercial simulator, **e.g.** Aspen Plus, there are some approaches for the reactor system: (**i**) using of Gibbs energy minimization based reactor, (**ii**) using conversion/ stoichiometric reactor or (**iii**) using of rigorous kinetic equations. Due to the lack of kinetic data available in the literature for this new reaction system, a stoichiometric reactor approach was used. It is important to highlight that this approach produce an estimate result for the reactor. This level of detail is in accordance with the prospective analysis considered in this study for a conceptual plant purpose. In order to define a robust and technologically consistent production scheme for this option, the plant was simulated using the Aspen Plus software.

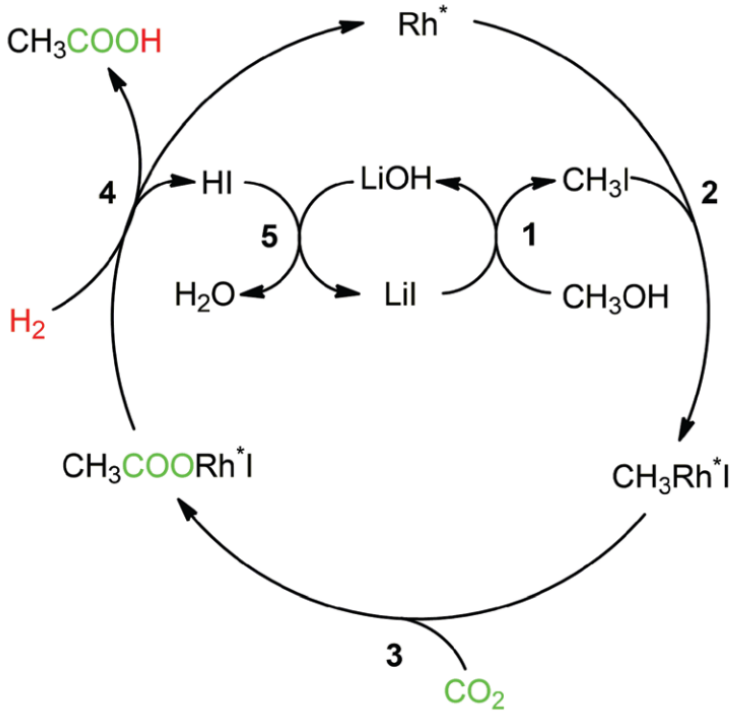

Figure 5.7: Mechanism of the reaction over the Rh-based catalytic system proposed by Cui *et al.* [202].

The conversion/stoichiometric reactor approach was used once there are literature data available to validate the set of independent reaction proposed.

5.5.2.2 Chemical Reaction Stoichiometry

Chemical Reaction Stoichiometry deals with constraints placed on changes in compositions of a closed system. It corresponds to the Law of Conservation of Mass (LCM) in the context of chemical reactions. It can be expressed as a set of linear equations, taking the conservation of atom types into account.

In the multi-reaction systems the matrix-method [254] can be applied to determine the appropriate number of independent chemical equations (R), a critical aspect of chemical equilibrium problems.

The constraints on chemical potentials at equilibrium can be imposed by *a priori* specifications, which reflects in the elemental abundances.

The algorithm proposed by Smith and Missen (1982) [254] was used to simultaneously determines the number of independent equations (rank ($\mathbf{A}$)) and a complete set of chemical equations. The first step is the reduction of the formula matrix $\mathbf{A}$ (Eq. 5.5.1) to unit matrix form. The task can be performed by Gauss-Jordan reduction [255].

$$\mathbf{A*} = \begin{pmatrix} \mathbf{I}_c & \mathbf{Z} \\ \mathbf{0} & \mathbf{0} \end{pmatrix} \tag{5.5.1}$$

where $\mathbf{I}_c$ represents the (C x C) identity matrix and $\mathbf{Z}$ represents the (C x R) matrix. C is the rank of $\mathbf{A}$. The complete stoichiometry matrix is obtained in the canonical form using Eq. 5.5.2

$$\mathbf{N} = \begin{pmatrix} -\mathbf{Z} \\ \mathbf{I}_c \end{pmatrix} \tag{5.5.2}$$

The stoichiometry procedure was implemented in Matlab and used to generate a set of reactions that represents the system.

Consider the hydrocarboxylation of methanol with carbon dioxide and hydrogen as introduced by Cui et al. [202], the system can be represented by the major components: methanol (CH_3OH), carbon dioxide (CO_2), hydrogen (H_2), water (H_2O), acetic acid (CH_3COOH), methane (CH_4), and minor by-products components: ethanol (C_2H_5OH), methyl-acetate ($C_3H_6O_2$), ethyl-acetate ($C_4H_8O_2$). One should refers to the original article for the details on the components. The Eq. 5.5.3 represent the system:

$$\{(CH_3OH, CO_2, H_2, H_2O, CH_3COOH, CH_4, C_2H_5OH, C_3H_6O_2, C_4H_8O_2), (C, H, O)\} \tag{5.5.3}$$

Moreover, an additional restriction was imposed to the system. From the experiments, it is known that CO_2 and H_2 do react, under certain conditions, in an equal amount [202]. This restriction was incorporated into the general description explicitly. Details are shown in Missen and Smith [256].

The formula matrix $\mathbf{A}$ for the given system is written including the chemical species and the restriction (Eq. 5.5.4).

$$\mathbf{A} = \begin{array}{c} \begin{matrix} (1) & (2) & (3) & (4) & (5) & (6) & (7) & (8) & (9) \end{matrix} \\ \begin{pmatrix} 1 & 1 & 0 & 0 & 2 & 1 & 2 & 3 & 4 \\ 4 & 0 & 2 & 2 & 4 & 4 & 6 & 6 & 8 \\ 1 & 2 & 0 & 1 & 2 & 0 & 1 & 2 & 2 \\ 0 & -1 & 1 & 0 & 0 & 0 & 0 & 0 & 0 \end{pmatrix} \end{array} \tag{5.5.4}$$

The numbers at the top stand for the species in the system (CH_3OH, CO_2, H_2, H_2O, CH_3COOH,

CH_4, C_2H_5OH, $C_3H_6O_2$, $C_4H_8O_2$) and the rows are in the order of the elements (C, H, O and restriction) given in Eq. 5.5.3. The number of species, $N = 9$ and M, that is the elements and the restriction of CO_2 and H_2 reacting in equal amount, therefore, resulting in 4. The formula matrix is transformed using Eq. 5.5.1 into **A***.

$$\mathbf{A^*} = \begin{pmatrix} 1 & 0 & 0 & 0 & 1 & 1.5 & 2 & 2 & 3 \\ 0 & 1 & 0 & 0 & 1 & -0.5 & 0 & 1 & 1 \\ 0 & 0 & 1 & 0 & 1 & -0.5 & 0 & 1 & 1 \\ 0 & 0 & 0 & 1 & -1 & -0.5 & -1 & -2 & -3 \end{pmatrix} \tag{5.5.5}$$

The rank (**A**) is then defined, and the maximum number of linearly independent stoichiometric equations is calculated as $R = N - M \therefore 9 - 4 = 5$. A complete stoichiometric matrix **N** in canonical form is presented in Eq. 5.5.6.

$$\mathbf{N} = \begin{pmatrix} -1 & -1.5 & -2 & -2 & -3 \\ -1 & 0.5 & 0 & -1 & -1 \\ -1 & 0.5 & 0 & -1 & -1 \\ 1 & 0.5 & 1 & 2 & 3 \\ 1 & 0 & 0 & 0 & 0 \\ 0 & 1 & 0 & 0 & 0 \\ 0 & 0 & 1 & 0 & 0 \\ 0 & 0 & 0 & 1 & 0 \\ 0 & 0 & 0 & 0 & 1 \end{pmatrix} \tag{5.5.6}$$

Each equation in a permissible set of chemical equations is retrieved from a column of **N** and rearranging, resulting in the six chemical equations described in Eq. 5.5.7

$$CH_3OH + CO_2 + H_2 = CH_3COOH + H_2O \tag{5.5.7a}$$

$$3CH_3OH = 2CH_4 + CO_2 + H_2 + H_2O \tag{5.5.7b}$$

$$2CH_3OH = C_2H_5OH + H_2O \tag{5.5.7c}$$

$$2CH_3OH + CO_2 + H_2 = C_3H_6O_2 + 2H_2O \tag{5.5.7d}$$

$$3CH_3OH + CO_2 + H_2 = C_4H_8O_2 + 3H_2O \tag{5.5.7e}$$

The reactor plays a key role in the process and to study extreme conditions, where these data are critical for the flowhseet design assessment. The reactor was simulated using RStoic module

(in Aspen Plus) and the reactions in Eq. 5.5.7 were used.

The reactor conditions were changed and the impact on the global environmental performance of the system were estimated.

For the sensitivity analysis, the literature data (yield of acetic acid for different temperatures) for the methanol hydrocarboxylation reaction [202] were fitted to a logistic regression curve.

The final expression was embedded into the Aspen Plus simulation as a Fortran code [257] and the yield of acetic acid in the reactor was retrieved based on the temperature of the reactor. According to the literature article from Cui et al. [202], the main side reaction is the production of methane (Eq. 5.5.7b), which is also adjusted to experimental results.

Figure 5.8 presents the results obtained for the analysis and the experimental data available in the literature.

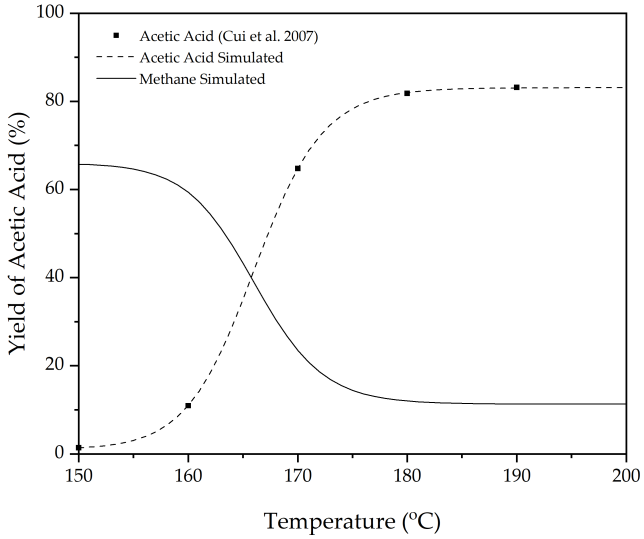

Figure 5.8: Yield of products based on reactor temperature.

The range of temperature of 190-200 °C presents a small increase in yield (1.28% and 1.35%, respectively) compared with 180 °C, while the energy required to increase the additional 10-20 °C is not environmental neither economical feasible. The curve at this region behaves asymptotically, and accordingly the temperature of 180 °C can be used as the extreme value.

On the other hand, the lower temperatures, for instance 170 °C reduces the required thermal energy (consequently the operation cost in the area and environmental metrics), however there is a decrease of 21% in the acetic acid yield, which can impact in the separation train (distillation columns) and also in the recycled streams (pumps and heat exchangers).

Thermodynamic analysis of the complete set of reactions (see Eq. 5.5.7) was carried out for understanding the behaviour of the system. The Gibbs free energy minimization method was

used [258, 259] (Eq. 5.5.8) and implemented in Aspen Plus software. The Peng-Robinson equation of state was employed to determine the fugacity in the calculation.

$$G = \sum_{i=1}^{NC} \sum_{k=1}^{NF} \mu_i^k n_i^k \tag{5.5.8}$$

where NC stands for number of components (i), NF the number of phases (k), G the Gibbs energy, n_i^k and μ_i^k the number of moles and chemical potential of component i in the phase k.

Table 5.10 presents the outcomes of the thermodynamic study carried out at 180 °C and 100 bars, which correspond to the conditions yielding the maximal acetic acid output according to the experimental data from Cui et al. [202]. To establish the thermodynamic boundary for the reaction under comparable circumstances as described in the referenced literature [202], an input of 12 mmol/h of methanol and equivalent amounts of hydrogen and carbon dioxide for the Gibbs reactor was assumed.

Table 5.10: Thermodynamic analysis results for the system.

Variable	**Molar Flow (mmol/h)**
$CO_{2,reacted}$	11.546
$H_{2,reacted}$	15.363
$MeOH_{in}$	12.000
$MeOH_{out}$	4.40×10^{-5}
Acetic $Acid_{out}$	10.705
$Water_{out}$	13.682
$Methane_{out}$	2.136
$Ethanol_{out}$	3.96×10^{-8}
Methyl $Acetate_{out}$	5.64×10^{-7}
Ethyl $Acetate_{out}$	2.17×10^{-8}

The results are the thermodynamic limit for the system under evaluation, **i.e.** the maximum amount of acetic acid that could be produced is 10.705 mmol, which corroborates the experimental results of Cui *et al.* [202] that obtained the value of 8.18 mmol in a batch mode.

Figure 5.9 presents the sensitivity analysis for the variation in temperature in the production of ethanol, methyl acetate and ethyl acetate.

The temperature range explored was between 150 to 200 °C for the three components, with the highest value observed at 200 °C. In the modeling of the reactor, the conversion of reactions in Eq. 5.5.7c-5.5.7e assumed fixed maximum values for each component (Ethanol, Methyl Acetate, and Ethyl Acetate). This was due to the thermodynamic limitation in achieving the production of those components.

The solvent 1,3-dimethyl-2-imidazolidinone (DMI) was also included in the simulation. The

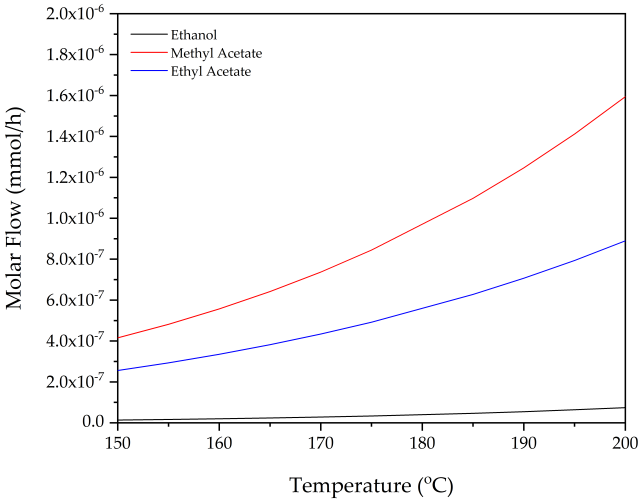

Figure 5.9: Molar flow of ethanol, methyl acetate and ethyl acetate.

temperature of the reactor was set to 180 °C and the pressure at 100 bar.

5.5.2.3 Reactor/Separator/Recycle

The input/output structure defines the material balance boundary of the flowsheet, which is often referred as the Inside Battery Limit Envelope (ISBL). The first decision regards the feed purification. In this case CO_2, H_2 (provided by alkaline water electrolysis [260]) and methanol enter in the reactor without previous purification and at the pressure and temperature specified.

The second key decision regards the recycling of reactants and auxiliary materials. In the proposed flowsheet, CO_2 and H_2 must be recycled to maintain the partial pressure in the reactor, and additionally the solvent and homogeneous catalyst must be recycled. Figure 5.10 presents the inside battery limit for the studied process flowsheet.

The third key decision is concerned the post-treatment of emissions and waste. In this process, the methane generated in the reactor is separated and directed to a flare system, where it is burned to produce energy for the plant. Simultaneously, the water produced undergoes purification and separation in the dehydration column.

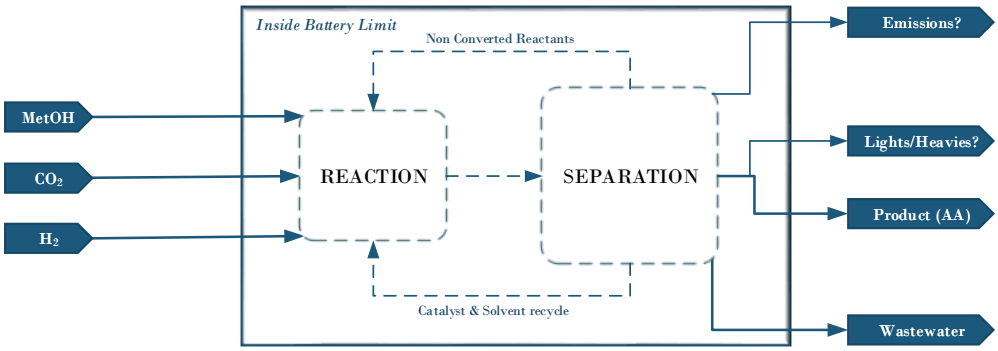

Figure 5.10: Input/Output structure of the acetic acid manufacturing.

5.5.2.4 Separation System

For the separation configuration, the formalism of task-oriented approach proposed by Barnicki and Fair [261, 262] was adopted. This methodology involves decomposing the separation synthesis problem into two main components: a gas/vapor recovery system and a liquid separation system. The reactor outlet is subjected to phase splitting before initiating the separation process.

The list-splitting technique, in which the components to be separated and their physical properties (**e.g.**, boiling points, melting points) are listed, and the list of techniques and the sequencing of these operations are obtained [263].

The main objective of the aforementioned scheme is to determine the alternatives for the separation system for further consideration, if coupled with short-cut screening techniques. The best alternative depends strongly on the Heat Exchanger Network (HEN) and design optimization for the complete process.

In the methodology of Dimian *et al.* [211], the Level 4 is the separation system. The first separation step (Level 4a) (see details in Section 5.4.2) is the split of the initial mixture in monophase submixtures (gas and liquid). According to Dimian *et al.* [211], simple flash or a sequence of flashes, adsorption/desorption and reboiled stripping, or the combination of these techniques can be employed. The reactor effluent is a heterogeneous gas/liquid stream, whose composition is shown in Table 5.11.

Table 5.11: Composition of the reactor effluent.

Component	**Mole Fraction (mol%)**	**Mole Flow (kmol/h)**
Methanol	1.46×10^{-6}	6.50×10^{-3}
CO_2	0.294	1309.897
H_2	0.323	1441.769
Acetic Acid	0.094	417.517
Methane	0.014	61.219
Methyl Acetate	1.36×10^{-6}	6.00×10^{-3}
Ehtyl Acetate	4.43×10^{-7}	1.98×10^{-3}
Ethanol	1.03×10^{-7}	4.58×10^{-4}
Solvent	0.175	781.725
Water	0.101	448.146

A first evaluation of phase separation may be obtained by performing a flash at 33 °C, where K-values larger than 10 are gas-phase components and smaller than 0.1 are condensing components. The K-values and the normal boiling points of the components are indicated in Table 5.12.

Table 5.12: Component ordered by boiling point.

Component	**Boiling Point (K)**	**K-value**	**Group**
H_2	20.39	4.75×10^{8}	Gas
Methane	111.66	87.37	Gas
CO_2	194.70	47.64	Gas
Methyl Acetate	330.09	1.09	Gas-Liquid
Methanol	337.85	4.42×10^{-1}	Gas-Liquid
Ehtyl Acetate	350.21	5.83×10^{-1}	Gas-Liquid
Ethanol	351.44	2.50×10^{-1}	Gas-Liquid
Water	373.15	1.03×10^{-1}	Gas-Liquid
Acetic Acid	391.05	6.77×10^{-2}	Liquid
Solvent	498.17	6.06×10^{-4}	Liquid

Pressure and temperature are optimisation variables against recovery of components in the corresponding vapour and liquid phases. In the study, two distinctive approaches were used: (A) one flash and (B) two flashes. The results are presented in Table 5.13.

Table 5.13: Molar flow in the vapor stream of flashes (kmol/h).

Component	**1 Flash**	**2 Flashes**				
	CO2 Recovery in vapor stream					
	98%	**98%**	**97%**	**96%**	**95%**	**94%**
H_2	1441.8	1441.8	1441.8	1441.8	1441.8	1441.8
CO_2	1231.6	1283.8	1270.6	1257.5	1244.4	1231.3
Methane	58.2	60.5	60.0	59.5	58.8	58.2
Water	16.8	49.3	33.7	25.4	20.3	16.8
Acetic Acid	10.7	30.7	21.0	15.9	12.7	10.6
Solvent	0.2	0.6	0.4	0.3	0.2	0.2
Methyl Acetate	1.73E-03	3.31E-03	2.71E-03	2.28E-03	1.97E-03	1.72E-03
Methanol	9.53E-04	2.20E-03	1.65E-03	1.33E-03	1.11E-03	9.50E-04
Ehtyl Acetate	3.54E-04	7.79E-04	6.02E-04	4.89E-04	4.10E-04	3.53E-04
Ethanol	4.13E-05	1.05E-04	7.57E-05	5.93E-05	4.86E-05	4.12E-05

The heuristic stated by Douglas [249] indicated that phase splits are the cheapest method of separation, therefore simple flash was used. A sensitivity analsys was carried out to pre-optimize the temperature and pressure of the flash (Figure 5.11).

The pre-optimized temperature of the flash was 38 °C, because of the restriction imposed by the lowest temperature available with cooling water (the cooling water approach ΔT is 5 °C), and pressure of 3.172 bar, selected as threshold between acetic acid recovery and CO_2 recovery.

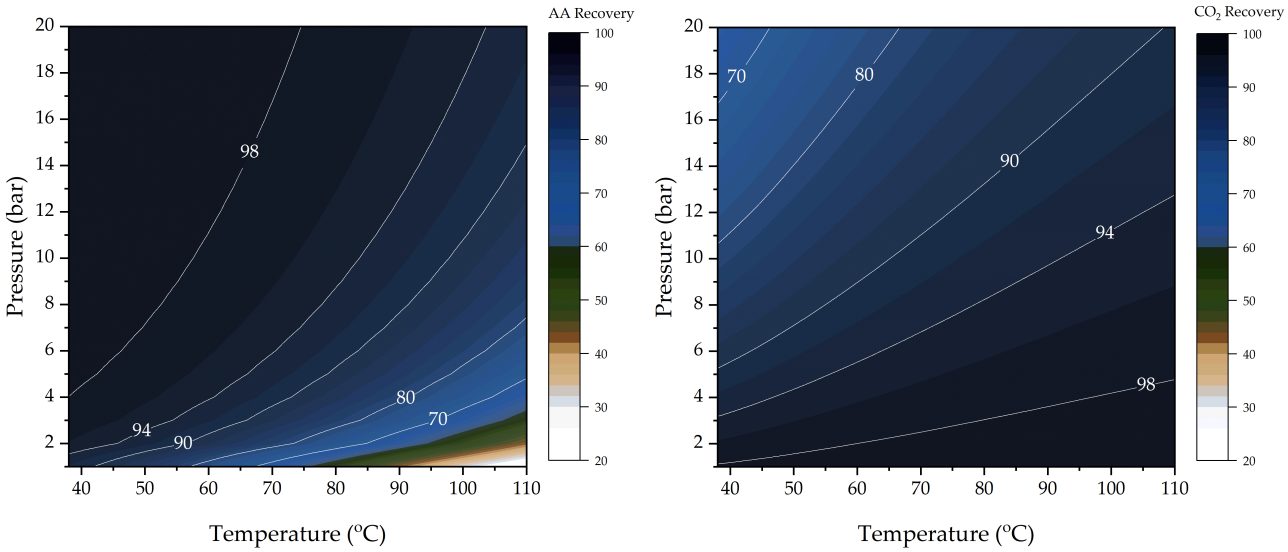

(a) (b)

Figure 5.11: Sensitivity analysis of pressure and temperature effect on recovery. (a) acetic acid recovery in liquid outlet stream and (b) CO_2 recovery in vapor outlet stream.

The pressure of the valve and the temperature of the cooler was adjusted to minimize the utility cooling requirements in the flash tank. Figure 5.12a depicts the schematic drawing and Figure 5.12b the results.

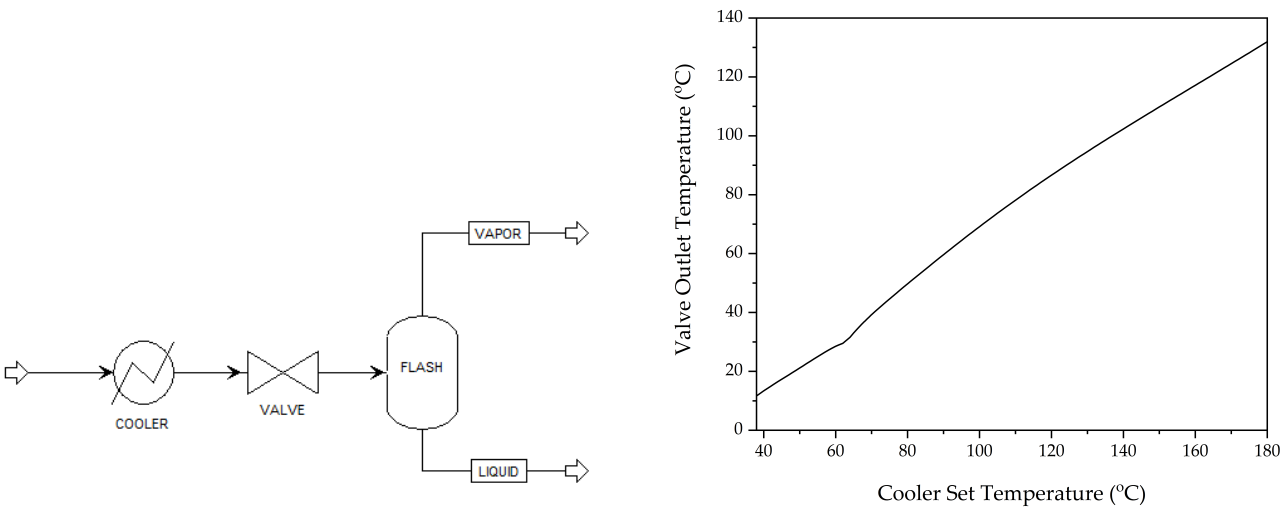

(a) (b)

Figure 5.12: Sensitivity analysis of temperature of the Cooler on the valve outlet stream. (a) schematic drawing and (b) cooler temperature.

Therefore, the most suitable temperature for the cooler before the valve is 70 °C, in order to achieve a temperature of the outlet of the valve around 38 °C.

5.5.2.5 Gas Separation System

The purpose of the gas recovery system is to remove or to recover valuable components from an exit gas stream or to prevent toxic components from leaving with a gas stream. According to [264] the most common techniques are a gas absorber, a refrigerated condenser with a flash drum, an adsorption bed, or a membrane.

For the generation of gas separation (Level 4b) (see details in [264]), an enrichment was coupled with purification to obtain a recycle stream with CO_2 and H_2 from the vapor split outlet.

The first part of the gas separation system is the removal of condensables and send them to the liquid separation system, while the non-condensable stream enters in the membrane module.

According to Ghasem et al. [265] the membrane technology offer a larger interfacial area while being significantly smaller and lighter than traditional CO_2 absorption towers, resulting in cost savings. Furthermore, their design promotes straightforward, linear scaling-up. Therefore, the membrane was selected as separation technology for this study.

A sensitivity analysis was carried out to select the best temperature and pressure of the condenser to remove the condensable components. The results are presented in Figure 5.13.

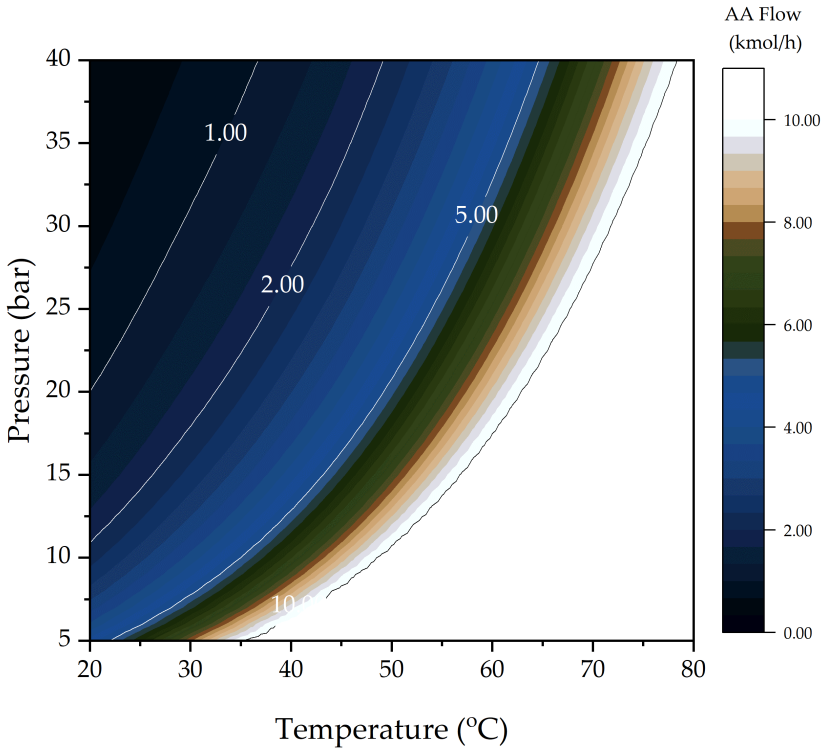

Figure 5.13: Sensitivity analysis of the vapor outlet stream of the condenser.

Higher pressures and lower temperatures favour the removal of acetic acid in the liquid flow of the condenser. The pre-optimized temperature and pressure were setted as 20 °C and 20 bar.

To simulate the membrane module, a model proposed by Pettersen and Lien (1994) [266] was used. It uses an analogy with the fundamental equation of heat exchangers as a shortcut design model for a hollow fiber module in counter-current operation. Several authors used the same model to simulate the membrane module [267–269]. The permeability and selectivity values for the polyimide membrane were obtained from Abetz et al. (2006) [270] and a connection with Aspen Plus and Excel was developed in the modeling. The outlet stream from the membrane module is recompressed and feeds the reactor.

Figure 5.14 depicts the sensitivity analysis for the membrane area on the outlet conditions. The selected area is 6000 m^2 to keep the impurities (methane, ethanol, ethyl-acetate and methyl-acetate), at least, below 2500 ppm, in order to have a cleaner recycle stream to the reaction system.

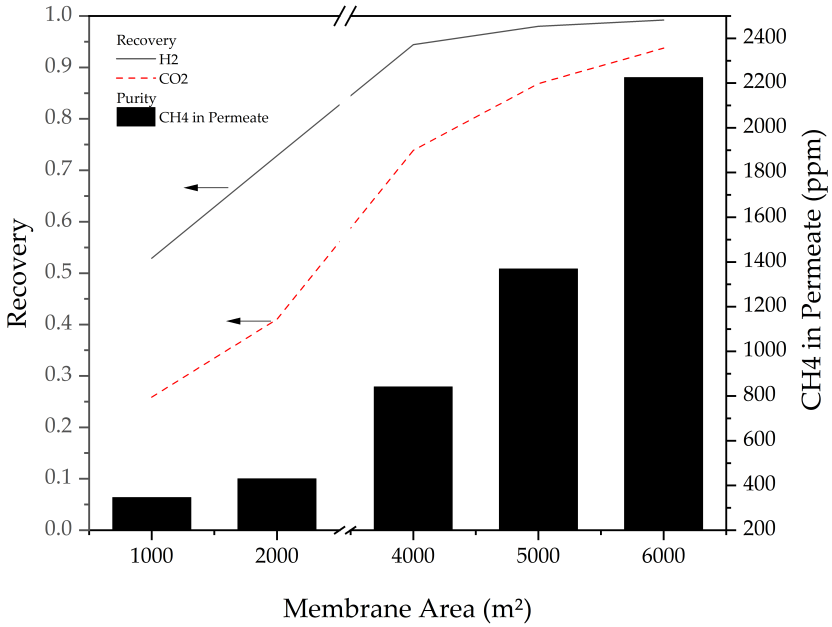

Figure 5.14: Sensitivity analysis of the conditions at oultet of the membrane module.

5.5.2.6 Liquid Separation System

The physical properties of acetic acid are well documented. In the design of distillation processes, accurate data is needed. Therefore, a thermodynamic analysis of the most important binary mixture in the system was performed.

Figure 5.15 depicts the prediction of the vapor liquid equilibria of the binary system acetic acid and water by three different thermodynamic models.

Some carboxylic acids can dimerize in the vapor phase due to the association between molecules and the association between different molecules. Acetic acid is one example and shows a high degree of non-ideality for the gas phase.

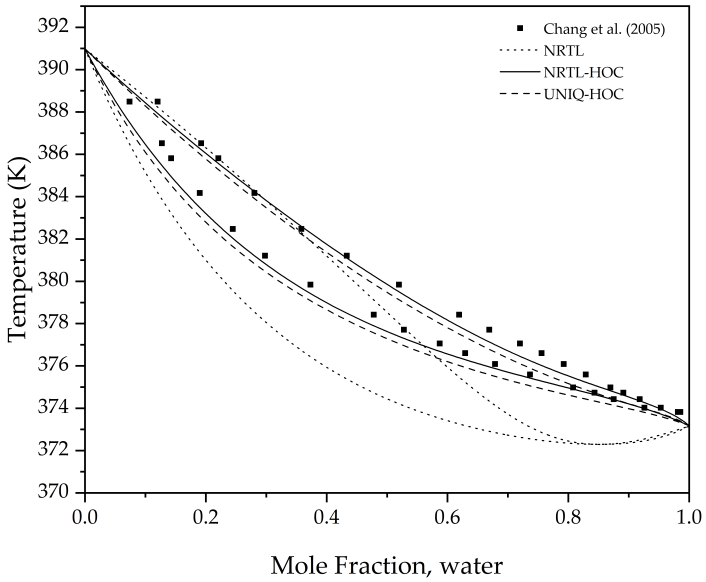

Figure 5.15: Vapor-liquid equilibria for the binary mixture acetic acid-water.

Hayden-O'Connell equation (HOC) applies to the fugacity calculation of gas mixture affected by association [271] and better predict the Vapor-Liquid Equilibrium (VLE) experimental data. Thus, the thermodynamic model NRTL-HOC was selected, where the Hayden-O'Connell equation correct the non-ideality of gas phase and the NRTL equation the liquid phase.

A Shortcut Distillation Column Model - Aspen Plus (DSTWU) was firstly used to estimate the parameters for a more Rigorous Distillation Column Model - Aspen Plus (RadFrac).

The solvent recovery column results for the shortcut column are present in Figure 5.16

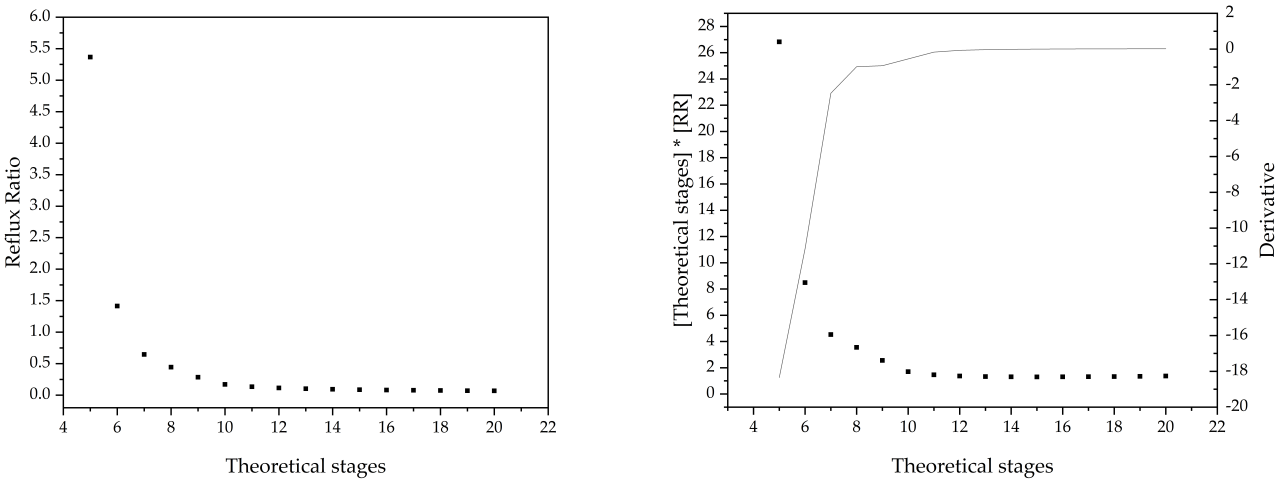

(a) (b)

Figure 5.16: Results for DSTWU column for solvent recovery. (a) reflux ratio and (b) cost estimation.

There is a relationship between the number of stages and reflux ratio in a separation process. At the extremes, a minimum number of stages would need infinite reflux, while a minimum reflux ratio would require an infinite number of stages. Between these extremes, there is an

approximately exponential decrease in reflux ratio with increasing stages. By plotting $N \cdot RR$ (number of stages times reflux ratio) on the y-axis, a curve with a minimum can be observed.

Increasing the number of stages results in higher capital costs for the column, while increasing the reflux ratio leads to higher operating costs due to increased material recycling and energy consumption. Hence, there is a tradeoff where larger columns have higher upfront costs but lower operating costs, while smaller columns have lower capital costs but are costlier to operate. The economic optimum typically lies around the minimum point of the $N \cdot RR$ vs. N curve, giving equal weight to both the number of stages and reflux ratio.

To account for real-world inefficiencies compared to the DSTWU model (which assumes complete equilibrium in each stage), a point slightly to the right of the minimum is chosen, signifying that additional stages may be needed in a real column to achieve the same separation efficiency as modeled in DSTWU.

The minimum value in the Figure 5.16b represents the lower cost for the operation and can be used as estimate in the RadFrac module. The parameters of purity were also optimized to meet the purity for the processing.

The dehydration column parameters were optimized based on the requirements for the final product [272]. The glacial acetic acid liquid is usually available as glacial acetic acid with 1 - 5 wt% water and over 95-99% purity [200, 272, 273].

The final stream meet the requirements (99.5%mol) and the lights contains ethanol, methyl acetate and ethyl acetate.

5.5.2.7 Process Flowsheet Analysis

Figure 5.17 introduces the proposed flowsheet. There are five distinct areas: (i) the feed conditioning and recompression, where the gases unreacted were recompressed, the solvent is mixed with the solvent make-up stream and the fresh reactants are introduced; (ii) the reaction system, where the reaction takes place; (iii) the liquid vapor split, to separate the effluent of the reactor into monophasic streams; (iv) the gas separation system and(v) the liquid separation system.

In the proposed flowsheet design methanol, (16.3 t/h), carbon dioxide (28.9 t/h) and hydrogen (0.8 t/h) react in a solvent media yielding acetic acid (25.1 t/h).

The gas separation system removes condensables, using compressors (6.5 MW), coolers (7.4 MW) and a membrane module (pressure drop of 23.9 bar), yielding a stream of 57.5 %mol of hydrogen and 42.4 %mol of carbon dioxide, requiring 14.8 MW of power for the recompression system.

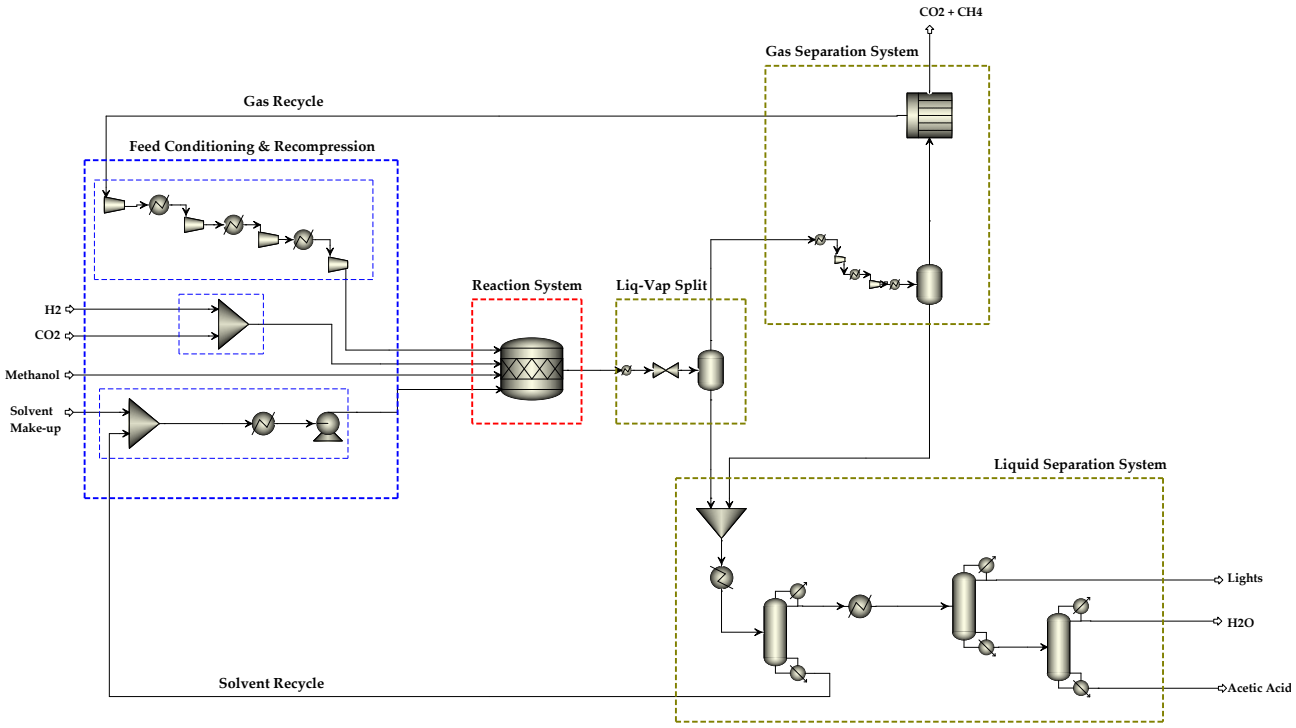

Figure 5.17: Proposed flowsheet for acetic acid production.

In the liquid separation system, the solvent recovery column (17 stages and the reflux ratio of 0.09) is followed by the second column (10 stages with a reflux ratio of 2.46) to remove the lights. The dehydration column is 40 stages with reflux ratio of 5.71. Similar results were found by Feyzi and Beheshti (2017) [274].

In comparison to the conventional method of methanol carbonylation, this innovative route from CO_2 exhibits a configuration that shares similarities with its conventional counterpart. Industrial applications of the methanol carbonylation process have employed various homogeneous metal-organic complexes as catalyst, based on cobalt, rhodium, ruthenium, or iridium. These catalysts operate at temperatures ranging from 150 to 300°C and pressures around 60 bar [275]. In this study, a catalyst and solvent are also utilized, with the temperature range between 170 and 190°C and a pressure of 100 bar, thus exhibiting similarities to the proposed process.

Commercialized methanol carbonylation processes by BASF, Monsanto, Cativa, and Acetica can be represented by a simplified flowsheet. These processes typically involve a liquid phase slurry reaction, a flash separation tank for catalyst separation, and a separation unit to obtain pure acetic acid. The catalyst remains in the liquid phase and is recycled back to the reactor. However, the separation of the homogeneous catalyst presents challenges [276]. Similarly, the proposed process incorporates a separation unit to separate and recycle the solvent and catalyst. Additionally, the inclusion of a final column in the proposed process aligns closely with the traditional route, primarily for water separation purposes and acetic acid purification.

5.5.3 Exergetic Results

In order to perform exergy analysis, an exergetic balance was performed for each subsystem of the flowsheet (feed conditioning and recompression, reaction system, liquid-vapor split, gas separation system and liquid separation system), according to Figure 5.17.

For identification of the magnitude and location of the inefficiencies, a Grassmann chart is useful as depicted in Figure 5.18.

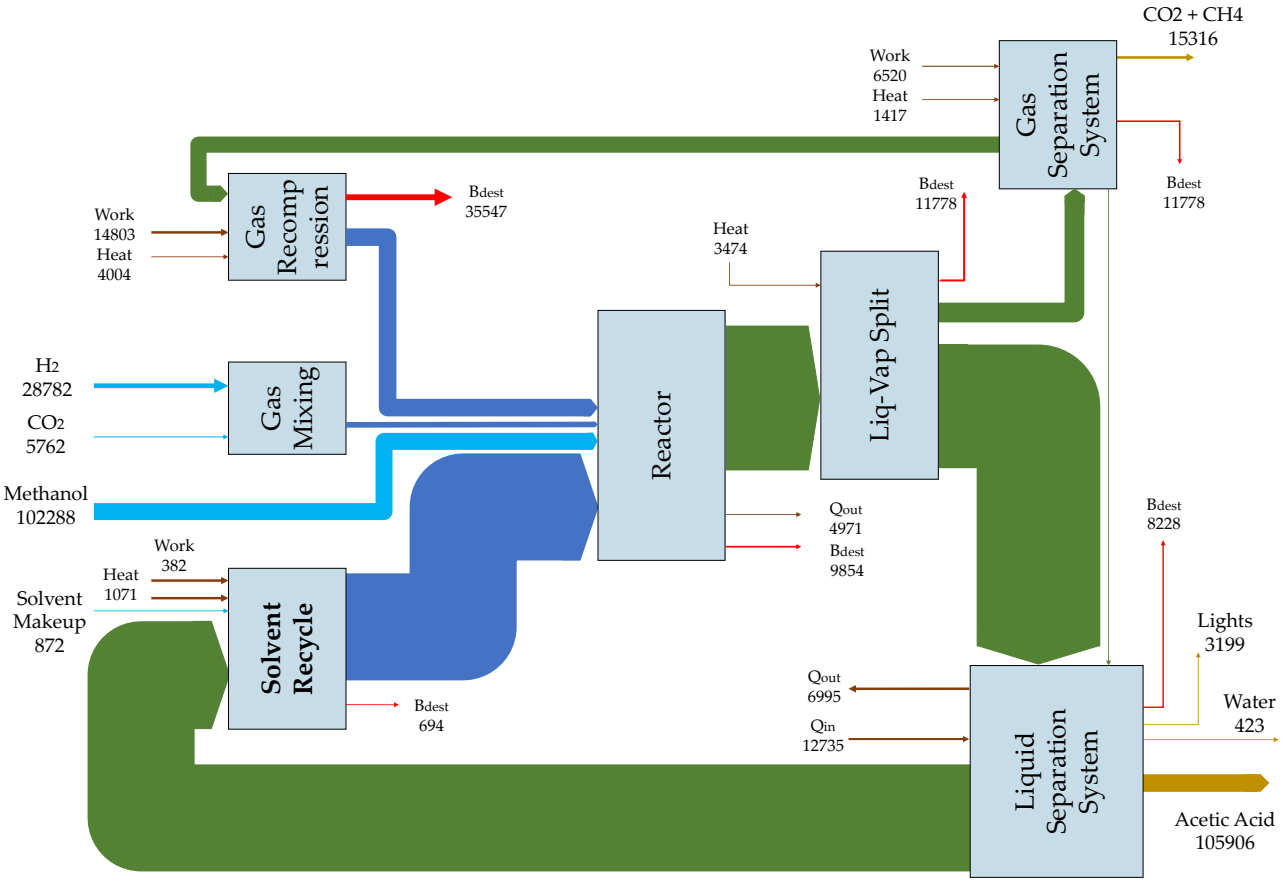

Figure 5.18: True to scale exergy flow diagram (Grassmann chart) for acetic acid production. The main flows are shown.

Blumberg *et al.* [41] performed an exergetic analysis for the synthesis of methanol from CO_2 and the integration with three different reforming processes. The author pointed out the locations of the main inefficiencies in the process.

Exergy destruction (also known as exergy loss or *Bdest*) refers to the irreversibilities and inefficiencies within a system that lead to a decrease in the potential of the energy to perform useful work. When energy undergoes transformations and interactions in a real-world system, it tends to degrade and disperse, resulting in a decrease in its ability to do work.

Common sources of exergy destruction include:

- Heat transfer across finite temperature differences: When heat is transferred from a high-temperature source to a low-temperature sink, there is an irreversibility that results in exergy destruction.
- Friction and mechanical losses: In mechanical systems, frictional forces and mechanical inefficiencies cause exergy destruction.
- Mixing of different substances: Mixing two substances at different states can lead to exergy destruction due to the non-recoverable nature of mixing.
- Chemical reactions: In chemical processes, irreversible reactions can lead to exergy destruction.

Similarly, in this work the areas with more inefficiencies can be mapped. The thermodynamic inefficiencies occur mainly within the gas separation system, the gas recompression and in the liquid separation system, indicating units or areas to be optimized, based on the values of $Bdest$.

Other methods of separation can also be used, for example: reactive distillation [277], azeotropic distillation [278, 279], membrane pervaporation ,liquid-liquid extraction [280] or hybrid extraction-distillation [281, 282]. The drawback of simulate such processes is the lack of experimental data regarding the specific system under assessment.

5.6 Conclusions

This study presented an assessment of acetic acid production routes from CO_2 through a multicriteria decision analysis, in order to select the most advantageous route in terms of process characteristic and energy demand.

The attributes of different routes were compared, and the methanol hydrocarboxylation route demonstrated to be the most promising and it was deeper studied. The exploration of alternative routes for acetic acid production within the field of chemical engineering has led to the development of an innovative process. While sharing a similar configuration with the traditional methanol carbonylation method, this process introduces adjustments in temperature and pressure ranges. By addressing the separation challenges associated with homogeneous catalysts and incorporating efficient separation units, the proposed process aims to enhance the overall sustainability and efficiency of acetic acid production. To the best of our knowledge the literature data regarding the process design of acetic acid production from CO_2 is scarce. Therefore, this work contributes to the field of process synthesis of CO_2 conversion to high added value products.

The flowsheet of the production process was designed based on process synthesis and demon-

strated to be feasible. The exergy analysis pointed out the locations and magnitude of thermodynamic inefficiencies that can be improved for better design.

Chapter 6

Process Flowsheet of CO_2 based Methanol and Dimethyl Ether

Drawing on the findings of Chapter 4, this chapter offers an evaluation of the processes related to Methanol and Dimethyl Ether (DME), recognizing the inherent synergies between them, they will be jointly examined. Following the analysis of acetic acid production in the previous chapter, this section completes the appraisal of potential products. The chosen flowsheets for these products were based on the current state of the art in carbon dioxide utilization. For methanol production, the CO_2 hydrogenation route was selected, while for DME production, the methanol dehydration route was chosen. The study's findings demonstrate the technical feasibility of these processes, resulting in the production of 170 kt/y of methanol (99%wt) and 150 kt/y of DME (99%wt). Process engineering and modeling play a crucial role in chemical engineering. By employing mathematical models and simulations, valuable insights into the behavior of the selected chemical processes can be gained. Furthermore, these tools help identify areas that can be optimized to enhance overall process efficiency.

Contents

6.1 Methanol Production Processes

Methanol (CH_3OH) is a chemical compound with numerous industrial applications, including the production of formaldehyde, acetic acid, and gasoline additives. Also, it is currently used in the chemical industry as an intermediate to formaldehyde, methyl tert-butyl ether, acetic acid, dimethyl ether, among others, and an emerging market for olefins. Methanol derived from renewable sources offers a major promise as the demand keeps growing [112].

Figure 6.1 describes a general process flow diagram for producing methanol either from syngas or by CO_2 hydrogenation. Initially, a mixture of CO_X and hydrogen undergoes a reaction in a heterogeneous reactor, resulting in the production of methanol. The effluent stream is subsequently cooled and separated in a flash. In this flash, methanol is separated as a liquid stream, while the unreacted gases are recycled back to the reactor. The liquid stream is then directed to a sequence of distillation columns to obtain high-purity methanol. Kiss *et al.* [283] provides further details on this process.

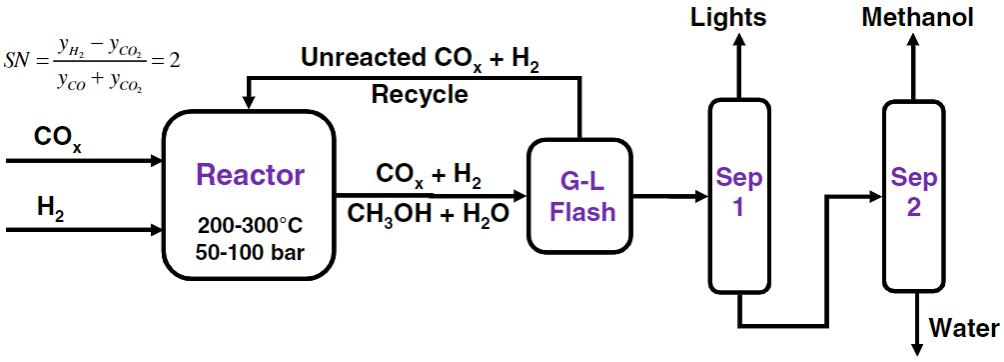

Figure 6.1: Generic process flow diagram used to produce methanol from syngas or CO_2 hydrogenation. Source: Kiss *et al.* [283].

6.1.1 Conventional Technological Route

The conventional technology for methanol production is the synthesis gas process developed during the 1920s. It involves the conversion of natural gas, coal, or biomass into synthesis gas (syngas), a mixture of carbon monoxide, carbon dioxide, and hydrogen. This syngas is then converted into methanol in a catalytic synthesis.

The technological aspects of the traditional methanol production process can be divided into three main stages: syngas production, syngas purification, and methanol synthesis.

In the first stage, syngas can be produced by natural gas reforming or biomass (or coal) gasification. In the case of natural gas, the gas is first desulfurized and then mixed with steam before being heated to high temperatures in a reformer. The resulting syngas contains varying amounts of carbon monoxide, carbon dioxide, and hydrogen, depending on the feedstock used.

The second stage involves the purification of the syngas to remove impurities such as sulfur compounds, ammonia, and particulates. This is accomplished through a series of processes, including cooling, compression, and scrubbing with chemicals such as amine and potassium carbonate. The resulting purified syngas is then ready for the methanol synthesis.

The final stage is the methanol synthesis, which involves the conversion of the purified syngas into methanol using a catalyst, typically copper or iron oxide. The syngas is first compressed to high pressures and then heated to around 250-300^{o}C in the presence of the catalyst. The resulting methanol vapors are cooled and condensed, resulting in a liquid product that is typically 99.5% pure. Overall, the traditional methanol production process is a complex and energy-intensive process that requires careful control and optimization of each stage to ensure maximum efficiency and product quality.

There are some specific technologies for process using syngas route, the Linde Process, Toyo Process and other minor contributing routes.

In the Linde process, methanol is produced from synthesis gas, using steam reforming or partial oxidation of hydrocarbons or a combination of both processes. The methanol synthesis occurs in an isothermal reactor. It is a fixed bed reactor cooled and maintained at optimum operating temperature through steam production in the pipe interiors [284].

In the Toyo process, syngas is generated in a top-fired steam-methane reformer at temperatures in the range of 750 - 875 ^{o}C and pressures of 15 - 30 atm. Prior steam reforming, the natural gas passes through an adiabatic pre-reforming step at 500 - 650 ^{o}C. The syngas generated is compressed at about 100 atm and feeds the Toyo's reactor (MRF-Z reactor). The reaction temperature is 464-500 ^{o}C and the catalyst is a cooper-based compound promoted by ZnO [285].

There are other technological processes, such as ICI Low Pressure Methanol Synthesis Process, Haldor Topsoe, DAVY technology. All these technologies use low pressure and combined reforming processes to obtain the best H_2/CO_2 molar ratio for increasing methanol synthesis yield and decrease the energy consumption and operational costs.

6.1.2 Innovative Technological Route

The production of methanol, like many other industrial processes, has significant environmental impacts. The traditional methanol production process, which relies on fossil fuels, can generate large amounts of greenhouse gas emissions, contribute to air pollution, and lead to water contamination. However, there are also opportunities to mitigate these environmental impacts through technological advancements, process improvements and alternative sources as raw materials.

Recently, the use of CO_2 has received attention as an alternative to replace the syngas in the methanol production. There are different routes to produce methanol. One of them is through direct hydrogenation of CO_2 [286]. Other options include reforming processes, namely bi-reforming [287, 288] or tri-reforming [289, 290]. In the direct hydrogenation process, carbon dioxide and hydrogen are converted in methanol and water [291].

Carbon Recycling International (CRI), a well-known global leader in converting CO2 into methanol, has been successfully operating on an industrial scale since 2012. In October 2022, the world witnessed the launch of the first-ever commercial-scale CO_2-to-methanol plant in Anyang, Henan Province, China. This state-of-the-art facility is unparalleled in its ability to produce methanol at such a large scale using captured waste carbon dioxide and hydrogen gases. The plant's production process relies on CRI's innovative Emissions-to-Liquids (ETL) technology, which was initially demonstrated in Iceland. The plant has the capacity to capture 160,000 tonnes of carbon dioxide emissions annually. These captured emissions are then combined with recovered hydrogen in CRI's exclusive ETL reactor system, capable of producing 110,000 tonnes of methanol per year. CRI's second large-scale project in China, a 100,000-tonne-per-year methanol plant for Jiangsu Sailboat Petrochemicals, is progressing as planned and is set to commence operations in the latter half of 2023 [292].

Wiesberg *et al.* [40] studied different routes to produce methanol using CO_2: (i) Route A: direct hydrogenation and (ii) Route B: bi-reforming of Natural Gas (NG). The results showed that the utilization of CO_2 in Route A (fed from an integrated bioethanol plant) is 5 times greater than Route B (0.28 $t_{CO2}/t_{methanol}$), for a given methanol production. Regarding the economic aspects, Route A is more competitive, however, both cases are infeasible due to the price of electricity and NG.

Nizami, Slamet and Purwanto [293] performed a techno-enviro-economics analysis for the synthesis of methanol by CO_2 hydrogenation using renewable hydrogen from photovoltaic-based electrolysis, the CO_2 was provided by a natural gas field processing. The results showed an increase in overall energy efficiency when heat integration was applied to the integrated hydrogen production and methanol synthesis.

Basini *et al.* [294] proposed an innovative process design for converting CO_2 into methanol, including a system for water electrolysis, an electrified reverse water gas shift reactor, and the methanol synthesis reactor. The authors pointed out that negative CO_2 emission can be achieved if a biogas plant CO_2 derived is used.

Yousaf *et al.* [295] studied the CO_2 hydrogenation process using different hydrogen production sources. They compared the cost of methanol production when H_2 is produced via Alkaline Water Electrolyzer (AWE) or via a high temperature Solid Oxide Electrolyzer Cell (SOEC). The

results indicated 22.3% reduction in the cost of hydrogen for SOEC as compared to the AWE as the source of hydrogen production when integrated with the CO_2 hydrogenation process.

Cordero-Lanzac *et al.* [296] presented a study for the production of green methanol from renewable H_2 and CO_2, including catalyst, plant and techno-economic/lifecycle analysis. The results indicated that CO_2 can be abated only if renewable energy is used to run the process (up to 1.75 $t_{CO2}/t_{methanol}$). A profitable methanol plant can be achieved if either a rock-bottom H_2 prices (1.5 \$/kg) or CO_2 taxation (300 \$/ton).

Campos *et al.* [297] evaluated the addition of two intermediate condensation units in methanol synthesis to increase CO_2 conversion. Detailed simulations and analyses compare the proposed process with the conventional approach. The new process achieves a significantly higher CO_2 conversion of 53.9% compared to the conventional process (28.5%) and equilibrium conversion (30.4%). This reduces the total recycle stream flow by half, resulting in lower operating costs (4.8% reduction) and fixed investment costs (22.7% decrease). Intermediate condensation steps are found to be beneficial, boosting CO_2 conversion and reducing both investment and operating costs in methanol synthesis.

6.2 Dimethyl Ether Production Routes

Dimethyl ether (DME) is a versatile gas that has a wide range of applications in various industries. One of the primary applications of DME is as a fuel, for transportation and heating. DME is a clean-burning fuel that produces very low emissions of particulate matter and sulfur oxides, making it an attractive alternative to diesel fuel in areas with strict emissions regulations [298, 299].

In addition to its use as a fuel, DME has several other applications in the chemical industry. For example, it can be used as a feedstock for the production of olefins, which are used in the production of plastics, fibers, and other materials. DME can also be used as a solvent in the production of pharmaceuticals and other chemicals, as well as a propellant in aerosol sprays.

Dimethyl Ether world production is increasing from 3740 kt/y in 2014 to 5000 kt/y today and the prevision of yearly growth of 19.65% between 2015 and 2020 and its global market is US\$ 6 billion in 2017 [300].

Major DME manufacturers are Akzo Nobel, Royal Dutch Shell, The Chemours Company, China Energy Limited, Mitsubishi Corporation, Ferrostal GmbH, Grillo Werke AG, Jiutai Energy Group, Oberon fuels and Zagros Petrochemical Company. Licensors of technology are installing a dehydration unit in high-capacity existing methanol plants, such as Toyo (6 kt/d) and Lurgi (5 kt/d) [301].

The traditional DME production process begins with the production of methanol, which is typically synthesized from natural gas or coal. Methanol is then converted into DME through a process known as dehydration. In this process, methanol is mixed with a catalyst, typically a zeolite, and heated to a high temperature, causing the methanol molecules to loose a molecule of water and form DME.

The conversion of methanol into DME can take place in either a fixed bed or fluidized bed reactor. In a fixed-bed reactor, the catalyst is placed in a fixed position within the reactor and the reactants are passed through it. In a fluidized bed reactor, the catalyst is suspended in a fluid, typically an inert gas such as nitrogen, and the reactants are passed through the fluid, causing the catalyst to become fluidized.

After the reaction is complete, the mixture of DME and unreacted methanol is separated from the catalyst and purified. The separation is typically achieved by distillation, with the DME and methanol being separated based on their boiling points. The purified DME can then be stored or transported for use as fuel or propellant [302].

Several technological aspects of the conventional DME production process are important for optimizing its efficiency and reducing its costs. The separation process is an important step because it affects the purity of the DME product and the amount of energy required to achieve the separation. Distillation is the most commonly used separation method, but it can be energy-intensive and costly. Other separation methods, such as membrane separation, may offer advantages in terms of energy efficiency and cost.

The manufacture of DME is currently based on fossil fuel derived syngas (indirect route or two steps process). However, alternative eco-efficient routes have been studied, e.g. CDU based routes, called direct route, using only one step. The indirect route involves: (i) the synthesis of synthesis gas (a mixture of hydrogen and carbon monoxide) by gasification of biomass or natural gas, (ii) the synthesis gas is then converted to methanol, which is subsequently dehydrated to produce DME. On the other hand, in the direct route, the synthesis of DME is directly from syngas or, more recently, from CO_2.

Schakel *et al.* [303] evaluated the techno-environmental performance of CO_2 utilization through dry reforming of methane into syngas for the production of DME in a refinery. The results show that although 94% of the captured CO_2 can be utilized for DME production, only 9% of CO_2 is avoided in the entire process due to direct CO_2 formation during DME synthesis and the syngas combustion. The study suggests that this utilization route lowers the Climate Change Potential (CCP) by 8%.

Dias *et al.* [304] discussed the estimation of CO_2 emissions from industrial processes for the production of dimethyl ether using two different processes. The results pointed out that the

process using a water-cooled reactor was more eco-efficient, providing opportunities for reducing CO_2 emissions through modifications in new projects or improvements in existing plants.

A process for direct production of DME from shale gas integrated with CO_2 capture has been developed by Mevawala, Jiang and Bhattacharyya [305]. The study evaluated the pre-reforming reactor, Autothermal Reforming (ATR) reactor, and DME synthesis reactors. The effects of key parameters like CO_2 recycle ratio and H_2/CO ratio on utility consumption in the syngas synthesis unit, Acid Gas Removal (AGR) unit, DME synthesis unit, and DME separation unit were studied. The direct shale gas to DME production process has a higher DME yield and overall equivalent electrical efficiency than the indirect process.

Michailos *et al.* [306] evaluated the technical and economic feasibility of producing DME via captured CO_2 hydrogenation within a power-to-liquid context, achieving 82.3% CO_2 conversion to DME with a 44.4% global energy efficiency. The electrolysis unit appears to be the main factor affecting the ecomomic feasibility.

A polygeneration plant with carbon capture for combined power and DME production is presented in the study of Farooqui *et al.* [307], integrating a chemical looping CO_2/H_2O splitting (CL) unit producing syngas for DME synthesis using oxyfuel power cycle exhaust gases. The process achieved 50.2% energy efficiency, 45% exergetic efficiency. The economic analysis showed the potential of integrating chemical looping CO_2/H_2O splitting for syngas production into polygeneration systems to increase overall efficiency while reducing the cost of carbon capture.

Fernández-Dacosta *et al.* [308] studied the one step process, that is a single reactor with a bifunctional catalyst that promotes the methanol synthesis and the methanol dehydration focuses on the economic and environmental performance. They concluded that CO_2-based fuels have limited practical relevance due to the lack of a favorable combination of cost and environmental performance, unless CO_2 is of non-fossil origin (from biomass combustion or captured from air). The study also highlights methodological challenges in carbon accounting for CO_2-based fuels, emphasizing the importance of considering the entire system (power and CO_2-fuel production) to avoid allocation issues.

The environmental performance of a CO_2-enhanced gasification based bio-DME production process was evaluated and compared to the conventional approach in terms of life cycle assessment impacts. The results showed that the CO_2-enhanced process significantly reduced the burden on climate change, toxicity, and eco-toxicity by at least 20%, mainly due to low feedstock consumption, high-energy recovery, and CO_2 utilization [309].

The production of DME is a complex process that involves several steps, each with its own set of challenges. One of the primary challenges faced in the production of DME is the efficient

removal of water from the reactor. The presence of water can interfere with the catalytic process and reduce the yield of DME.

Lastly, plant optimization is critical for improving the overall efficiency of the DME production process. This involves identifying areas where energy consumption can be reduced, optimizing process conditions, and minimizing waste generation. Plant optimization can lead to significant cost savings, improve the sustainability of the production process, and increase the competitiveness of the DME industry. Overall, the challenges faced in the production of DME are significant, and addressing them requires a thorough understanding of the process.

6.3 Methods

On the basis of the most recent developments in CDU, an integrated flowsheet were proposed to produce methanol and dimethyl ether from carbon dioxide.

6.3.1 Methanol Process Synthesis

The route of hydrogenation of CO_2 was evaluated by modeling and simulation. Literature data are available to validate the model [286].

The synthesis of methanol from CO_2 over Cu/ZnO catalyst can be represented by two main kinetic models: the work of Graaf, Stamhuis and Beenackers [310], where the authors proposed a kinetic model based on three independent reactions; and Bussche and Froment [311] that assumed that the main source of carbon in methanol is from CO_2, while the conversion of CO is given by the Water Gas Shift (WGS) reaction.

In this work, the kinetic model from Bussche and Froment [311] with modifications proposed by Mignard and Pritchard [312] was implemented in Aspen Plus. The corresponding rate equations for the kinetic model are described in Eq. 6.3.1 - 6.3.2.

$$r_{MeOH} = \frac{k'_{5a} K'_2 K_3 K_4 K_{H_2} \cdot P_{CO_2} P_{H_2} \left[1 - \left(\frac{1}{K*}\right)\left(\frac{P_{H_2O} P_{CH_3OH}}{P^3_{H_2} P_{CO_2}}\right)\right]}{\left[1 + \left(\frac{K_{H_2O}}{K_8 K_9 K_{H_2}}\right)\left(\frac{P_{H_2O}}{P_{H_2}}\right) + \sqrt{K_{H_2} \cdot P_{H_2}} + K_{H_2O} \cdot P_{H_2O}\right]^3} \tag{6.3.1}$$

$$r_{RWGS} = \frac{k'_1 \cdot P_{CO_2} \left[1 - K^*_3 \left(\frac{P_{H_2O} P_{CO}}{P_{H_2} P_{CO_2}}\right)\right]}{\left[1 + \left(\frac{K_{H_2O}}{K_8 K_9 K_{H_2}}\right)\left(\frac{P_{H_2O}}{P_{H_2}}\right) + \sqrt{K_{H_2} \cdot P_{H_2}} + K_{H_2O} \cdot P_{H_2O}\right]} \tag{6.3.2}$$

The generalized rate expression to be used in Aspen Plus is:

$$r = \frac{(\text{kinetic factor})\,(\text{driving force expression})}{(\text{adsorption term})} \tag{6.3.3}$$

when a reference temperature T_0 is not specified, the kinetic factor in Aspen Plus is expressed by a pre-exponential factor and an Arrhenius term:

$$\text{kinetic factor} = kT^n e^{\frac{-E_a}{RT}} \tag{6.3.4}$$

To rearrange Eq. 6.3.1 for the process simulator as described in Eq. 6.3.4, the numerator must be rearranged.

$$\begin{aligned} k_A &= k_{5a}^{'} K_2^{'} K_3 K_4 K_{H_2} \\ k_A &= 1.07 \times 10^{-13} \qquad \text{kmol/kg}_{cat}\text{.s.Pa}^2 \end{aligned} \tag{6.3.5}$$

The kinetic model can not be inputted directly into the process simulator, and a rearrangement in the equations must be performed as presented in Eq. 6.3.6.

$$r_{MeOH} = \frac{\overbrace{k_A \cdot P_{CO_2} P_{H_2}}^{\substack{\text{Driving Force Expression} \\ \text{(TERM 1)}}} \quad \overbrace{- k_B \cdot \frac{P_{H_2O} P_{CH_3OH}}{P_{H_2}^2}}^{\substack{\text{Driving Force Expression} \\ \text{(TERM 2)}}}}{\underbrace{\left(1 + k_C \cdot \frac{P_{H_2O}}{P_{H_2}} + k_D \cdot \sqrt{P_{H_2}} + k_E \cdot P_{H_2O}\right)^3}_{\text{Adsorption Expression}}} \tag{6.3.6}$$

A similar procedure was done for Eq. 6.3.2, as described in Eq. 6.3.7.

$$r_{RWGS} = \frac{k_F \cdot P_{CO_2} - k_G \cdot \frac{P_{H_2O} \cdot P_{CO}}{P_{H_2}}}{1 + k_C \cdot \frac{P_{H_2O}}{P_{H_2}} + k_D \cdot \sqrt{P_{H_2}} + k_E \cdot P_{H_2O}} \tag{6.3.7}$$

The original parameters for the Eq. 6.3.1 - 6.3.2 are described in Table 6.1. The rearranged values are described in details in Appendix E.

In this study, the byproducts were not considered [313]. To describe the thermodynamic behavior of the vapor-liquid equilibrium, the NRTL-RK model was employed. The model incorporates thermodynamic parameters and activity coefficients to capture the non-ideal behavior of the components and ensure a realistic representation of the system under study.

For the raw materials input, the CO_2 stream is considered to be provided by a typical CO_2

Table 6.1: Original Parameters for the kinetic model from Bussche and Froment [311].

κ		**Value**
$\sqrt{K_{H_2}}$	A	0.499
	B	17,197
K_{H_2O}	A	6.62 x 10-11
	B	124,119
$\frac{K_{H_2O}}{K_8 K_9 K_{H_2}}$	A	3,453.38
	B	-
$k'_{5a} K'_2 K_3 K_4 K_{H_2}$	A	1.07
	B	36,696
k'_1	A	1.22 x 10-10
	B	-94,765

separation process with amine-based absorption-regeneration method for capturing CO_2 (MDEA), developed at industrial scale and widely considered as the benchmark for the purification of large industrial CO_2 emitters [291, 314].

The H_2 feed stream is considered to be provided alkaline water electrolysis due to the main commercialized technique producing hydrogen (purity level of 99%) [260].

6.3.2 DME Process Synthesis

The dehydration of methanol route (two steps process) was selected for this study. Methanol is feed to the DME reactor with a mono functional catalyst where dehydration occurs as described in Eq. 6.3.8.

$$2\,\mathrm{CH3OH} \rightleftharpoons \mathrm{CH3OCH3} + \mathrm{H2O} \tag{6.3.8}$$

The kinetics of the methanol dehydration reaction over an acidic γ-Al_2O_3 catalyst was proposed by Berčič and Levec [315, 316], as presented in Eq. 6.3.9.

$$r_{MeOHdehydration} = \frac{k_H K^2_{\mathrm{CH3OH}} \cdot \left(C^2_{\mathrm{CH3OH}} - \frac{C_{\mathrm{H2O}} C_{DME}}{K_{eq,MeOHdeh}}\right)}{\left(1 + 2\sqrt{K_{\mathrm{CH3OH}} C_{\mathrm{CH3OH}}} + K_{\mathrm{H2O}} C_{\mathrm{H2O}}\right)^4} \tag{6.3.9}$$

The original parameters from Berčič and Levec [315] were used in the simulation. The equilibrium constants (K_i) and constant rate values (k_i) used to determine the reaction rate are described in Table 6.2. The thermodynamic equilibrium constant parameters ($K_{eq,MeOHdeh}$) were obtained from Diep [317].

The methanol dehydration reactor is modeled as a Plug Flow Reactor (PFR) with Langmuir-

Table 6.2: Kinetics coefficients for methanol dehydration [315].

parameter	equation
k_H	5.35×10^{13} exp(-17280/T)
K_{CH3OH}	5.39×10^{-4} exp(8487/T)
K_{H2O}	8.47×10^{-2} exp(5070/T)

Hinshelwood-Hougen-Watson (LHHW) kinetics (the detailed Aspen Plus implementation is presented in Appendix F), operating adiabatically at 12 bar, in accordance with literature range of pressures [304, 305]. The reaction takes place over Al_2O_3 catalyst with particle density of 1470 kg/m^3 and bed voidage of 0.4 [305, 318]. The reactor lenght is 10 meters to meet the DME production specified. The DME purification column and methanol-water separation column are modeled as equilibrium-based models.

When it comes to the synthesis of DME, a specific aspect to consider is that only methanol derived from the methanol synthesis unit is utilized in the process. This means that no other feedstocks or reactants are introduced during the synthesis of DME.

The selectivity for the DME synthesis via methanol dehydration is close to 100%. By-products are therefore neglected in the simulation. The mixing gap of the ternary component system methanol/water/DME is bypassed [302].

For the separation system, a shortcut distillation column model was firstly used to estimate the parameters for a rigorous distillation column (RadFrac), in which the parameters were optimized to meet the purity requirement for AA grade methanol and DME, and also fulfill the requirements for DME as a fuel according to ISO 16861 [319]. The process of purifying the product is comparable to those described in the literature [291, 318].

6.4 Results and Discussion

In this section, the results and discussions of the simulation of the selected processes are presented. The kinetics validation comparing the implementation in the simulator are also presented.

6.4.1 Kinetics Validation

In order to validate the kinetics of methanol synthesis and DME synthesis, a comprehensive simulation was carried out using Aspen Plus software. This simulation aimed to assess the accuracy and reliability of the implemented reaction kinetics involved in these processes. The simulation results were compared with available literature data as depicted in Figure 6.2. This

comparison served as a means to assess the agreement between the modeled reactions kinetics and the experimental data reported in previous studies [311, 315].

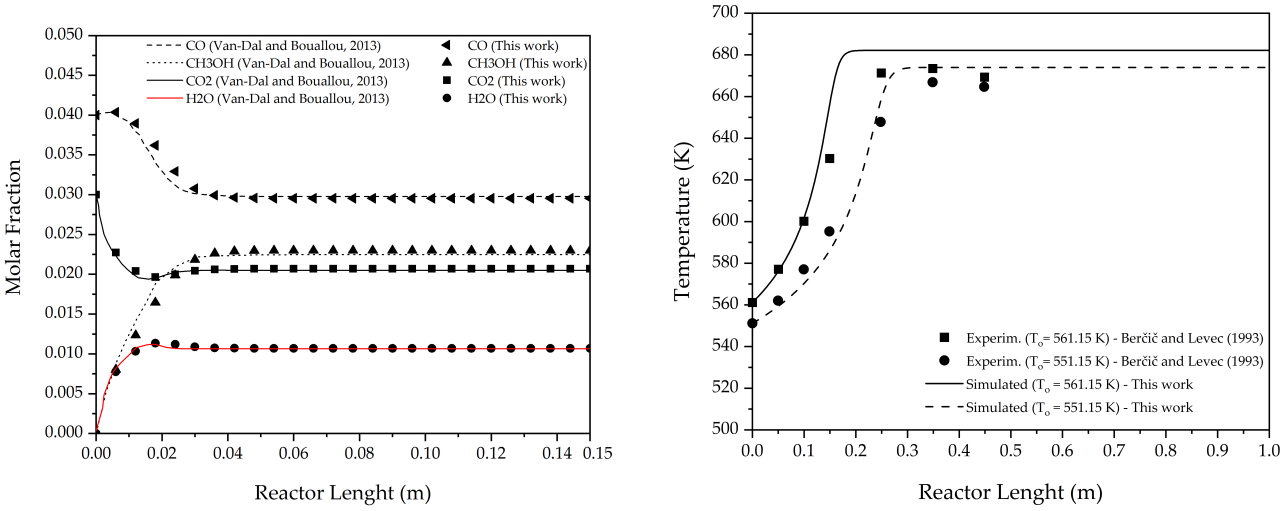

(a) (b)

Figure 6.2: Validation of kinetics equations implementation for (a) Methanol Synthesis and (b) DME Synthesis.

It is possible to verify the good agreement between this study and the reported literature values. The Figure 6.2a depicts the behaviour of the methanol synthesis, the results follow the pattern of the literature, and deviations are observed in the first portions of the reactor, however all within 10% difference.

Van-Dal and Bouallou [320] pointed out that their simulated results are comparable to the original experimental values from Bussche *et al.* [311]. This comparison between the simulation and experimental data provided a strong indication that the modeled reaction kinetics accurately captured the behavior of the system.

The comparions of different kinetic models for methanol synthesis from CO_2 was performed by [321], indicating that an optimal temperature range of 200 to 250 ^oC exists for both mechanisms. This temperature range is favorable for maximizing methanol yield in the studied process. These results revealed valuable insights into the reaction kinetics and conversion rates of the studied process, therefore one can analyze the influence of such variables in the final product.

The Figure 6.2b depicts the behaviour of temperature in function of the reactor lenght for the DME synthesis. The experimental values from Berčič and Levec [315] were compared with the simulated values from this study. One can see that the simulated values are in good agreement with the experimental values in the first 30 cm for the lower temperature (551.15 K), while 15 cm for the higher temperature (561.15 K), that can have implications for the process, mainly in

product yields and conversion rates.

Raoof *et al.* [322] conducted a sensitivity analysis for the methanol dehydration to DME, varying the feed temperature and other parameters, and the results indicated a limit of 83% conversion under 270 ^{o}C.

This indicates that the simulation model is reliable and can be used to predict the behavior of the process at different conditions. The results also suggest that the temperature has a significant impact on the DME synthesis process, and optimizing the temperature can improve the efficiency of the process.

6.4.2 Proposed Flowsheet

Figure 6.3 introduces the proposed flowsheet for the synthesis of methanol and Figure 6.4 the DME synthesis and purification of products. There are five distinct areas: (**i**) the feed conditioning and recompression, here the unreacted gases are recompressed and the fresh reactants are introduced; (**ii**) the methanol reaction section, where the CO_2 hydrogenation reaction takes place; (**iii**) methanol separation and purification section; (**iv**) the DME reaction section, where the methanol dehydration reaction takes place, (**v**) DME purification section.

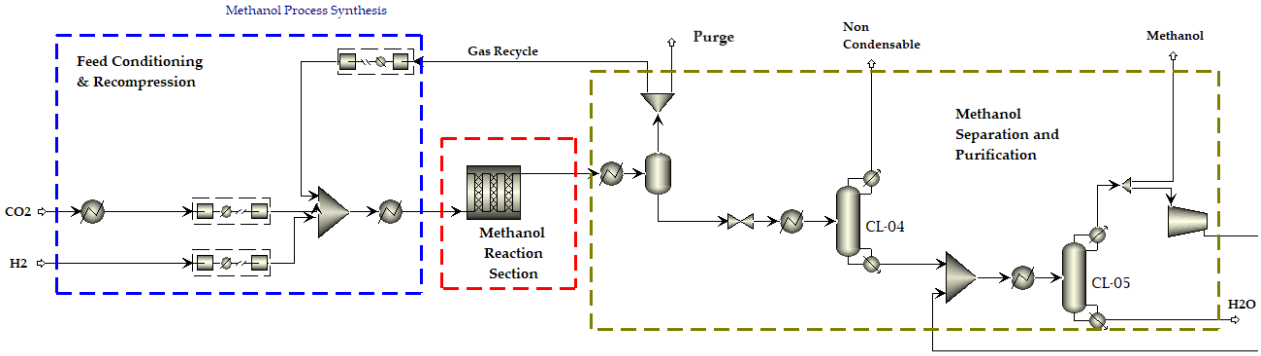

Figure 6.3: Methanol process synthesis flowsheet.

The fresh reactants, carbon dioxide (88 t/h) and hydrogen (4.3 t/h) at 20 bar and 37 ^{o}C, are mixed with the unreacted gases and fed into the reactor. These flowrates were chosen to garantee the product flowrates defined for the chemical plant. The unreacted gases are separated from the raw methanol using a flash separator and recycled back to the methanol reactor.

A column (CL-04) with 4 equilibrium stages and a reflux ratio of 0.302 is used to remove the non-condensable gases to send to the flare. The resulting vapor stream consists of 97.45%wt of CO2 and 2.54%wt of CO, while the liquid stream contains 38.43% water and 61.56% methanol. The condenser and reboiler consume 0.88 MW and 5.9 MW, respectively, for the removal of non-condensable gases.

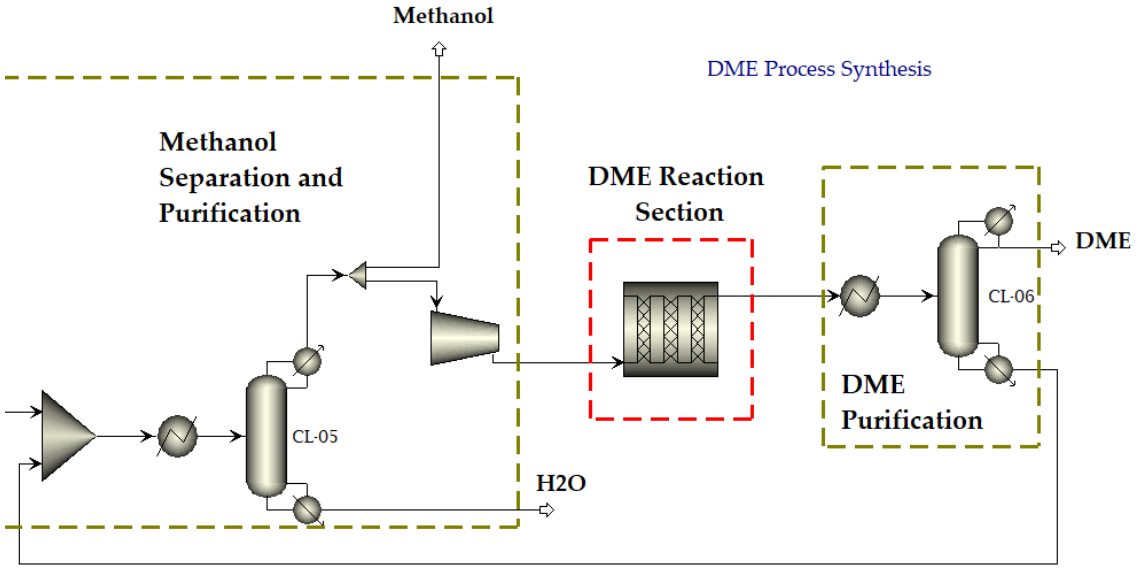

Figure 6.4: DME process synthesis flowsheet.

The methanol tower (CL-05) consists of 20 stages with a reflux ratio of 2.02. The condenser and reboiler consume 29.8 MW and 41.5 MW, respectively. The top stream from the tower is AA grade methanol, which can be sold or used as a raw material for other processes. The bottom stream is 99.98%wt water, indicating a high degree of purification.

The pure methanol stream is fed into an adiabatic reactor, resulting in the production of raw DME at 375^{o}C. Subsequently, a DME purification tower (CL-06) with 12 stages and a reflux ratio of 7.9 is used. The tower separates a top stream containing 99.9%wt DME (17 t/h) and a bottom stream consisting of 0.566 water/0.431 methanol (11.8 t/h).

The feasibility of the proposed flowsheet is established based on the separation and purification of the desired products (methanol and DME) and the efficient recycling of unreacted gases. Further optimization could focus on enhancing the energy efficiency of the system, minimizing the consumption of resources, and optimizing the separation processes to improve product purity.

6.5 Conclusion

The study conducted a thorough evaluation of carbon dioxide conversion into methanol and dimethyl ether. The proposed integrated flowsheet for these products was based on the latest carbon dioxide utilization techniques, it was based on five distinct stages: feed conditioning and recompression, the methanol reaction, methanol separation and purification, the DME reaction, and DME purification. The system utilizes carbon dioxide and hydrogen as raw materials, efficiently recycling the unreacted gases, while maintaining optimal conditions to achieve the

desired product flowrates.

The combination of accurate modeling and advanced visualization tools offers a powerful approach for studying complex chemical reactions. This study confirms the viability and functionality of the proposed flowsheet, with all sections demonstrating proficient operational capabilities and yielding high-purity products. However, there is room for further optimization, specifically concerning the system's energy efficiency and resource consumption. Future research can be developed upon these findings to explore additional optmiziation aspects. This study contributes to the advancement of more sustainable methods of utilizing carbon dioxide as a resource in the chemical industry.

Chapter 7

Surrogate-based Optimization of Chemical Plants

This chapter explores the utilization of Artificial Neural Networks (ANN) in the field of process engineering and optimization. The use of ANNs for generating surrogate models has proven to be advantageous in representing entire subsystems, comprising multiple units, within an industrial plant. Surrogate models are mathematically simple models that map, or regress, the input-output relationships of a more complex model. The study employs a simulation-based optimization framework that combines the capabilities of Aspen Plus, a widely used process simulator, with an external platform housing rigorous optimization algorithms. By leveraging simulation data, surrogate models are developed as simplified versions of the original models. The integration of ANNs and simulation-based optimization enables the exploration of various configurations and potential scenarios. The multi-objective included minimizing the total annualized cost and reducing $CO_{2,eq}$ emissions, it was possible to identify optimal solutions that can achieve cost-effectiveness while simultaneously addressing environmental concerns.

Contents

7.1 Introduction

The economic performance of individual plants and whole production sites is heavily reliant on the modeling, simulation and optimization of their operations. Process optimization and synthesis enhance process designs through optimization, reaching higher efficiency, lower costs and improves plant operability [323]. The unit operations are represented by complex first principle models, including transport, thermodynamic and kinetic relationships. The set of

rigorous models are accessed by the use of modern simulators, where a detailed flowsheet can be designed. However, they are computationally expensive when included directly in the optimization formulation [324].

In recent decades, a large number of studies using ANN in chemical engineering has been carried out, from molecular property prediction [325], catalysis [326, 327], fault diagnosis [328], predictive control [329] and optimization [330, 331]. The use of first-principles knowledge must be integrated with the neural network in order to retain more physical knowledge of the system [329].

ANN-based modeling is notable for not requiring prior, specific mathematical information concerning the process, making it a powerful tool for nonlinear systems.

In their study, Alves and Nascimento [332] focused on producing high purity isoprene from a C_5 cut derived from a pyrolysis gasoline unit. The authors utilized neural networks to replace the operation models of the units in order to find the optimal parameters for the process through a grid search. A set of 10 neural networks was employed to represent the entire flowsheeting, with the number of hidden layers determined based on the minimum error in the test set. Ultimately, this framework successfully optimized a chemical plant using neural networks and industrial data.

Hang, Zhou and Liu [333] improved neural network models for the reactor and distillation column, in an ethylbenzene unit, which is simulated and optimized by the proposed method reducing 55.25% the heating utility consumption.

Khezri *et al.* [330] proposed a hybrid model for optimizing a large-scale gas-to-liquids process. They constructed a dataset by simulating the GTL process and compared various topologies to identify the most promising one. Different configurations with one and two hidden layers and varying numbers of neurons were tested. The optimal configuration consisted of two hidden layers with 7 and 15 hidden neurons, respectively. The ANN model was developed using input features such as the tail gas unpurged ratio, recycled tail gas to FT ratio, H_2O/C in the syngas section, and CO_2 removal percentage. The output feature was the wax production rate. The ANN model was subsequently utilized for optimization purposes, allowing for the improvement and fine-tuning of the GTL process.

Savage *et al.* [334] introduced a hybrid framework based on machine learning to optimize a CryoMan Cascade cycle system. The authors conducted a comparison between different surrogate models, namely ANN and Kriging Partial Least Squares. The results demonstrated a notable reduction in the optimization time compared to the rigorous model. Furthermore, the study revealed that a single large ANN was insufficient to capture the complex nonlinearity inherent in the process, as indicated by the final accuracy. Consequently, the authors devised a

strategy to divide the surrogate model into multiple parallel sub-models, which significantly improved the overall accuracy of the optimization process.

In order to circumvent the solution problem of a superstructure, Henao and Maravelias [335] proposed a framework to replace complex unit models, based on first-principle, by surrogate models, developed through artificial neural networks.

Leperi *et al.* [336] proposed a model reduction-based approach to generate surrogate models of a rigorous Pressure Swing Adsorption (PSA) models, by training artificial neural networks on data collected from full partial differential algebraic equation simulation.

Zapf and Wallek [337] study a multi-objective optimization for a petrochemical production plant. The authors used Black Box Model (BB) or Gray Box Model (GB) based process models from process data and the results indicated the better performance when used ANN.

Wu *et al.* [329] proposed a hybrid machine-learning model incorporation first principles into a Recurrent Neural Network (RNN). The authors studied two models, a partially-connected RNN model and a weight-constrained RNN model and applied to a chemical process containing two well-mixed, non- isothermal continuous stirred tank reactors in series. The two proposed models outperformed a Lyapunov-based model predictive controller based on prediction accuracy, smoother state trajectories and the economic advantages.

The development of an industrial process involves numerous steps that take into account many different levels of detail. The more precise the scale, the more intricate and complicated the process becomes [338, 339].

As the number of interconnected plants increases, the negative effects of these issues become more severe. This leads to a difficult, mixed-integer nonlinear problem when trying to optimize an entire production site. As a result, there is a wide range of research devoted to finding solutions for this problem in order to make decisions that will help meet business objectives through optimizing production operations across all sites.

The optimization of conceptual plants is motivated by the opportunities of this research domain owing to environmental concerns, industrial and economic context. The objective of this study is to propose a methodology to optimize a chemical plant related to economics and enviromental parameters. A complete subsystem of a chemical plant (units or group of units) are modeled as black box surrogate models, based on artificial neural networks and incorporated into the optimiziation procedure.

Employing simplified models or surrogates at the unit operation level offers several advantages, primarily because these surrogates can effectively represent entire subsystems composed of a specific number of units [332]. Artificial Neural Networks (ANN) are well-suited for generating

surrogate models due to their exceptional fitting capabilities [31].

7.2 Methods

An overview of the procedure proposed is provided in Figure 7.1. The framework incorporates the benefits of using a process simulator, in which rigorous calculations can be performed, including thermodynamic model, to the equation oriented environment.

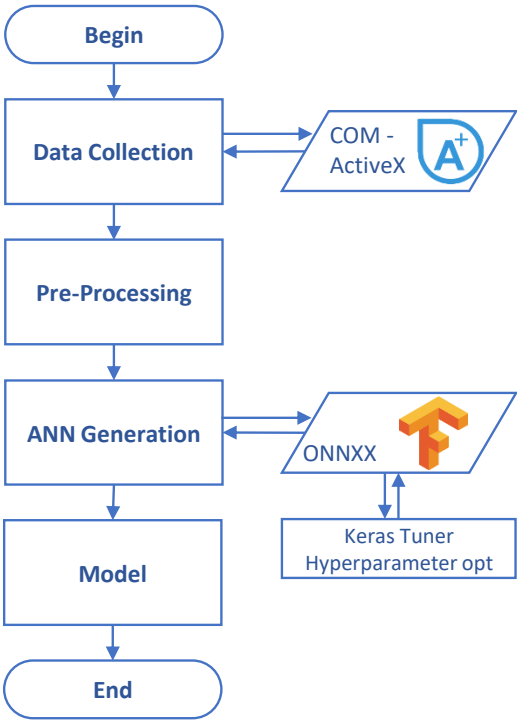

Figure 7.1: Procedure for Surrogate artificial neural network model generation.

The connection between Aspen Plus and Matalb is estabilished by a Component Object Model (COM) in ActiveX. The dataset is, then, ready for pre-processing. The differences in the scales across input variables may increase the difficulty of the problem being modeled, and therefore the input were normalized. The output were also normalized to avoid large error gradient values, which can change the weight values dramatically, making the ANN learning process unstable.

The neural network model was developed using the TensorFlow library, while the integration with Matlab was established through the ONNX connection. In the Python environment, the hyperparameters were fine-tuned using the Keras Tuner library. The last step is the surrogate model expressed as a function of weights and biases.

The simultaneous use of various software programs, such as Aspen Plus, Matlab, TensorFlow, and GAMS, brings together the strengths of each tool, allowing for rigorous modeling, calculation, and optimization of chemical plants. Aspen Plus simulator contains implementations for the

rigorous modelling of unit operations, moreover it allows the use of a thermodynamic package selected according to the system under evaluation. Matlab can connect with several other applications and also calculate and store functions and values in an efficient way. Python open source library tensorflow is very detailed in exploring the best of neural networks, and finally the GAMS is a high-level modeling system for mathematical optimization.

7.2.1 Data Collection

The precise determination of the states of a system in the chemical industry is derived from mass and energy balances rigorously modelled. The computer-aided process systems provide a large variety of tools and packages (Aspen Plus, COCO and cantera-python).

The proposed framework incorporates the simulations performed in the Aspen Plus environment (see Chapter 5 for acetic acid and Chapter 6 for methanol and DME). Figure 7.2 introduces the diagram of the data collection and storage in a dataset, representing the first part of the framework.

The Latin Hypercube Sampling (LHS) [340, 341] was selected for generation of the design variables. The algorithm generates random values by dividing the range of given random variables into equal probability intervals or stripes, and each stripe is sampled only once. It ensures a homogeneous cover of the sampling space.

Once the initial design has been generated, it serves as the input for the simulation process (Part 1). The connection between Aspen Plus and Matlab is established using a Component Object Model (COM) in ActiveX. The simulation's proper execution is accounted for in Part 2, wherein Aspen Plus receives all the defined input variables, resets any previous values, and initiates the simulation run.

The framework is capable of handling various unit operations, regardless of their quantity or type. This is achieved by implementing a loop for each unit operation within the subsystem being evaluated. Prior to proceeding to the next step, each unit operation undergoes a convergence evaluation (Part 3). The convergence criteria may differ depending on the specific unit. For instance, in the case of a rigorous column (using the RadFrac module in Aspen Plus), the option to automatically attempt different solvers for convergence is incorporated.

Part 4 is concerned with the sizing and costing aspects. Once a unit operation has converged, a utility is assigned to it, selected from a standardized list of utilities based on the prevailing conditions.

To determine the capacity of each unit operation, a sizing function is called. This function calculates the unit capacity based on process data and specifications. For some equipment, such

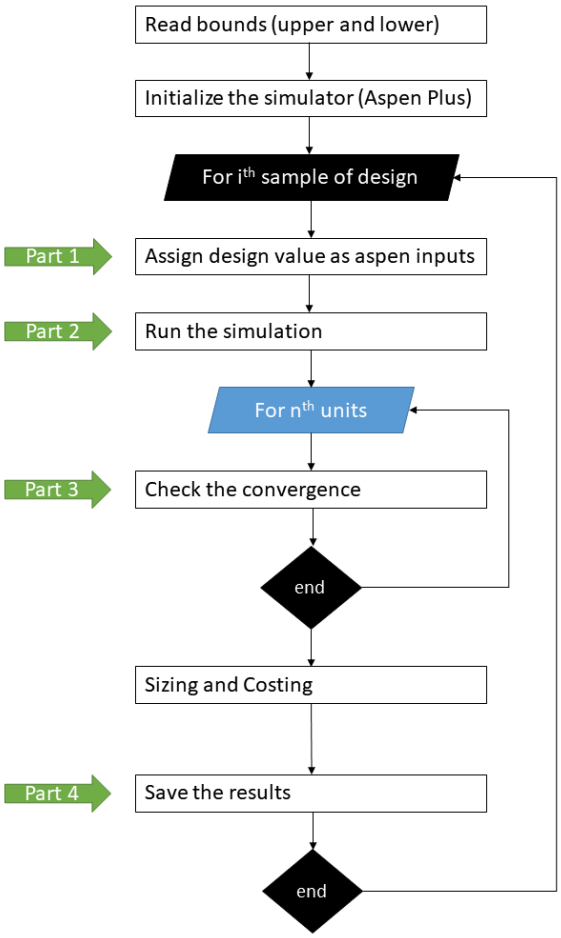

Figure 7.2: Diagram for data collection and storage.

as pumps, the simulation results directly yield the unit capacity. However, for equipment like columns, the unit capacity needs to be calculated using specific procedures and correlations. The details of these sizing procedures can be found in the referenced literature [342, 343].

Once the unit capacity is determined, the cost can be calculated. The algorithm proposed by Turton *et al.* [343] is employed to calculate the bare module cost of equipment ($C_{BM,i}$). This cost estimation takes into account factors such as the material of construction, operating pressure, correlations based on individual pieces of equipment, and adjustment for inflation using the Chemical Engineering Plant Cost Index (CEPCI - 2020).

Finally, the code saves all the results in a database (Part 5) for further use in the artificial neural network generation.

7.2.2 Surrogate Model Approach

An overview of the procedure proposed for the generation of a surrogate model using neural networks is provided in Figure 7.3.

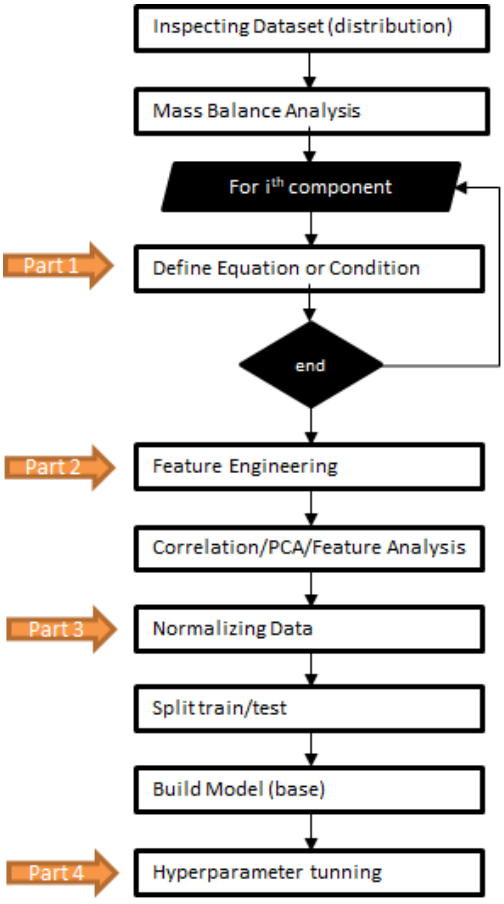

Figure 7.3: Procedure for the generation of surrogate models based on artificial neural networks.

The framework first builds a hybrid machine learning based surrogate model to reduce the

system dimensionality and capture the nonlinearity of the underlying the chemical process. A mass balance analysis (Part 1) can identify possible correlation between streams. Therefore, a phenomenological model is used together with the machine learning model to represent the subsystem of the chemical plant, if needed.

A feature engineering can reduce correlated features or merge features. This procedure aids to the reduction of the dimensionality of the inputs and outputs for the neural networks.

The dataset is, then, ready for pre-processing. The differences in the scales across input variables may increase the difficulty of the problem being modeled and therefore the input were normalized. The output were also normalized to avoid large error gradient values, which can change weight values dramatically, making the learning process unstable.

The neural network was modeled using the tensorflow library. Tuning hyperparameters for a neural network involves optimizing the values of parameters such as learning rate, batch size, and activation functions to enhance the network's performance and achieve better accuracy. The hyperparameter has been tuned using keras tuner library in python environment as presented in Part 4 (Figure 7.3).

7.2.3 Description and training of ANNs

The Artificial Neural Network (ANN) is a class of machine learning algorithm which its inner function is based on the biological neural networks of human brains [344]. Simple units (or nodes) are interconnected in an assembly structure, where the ability of processing is established by the weights through a learning process [345].

Figure 7.4 depicts the structure of a neural network, the inputs are represented by the single units or nodes in the input layer. The summation junction is a simple arithmetic addition of a unit value multiplied by its weight and the bias [345].

The next step incorporates a non-linearity to the model using an activation function in a form of $\phi()$. This procedure allows the modelling of non-linear relationships between inputs, not possible if one uses only the summation junction [345].

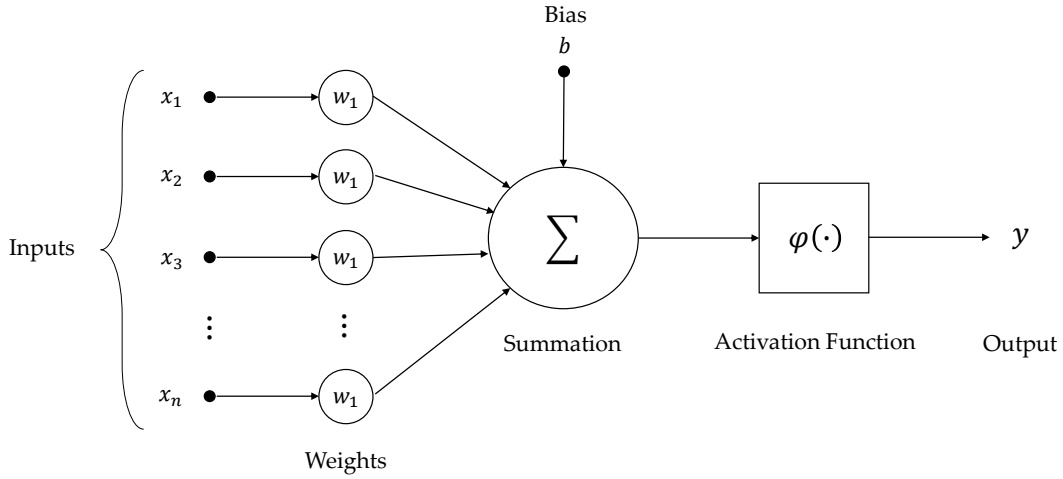

Figure 7.4: Basic structure of an artificial neural network.

The architecture of a neural network can contains several hidden layers stacked, based on the principle described, called Deep Netural Networks [346]; however, is out of the scope of the current study.

The superior prediction capabilities of deep neural networks over shallow neural networks is demonstrated for a wide range of applications [347, 348]. One of the disadvantage is that deep networks require a large amount of data for training.

The training stage is defined as the stage to fit the model to the data (where an optimizer and a loss function must be assigned). All the learnable parameters are calculated, in the training process, through the backpropagation algorithm. Some parameters, called hyperparameters, must be set prior training [344, 345]. These hyperparameters must be to be tuned in order to achieve the best ANN architecture. The visualization of the data prior to training and hyperparameters settings is essential in order to define the best choice of the activation function, for example.

Among the major and more important hyperparameters to be tunned are: (i) number of hidden neurons, (ii) activation function, (iii) optimizer, (iv) regularization and their dependencies (learning rate, optimizer specific, dropout rate, etc).

Activation functions play a crucial role in the neural network architecture by introducing non-linearity and enabling complex mapping between inputs and outputs, additionally to the computational efficiency of training a model. Sigmoid function, Hyperbolic Tangent (TanH)

and Rectified Linear Unit (ReLU) are some examples of activation functions. Recent studies improve the classical activation functions, defining new functions (Leaky ReLU, Swish, H-Swish) [349]. In the Sigmoid activation function, the output values bound between 0 and 1, normalizing the output of each neuron, although there is a problem of vanishing gradient and outputs are not zero centered. In the TanH, the outputs are zero centered, i.e. when the inputs contain strongly negative, neutral, and strongly positive values the modeling is easier. The ReLU is a computationally efficient activation function that will output the input directly if it is positive, otherwise, it will output zero. In the Leaky ReLU, the slope is changed left of x=0 avoiding the dying ReLU problem (some neurons can die for all inputs and remain inactive).

For the optimizer, the Stochastic Gradient Descent (SGD) is a variant of the gradient descent algorithm. It only performs computations on a small subset or random selection of data examples. The Adam optimizer combines the advantages of two SGD extensions — Root Mean Square Propagation (RMSProp) and Adaptive Gradient Algorithm (AdaGrad) — and computes individual adaptive learning rates for different parameters. Other optimizers like Adamax, Adadelta, Adagrad, and Nadam offer further enhancements, such as adaptive learning rates, momentum, and moment-based gradient adaptations.

Regularization is a technique for preventing over-fitting by penalizing a model for having large weights. There are two main regularization parameters: L1 (lasso) and L2 (ridge). L1 regularization adds a penalty to the loss function based on the absolute value of the model's weights, encouraging sparsity. L2 regularization, also known as weight decay, penalizes the sum of squared weights, discouraging large weight values. Regularization techniques promote simplicity, reduce overfitting, and improve the model's ability to generalize to unseen data. They play a crucial role in neural network architecture by striking a balance between model complexity and performance, leading to more robust and accurate models

7.2.4 Superstructure Optimization Approach

Considering environmental aspects in the design of chemical processes is important for promoting sustainability, minimizing environmental impact, and complying with regulations. By incorporating eco-friendly practices, such as emissions control and waste reduction, the design can promote environmental-friendly practices and reduction in industrial impact. Addressing environmental factors early in the design phase avoids costly retrofits and aligns business interests with environmental protection.

It should be noted that economic and environmental objectives often conflict. Therefore, a multiobjective optimization algorithm that can identify the tradeoffs between these competing criteria must be used in order to develop chemical processes automatically. Single-objective optimization is not enough to achieve this [350].

The objective function for optimization problems are normally the maximization of the net present value (NPV) [351] or the minimization of the total annualized cost (TAC) [352–356]. The initial step for both situations is to calculate the capital cost, which includes the cost of constructing the plant and the operating costs.

The selected objective function for the current work is the total annualized cost (TAC) used to measure the economic viability and profitability of a chemical production process and the Total $CO_{2,eq}$ usage.

The total annualized cost of a chemical plant is the sum of all the costs associated with the operation of the plant over the course of one year. This includes the cost of labor, raw materials, energy, maintenance, and any other associated costs. To calculate the total annualized cost, one must first identify all the costs associated with the operation of the plant and then calculate the total cost for each of these components. The total cost for each of the components are summed to get the total annualized cost.

The TAC must be minimized and contains two terms, one for operating costs and one capital costs, as shown in Eq. 7.2.1 [342].

$$\text{TAC (US\$/year)} = OPEX + \frac{i\,(1+i)^n}{(1+i)^n - 1} \cdot (\text{CAPEX}) \tag{7.2.1}$$

where OPEX is the operating cost per year and CAPEX is the total grassroots cost for the purchase and installation of all major equipment. The term $\left[\frac{i(1+i)^n}{(1+i)^n-1}\right]$ is the annualization factor (F) [357] of the capital cost, where i stands for the fractional interest rate per year, considered 10% in this study, and n is the lifespan of plant equipment, the value of 15 years was adopted [358, 359]. The plant will run 8000 hours a year.

Cost parameters and correlations for both CAPEX and OPEX follow the methodology defined by Turton *et al.* [343]. The Eq. 7.2.2 defines the CAPEX, while Eq. 7.2.3 defines the OPEX.

$$\text{CAPEX} = 1.18 \cdot C_{BM} + 0.50 \cdot C_{BM,0} \tag{7.2.2}$$

$$\text{OPEX} = 1.23 \cdot (C_{RM} + C_{WT} + C_{UT}) + 2.73 \cdot C_{OL} + 0.18 \cdot CAPEX \tag{7.2.3}$$

C_{BM} stands for bare module equipment cost: direct and indirect costs for each unit and $C_{BM,0}$ the bare module cost for the base conditions [343].

C_{RM} stands for raw material cost, which is estimated based on the input streams of the raw materials. It may be important to consider the average price of a given chemical product over

a long period of time, as there may be significant seasonal fluctuations in pricing. Such price variations are usually caused by changes in the supply and demand of the product, which have a major impact on the cost at any given moment.

C_{WT} stands for treatment of the residue. Since environmental regulations are more strict, the issues and costs associated with the treatment of waste chemical streams also significantly increase. Therefore, waste minimization strategies or other solutions are crucial. According to Towler [342], the cost of wastewater treatment is typically about $1.5 per metric ton.

C_{UT} stands for cost of utility, which is calculated using the output - utility usage - of each neural network; and C_{OL} is the labor cost.

The emission factors for CO_2 associated with utility usage were obtained from the U.S. Environmental Protection Agency's regulation E9-5711, also known as the "Mandatory Reporting of Greenhouse Gases." [360]. This regulation encompasses all sectors of the U.S. economy, including both fossil fuel suppliers and direct greenhouse gas emitters. The emission factors specific to utilities can be found in Table 7.1. The utility usage is aggregated into the variable Total $CO_{2,eq}$ and employed in the optimization problem.

Table 7.1: Utilities Emission Factors.

Utility	CO_2 emission factor (tonne/GJ)
Electricity	0.0964
Low Pressure Steam	0.0658
High Pressure Steam	0.0658
Low Temperature Refrigerant	0.0558
Very Low Temperature Refrigerant	0.2012

7.2.5 Surrogate model reimplementation

The surrogate model is expressed as a function of weights and biases and can be rewritten directly in the optimization environment of the General Algebraic Modelling System (GAMS) software using GDXMRW (GDX-Matlab Read/Write), a suite of utilities to exchange data between GAMS and MATLAB.

A special case occurs when the best activation function, retrieved from the hyperparameter tunning step, the Rectified Linear Unit (ReLU). In this case, the big-M formalism was used in order to accommodate the non-linear nature of the equation: $x^k = \sigma(W^k \cdot x^{k-1} + b^k)$, where $\sigma(y) := max\{0, y\}$ [361].

The final optimization model is represented in Eq. 7.2.4. The weighted sum multi-objective approach was used [362].

$$
\begin{aligned}
\textbf{min} \quad & \alpha \cdot \text{TAC} + (1-\alpha) \cdot \text{Total } \text{CO}_{2,eq} \\
\\
\textbf{s.t.} \quad & \textit{auxiliary equations} \\
& \text{TAC} = \text{OPEX} + \frac{i\,(1+i)^n}{(1+i)^n - 1} \cdot (\text{CAPEX}) \\
& \text{CAPEX} = 1.18 \cdot C_{BM} + 0.50 \cdot C_{BM,0} \\
& C_{BM} = \sum_{1}^{k} y^k_{C_{BM}} \quad \forall\, k \in \mathcal{K} \\
& C_{BM,0} = \sum_{1}^{k} y^k_{C_{BM,0}} \quad \forall\, k \in \mathcal{K} \\
& \text{OPEX} = 1.23 \cdot (C_{RM} + C_{WT} + C_{UT}) + 2.73 \cdot C_{OL} + 0.18 \cdot \text{CAPEX} \\
& C_{RM} = \sum_{1}^{r} (\text{RMusage}_r \cdot \text{RMcost}_r) \quad \forall\, r \in \mathcal{R} \\
& C_{WT} = \sum_{1}^{k} y^k_{\text{water}} \cdot \text{WTcost} \\
& C_{OL} = \text{AHW} \cdot \left(6.29 + 31.7 \cdot P^2 + 0.23 \cdot N_{np}\right)^{0.5} \\
& C_{UT} = \sum_{1}^{k} \sum_{1}^{u} y^k_u \quad \forall\, k \in \mathcal{K}, u \in \mathcal{U} \\
& \text{Total } \text{CO}_{2,eq} = \sum_{1}^{k} y^k_{CO_{2,eq}} \quad \forall\, k \in \mathcal{K} \\
& \textit{surrogate models} \\
& y^k_p = \text{ANN}^k(x^k_p) \quad \forall\, k \in \mathcal{K}, p \in \mathcal{P} \\
& \textit{operating region} \\
& lb \leq x^k_p, x^k_q \geq ub \\
& \textit{purity product specifications} \\
& y^k_{\text{purity product}_i} \geq 0.98 \quad \forall\, i \in [\text{ME, AA, DME}]
\end{aligned}
\tag{7.2.4}
$$

where $\mathcal{K}$ represent the list of neural networks, $\mathcal{P}$ the list of properties estimated from the neural networks, $\mathcal{U}$ the list of utilities, $\mathcal{R}$ the raw materials,

7.3 Results and Discussion

The application of the framework to two case studies is presented in this section.

7.3.1 Case Study 1 - Methanol and DME Production Process

The process assessed in the case study #1 is the methanol and DME synthesis presented in Chapter 6. The detailed process flowsheet is depicted in Figure 7.5.

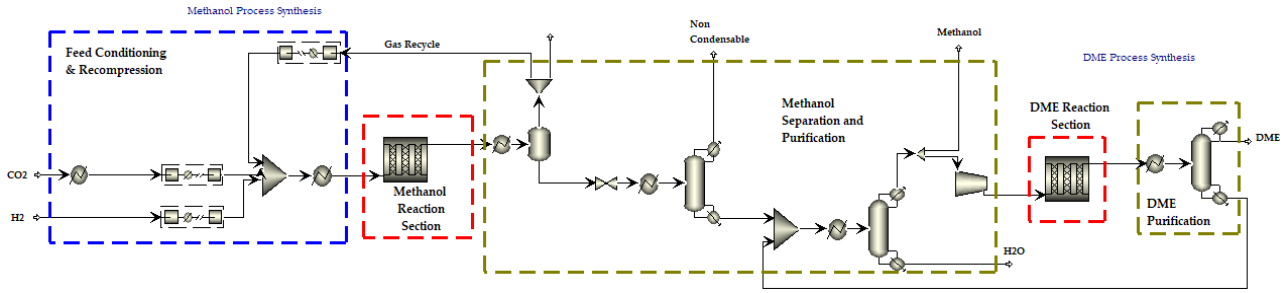

Figure 7.5: Methanol and DME Production Process Flowsheet.

7.3.1.1 Variable Selection and Data Collection

The first step of the framework is to define the variables to be evaluated as presented in Figure 7.2.

According to Srinivasan *et al.* [363], developing a comprehensive model for a chemical process poses considerable challenges owing to the sheer multitude of variables and the complex series of steps it entails. Moreover, the process is heavily reliant on conditions that exhibit non-linearity and transience, further exacerbating the difficulty.

The intricate nature of chemical processes needs a thorough understanding and careful consideration of numerous factors. With a multitude of variables at play, ranging from reactant concentrations and reaction rates to temperature, pressure, and catalyst properties, capturing the interplay and interdependencies between these elements becomes an intricate task.

For the case of methanol and DME production, the main variables defined are temperature of the heat exchangers, lenght of reactors, reflux ratio and distillate to feed molar ratio of the columns. The variables collected after the simulation are utility $CO_{2,equivalent}$ usage, utility usage, mass flows and bare module cost for capital cost calculations.

The Figure 7.6 translates the variables into a neural network. It is a feed-forward neural network with only one hidden layer. The number of neurons is defined in the hyperparameter tuning step.

There are 13 input variables: *T_HT-12* to *T_HT-16* are temperatures in degrees Celsius (°C) of the heat exchangers from 12 to 16. *Lenght_RT-02* and *Lenght_RT-03* are the length of the reactors 2 (Methanol) and 3 (DME) in meters. *RR_CL_4* to *RR_CL_6* are the reflux ratio of the columns 4 to 6, while *D-F_CL-04* to *D-F_CL-06* are the distillate to feed ratio of the columns 4 to 6.

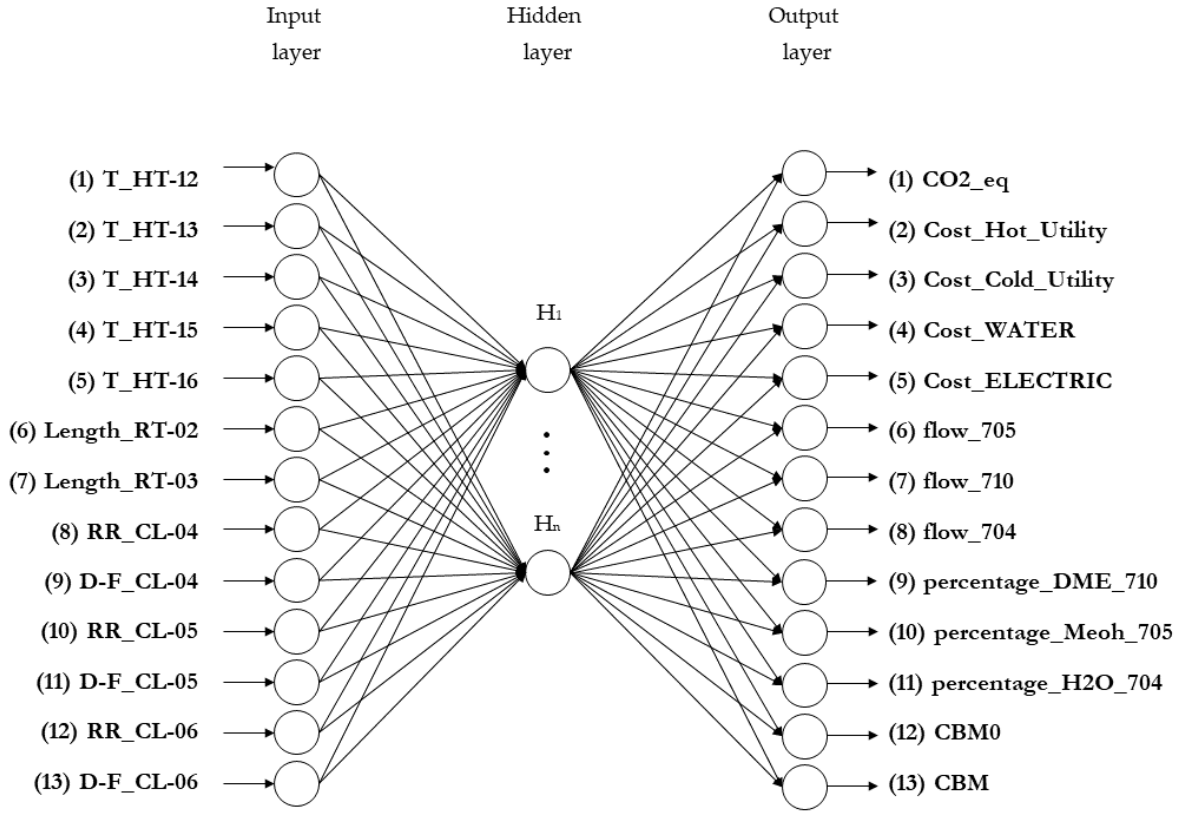

Figure 7.6: Detailed architecture for methanol and DME ANN.

After the simulation and data collection, the output are aggregated into groups, for example the $CO_2 eq$ is the sum of all $CO_{2,equivalent}$ from the utility usage. Reducing the number of output features, often leads to an in increase in the overall performace of the final neural network model. The final output features are CO_{2eq}, cost of utilities, total flow of the main streams, purity of the selected streams and total capital cost (bare cost module).

The final set of outputs analyzed is *CO2_eq* that is the CO_2 equivalent for utility usage in kilograms (kg). The utility cost variables are *Cost_Hot_Utility*, *Cost_Cold_Utility*, *Cost_WATER*, and *Cost_ELECTRIC* expressed in US$. The *flow_705*, *flow_710* and *flow_704* are the flow of the methanol, DME and wastewater stream in kg. The *percentage_DME_710*, *percentage_Meoh_705* and *percentage_H2O_704* represent the purity of the component in the stream. The *CBM0* and *CBM* represent the bare cost module used in economic calculations.

Based on the selected variables used as inputs, a design of experiments based on latin hypercube sampling (LHS) was used. It ensures uniform coverage of the parameter space, enhancing the exploration of the design problem. LHS is efficient, requiring fewer experiments to achieve a desired level of precision. It reduces bias by evenly distributing samples, enabling reliable statistical analysis. LHS is flexible, accommodating both continuous and discrete variables, and is scalable to higher dimensions.

The data distribution of the input variables used for the phenomenological model are presented in Figure 7.7 using a pair plot. This visualization technique is used to examine the relationships between pairs of variables in a dataset and to explore the correlation between multiple variables in a single plot, making it easy to identify patterns and relationships that might not be apparent in a single scatter plot.

A uniform distribution was successfully attained, using the lhs sampling technique. The data points are evenly distributed throughout the parameter space, resulting in a more comprehensive and representative sample. It is worth noting that the same pattern and distribution were observed across all assessed variables.

The collected data from the simulation are depicted in Figure 7.8. It is important to note that the raw output from the simulations were aggragated through feature engineering, helping to reduce the complexity of the input data by removing irrelevant or redundant features.

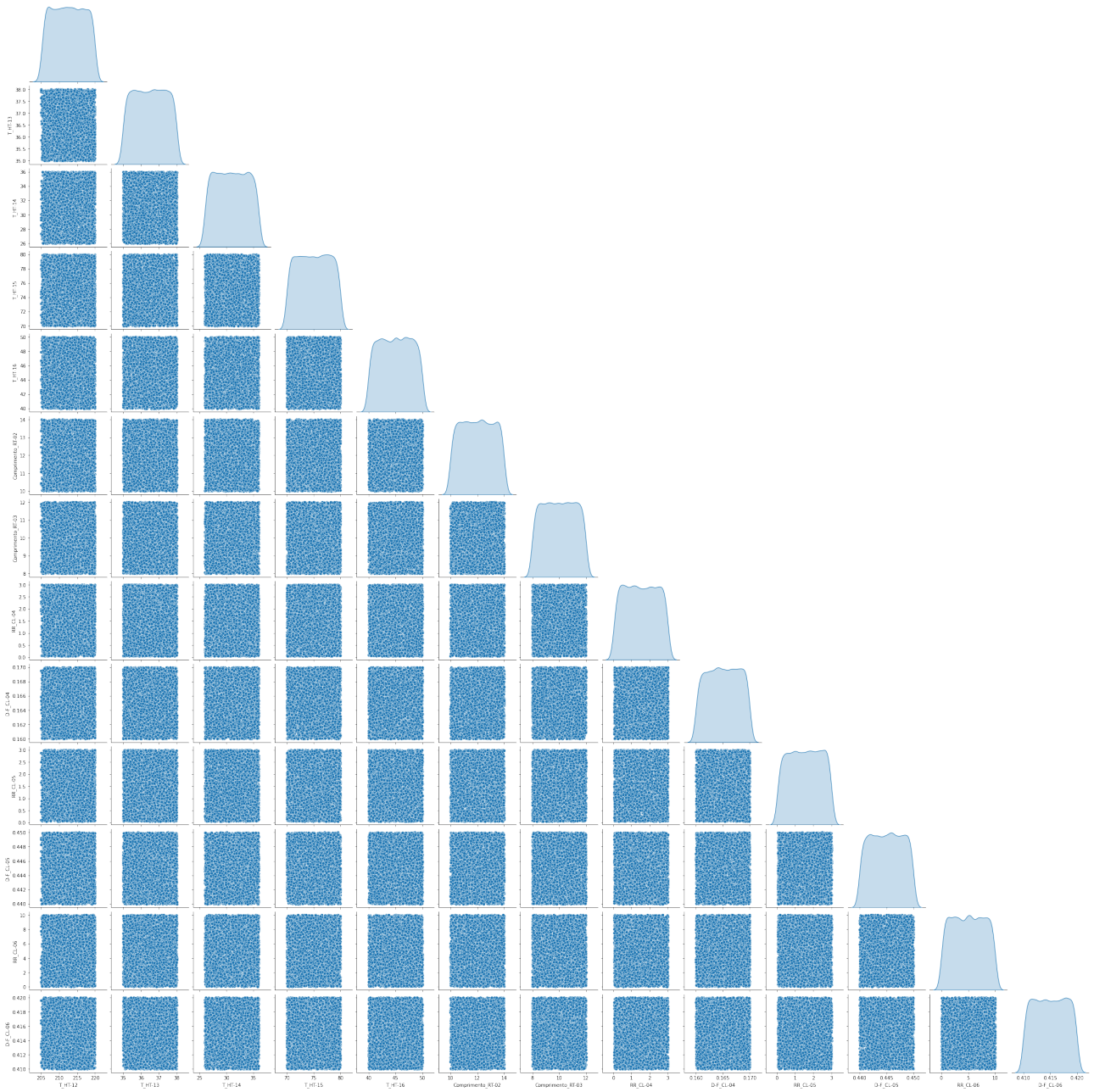

Figure 7.7: Input data distribution for Methanol and DME Neural Network.

From Figure 7.8, it is possible to identify a linear relationship between some variables, for example the purity in the methanol stream and wastewater stream, since this streams are outputs of the same separation column in the flowsheet.

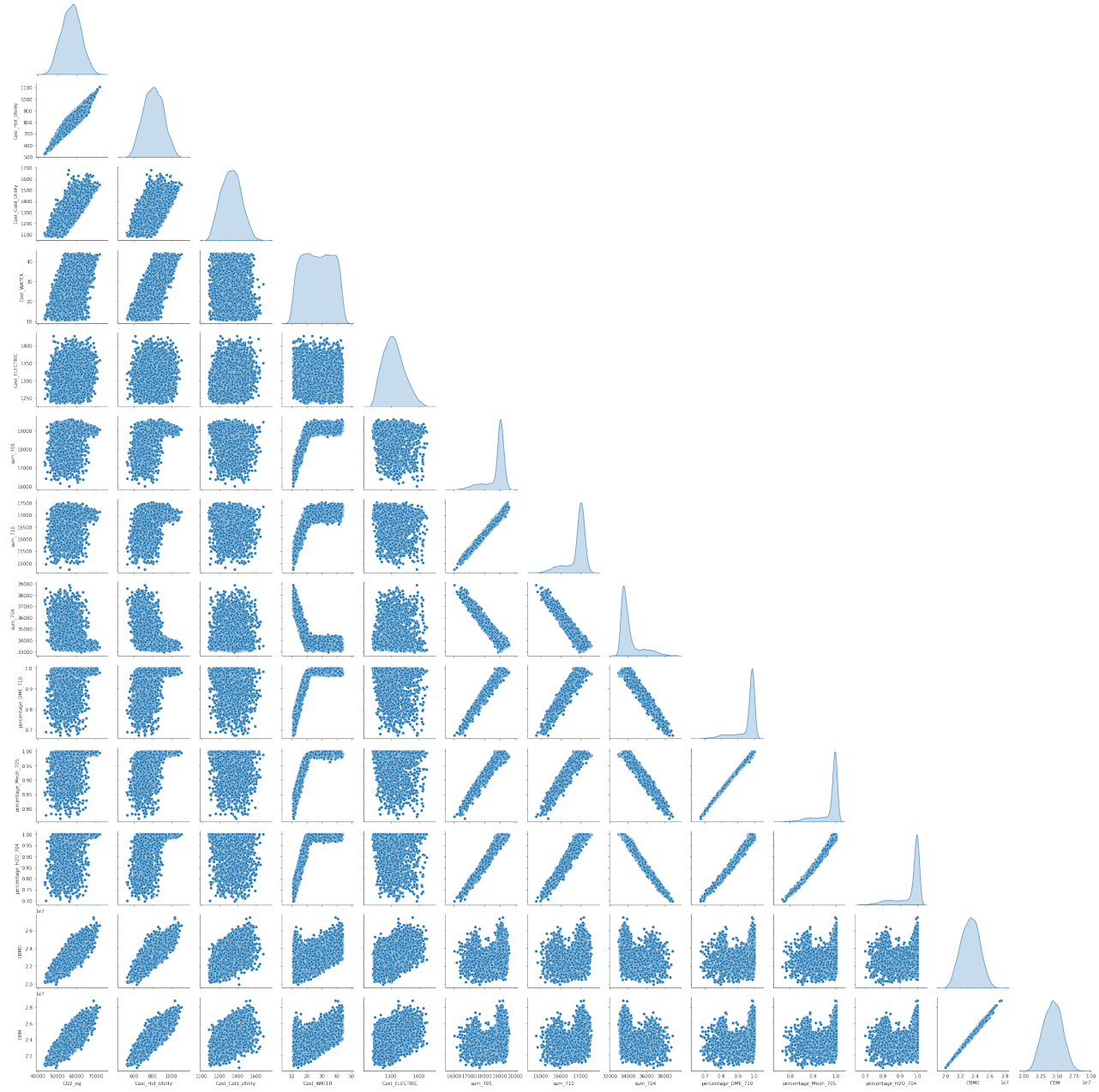

Figure 7.8: Output data distribution for Methanol and DME Neural Network.

Based on the simulation results, it seems that there are no outliers or unusual observations. An interesting observation is the relationship between the cost of water and the percentage of DME in the stream 710. The results indicate that as more water is used, the percentage of DME in the stream 710 increases linearly. However, there is a limit to the purity of the DME in this stream, beyond which increasing the amount of water used does not result in any further increase (or decrease) in DME purity. This observation could has important implications for the design and operation of the chemical plant. For example, it suggests that there may be an optimal amount of water usage that maximizes the purity of DME in the stream 710 while minimizing the cost of water.

7.3.1.2 Neural Network Generation

As previously describe, in this case study, only one neural network will represent the entire process flowsheet described in Figure 7.5.

Hyperband is a powerful technique for efficient neural network hyperparameter tuning. It combines random search with early stopping, allowing for the exploration of a wide range of hyperparameter configurations in a time-effective manner. The process involves training multiple configurations in parallel, progressively eliminating poor performers. This helps identify promising hyperparameter settings and allocate more resources to them, maximizing the chances of finding optimal solutions. By dynamically adapting the resource allocation and termination criteria, hyperband achieves significant time savings compared to traditional grid or random search methods [364]. Hyperband Tuner Search using the library keras-tuner was used for select the best hyperparameters. The results are depicted in Figure 7.9.

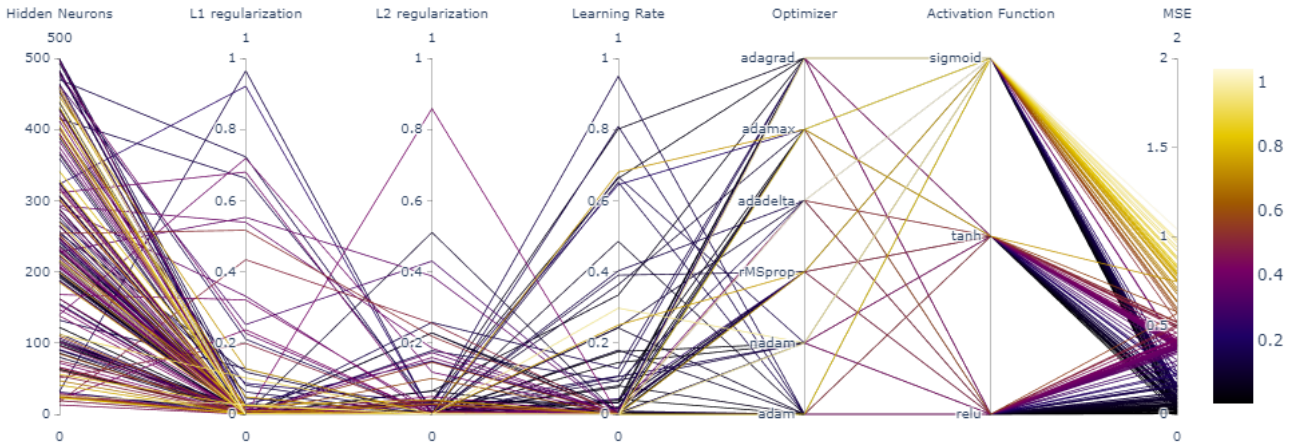

Figure 7.9: Hyperparameter Search for Methanol and DME Neural Network.

The hyperparameters tuned are the number of hidden neurons, L1 and L2 regularization, learning rate, optimizer and the activation function. The activation function play an important role in the configuration of a neural network, Figure 7.9 shows the impact on the mean square error. The sigmoid activation function usually produces models with higher errors compared with tanh and ReLU functions.

The evaluation metric used to define the best model is the Mean Squared Error (MSE), a commonly loss function used for regression tasks. The final model is the one that achieved the lowest MSE (using 3 trials). For the methanol and DME neural network, the calculated MSE value of 2.467×10^{-3}.

The neural network model consists of a hidden layer with 63 neurons, responsible for performing computations and learning representations from the input data. The dense activation function parameter is the ReLU.

Regularization techniques are applied to the model to prevent overfitting and control the model complexity. The 'regularizer_1' parameter represents the strength of L1 regularization, which adds a penalty proportional to the absolute values of the weights. This helps to reduce the impact of less important features in the model. The best value for this parameter was 1.354×10^{-8}. On the other hand, the 'regularizer_2' parameter indicates the strength of L2 regularization, which adds a penalty proportional to the squared values of the weights. This regularization technique further reduces the model complexity and encourages the model to generalize well. The best value for this parameter was 7.331×10^{-6}.

The optimization algorithm used to train the model is specified by the 'optimizer' parameter. The hyperparameter search indicated 'adamax' as the best one. Adamax is a variant of the Adam optimizer, known for its adaptive learning rates and momentum. This optimizer helps to efficiently update the model's parameters during training and improve convergence.

The learning rate determines the step size taken during each iteration of the training process. A learning rate of 3.330×10^{-2} is chosen for this model. Finding an appropriate learning rate is crucial, since a higher learning rate can lead to faster convergence, but it may also risk overshooting and instability during training.

The performance of the neural network results were evaluated by comparing the predicted values with the actual observed values. Figure 7.10 shows the observed value and the value predicted using the best model from the hyperparameter tunning.

The training dataset contains 3472 samples and the test dataset contains 613 samples. A high degree of concordance was observed between the predicted and observed values across the evaluated variables. The neural network consistently achieved accurate predictions. The model's performance was also evaluated using the coefficient of determination (R^2), and the results vary from the lowest of 0.935 (for *CBM0*) to the highest of 0.998 (for *Cost_WATER*).

The results demonstrated the effectiveness of the neural network in accurately predicting various outcomes, highlighting its potential for real-world applications.

The key advantage of ANN-based modeling is that it does not rely on predetermined mathematical information about the process steps, but rather learns from training examples. As a result, ANN-based modeling can be employed for predicting the results of chemical processes and also in the optimization framework.

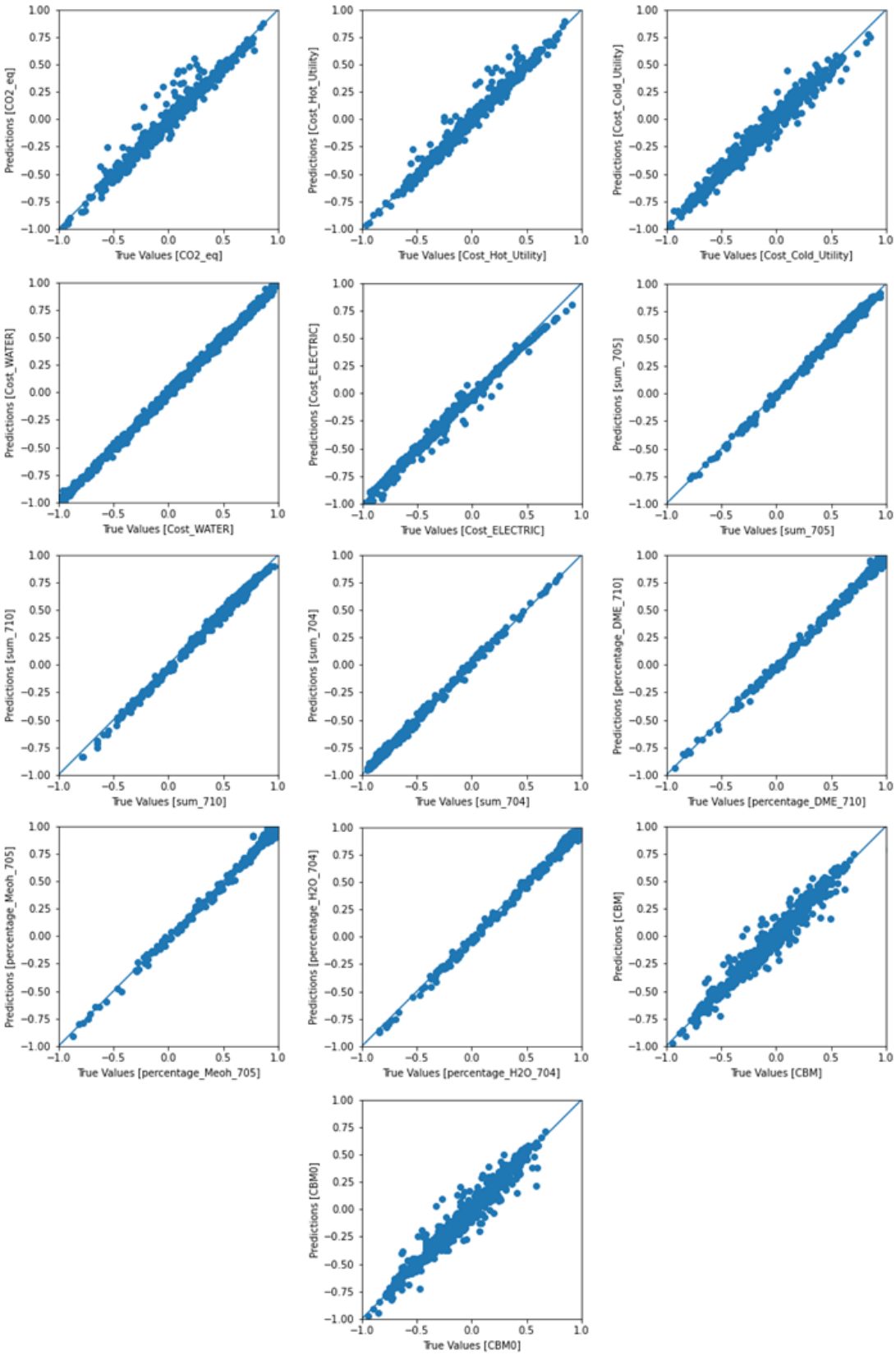

Figure 7.10: Predictions for the Methanol and DME Neural Network.

7.3.1.3 Optimization Aspects

The optimization problem is classified as MINLP due to discrete variables of the neural network and non-linear functions, such as the activation function.

Eq. 7.2.4 represents the proposed set of equations assessed. The combination of Total Annualized Cost and Total CO_2 was set as objective function to be minimized.

The neural network generated in Section 7.3.1.2 was also used in the optimization framework. The input variables for the optimization are the same as the inputs for the neural network, Table 7.2 present the minimum and maximum values set as restrictions for the optimization.

Table 7.2: Free variables for the optimization of case study #1.

Input Variable	Minimum	Maximum	Base Case (no opt)
T_HT-12	205.01	220.00	210
T_HT-13	35.00	38.00	35
T_HT-14	26.00	35.99	27
T_HT-15	70.00	80.00	75
T_HT-16	40.00	50.00	45
Length_RT-02	10.00	14.00	12
Length_RT-03	8.00	12.00	10
RR_CL-04	0.05	3.00	0.302
D-F_CL-04	0.16	0.17	0.163
RR_CL-05	0.05	3.00	2.020
D-F_CL-05	0.44	0.45	0.447
RR_CL-06	0.05	10.00	7.943
D-F_CL-06	0.41	0.42	0.411

In this optimization problem, the complete model consists of 23 blocks of equations, encompassing a total of 504 unique equations. These equations are derived from various aspects of the problem (see Eq. 7.2.4). Additionally, the model comprises 20 blocks of variables, with a total of 328 unique variables. These variables represent the decision-making variables (Table 7.2) that are subject to optimization and also including the internal hidden variables of the neural network. Furthermore, the problem involves 126 discrete variables, which introduce discrete choices and further complexity to the optimization process. The non-linear matrix, a key component of the problem, is composed of three coefficient entries. These coefficients contribute to the non-linear relationships within the model and influence the optimization outcomes.

Base Case from Simulation

The base case contains the original values from the simulation developed in Chapter 6, and the free variables in the base case are presented in Table 7.2.

The economic analysis of the proposed chemical plant reveals that the total annualized cost is \$276.58M, while the total $CO_{2,eq}$ emitted, represents the total amount of carbon dioxide emitted by the chemical plant during its operation based on utilities usage. This value highlights the plant's environmental impact and carbon footprint and, for the base case, the calculated value is 458.23M kg/year.

Different Solvers Comparison

Comparing different solvers in MINLP optimization is crucial for selecting the most suitable solver. By comparing solvers, one can assess their performance in terms of solution quality, convergence speed, and robustness. Different solvers employ diverse algorithms, heuristics, and optimization techniques, making their performance vary. Additionally, solvers may excel at specific problem characteristics, such as handling non-convex functions or supporting certain constraints [365, 366].

For the sake of simplicity in this evaluation, a alpha (α) of 1 was adopted. Table 7.3 displays the comparison results for various solvers. The software GAMS (version 25.0.3) was employed.

Table 7.3: MINLP solver comparison for optimization problem.

Solver	Objective Value	Resource Usage	Iteration Count	Version
antigone	2.727×10^8	0.188	0	1.1
baron	2.675×10^8	0.730	0	17.10.16
dicopt	2.675×10^8	0.234	453	2
lindo	2.696×10^8	0.765	58278	11.0.3802.300
scip	2.694×10^8	0.000	87	-

The differences can be due to relative optimality tolerance or due to the nature of the algorithm used for the solver. The concept of critical optimality tolerance and its implications in solving optimization problems meaning that the solver will stop when it finds a feasible integer solution within a gap (tolerance) of the global optimum.

In case of nonlinear nonconvex problems, local solvers can find an optimum that is better than neighboring points, but it may not be the global optimum. The optimal solution depends on the starting point and the path taken by the solver, which can vary due to numerical differences in data, initial values, and bounds.

Multi-Objective Results

The base case was compared with an optimized case, using the parameter α fixed in 1 (see Eq. 7.2.4). The optimization process, with variables left free for adjustment, reduced the total

annualized cost of the chemical plant from $276.58 million in the base case to to $267.55 million, a reduction of approximately $9 million (3.26%).

The more significant improvement is observed in the total $CO_{2,eq}$ emissions, which decreased from 458.23 million kilograms per year in the base case to 338.77 million kilograms per year in the optimized scenario. This reduction in $CO_{2,eq}$ emissions is crucial from an environmental standpoint as it signifies a substantial decrease in the plant's carbon footprint and an improvement in the plant's environmental performance.

The environmental importance of this reduction is due the variables related to utilities usage, including steam pressures and temperatures, cooling water flow rates, electricity consumption targets, fuel usage, and other energy-related parameters.

Table 7.4 provides a comprehensive comparison between the variable values of the base case and the values achieved after the optimization process. This table serves as a valuable reference for understanding the specific changes made during the optimization and their effects on the overall performance.

By comparing the optimized variable values with those of the base case, it becomes evident which specific parameters have been modified to achieve the desired improvements. This comparison helps identify the key drivers behind the cost reduction and $CO_{2,eq}$ equivalent emission reduction.

Table 7.4: Comaprison of variables in the base case and after optimization.

Input Variable	Case Base (no opt)	Optimized
T_HT-12	210	206.16
T_HT-13	35	35.00
T_HT-14	27	26.00
T_HT-15	75	77.65
T_HT-16	45	50.00
Length_RT-02	12	10.00
Length_RT-03	10	8.00
RR_CL-04	0.302	0.053
D-F_CL-04	0.163	0.161
RR_CL-05	2.020	0.968
D-F_CL-05	0.447	0.449
RR_CL-06	7.943	0.055
D-F_CL-06	0.411	0.419

The optimization process revealed that the optimal temperatures for Heater 12 and Heater 14 are slightly lower than the initial values, suggesting potential energy savings. Conversely, the optimal temperature for Heater 15 is slightly higher, indicating improved reaction efficiency at a slightly elevated temperature. The temperature of Heater 16 was found to be more favorable at a higher value.

Relating the reactor length, the optimization indicated that shorter lengths for Reactor 02 and Reactor 03 are preferred, suggesting potential cost savings and improved productivity.

For the column variables, the optimization process resulted in significant improvements in the reflux ratios of Columns 4, 5, and 6. Lower reflux ratios imply reduced energy consumption and potentially enhanced separation efficiency in these columns. The distillate to feed ratios of Columns 4 and 5 remained relatively unchanged, indicating that the optimization did not significantly affect the separation efficiency in those columns. The distillate to feed ratio of Column 6 showed a minor improvement after optimization.

The optimization results highlight the sensitivity of certain variables compared to others. Variables such as reflux ratios and temperature showed more significant changes, indicating their crucial role in process optimization. On the other hand, variables like distillate to feed ratios exhibited smaller variations, suggesting they are already close to the optimal values or less influential in achieving the desired optimization objectives.

The optimized variables from the surrogate model were used back into the phenomenological simulation to assess the accuracy the model in the optimal scenario. The output variables, as described in Section 7.3.1.1 were compared. The CO_2_eq variable showed a 7.2% discrepancy, indicating reasonable accuracy but room for improvement. Utility costs displayed mixed accuracy with the highest discrepancy in *Cost_Hot_Utility* (7.28%) and *Cost_Cold_Utility* (4.82%). Variables *flow_705*, *flow_710* and *flow_704* were predicted with remarkable accuracy, particularly *flow_704* with a tiny 0.0446% difference. Finally, large-scale variables *CBM* and *CBM0* showed minor percentage errors (1.76% and 1.48%, respectively). Notably, the results showcased a close match, within a 7.2% error rate for the variables. Given the complex and multifaceted nature of chemical processes and plant operations, an error within this range suggests that the surrogate models effectively capture the dynamics of the actual chemical process, taking into account various aspects including chemical reactions, mass transfer, heat transfer, and equipment-specific dynamics.

The optimization efforts in the Methanol and DME process have yielded positive outcomes from both economic and environmental perspectives. The reduction in the total annualized cost indicates improved financial efficiency, while the decrease in $CO_{22,eq}$ equivalent emissions signifies a commendable step towards environmental sustainability. These results highlight the significance of employing optimization techniques in chemical engineering to strike a balance between economic viability and environmental responsibility.

Pareto Frontier Analysis

The Pareto frontier represents a set of solutions where it is not possible to improve one objective without sacrificing another. In other words, it represents the trade-off between different objectives that cannot be simultaneously optimized [337].

The Pareto frontier, as described in Figure 7.11, is a graphical representation that shows the various trade-off options between the two objectives. It would depict the possible combinations of total annualized cost and total CO_2 equivalent emissions that cannot be further improved without sacrificing one objective for the other.

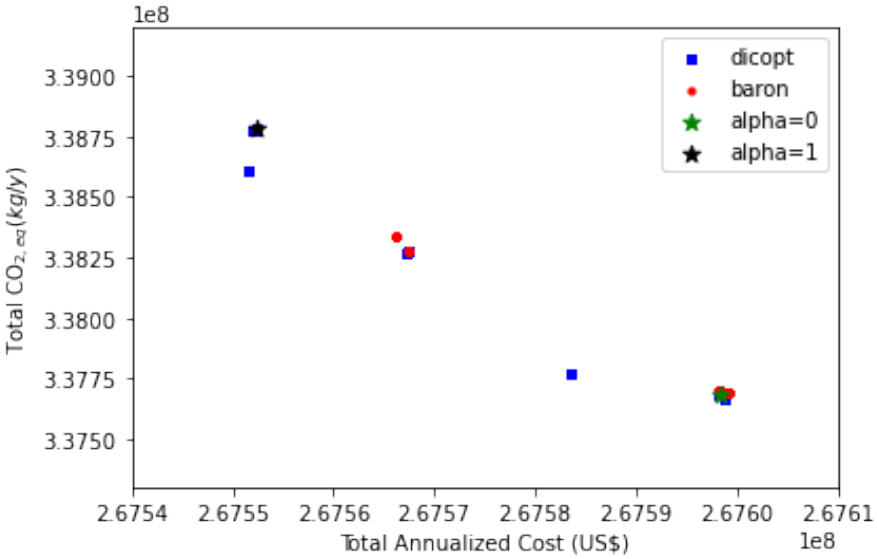

Figure 7.11: Pareto Frontier for the Multi-Objective Optimization of Methanol and DME Process.

The points on the frontier represent the best compromise between economic cost and environmental impact, and any point outside the frontier would represent a suboptimal solution.

When the alpha parameter (α) in the multiobjective optimization is set to 0, indicating a higher importance placed on minimizing total CO_2 equivalent emissions, the best solution achieved is a total annualized cost of US$267.59M and a total CO_2 equivalent emission of 338.77M kg/year. This solution demonstrates a strong emphasis on environmental sustainability by significantly reducing emissions while still maintaining a reasonable cost.

Conversely, when the alpha parameter is set to 1, meaning a higher importance is placed on minimizing total annualized cost, the results show a total annualized cost of US$267.55M and a total CO_2 equivalent emission of 338.78M kg/year. This solution prioritizes cost reduction while still meeting the emission targets.

These results highlight the strengths and trade-offs of the different solutions along the Pareto frontier. Some solutions achieve significant emissions reductions while maintaining reasonable

costs, making them favorable for environmental sustainability. On the other hand, there are solutions that focus on achieving the lowest costs possible while still meeting emission targets.

The relevance of these solutions to the specific context of the chemical plant depends on various factors such as industry regulations, stakeholder expectations, and long-term sustainability goals. For instance, if the chemical plant operates in a region with strict environmental regulations or is committed to corporate social responsibility, solutions with significant emissions reductions may be more relevant and aligned with their objectives.

Additionally, the trade-offs between economic cost and environmental impact should be carefully considered. While some solutions may achieve lower costs, they might have a higher environmental impact. Conversely, solutions with significant emissions reductions may come with slightly higher costs. Decision-makers must evaluate these trade-offs and consider the plant's financial capabilities, environmental targets, and overall sustainability strategy to select the most appropriate solution.

Sensitivity Analysis for Raw Material Cost

Sensitivity analysis is a valuable tool used to assess the impact of changes in key variables on a particular outcome. The sensitivity analysis was performed to evaluate the effect of fluctuations in raw material costs on the overall profitability of the plant. One critical aspect of this analysis is comparing only the raw material cost with the sales revenue, considering the price sensitivity of key components such as hydrogen and carbon dioxide, the pricing information are described in Table 7.5.

Table 7.5: Pricing information for the products.

Component	Price	Ref.
Methanol	\$0.498/kg	[367]
Hydrogen	\$2.000/kg	[368]
CO_2	\$0.060/kg	[369]
DME	\$0.600/kg	[370]

The cost of raw material (refer to Eq. 7.3.1) can be calculated using the pricing information for hydrogen and carbon dioxide, as well as the specific amounts of raw material intake for these components. In this case, the optimization case described in Section 7.3.1.3 provides the necessary values for the amount of raw material intake, which are 8668.284 kg/h for hydrogen and 88000 kg/h for carbon dioxide.

$$C_{RM} = \sum_{1}^{r} (\text{RMusage}_r \cdot \text{RMcost}_r) \quad \forall\, r \in [\text{H}_2, \text{CO}_2] \tag{7.3.1}$$

Additionally, the sales revenue can be determined based on the prices of methanol and dimethyl ether, by summing the product price and amount for each product stream, following the Eq. 7.3.2.

$$\text{Revenue} = \sum_{1}^{p} \left(\text{Pamount}_p \cdot \text{Pprice}_p \right) \quad \forall\, p \in [\text{Methanol}, \text{DME}] \tag{7.3.2}$$

It is important to consider the product streams, that were set as constraints in the optimization process. In this scenario, the optimization case (referenced in Section 7.3.1.3) sets the specific amounts for methanol and dimethyl ether product streams. It states that the plant produces 19,300 kg/h of methanol and 17,100 kg/h of dimethyl ether.

The results of the sensitivity analysis comparison between the prices of raw materials (hydrogen and carbon dioxide) and the corresponding raw material costs are presented in Figure 7.12.

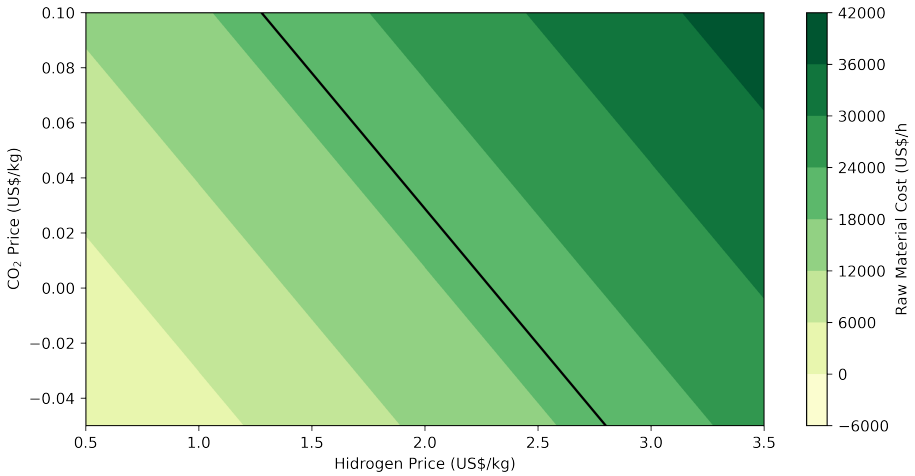

Figure 7.12: Sensitivity Analysis of Hydrogen and CO_2 Price.

Given that the sales revenue is \$19871, it is important to ensure that the cost of raw material (CRM) remains, at least, lower than this value to maintain profitability, considering only the cost of raw material.

Based on the optimized case, the calculated CRM is \$22616 using the provided pricing information. In this scenario, it becomes apparent that the plant would not be profitable if the prices of hydrogen and carbon dioxide are kept at that level.

To achieve profitability, adjustments in the prices of H_2 and CO_2 need to be made. If the CO_2 price remains at \$0.06 per kg, the price of H_2 must be reduced to \$1.683 per kg. Conversely, if the H_2 price is maintained at \$2 per kg, the price of CO_2 should be reduced to \$0.0288 per kg.

The sensitivity analysis also reveals a linear relationship between the prices of H_2 and CO_2 that yields profitability. The black line on the graph represents the exact combination of H_2

price and CO_2 price where the CRM equals the sales revenue. This relationship highlights the importance of finding the optimal balance between the prices of these raw materials.

The price of carbon dioxide is also evaluated. Carbon pricing incentivizes the reduction of greenhouse gas emissions by applying costs to polluters. In a scenario where CO_2 capture is incentivized through economic incentives, if the price of carbon dioxide is reduced to zero (free of charge), the price of H_2 can increase up to \$2.292 per kg.

By examining Figure 7.12, one can gain valuable insights into the relationship between price fluctuations and their impact on the overall cost of raw materials. It allows the identification of critical price ranges where the cost of raw materials may exceed the sales revenue.

It is crucial to note that there are additional costs beyond the raw material costs analyzed in this section that can significantly impact the profitability of the chemical plant. While the sensitivity analysis focused specifically on the relationship between raw material prices and sales revenue, other expenses, such as operational costs, energy costs, must also be evaluated. These factors, along with market conditions and demand fluctuations influence the profitability.

7.3.2 Case Study 2 - Acetic Acid Production Process

In order to apply the framework proposed in Section 7.2 to the acetic acid process, the first step involves the determination of variables and the development of simplified models using neural networks.

In Chapter 5, the base case flowsheeting was introduced as a starting point for further analysis, as depicted in Figure 7.13. The focus of this research is to propose a synthesis route for acetic acid production that utilizes CO_2 as a building block.

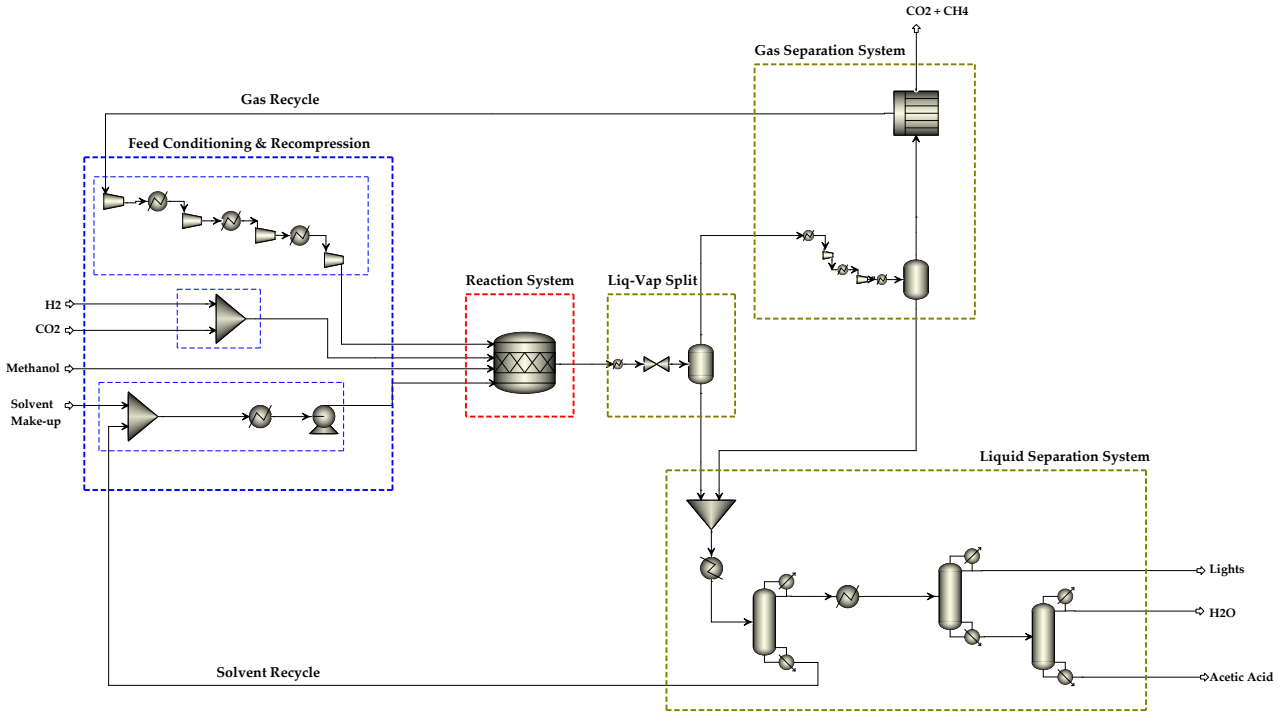

Figure 7.13: Acetic Acid Production Process Flowsheet.

The scales under consideration are determined based on the objectives, scope of the study, and the hypothesis or available information. For instance, Zondervan et al. [371] adopted an approach where they specifically examined three consecutive scales: the unit operation scale, unit scale, and plant scale. Their main goal was to thoroughly explore various processing options and identify the most optimal processing route among them.

These scales can be further expanded in both directions. When focusing on larger scales, there is a current trend to surpass the process scale and broaden the perspective of process synthesis. This involves enhancing the integration of the process within its ecosystem, thereby considering the larger context and interconnections beyond just the immediate process.

7.3.2.1 Definition of Neural Networks for the Subsystems

To effectively analyze and optimize the process, the flowsheet (Figure 7.13) was divided into six distinct subsystems. These subsystems are depicted in Figure 7.14. By breaking down the flowsheet into smaller components, it becomes easier to study and understand the individual processes occurring within the overall system.

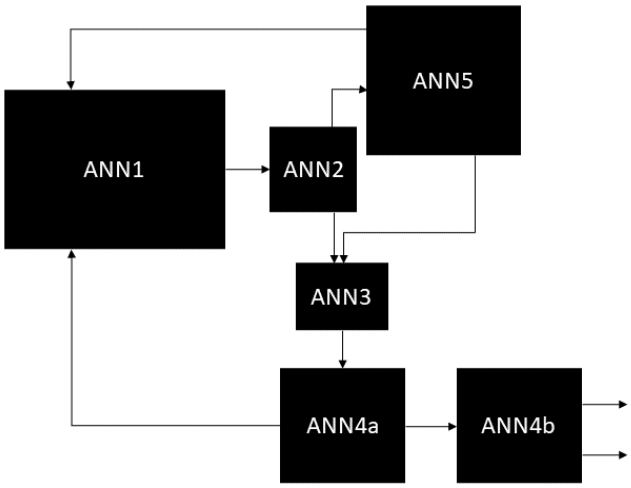

Figure 7.14: Acetic Acid Production Process Flowsheet.

The first subsystem (see details in Appendix G) involves the preparation and handling of the raw materials required for acetic acid production. This includes the CO_2 feedstock, which is a crucial building block in the proposed synthesis route. The handling of other necessary reactants, such as methanol and hydrogen, is also part of this subsystem. It is also included the reactor design and operation. This stage involves the interaction between the reactants and the catalysts, where chemical reactions take place to convert CO_2 and methanol into acetic acid. The optimal reactor conditions, such as temperature, need to be determined to achieve desired conversion and selectivity.

The second subsystem (see details in Appendix H) involves the separation and purification of the reaction products. The first separation step is the split of the initial mixture in monophase submixtures (gas and liquid) using a simple flash. The third subsystem (see details in Appendix I) is the mixing of liquid streams from the gas separation system and the flash.

The liquid separation subsystem plays a crucial role in the acetic acid production process. Its primary objective is to separate and purify the desired acetic acid from the reaction mixture, while also considering the recovery of any valuable byproducts and the recycling of unreacted materials. Therefore, the liquid separation system was divided into two subsystems: 4a (see details in Appendix J) and 4b (see details in Appendix K).

The fifth subsystem (see details in Appendix L) addresses the gas separation system. This involves the removal of impurities from gaseous stream through a membrane module. The recycling of unreacted materials are also considered in this subsystem.

By dividing the acetic acid production flowsheet into these six subsystems, a comprehensive framework for analysis and optimization can be established. This approach allows for a detailed investigation of each subsystems while considering the interactions and dependencies between them.

7.3.2.2 Surrogate Modeling Aspects - Normalization

The normalization of data before entering it into a neural network can have a significant impact on the performance and effectiveness of the model. Normalization refers to the process of scaling and standardizing the input data to a consistent range or distribution.

Normalizing the input data helps to ensure that the optimization algorithm converges more effectively during the training process. When the input features have widely varying scales, it can lead to slower convergence or even the failure of the training process. Additionally, certain features with larger scales can dominate the learning process compared to features with smaller scales. This can lead to biased influence and less meaningful learning. Normalizing the data mitigates this bias by placing all features on a similar scale, allowing each feature to contribute more equally during the training process.

To exemplify, the neural network 1 (Appendix G) was used. The normalization results are depicted in Figure 7.15. The applied technique was min-max normalization, which rescales the input features to a range between -1 and 1. This is achieved through a linear transformation of the data using the minimum and maximum values of each feature.

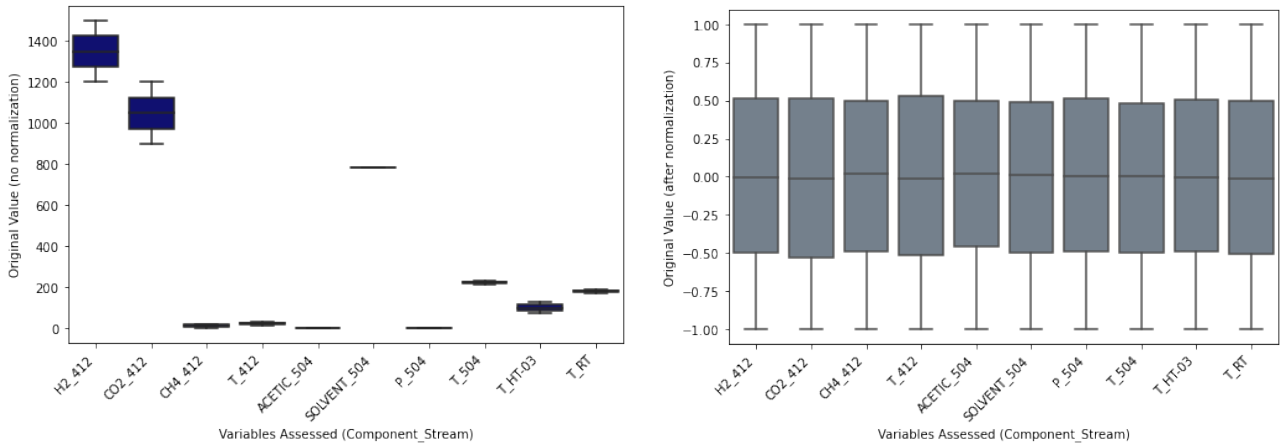

(a) (b)

Figure 7.15: Input Distribution for ANN1. (a) Original Values and (b) After Normalization.

Before normalization, the scales of the features differ significantly in terms of magnitude. However, after applying min-max normalization, all the features are transformed to a consistent range, eliminating the variations in magnitude.

By applying Min-Max Normalization, the features are scaled consistently, allowing for easier comparison and analysis. The method is straightforward to implement and helps prevent the dominance of certain features in neural network training, while it maintains the original range of the data.

The same procedure of data normalization was applied to all the neural networks generated within this study, ensuring consistency and comparability across the various subsystems. For each subsystem, the input data used to train and test the neural networks contained multiple features that represented different aspects of the corresponding process. These features often exhibited different orders of magnitude and ranges, making direct comparison and analysis challenging.

Data normalization before entering it into a neural network is crucial for ensuring better convergence, avoiding biased influence, improving gradient descent, promoting regularization, enhancing model interpretability, and facilitating generalization to unseen data, therefore making more accurate predictions.

7.3.2.3 Mass balance analysis in ANN4a

To integrate phenomenological aspects, like mass balance, into the neural networks, an assessment was performed in the neural network 4a (Appendix J), which represents the subsystem of the liquid separation system, according to Figure 7.16.

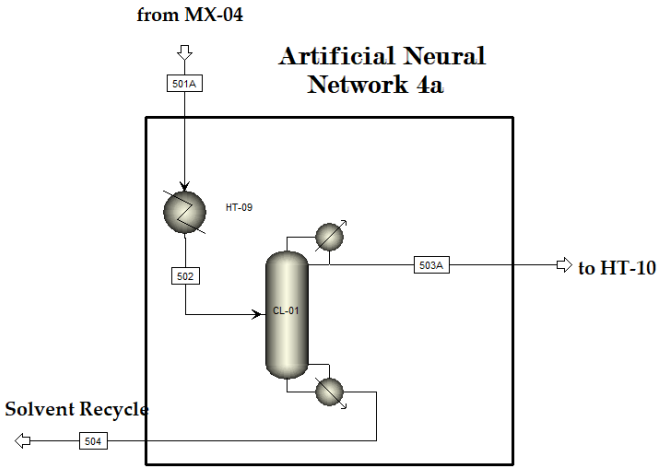

Figure 7.16: Process flowsheet for Liquid Separation System for ANN4a.

The molar flow rates of the components in the input stream (501) were analyzed and compared with the corresponding output streams (503 and 504). The findings for CO_2 and CH_4 are illustrated in Figure 7.17.

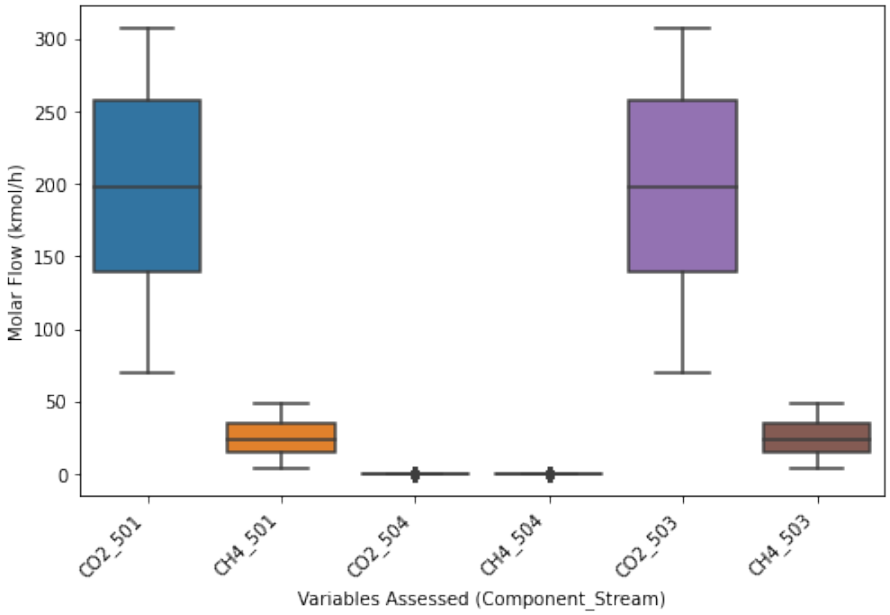

Figure 7.17: Distribution of data for CO_2 and CH_4.

The analysis of Figure 7.17 provides valuable insights into the numerical data distribution and important statistical characteristics, including the median, quartiles, and potential outliers. The results clearly indicate that the molar flow of CO_2 and CH_4 in the input stream (501) is predominantly found in stream 503. Moreover, similarities can be observed in their central tendencies, spreads, and skewness.

Based on these observations, we can approximate the mass balance equations as:

$$z^{in}_{CO_2} = z^{503}_{CO_2}$$

$$z^{in}_{CH_4} = z^{503}_{CH_4}$$

$$z^{504}_{CO_2} \approx 0$$

$$z^{504}_{CH_4} \approx 0$$

It can be assumed that the molar flow of CO_2 in stream 504 is approximately negligible, and the same applies to the molar flow of CH_4 in stream 504. Similarly, the aforementioned approach was also applied to the other components, namely hydrogen, methanol, ethanol, methyl acetate, and ethyl acetate. The molar flow rates of these components in the input stream (501) were carefully examined and compared to their respective output streams (503 and 504). The results obtained from this analysis are visually presented in Figure 7.18, providing a comprehensive

overview of the distribution and behavior of these components.

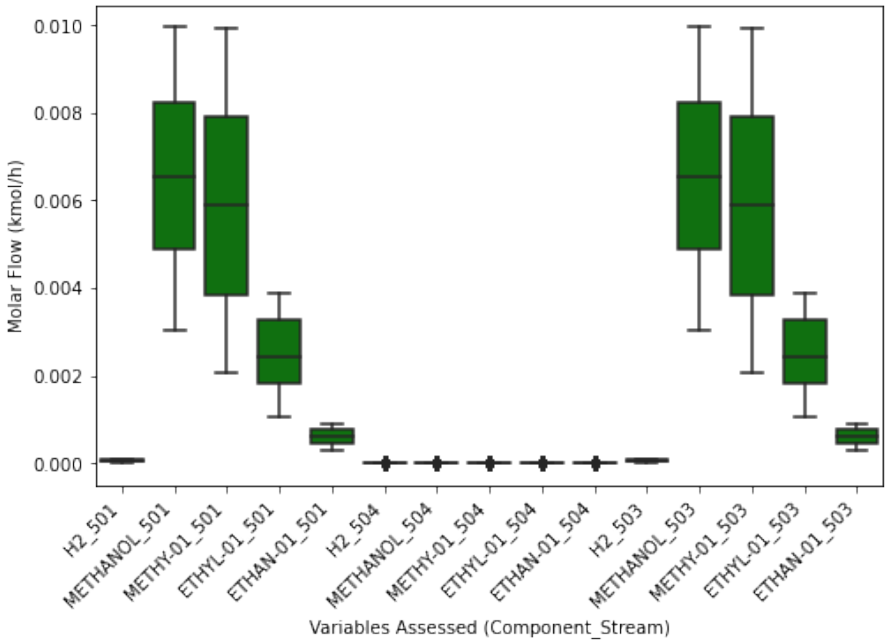

Figure 7.18: Distribution of data for minor components in liquid separation system.

Upon conducting the comparisons, it becomes evident that the molar flows of hydrogen, methanol, ethanol, methyl acetate, and ethyl acetate from the input stream (501) are predominantly observed in the output stream (503). Consequently, the quantity of these components remaining in stream 504 is minimal and can be considered negligible..

The findings presented in Figure 7.18 serve to enhance our understanding of the system's mass balance for each component. They provide a visual representation of the distribution of the molar flow rates and highlight any significant variations or trends that may exist between the input and output streams. It also allow to reduce the dimensionality of the neural networks, due to mass balance considerations.

7.3.2.4 Analysis of Neural Network Predictions

A comprehensive examination of specific parameters in the input variables was carried out. This involved conducting a study with neural network 2, as depicted in Figure 7.19, while systematically varying the key parameters related to a one output. This detailed analysis aimed to assess the impact of the parameter variations on the performance and reliability of the neural network. By investigating the specific parameters and their effects on the output, a more thorough understanding of the neural network's behavior and its sensitivity to input variations was achieved.

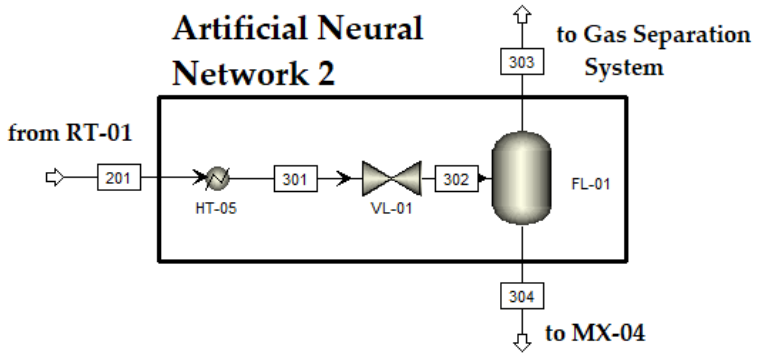

Figure 7.19: Process flowsheet for gas liquid split.

Figure 7.20 illustrates the examination of variations in the molar flow of acetic acid in stream 201 and the temperature of the heat exchanger (HT-05), specifically in relation to their impact on the molar flowrate of acetic acid. The analysis provides a visual representation of the relationship between these variables, shedding light on how changes in the molar flow and temperature influence the molar flowrate of acetic acid.

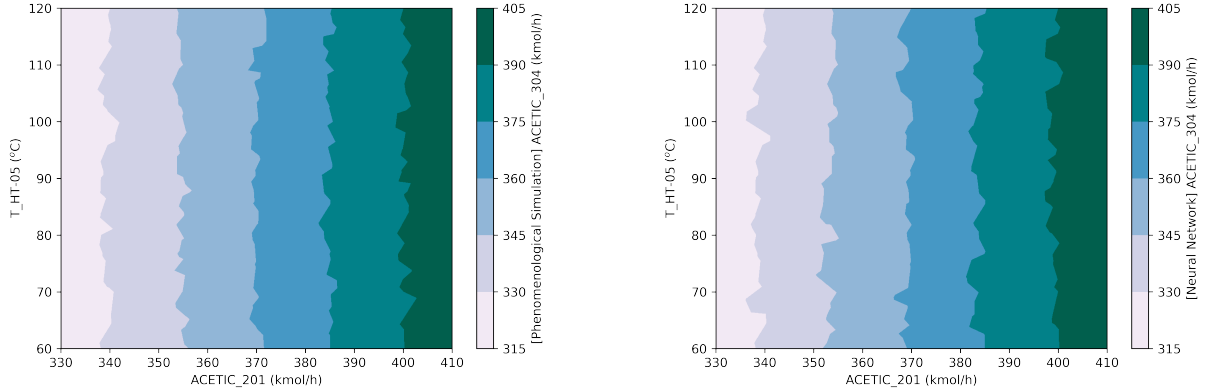

(a) (b)

Figure 7.20: Contourn of molar flow rate of acetic acid in stream 201 from (a) phenomenological simulation and (b) neural networks.

In Figure 7.20a, the outcomes of the phenomenological simulation are displayed, where the molar flow rate of acetic acid and the temperature of the heat exchanger (HT-05) were varied while keeping other variables constant. On the other hand, Figure 7.20b showcases the response of the trained neural network to the same inputs. A notable observation is the presence of similarities and patterns between the neural network and the phenomenological model. It is important to note that the Figure 7.20 is an interpolation between the collected data, either for the phenomenological data and for the neural network.

Furthermore, these findings were consistent with a previous study conducted by Chakkingal *et al.* [372], which also involved comparing different machine learning models. The similar results obtained in both studies emphasized the reliability and potential of machine learning approaches in accurately modeling and predicting chemical processes. They highlighted the ability of the trained neural network to capture and replicate the behavior observed in the phenomenological model, indicating its potential for practical application in process optimization. The same procedure described for constructing the neural network was also employed for all other networks utilized in the case study #2. These additional networks, which focused on different section of the flowsheet, are thoroughly explained in the Appendices G to L. In the appendices, detailed information regarding the network architectures, hyperparameter settings, training methodologies, and any specific modifications or enhancements implemented can be found.

7.3.2.5 Surface response for the optimization procedure

The initial scenario contains the original values obtained from the simulation conducted in Chapter 5.

Combining CAPEX and OPEX, the total annualized cost amounts to $156.80M, representing the comprehensive cost of running the plant anuallized for a year. Furthermore, the total CO_2 emissions of 199.13M kg/y highlight the environmental impact and carbon footprint of the plant. This value provides insights into the amount of carbon dioxide emitted during the plant's operation based on utilities usage.

To perform a sensitivity analysis on the plant's performance, a modification of the Response Surface Methodology (RSM) was employed. The methodology is used to model and analyze the relationship between input variables (process variables or factors) on the output variables. RSM is particularly useful when the relationship between the inputs and the response is complex and nonlinear. By varying the levels of the input variables within a defined range, RSM enables the exploration of the response surface, which is a graphical representation of the relationship between the inputs and the output.

In the context of the analysis described, the results were obtained by varying 21 free variables, which play a crucial role in determining the performance of the chemical plant. These variables include the temperature of heat exchangers and reactor, pressure on the valve, reflux ratio, distillate to feed ratio, feed stage of the columns, and membrane area.

The range of variation for these free variables is specified in the Appendices G to L, indicating the boundaries within which they were explored during the sensitivity process. By considering different values within these ranges, the calculated function ($f = alpha \cdot TAC + (1 - alpha) \cdot$

$TotalCO_2$) aims to identify the optimal combination of these variables that leads to improved function.

It is important to note that the molar flows in the process are calculated using neural networks, as depicted in Figure Figure 7.14. The outputs of one neural network serve as inputs to the next neural network in a cascaded manner. This approach allows for the integration of various process stages and enables the modeling of complex relationships between variables and responses.

By utilizing neural networks, the optimization process can handle the nonlinear and complex nature of the chemical plant system. These networks capture the underlying patterns and correlations within the process data, providing insights into the relationships between the free variables and the desired outcomes, such as reducing the total annualized cost (TAC) and minimizing CO2 emissions.

Figure 7.21 presents the results of the evaluation of a range of conditions on the Total Annualized Cost (TAC) and Total $CO_{2,eq}$ emissions. In Figure 7.21a, the scenario considers alpha=1, aiming to evaluate the best case for TAC optimization. In Figure 7.21b, alpha=0 is considered, focusing on Total $CO_{2,eq}$ emissions.

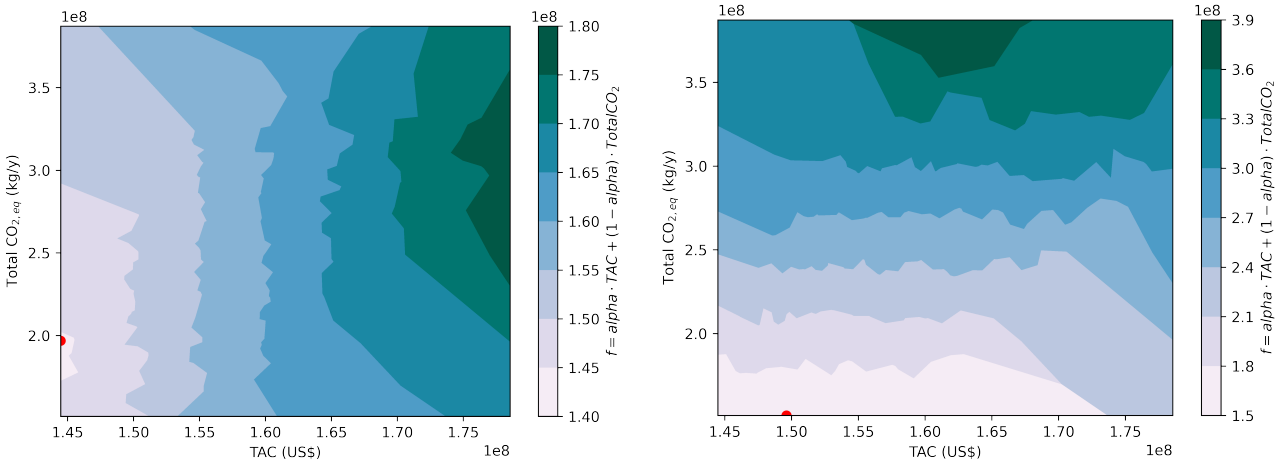

(a) (b)

Figure 7.21: Response for the acetic acid complete process (a) alpha=1 and (b) alpha=0.

The results indicate a reduction in the TAC for both scenarios. In the case where alpha=1, the TAC is reduced from \$156.80M (base case) to \$144.47M, indicating a significant improvement in cost efficiency. Similarly, when alpha=0, the TAC is reduced to \$149.61M.

Moreover, the total CO_2 equivalent emissions are also reduced through optimization. In the scenario with alpha=1, the emissions decrease from 199.13M kg/y (base case) to 196.86M kg/y,

showcasing a reduction in the environmental impact. In the scenario with alpha=0, the emissions are further reduced to 151.09M kg/y.

The optimal variables were tested back in the simulation, the results are in good agreement in average of 3.73% in the outputs. The results corroborate the predictions of the neural networks. These results demonstrate the effectiveness of the data-driven optimization approach efforts using RSM modified in achieving cost savings and environmental improvements for the chemical plant. By identifying optimal combinations of input variables, the plant's performance can be enhanced, leading to reduced costs and a smaller carbon footprint.

7.4 Conclusions

This study introduces a framework for the optimization of chemical plants, considering both the total annualized cost and the total CO_2 emissions resulting from the utility usage. Addressing economic and environmental factors simultaneously promotes sustainable practices in the chemical engineering field.

The proposed framework leverages simplified models, particularly neural networks, to accurately represent the plant's behavior. Simplified models or surrogates can be used to represent an entire subsystem consisting of a definite number of units or even an entire chemical plant.

The results obtained from the optimization process provide valuable insights into the plant's performance and financial implications. By considering the total annualized cost, encompassing both capital expenditure (CAPEX) and operating expenditure (OPEX), the framework offers a comprehensive evaluation of the plant's financial economics. Additionally, by factoring in the total CO_2 emissions resulting from utility usage, the environmental impact and carbon footprint of the plant are assessed.

Therefore, this study contributes to the advancement of optimization techniques in chemical engineering, emphasizing the importance of integrating economic and environmental factors. The proposed framework opens new avenues for future research and development, ultimately driving the industry towards more sustainable and efficient chemical plant operations.

Chapter 8

Conclusions and Recommended Future Works

In this chapter, the final conclusions drawn from the extensive research conducted throughout the study are presented. These conclusions reflect the comprehensive analysis of the data collected, the insights gained, and the patterns and trends identified. Moreover, based on these conclusions, valuable recommendations for future works and further research will be provided.

8.1 Conclusions

In recent years, there has been a shift in the scientific community's perspective regarding carbon dioxide. Rather than considering it solely as an expensive waste, particularly in countries with carbon taxes, CO_2 is now seen as a potential carbon source, offering an alternative to fossil fuels. As a result, future perspectives on reducing carbon dioxide emissions will not only focus on the advancement of more efficient Carbon Capture and Storage technologies but will also involve the development of new strategies for recycling CO_2 into energy vectors and chemical intermediates.

This shift in mindset opens up novel opportunities for utilizing CO_2 as a valuable resource and exploring innovative pathways for transforming it into useful products, thereby contributing to the reduction of greenhouse gas emissions and promoting a more sustainable and circular economy. The contribution of CO_2 conversion goes beyond lowering global warming, by means of reducing fossil resource depletion or even yielding more benign production pathways.

The literature data regarding the quantity of energy needed to convert CO_2 into chemicals is limited and narrowed to the most studied processes and products. Different procedures to estimate the basic thermodynamic properties of the reactants and products of these reactions were investigated. The availability of experimental thermochemistry data is often limited due to the destructive nature and material requirements of calorimetry measurements. To overcome this challenge, computational chemistry methods offer a promising approach for modeling

physiochemical properties and determining optimal molecular structures. While previous studies in CO_2 utilization have focused on a limited number of compounds, this research specifically addressed the scarcity of energy-related content related to CO_2 products. Carbon dioxide-derived products are categorized into sixteen chemical classes, providing valuable insights into the reaction enthalpy associated with their direct production. The findings reveal significant variations in reaction enthalpy across the different chemical classes. This knowledge contributes to a deeper understanding of the design considerations for chemical products in CO_2 utilization. By expanding the scope of investigation and exploring a broader range of CO_2 products, this research enhances our understanding of their thermodynamic properties and their potential as sustainable alternatives.

A Brazilian local market analysis for potential products from CO_2 chemical conversion was performed. The proposed approach demonstrated its effectiveness in selecting the most favorable products for CO_2 conversion. The concern over CO_2 emissions from power plants in Brazil served as the motivation to map these emissions and conduct a local market analysis for potential products derived from CO_2 chemical conversion. Among the assessed products, methanol, polycarbonates, formic acid, and acetaldehyde emerged as the most promising options for implementation in Brazil. The research highlighted that power plants with higher capacities, and consequently, higher CO_2 emissions, are primarily located in São Paulo and Rio de Janeiro. São Paulo exhibited both a greater demand for the evaluated products and a significant availability of CO_2, suggesting it as a potential location for the installation of a new CO_2 conversion plant.

The challenge of evaluating carbon dioxide utilization technologies and identifying promising products from a wide range of candidates were addressed. A systematic search was conducted to establish specific criteria for carbon dioxide conversion, which were then applied in a three-level assessment to select the most suitable CO_2 conversion products. The proposed methodological framework allows decision-makers to prioritize products for further development and commercialization, considering economic viability, technological maturity, and scientific significance. Dimethyl carbonate, dimethyl ether, and acetic acid emerged as the most favorable products for further rigorous process design studies. Furthermore, this study offers the flexibility to consider variations in prices, maturity levels, and scientific relevance of the evaluated products.

The focus on assessing various routes for acetic acid production from CO_2 using a multicriteria decision analysis approach revealed the methanol hydrocarboxylation route to be the most promising, leading to further in-depth analysis. Through exploration within the field of chemical engineering, an innovative process was developed for acetic acid production. While sharing similarities with the traditional methanol carbonylation method, this process incorporates adjustments in CO_2 as feedstock, temperature and pressure ranges and efficient separation units

leading to a technically feasible process. It is worth noting that there is a scarcity of literature data regarding the process design of acetic acid production from CO_2, methanol and hydrogen. Thus, this study contributes to the field of process synthesis for converting CO_2 into high-value products.

A comprehensive evaluation of carbon dioxide conversion into methanol and dimethyl ether, focusing on the integration of the latest carbon dioxide utilization techniques was conducted. The proposed integrated flowsheet considered key chemical engineering aspects, such as process design, to ensure efficient and sustainable production of these products. The feasibility of the proposed flowsheet has been established through the successful separation and purification of the desired products, as well as the efficient recycling of unreacted gases. Further optimization efforts can concentrate on enhancing the energy efficiency of the system, reducing resource consumption, and optimizing the separation processes to enhance product purity. By addressing these areas, the overall performance and sustainability of the process can be improved, leading to more efficient utilization of resources and higher product quality.

A framework that optimizes chemical plants by considering both the total annualized cost and the resulting CO_2 emissions from utility usage was proposed. By leveraging simplified models, particularly neural networks, the framework accurately represents plant behavior, enabling efficient optimization. The comprehensive evaluation of the plant's financial economics and environmental impact contributes to the advancement of optimization techniques in chemical engineering. Some solutions prioritize environmental sustainability by achieving substantial emissions reductions, while others focus on cost reduction while meeting emission targets. The relevance of these solutions depends on factors such as industry regulations, stakeholder expectations, and long-term sustainability goals of the chemical plant. Aslo, the optimized case reveals that the chemical plant would not be profitable based on the provided pricing information. Adjustments in the prices of hydrogen and carbon dioxide are necessary to achieve profitability. Carbon pricing and incentives for CO_2 capture are considered, indicating that if the price of CO_2 is reduced to zero, the price of H_2 can increase to a certain extent. The proposed framework opens new avenues for research and development, ultimately driving the industry towards more sustainable and efficient chemical plant operations.

8.2 Recommendations for Future Works

The recommendations for future works serve as a roadmap for researchers interested in further advancing the knowledge and understanding in the chemical engineering aspects. These recommendations are based on the identified limitations of the current study and aim to guide future research toward addressing these limitations and exploring new avenues of investigation.

The process of evaluating carbon dioxide utilization technologies, as well as identifying potential products from a broad assortment of candidates, posed a considerable challenge that has now been addressed. In the proposed methodological framework one can also incorporate information about the energy needed for separation of each product assessed and the thermodynamics for the reaction synthesis. This comprehensive approach provides a more realistic evaluation of the energy consumption and associated costs involved in the production of a particular product. By factoring in these elements, the framework aids in establishing a more effective and economical CO_2 utilization process.

To maximize the utilization of phenomenological aspects and prior knowledge, it is crucial to integrate the understanding of physical systems into neural network frameworks. This involves incorporating the first principles and insights gained from chemical process knowledge into data-driven modeling, as an example of hybrid models and gray-box models.

Future research must focus on challenges that process synthesis will encounter. This entails incorporating multi-product processes into a superstructure, enabling optimization based on various pathways for chemical production (via route A or route B). Additionally, environmental and economic factors must be taken into consideration throughout the decision-making process.

References

[1] Agency, I. E. **World energy outlook 2016**: IEA, 2016. 684 p.

[2] Song, C. Global challenges and strategies for control, conversion and utilization of co2for sustainable development involving energy, catalysis, adsorption and chemical processing. **Catalysis Today**, v. 115, p. 2–32, 2006.

[3] Economics, B. E. **Bp energy outlook: 2018 edition**: BP, 2018. 125 p.

[4] Hunt, A. J.; Sin, E. H.; Marriott, R. and Clark, J. H. Generation, capture, and utilization of industrial carbon dioxide. **ChemSusChem**, v. 3, p. 306–322, 2010.

[5] ExxonMobil. **2018 outlook for energy: A view to 2040**: 2018. 63 p.

[6] Bertran, M. O.; Frauzem, R.; Sanchez-Arcilla, A. S.; Zhang, L.; Woodley, J. M. and Gani, R. A generic methodology for processing route synthesis and design based on superstructure optimization. **Computers and Chemical Engineering**, v. 106, p. 892–910, 2017.

[7] Aresta, M. and Dibenedetto, A. Utilisation of co2 as a chemical feedstock: opportunities and challenges. **Dalton Transactions**, p. 2975, 2007.

[8] Fan, J. L.; Zhang, X.; Zhang, J. and Peng, S. Efficiency evaluation of co2 utilization technologies in china: A super-efficiency dea analysis based on expert survey. **Journal of CO2 Utilization**, v. 11, p. 54–62, 2014.

[9] Artz, J.; Müller, T. E.; Thenert, K.; Kleinekorte, J.; Meys, R.; Sternberg, A.; Bardow, A. and Leitner, W. Sustainable conversion of carbon dioxide: An integrated review of catalysis and life cycle assessment. **Chemical Reviews**, p. acs.chemrev.7b00435, 2017.

[10] Gale, J.; Bradshaw, J.; Chen, Z.; Garg, A.; Gomez, D.; Rogner, H.; Simbeck, D.; Williams, R.; Toth, F. and van Vuuren, D. Sources of co2: Cambridge University Press, 2005. p. 75 – 104.

[11] Peters, M.; Köhler, B.; Kuckshinrichs, W.; Leitner, W.; Markewitz, P. and Müller, T. E. Chemical technologies for exploiting and recycling carbon dioxide into the value chain. **ChemSusChem**, v. 4, p. 1216–1240, 2011.

[12] Zimmermann, A. and Kant, M. The business side of innovative co2 utilisation. *Technical report*, Technische Universitat Berlin, 2015.

[13] Aresta, M.; Dibenedetto, A. and Angelini, A. The changing paradigm in co2 utilization. **Journal of CO2 Utilization**, v. 3-4, p. 65–73, 2013.

[14] et al. BRINCKERHOFF, P. **Accelerating the uptake of ccs: industrial use of captured carbon dioxide**: Global CCS Institute, 2011. 260 p.

[15] Mikkelsen, M.; Jørgensen, M. and Krebs, F. C. The teraton challenge. a review of fixation and transformation of carbon dioxide. **Energy Environ. Sci.**, v. 3, p. 43–81, 2010.

[16] Aresta, M.; Dibenedetto, A. and Angelini, A. Catalysis for the valorization of exhaust carbon: From co2 to chemicals, materials, and fuels. technological use of co2. **Chemical Reviews**, v. 114, p. 1709–1742, 2014.

[17] Li, B. H.; Zhang, N. and Smith, R. Simulation and analysis of co2 capture process with aqueous monoethanolamine solution. **Applied Energy**, v. 161, p. 707–717, 2016.

[18] Pakhare, D. and Spivey, J. A review of dry (co2) reforming of methane over noble metal catalysts. **Chem. Soc. Rev.**, v. 43, p. 7813–7837, 2014.

[19] Albo, J.; Alvarez-Guerra, M.; Castaño, P. and Irabien, A. Towards the electrochemical conversion of carbon dioxide into methanol. **Green Chem.**, p. 2304–2324, 2015.

[20] Pekdemir, T. Integrated capture and conversion. **Carbon Dioxide Utilisation: Closing the Carbon Cycle: First Edition**, p. 253–272, 2014.

[21] Martín, A. J.; Larrazábal, G. O. and Pérez-Ramírez, J. Towards sustainable fuels and chemicals through the electrochemical reduction of co2: lessons from water electrolysis. **Green Chem.**, v. 17, p. 5114–5130, 2015.

[22] Zheng, Y.; Zhang, W.; Li, Y.; Chen, J.; Yu, B.; Wang, J.; Zhang, L. and Zhang, J. Energy related co2conversion and utilization: Advanced materials/nanomaterials, reaction mechanisms and technologies. **Nano Energy**, v. 40, p. 512–539, 2017.

[23] Ampelli, C.; Perathoner, S. and Centi, G. Co2 utilization: an enabling element to move to a resource- and energy-efficient chemical and fuel production. **Philosophical Transactions of the Royal Society A: Mathematical, Physical and Engineering Sciences**, v. 373, p. 20140177–20140177, 2015.

[24] Fernández-Dacosta, C.; Stojcheva, V. and Ramirez, A. Closing carbon cycles: Evaluating the performance of multi-product co2 utilisation and storage configurations in a refinery. **Journal of CO2 Utilization**, v. 23, p. 128–142, 2018.

[25] Graciano, J. E. and Roux, G. A. L. Improvements in surrogate models for process synthesis. application to water network system design. **Computers and Chemical Engineering**, v. 59, p. 197–210, 2013.

[26] Wu, W.; Yenkie, K. and Maravelias, C. T. A superstructure-based framework for bio-separation network synthesis. **Computers and Chemical Engineering**, v. 96, p. 1–17, 2017.

[27] Yeomans, H. and Grossmann, I. E. A systematic modeling framework of superstructure optimization in process synthesis. **Computers and Chemical Engineering**, v. 23, p. 709–731, 1999.

[28] Biegler, L. T.; Grossmann, I. E. and Westerberg, A. W. **Systematic methods of chemical process design**: Prentice Hall PTR, 1999. 808 p.

[29] Grossmann, I. E. and Daichendt, M. M. New trends in optimization-based approaches to process synthesis. **Computers & Chemical Engineering**, v. 20, p. 665–683, 2003.

[30] Henao, C. A. and Maravelias, C. T. **Surrogate-based process synthesis**. v. 28: Elsevier B.V., 2010. 1129-1134 p.

[31] Haykin, S. **Neural networks: a comprehensive foundation**: Prentice Hall PTR, 1994.

[32] Haunschild, R. Theoretical study on the reaction mechanism of carbon dioxide reduction to methanol using a homogeneous ruthenium(ii) phosphine catalyst. **Polyhedron**, v. 85, p. 543–548, 2015.

[33] Milani, D.; Khalilpour, R.; Zahedi, G. and Abbas, A. A model-based analysis of co2 utilization in methanol synthesis plant. **Journal of CO2 Utilization**, v. 10, p. 12–22, 2015.

[34] Pérez-Fortes, M.; Schöneberger, J. C.; Boulamanti, A.; Harrison, G. and Tzimas, E. Formic acid synthesis using co2 as raw material: Techno-economic and environmental evaluation and market potential. **International Journal of Hydrogen Energy**, v. 41, p. 16444–16462, 2016.

[35] Pacheco, K. A.; Bresciani, A. E.; Nascimento, C. A. and Alves, R. M. Assessment of property estimation methods for the thermodynamics of carbon dioxide-based products. **Energy Conversion and Management**, v. 211, p. 112756, 5 2020.

[36] Pacheco, K. A.; Reis, A. C.; Bresciani, A. E.; Nascimento, C. A. O. and Alves, R. M. B. Assessment of the brazilian market for products by carbon dioxide conversion. **Frontiers in Energy Research**, v. 7, p. 1–16, 2019.

[37] Pacheco, K. A.; Bresciani, A. E. and Alves, R. M. Multi criteria decision analysis for screening carbon dioxide conversion products. **Journal of CO2 Utilization**, v. 43, 1 2021.

[38] Pacheco, K. A.; Bresciani, A. E.; Nascimento, C. A. O. and Alves, R. M. B. Co2-based acetic acid production assessment. **30 European Symposium on Computer Aided Process Engineering**, v. 48, p. 1027–1032, 2020.

[39] Mago, P. J. and Luck, R. Potential reduction of carbon dioxide emissions from the use of electric energy storage on a power generation unit/organic rankine system. **Energy Conversion and Management**, v. 133, p. 67–75, 2017.

[40] Wiesberg, I. L.; de Medeiros, J. L.; Alves, R. M.; Coutinho, P. L. and Araújo, O. Q. Carbon dioxide management by chemical conversion to methanol: Hydrogenation and bi-reforming. **Energy Conversion and Management**, v. 125, p. 320–335, 2016.

[41] Blumberg, T.; Morosuk, T. and Tsatsaronis, G. Co 2 -utilization in the synthesis of methanol: Potential analysis and exergetic assessment. **Energy**, v. 175, p. 730–744, 2019.

[42] Dabral, S. and Schaub, T. The use of carbon dioxide (co2) as a building block in organic synthesis from an industrial perspective. **Advanced Synthesis and Catalysis**, v. 361, p. 223–246, 2019.

[43] Chauvy, R.; Meunier, N.; Thomas, D. and Weireld, G. D. Selecting emerging co2 utilization products for short- to mid-term deployment. **Applied Energy**, v. 236, p. 662–680, 2019.

[44] Koytsoumpa, E. I.; Bergins, C. and Kakaras, E. The co2economy: Review of co2capture and reuse technologies. **Journal of Supercritical Fluids**, v. 132, p. 3–16, 2018.

[45] Shell. Shell energy transition report. p. 157–166, 2018.

[46] Jr, E. L. C. and Moggridge, G. D. **Chemical product design**. 2 ed: Cambridge University Press, 2011.

[47] Bagheri, M.; Yerramsetty, K.; Gasem, K. A. M. and Neely, B. J. Molecular modeling of the standard state heat of formation. **Energy Conversion and Management**, v. 65, p. 587–596, 2013.

[48] Poling, B. E.; Prausnitz, J. M. and O'connell, J. P. **The properties of gases and liquids**. v. 5: McGraw-Hill, 2001.

[49] JOBACK, K. and REID, R. Estimation of pure-component properties from group-contributions. **Chemical Engineering Communications**, v. 57, p. 233–243, 1987.

[50] Benson, S. W.; Golden, D. M.; Haugen, G. R.; Shaw, R.; Cruickshank, F. R.; Rodgers, A. S.; O'neal, H. E. and Walsh, R. Additivity rules for the estimation of thermochemical properties. **Chemical Reviews**, v. 69, p. 279–324, 1969.

[51] Austin, N. D.; Sahinidis, N. V. and Trahan, D. W. Computer-aided molecular design: An introduction and review of tools, applications, and solution techniques. **Chemical Engineering Research and Design**, v. 116, p. 2–26, 2016.

[52] Thiel, W. Semiempirical quantum-chemical methods. **Wiley Interdisciplinary Reviews: Computational Molecular Science**, v. 4, p. 145–157, 2014.

[53] Dewar, M. J.; Zoebisch, E. G.; Healy, E. F. and Stewart, J. J. Am1: A new general purpose quantum mechanical molecular model1. **Journal of the American Chemical Society**, v. 107, p. 3902–3909, 1985.

[54] Stewart, J. J. P. Optimization of parameters for semiempirical methods vi: more modifications to the nddo approximations and re-optimization of parameters. **J Mol Model**, p. 1–32, 2013.

[55] Stewart, J. J. Optimization of parameters for semiempirical methods v: Modification of nddo approximations and application to 70 elements. **Journal of Molecular Modeling**, v. 13, p. 1173–1213, 2007.

[56] Otto, A.; Grube, T.; Schiebahn, S. and Stolten, D. Closing the loop: captured co ₂ as a feedstock in the chemical industry. **Energy Environ. Sci.**, v. 8, p. 3283–3297, 2015.

[57] Plus, T. A. Aspen plus v9. 2016.

[58] Hanwell, M. D.; Curtis, D. E.; Lonie, D. C.; Vandermeersch, T.; Zurek, E. and Hutchison, G. R. Avogadro: an advanced semantic chemical editor, visualization, and analysis platform. **Journal of Cheminformatics**, v. 4, p. 17, 2012.

[59] O'Boyle, N. M.; Morley, C. and Hutchison, G. R. Pybel: a python wrapper for the openbabel cheminformatics toolkit. **Chemistry Central Journal**, v. 2, p. 5, 2008.

[60] Halgren, T. A. Merck molecular force field. ii. mmff94 van der waals and electrostatic parameters for intermolecular interactions. **Journal of Computational Chemistry**, v. 17, p. 520–552, 1996.

[61] Halgren, T. A. Merck molecular force field. iii. molecular geometries and vibrational frequencies for mmff94. **Journal of Computational Chemistry**, v. 17, p. 553–586, 1996.

[62] MOPAC2016 and Stewart, J. J. P. Stewart computational chemistry. 2016.

[63] Willmott, C. J. Some comments on the evaluation of model performance. **Bulletin of the American Meteorological Society**, v. 63, p. 1309–1313, 1982.

[64] Chai, T. and Draxler, R. R. Root mean square error (rmse) or mean absolute error (mae)? -arguments against avoiding rmse in the literature. **Geoscientific Model Development**, v. 7, p. 1247–1250, 2014.

[65] Li, J. A review of spatial interpolation methods for environmental scientists. **Canberra: Geoscience Australia**, v. 137, p. 154, 2008.

[66] Nash, E. and Sutcliffe, V. River flow forecasting through conceptual models part i - a discussion of principles. **Journal of Hydrology**, v. 10, p. 282–290, 1970.

[67] Legates, D. R. and Jr., G. J. M. Evaluating the use of "goodness-of-fit" measures in hydrologic and hydroclimatic model validation. **Water Resources Research**, v. 35, p. 233–241, 1 1999.

[68] Koretsky, M. D. **Engineering and chemical thermodynamics**. v. 2: Wiley New York, 2004.

[69] Y. B. Razali, . W., N. M. Power comparisons of shapiro-wilk, kolmogorov-smirnov, lilliefors and anderson-darling tests. **Journal of Statistical Modeling and Analytics**, v. 2, p. 21–33, 2011.

[70] Cramer, D. **Fundamental statistics for social research: Step-by-step calculations and computer techniques using spss for windows**: Routledge, 1998.

[71] Guthrie, J. P. Hydration of carboxamides. evaluation of the free energy change for addition of water to acetamide and formamide derivatives. **Journal of the American Chemical Society**, v. 96, p. 3608–3615, 5 1974.

[72] Lide, D. R. **Crc handbook of chemistry and physics**. 90th ed: 2009.

[73] NIST. Nist chemistry webook. 2018.

[74] Yaws, C. L. **Yaws' handbook of thermodynamic properties for hydrocarbons and chemicals (knovel, 2009)**: 2009.

[75] Verkade, P.-E. L'acide salicylique comme substance étalon secondaire de calorimétrie. **J. Chim. Phys.**, v. 29, p. 297–301, 1932.

[76] Bernard, M. A.; Boukari, Y. and Busnot, F. Étude thermodynamique des carbamates de méthyle, d'éthyle et de leur eutectique. **Thermochimica Acta**, v. 16, p. 267–275, 1976.

[77] Kabo, G. Y.; Miroshnichenko, E. A.; Frenkel', M. L.; Kozyro, A. A.; Simirskii, V. V.; Krasulin, A. P.; Vorob'eva, V. P. and Lebedev, Y. A. Thermochemistry of alkyl derivatives of urea. **Bulletin of the Academy of Sciences of the USSR, Division of chemical science**, v. 39, p. 662–667, 1990.

[78] das Dores M.C. Ribeiro da Silva, M.; da Silva, M. A. R.; Freitas, V. L.; Roux, M. V.; Jiménez, P.; Temprado, M.; Dávalos, J. Z.; Cabildo, P.; Claramunt, R. M. and Elguero, J. Structural studies of cyclic ureas: 1. enthalpies of formation of imidazolidin-2-one and n,n-trimethyleneurea. **Journal of Chemical Thermodynamics**, v. 40, p. 386–393, 2008.

[79] Elioff, M. S.; Hoy, J. and Bumpus, J. A. Calculating heat of formation values of energetic compounds: A comparative study. **Advances in Physical Chemistry**, v. 2016, 2016.

[80] Kuhn, M. and Johnson, K. **Applied predictive modeling**. v. 26: Springer, 2013.

[81] Li, J. Assessing the accuracy of predictive models for numerical data: Not r nor r2, why not? then what? **PLoS ONE**, v. 12, p. 1–16, 2017.

[82] Ghahremanpour, M. M.; van Maaren, P. J.; Ditz, J. C.; Lindh, R. and van der Spoel, D. Large-scale calculations of gas phase thermochemistry: Enthalpy of formation, standard entropy, and heat capacity. **The Journal of Chemical Physics**, v. 145, p. 114305, 9 2016.

[83] Curtiss, L. A.; Raghavachari, K.; Trucks, G. W. and Pople, J. A. Gaussian-2 theory for molecular energies of first- and second-row compounds. **The Journal of Chemical Physics**, v. 94, p. 7221–7230, 6 1991.

[84] Curtiss, L. A.; Raghavachari, K.; Redfern, P. C.; Rassolov, V. and Pople, J. A. Gaussian-3 (g3) theory for molecules containing first and second-row atoms. **The Journal of Chemical Physics**, v. 109, p. 7764–7776, 11 1998.

[85] Curtiss, L. A.; Redfern, P. C. and Raghavachari, K. Gaussian-4 theory. **The Journal of Chemical Physics**, v. 126, p. 84108, 2 2007.

[86] Montgomery, J. A.; Frisch, M. J.; Ochterski, J. W. and Petersson, G. A. A complete basis set model chemistry. vi. use of density functional geometries and frequencies. **The Journal of Chemical Physics**, v. 110, p. 2822–2827, 1 1999.

[87] Barnes, E. C.; Petersson, G. A.; Montgomery, J. A.; Frisch, M. J. and Martin, J. M. L. Unrestricted coupled cluster and brueckner doubles variations of w1 theory. **Journal of Chemical Theory and Computation**, v. 5, p. 2687–2693, 10 2009.

[88] Bustamante, F.; Orrego, A. F.; Villegas, S. and Villa, A. L. Modeling of chemical equilibrium and gas phase behavior for the direct synthesis of dimethyl carbonate from co ₂ and methanol. **Industrial & Engineering Chemistry Research**, v. 51, p. 8945–8956, 2012.

[89] Nations, U. Kyoto protocol to the united nations framework convention on climate change. **Review of European Community & International Environmental Law**, v. 7, p. 214–217, 7 1998.

[90] on Climate Change (UNFCCC), U. N. F. C. Adoption of the paris agreement (fccc/cp/2015/l. 9/rev. 1). 2015.

[91] Olivier, J. G. J.; Schure, K. M. and Peters, J. A. H. W. Trends in global co2 and total greenhouse gas emissions. **PBL Netherlands Environmental Assessment Agency**, p. 8, 2017.

[92] IPCC. **Climate change 2014: Mitigation of climate change. contribution of working group iii to the fifth assessment report of the intergovernmental panel on climate change**: Cambridge University Press, 2014.

[93] Bogmans, C. W.; Dijkema, G. P. and van Vliet, M. T. Adaptation of thermal power plants: The (ir)relevance of climate (change) information. **Energy Economics**, v. 62, p. 1–18, 2017.

[94] Azevedo, T. R. and Angelo, C. **Emissões de gee no brasil e suas implicações para políticas públicas e a contribuição brasileira para o acordo de paris. sistema de estimativas de emissões e remoções de gases de efeito estufa (seeg).**: Observatorio do Clima, 2018. 51 p.

[95] de Pesquisa Energética, E. Plano decenal de expansão de energia 2026. 2017. Http://www.epe.gov.br/PDE/Documents/Arquivos/PDE2026/PDE2026_versao_para_ConsultaPub

[96] Campos, A. F.; da Silva, N. F.; Pereira, M. G. and Freitas, M. A. V. A review of brazilian natural gas industry: Challenges and strategies. **Renewable and Sustainable Energy Reviews**, v. 75, p. 1207–1216, 2017.

[97] do Espirito Santo, D. B. and Gallo, W. L. R. Utilizing primary energy savings and exergy destruction to compare centralized thermal plants and cogeneration/trigeneration systems. **Energy**, v. 120, p. 785–795, 2017.

[98] von der Assen, N.; Jung, J. and Bardow, A. Life-cycle assessment of carbon dioxide capture and utilization: Avoiding the pitfalls. **Energy & Environmental Science**, p. 2721–2734, 2013.

[99] Pérez-Fortes, M.; Schöneberger, J. C.; Boulamanti, A. and Tzimas, E. Methanol synthesis using captured co2 as raw material: Techno-economic and environmental assessment. **Applied Energy**, v. 161, p. 718–732, 2016.

[100] Inagendo. Carbon capture use & storage (ccus). 2015. Http://www.inagendo.com/res/default/inagendo_ccus.pdf.

[101] Li, X.; Anderson, P.; Jhong, H.-R. M.; Paster, M.; Stubbins, J. F. and Kenis, P. J. A. Greenhouse gas emissions, energy efficiency, and cost of synthetic fuel production using electrochemical co2 conversion and the fischer–tropsch process. **Energy & Fuels**, v. 30, p. 5980–5989, 2016.

[102] Markewitz, P.; Kuckshinrichs, W.; Leitner, W.; Linssen, J.; Zapp, P.; Bongartz, R.; Schreiber, A. and Müller, T. E. Worldwide innovations in the development of carbon capture technologies and the utilization of co2. **Energy & Environmental Science**, v. 5, p. 7281, 2012.

[103] Dairanieh, I. Converting a liability into an asset: CSLF, 2016.

[104] Saaty, T. L. A scaling method for priorities in hierarchical structures. **Journal of Mathematical Psychology**, v. 15, p. 234–281, 1977.

[105] Brans, J. P. and Vincke, P. A preference ranking organisation method. **Management Science**, v. 31, p. 647–656, 1985.

[106] Behzadian, M.; Otaghsara, S. K.; Yazdani, M. and Ignatius, J. A state-of the-art survey of topsis applications. **Expert Systems with Applications**, v. 39, p. 13051–13069, 2012.

[107] Hwang, C.-L. and Yoon, K. **Multiple attribute decision making: methods and applications a state-of-the-art survey**. v. 186: Springer Science & Business Media, 2012.

[108] Kirkwood, C. W. and Corner, J. L. The effectiveness of partial information about attribute weights for ranking alternatives in multiattribute decision making. **Organizational Behavior and Human Decision Processes**, v. 54, p. 456–476, 1993.

[109] Cabral, J. B.; Luczywo, N. A. and Zanazzi, J. L. Scikit-criteria: Colección de métodos de análisis multi-criterio integrado al stack científico de python. **XLV Jornadas Argentinas de Informática e Investigación Operativa (45JAIIO)-XIV Simposio Argentino de Investigación Operativa**, p. 59–66, 2016.

[110] Commission, E. **From research to innovation. lessons learnt from the fp7 nmp materials call 2013: "substantial steps forward in the industrial use of european intellectual assets, stimulating the use of newly developed materials"**: RTD-PUBLICATIONS, 2013. 24 p.

[111] Bocin-dumitriu, A.; del MAR Perez Fortes, M.; Tzimas, E. and Sveen, T. **Carbon capture and utilisation workshop background and proceedings**: Joint Research Centre of the European Commission, 2013. 77 p.

[112] Sciences, C. and Initiative, T. G. C. **Global roadmap for implementing co2 utilization**: 2016. 62 p.

[113] Zimmermann, A. W. and Schomäcker, R. Assessing early-stage co ₂ utilization technologies-comparing apples and oranges? **Energy Technology**, v. 5, p. 850–860, 2017.

[114] Zimmermann, A.; Kant, M.; Strunge, T.; Tzimas, E.; Leitner, W.; Arlt, W.; Styring, P.; Arning, K.; Ziefle, M.; Meys, R.; Kätelhön, A.; Bardow, A.; Castillo, A. C.; Flanders, N.; Marinić, S. and Mechnig, S.-P. Co2 utilisation today - report 2017. p. 45, 2017.

[115] AliceWeb. Sistema de análise das informaçoes de comércio exterior - analysis system of foreign trade information. 2018. Http://aliceweb.mdic.gov.br/.

[116] Wei, W. W. S. **Time series analysis: univariate and multivariate methods**. 2 ed, v. 10: 2006. 212-235 p.

[117] Papacharalampous, G.; Tyralis, H. and Koutsoyiannis, D. Predictability of monthly temperature and precipitation using automatic time series forecasting methods. **Acta Geophysica**, v. 7, p. 1–25, 2018.

[118] Taylor, S. J. and Letham, B. prophet: automatic forecasting procedure. r package version 0.2.1 (2017.11.08). 2017. Https://cran.r-project.org/pack age=prophet.

[119] Taylor, S. J. and Letham, B. Forecasting at scale. **The American Statistician**, p. 0–0, 2017.

[120] Aresta, M.; Quaranta, E. and Tommasi, I. Carbon dioxide utilisation in the chemical industry. **ACS Division of Fuel Chemistry, Preprints**, v. 41, p. 1341–1344, 1996.

[121] Aresta, M. **Carbon dioxide as a chemical feedstock**: Wiley-VCH Verlag GmbH & Co. KGaA, 2010. 394 p.

[122] Styring, P.; Jansen, D.; de Coninck, H.; Reith, H. and Armstrong, K. **Carbon capture and utilisation in the green economy**: 2011. 60 p.

[123] Aresta, M.; Dibenedetto, A. and Quaranta, E. **Reaction mechanisms in carbon dioxide conversion**: 2015. 1-409 p.

[124] Chu, A. T. W.; Kalaba, R. E. and Spingarn, K. A comparison of two methods for determining the weights of belonging to fuzzy sets. **Journal of Optimization Theory and Applications**, v. 27, p. 531–538, 1979.

[125] Hwang, C.-L. and Lin, M.-J. **Group decision making under multiple criteria: methods and applications**. v. 281: Springer Science & Business Media, 2012.

[126] Shannon, C. E. A mathematical theory of communication. **Bell system technical journal**, v. 27, p. 379–423, 1948.

[127] Zeleny, M. **Multiple criteria decision making kyoto 1975**. v. 123: Springer Science & Business Media, 2012.

[128] Choo, E. U. and Wedley, W. C. Optimal criterion weights in repetitive multicriteria decision-making. **Journal of the Operational Research Society**, v. 36, p. 983–992, 11 1985.

[129] Patricio, J.; Angelis-Dimakis, A.; Castillo-Castillo, A.; Kalmykova, Y. and Rosado, L. Region prioritization for the development of carbon capture and utilization technologies. **Journal of CO2 Utilization**, v. 17, p. 50–59, 2017.

[130] Patricio, J.; Angelis-Dimakis, A.; Castillo-Castillo, A.; Kalmykova, Y. and Rosado, L. Method to identify opportunities for ccu at regional level — matching sources and receivers. **Journal of CO2 Utilization**, v. 22, p. 330–345, 12 2017.

[131] U.S.NRC. Nrc: Glossary – capacity factor (net). 2018. Https://www.nrc.gov/reading-rm/basic-ref/glossary/capacity-factor-net.html.

[132] Ruggero, B. **Perspectives for geothermal energy in europe**: World Scientific Publishing Company, 2017.

[133] ENERGIA, M. M. D. M. E. Capacidade instalada de geração elétrica. 2017. Http://www.mme.gov.br/web/guest/publicacoes-e-indicadores/boletins-de-energia?p_p_id=20&p_p_lifecycle=0&p_p_state=normal&p_p_mode=view&p_p_col_id=colum 1&p_p_col_count=1&_20_struts_action=

[134] de Queiroz Fernandes Araújo, O.; de Carvalho Reis, A.; de Medeiros, J. L.; do Nascimento, J. F.; Grava, W. M. and Musse, A. P. S. Comparative analysis of separation technologies for processing carbon dioxide rich natural gas in ultra-deepwater oil fields. **Journal of Cleaner Production**, v. 155, p. 12–22, 2017.

[135] Artz, J.; Müller, T. E.; Thenert, K.; Kleinekorte, J.; Meys, R.; Sternberg, A.; Bardow, A. and Leitner, W. Sustainable conversion of carbon dioxide: An integrated review of catalysis and life cycle assessment. **Chemical Reviews**, v. 118, p. 434–504, 2018.

[136] BP. Bp statistical review of world enegy. p. 56, 2018.

[137] Administration, U. E. I. **International energy outlook 2017**: 2017. 76 p.

[138] Agency, I. E. Chapter 1: Introduction and scope. **World Energy Outlook 2017**, p. 33–61, 2017.

[139] of Energy Economics Japan, T. I. Ieej outlook 2018 - prospects and challenges until 2050. p. 22, 2018.

[140] Gabrielli, P.; Gazzani, M. and Mazzotti, M. The role of ccu , ccs and biomass to enable a net-zero-co emissions chemical industry. **Industrial & Engineering Chemistry Research**, 2020.

[141] Kozonoe, C. E.; Alves, R. M. B. and Schmal, M. Influence of feed rate and testing variables for low-temperature tri-reforming of methane on the ni@mwcnt/ce catalyst. **Fuel**, v. 281, p. 118749, 2020.

[142] Figueira, C. E.; Moreira, P. F.; Giudici, R.; Alves, R. M. B. and Schmal, M. Nanoparticles of ce, sr, co in and out the multi-walled carbon nanotubes applied for dry reforming of methane. **Applied Catalysis A: General**, v. 550, p. 297–307, 2018.

[143] Jardim, S. S. Q.; Graciano, J. E. A. and Alves, R. M. B. Analysis of the tri-reforming of methane in a membrane reactor. **29 European Symposium on Computer Aided Process Engineering**, v. 46, p. 517–522, 2019.

[144] Mantzalis, D.; Asproulis, N. and Drikakis, D. Filtering carbon dioxide through carbon nanotubes. **Chemical Physics Letters**, v. 506, p. 81–85, 2011.

[145] Mantzalis, D.; Asproulis, N. and Drikakis, D. Enhanced carbon dioxide adsorption through carbon nanoscrolls. **Physical Review E - Statistical, Nonlinear, and Soft Matter Physics**, v. 84, p. 1–8, 2011.

[146] Meza, A. and Koç, M. The lng trade between qatar and east asia: Potential impacts of unconventional energy resources on the lng sector and qatar's economic development goals. **Resources Policy**, p. 101886, 2020.

[147] Greco, S.; Ehrgott, M. and Figueira, J. R. **Multi-criteria decision analysis: State of the art surveys**. 2 ed: Springer, 2016. 1355 p.

[148] Ishizaka, A. and Nemery, P. **Multi-criteria decision analysis: Methods and software**: 2013. 1-296 p.

[149] Aissi, H. and Roy, B. **Robustness in multi-criteria decision aiding bt - trends in multiple criteria decision analysis**: Springer US, 2010. 87-121 p.

[150] Taylan, O.; Kaya, D. and Demirbas, A. An integrated multi attribute decision model for energy efficiency processes in petrochemical industry applying fuzzy set theory. **Energy Conversion and Management**, v. 117, p. 501–512, 2016.

[151] Zhang, H.; Peng, Y.; Tian, G.; Wang, D. and Xie, P. Green material selection for sustainability: A hybrid mcdm approach. **PLoS ONE**, v. 12, p. 1–26, 2017.

[152] Daim, T.; Yates, D.; Peng, Y. and Jimenez, B. Technology assessment for clean energy technologies: The case of the pacific northwest. **Technology in Society**, v. 31, p. 232–243, 2009.

[153] Akber, M. Z.; Thaheem, M. J. and Arshad, H. Life cycle sustainability assessment of electricity generation in pakistan: Policy regime for a sustainable energy mix. **Energy Policy**, v. 111, p. 111–126, 2017.

[154] Pacheco, K. A.; Bresciani, A. E.; Nascimento, C. A. O. and Alves, R. M. B. Thermodynamics of carbon dioxide related compounds: 2019, p. submitted.

[155] Reuters, T. **Web of science 2018**: 2018.

[156] Scopus. **Scopus**: 2018.

[157] Lajeunesse, M. J. Facilitating systematic reviews, data extraction and meta-analysis with the metagear package for r. **Methods in Ecology and Evolution**, v. 7, p. 323–330, 2016.

[158] Daim, T.; Oliver, T. and Kim, J. Multi-criteria applications in renewable energy analysis, a literature review. **Research and Technology Management in the Electricity Industry**, v. 1, p. 17–31, 2013.

[159] Saaty, T. L. The modern science of multicriteria decision making and its practical applications: The ahp/anp approach. **Operations Research**, v. 61, p. 1101–1118, 2013.

[160] Roy, B. Classement et choix en présence de points de vue multiples. **Revue française d'informatique et de recherche opérationnelle**, v. 2, p. 57–75, 2017.

[161] Dyer, J. S. **Maut—multiattribute utility theory**: Springer, 2005. 265-292 p.

[162] Guarini, M.; Battisti, F. and Chiovitti, A. Public initiatives of settlement transformation: A theoretical-methodological approach to selecting tools of multi-criteria decision analysis. **Buildings**, v. 8, p. 1, 2017.

[163] Seixedo, C. and Tereso, A. P. A multicriteria decision aid software application for selecting mcda software using ahp. **2nd International Conference on Engineering Optimization, September 6-9, 2010.**, p. 1–11, 2010.

[164] Wang, J. J.; Jing, Y. Y.; Zhang, C. F. and Zhao, J. H. Review on multi-criteria decision analysis aid in sustainable energy decision-making. **Renewable and Sustainable Energy Reviews**, v. 13, p. 2263–2278, 2009.

[165] Broekhuizen, H.; Groothuis-Oudshoorn, C. G.; van Til, J. A.; Hummel, J. M. and IJzerman, M. J. A review and classification of approaches for dealing with uncertainty in multi-criteria decision analysis for healthcare decisions. **PharmacoEconomics**, v. 33, p. 445–455, 2015.

[166] Chen, J.; Wang, J.; Baležentis, T.; Zagurskaite, F.; Streimikiene, D. and Makuteniene, D. Multicriteria approach towards the sustainable selection of a teahouse location with sensitivity analysis. **Sustainability (Switzerland)**, v. 10, p. 1–17, 2018.

[167] Asif, M.; Gao, X.; Lv, H.; Xi, X. and Dong, P. Catalytic hydrogenation of co2 from 600 mw supercritical coal power plant to produce methanol: A techno-economic analysis. **INTERNATIONAL JOURNAL OF HYDROGEN ENERGY**, v. 43, p. 2726–2741, 2018.

[168] Jones, C. R.; Olfe-Kraeutlein, B. and Kaklamanou, D. Lay perceptions of carbon dioxide utilisation technologies in the united kingdom and germany: An exploratory qualitative interview study. **ENERGY RESEARCH & SOCIAL SCIENCE**, v. 34, p. 283–293, 2017.

[169] Chen, Q.; Gu, Y.; Tang, Z.; Wei, W. and Sun, Y. Assessment of low-carbon iron and steel production with co2 recycling and utilization technologies: A case study in china. **APPLIED ENERGY**, v. 220, p. 192–207, 6 2018.

[170] Meunier, N.; Chauvy, R.; Thomas, D. and Weireld, G. D. E. Techno-economic and environmental assessment of the conversion of co 2 into methanol: 2017.

[171] Mourits, F.; Kulichenko-Lotz, N.; González, G. H. and Nieta, J. M. Overview of world bank ccus program activities in mexico. **Energy Procedia**, v. 114, p. 5916–5932, 2017.

[172] González-Aparicio, I.; Kapetaki, Z. and Tzimas, E. Wind energy and carbon dioxide utilisation as an alternative business model for energy producers: A case study in spain. **Applied Energy**, v. 222, p. 216–227, 7 2018.

[173] Zhang, C.; Jun, K.-W.; Gao, R.; Kwak, G. and Park, H.-G. Carbon dioxide utilization in a gas-to-methanol process combined with co2/steam-mixed reforming: Techno-economic analysis. **FUEL**, v. 190, p. 303–311, 2017.

[174] Lee, J. H.; Lee, J. H.; Park, I. K. and Lee, C. H. Techno-economic and environmental evaluation of co2 mineralization technology based on bench-scale experiments. **JOURNAL OF CO2 UTILIZATION**, v. 26, p. 522–536, 7 2018.

[175] Zheng, Y.; Zhang, W.; Li, Y.; Chen, J.; Yu, B.; Wang, J.; Zhang, L. and Zhang, J. Energy related co2 conversion and utilization: Advanced materials/nanomaterials, reaction mechanisms and technologies. **Nano Energy**, v. 40, p. 512–539, 10 2017.

[176] Roh, K.; Lim, H.; Chung, W.; Oh, J.; Yoo, H.; Al-Hunaidy, A. S.; Imran, H. and Lee, J. H. Sustainability analysis of co2 capture and utilization processes using a computer-aided tool. **JOURNAL OF CO2 UTILIZATION**, v. 26, p. 60–69, 7 2018.

[177] Chiuta, S.; Engelbrecht, N.; Human, G. and Bessarabov, D. Techno-economic assessment of power-to-methane and power-to-syngas business models for sustainable carbon dioxide utilization in coal-to-liquid facilities. **Journal of CO2 Utilization**, v. 16, p. 399–411, 2016.

[178] Rudin, S.; Muis, Z. A.; Hashim, H. and Ho, W. Techno-economic assessment of integrated power plant with methanation. **Chemical Engineering Transactions**, v. 63, p. 451–456, 2018.

[179] Rumayor, M.; Dominguez-Ramos, A. and Irabien, A. Formic acid manufacture: Carbon dioxide utilization alternatives. **Applied Sciences 2018, Vol. 8, Page 914**, v. 8, p. 914, 2018.

[180] Mondal, K.; Sasmal, S.; Badgandi, S.; Chowdhury, D. R. and Nair, V. Dry reforming of methane to syngas: a potential alternative process for value added chemicals-a techno-economic perspective. **ENVIRONMENTAL SCIENCE AND POLLUTION RESEARCH**, v. 23, p. 22267–22273, 11 2016.

[181] Szima, S. and Cormos, C.-C. Improving methanol synthesis from carbon-free h-2 and captured co2: A techno-economic and environmental evaluation. **JOURNAL OF CO2 UTILIZATION**, v. 24, p. 555–563, 3 2018.

[182] Alper, E. and Orhan, O. Y. Co2 utilization: Developments in conversion processes. **Petroleum**, v. 3, p. 109–126, 2017.

[183] Álvarez, A.; Bansode, A.; Urakawa, A.; Bavykina, A. V.; Wezendonk, T. A.; Makkee, M.; Gascon, J. and Kapteijn, F. Challenges in the greener production of formates/formic acid, methanol, and dme by heterogeneously catalyzed co2 hydrogenation processes. **Chemical Reviews**, v. 117, p. 9804–9838, 2017.

[184] Roh, K.; Lee, J. H. and Gani, R. A methodological framework for the development of feasible co2conversion processes. **International Journal of Greenhouse Gas Control**, v. 47, p. 250–265, 2016.

[185] Collodi, G.; Azzaro, G.; Ferrari, N. and Santos, S. Demonstrating large scale industrial ccs through ccu - a case study for methanol production. **Energy Procedia**, v. 114, p. 122–138, 2017.

[186] Meylan, F. D.; Moreau, V. and Erkman, S. Co2 utilization in the perspective of industrial ecology, an overview. **JOURNAL OF CO2 UTILIZATION**, v. 12, p. 101–108, 2015.

[187] Fernández-Dacosta, C.; Spek, M. V. D.; Hung, C. R.; Oregionni, G. D.; Skagestad, R.; Parihar, P.; Gokak, D. T.; Strømman, A. H. and Ramirez, A. Prospective techno-economic and environmental assessment of carbon capture at a refinery and co2 utilisation in polyol synthesis. **Journal of CO2 Utilization**, v. 21, p. 405–422, 2017.

[188] Poliakoff, M.; Leitner, W. and Streng, E. S. The twelve principles of co2 chemistry. **Faraday Discussions**, v. 183, p. 9–17, 2015.

[189] Frauzem, R.; Woodley, J. M. and Gani, R. Application of a computer-aided framework for the design of co2 capture and utilization processes. **Computer Aided Chemical Engineering**, v. 40, p. 2653–2658, 2017.

[190] Hart, P. W. and Sommerfeld, J. T. Cost estimation of specialty chemicals from laboratory-scale prices. **Cost Engineering**, v. 39, p. 31–35, 1997.

[191] Ackiewicz, M.; Foster, C.; Bonijoly, D.; Ramsak, P.; Al-Eidan, A.; Surridge, T. and Sharman, P. Final phase ii report by the cslf task force on co2 utilization options. **Report Prepared for the CSLF Technical Group By the CSLF Task Force on Utilization Options of CO2**, p. 69, 2013.

[192] IHS. Acetic acid - chemical economics handbook. 2016. Https://ihsmarkit.com/products/acetic-acid-chemical-economics-handbook.html.

[193] Dimian, A. C. and Kiss, A. A. Novel energy efficient process for acetic acid production by methanol carbonylation. **Chemical Engineering Research and Design**, v. 159, p. 1–12, 7 2020.

[194] Mordor. Acetic acid market | growth, trends, and forecasts (2019 - 2024). 2019. Https://www.mordorintelligence.com/industry-reports/acetic-acid-market.

[195] Pal, P. and Nayak, J. Acetic acid production and purification: Critical review towards process intensification. **Separation and Purification Reviews**, v. 46, p. 44–61, 2017.

[196] Intelligence, M. Acetic acid market - segmented by application, and geography - trends and forecasts (2018- 2023). 2017. Https://www.mordorintelligence.com/industry-reports/global-acetic-acid-market-industry.

[197] Processing. Asian chemical industry surge benefits acetic acid market - processing magazine. 2020. Https://www.processingmagazine.com/asian-chemical-industry-surge-benefits-acetic-acid-market/.

[198] GVR, G. V. R. Acetic acid market size. 2015. Https://www.grandviewresearch.com/industry-analysis/acetic-acid-market.

[199] statista. Market volume of acetic acid worldwide from 2015 to 2021, with a forecast for 2022 to 2029. 2022. Https://www.statista.com/statistics/1245203/acetic-acid-market-volume-worldwide/.

[200] Berre, C. L.; Serp, P.; Kalck, P. and Torrence, G. P. **Ullmann's encyclopedia of industrial chemistry - acetic acid**. v. 1603: Wiley-VCH Verlag GmbH & Co. KGaA, 2013. 90-93 p.

[201] Wu, J.-F.; Yu, S.-M.; Wang, W. D.; Fan, Y.-X.; Bai, S.; Zhang, C.-W.; Gao, Q.; Huang, J. and Wang, W. Mechanistic insight into the formation of acetic acid from the direct conversion of methane and carbon dioxide on zinc-modified h–zsm-5 zeolite. **Journal of the American Chemical Society**, v. 135, p. 13567–13573, 2013.

[202] Cui, M.; Qian, Q.; Zhang, J.; Chen, C. and Han, B. Efficient synthesis of acetic acid via rh catalyzed methanol hydrocarboxylation with co2 and h2 under milder conditions. **Green Chem.**, p. 3558–3565, 2017.

[203] Wang, H.; Zhao, Y.; Ke, Z.; Yu, B.; Li, R.; Wu, Y.; Wang, Z.; Han, J. and Liu, Z. Synthesis of renewable acetic acid from co 2 and lignin over an ionic liquid-based catalytic system. **Chemical Communications**, v. 55, p. 3069–3072, 2019.

[204] Ikehara, N.; Hara, K.; Satsuma, A.; Hattori, T. and Murakami, Y. Unique temperature dependence of acetic acid formation in co2 hydrogenation on ag-promoted rh/sio2 catalyst. **Chemistry Letters**, v. 23, p. 263–264, 2 1994.

[205] Feyzi, V. and Beheshti, M. Application of exergy analysis and response surface methodology (rsm) for reduction of exergy loss in acetic acid production process. **Gas Processing Journal**, v. 3, p. 51–66, 2015.

[206] Smith, R. L.; Ruiz-Mercado, G. J.; Meyer, D. E.; Gonzalez, M. A.; Abraham, J. P.; Barrett, W. M. and Randall, P. M. Coupling computer-aided process simulation and estimations of emissions and land use for rapid life cycle inventory modeling. **ACS Sustainable Chemistry and Engineering**, v. 5, p. 3786–3794, 2017.

[207] Noriyuki, Y.; Takeshi, M.; Joe, W. and Ben, S. The chiyoda/uop acetica™ process: A novel acetic acid technology. v. 121: Elsevier, 1999. p. 93–98.

[208] Roh, K.; Lim, H.; Chung, W.; Oh, J.; Yoo, H.; Al-Hunaidy, A. S.; Imran, H. and Lee, J. H. Sustainability analysis of co2capture and utilization processes using a computer-aided tool. **Journal of CO2 Utilization**, v. 26, p. 60–69, 2018.

[209] Audus, H. and Oonk, H. An assessment procedure for chemical utilisation schemes intended to reduce co2 emissions to atmosphere. **Energy Convers. Mgmt**, v. 38, p. S409–S414, 1997.

[210] Müller, K. and Arlt, W. Shortcut evaluation of chemical carbon dioxide utilization processes. **Chemical Engineering and Technology**, v. 37, p. 1612–1615, 2014.

[211] Dimian, A. C. and Bildea, C. S. **Chemical process design: Computer-aided case studies**: John Wiley & Sons, 2008.

[212] Ramachandriya, K. D.; Kundiyana, D. K.; Wilkins, M. R.; Terrill, J. B.; Atiyeh, H. K. and Huhnke, R. L. Carbon dioxide conversion to fuels and chemicals using a hybrid green process. **Applied Energy**, v. 112, p. 289–299, 2013.

[213] Engine, M. R. Acetic acid market forecast to touch uss 15 billion by 2023. 2018. Https://www.marketwatch.com/press-release/acetic-acid-market-forecast-to-touch-us-15-billion-by-2023-2018-12-21.

[214] ICIS. Acetic acid production and manufacturing process. 2010. Https://www.icis.com/resources/news/2007/10/31/9074780/acetic-acid-production-and-manufacturing-process/.

[215] Howard, M. J.; Jones, M. D.; Roberts, M. S. and Taylor, S. A. C1to acetyls: catalysis and process. **Catalysis Today**, v. 18, p. 325–354, 1993.

[216] Kutepow, N. V.; Himmele, W. and Hohenschutz, H. Die synthese von essigsäure aus methanol und kohlenoxyd. **Chemie Ingenieur Technik**, v. 37, p. 383–388, 4 1965.

[217] Paulik, F. E. and Roth, J. F. Novel catalysts for the low-pressure carbonylation of methanol to acetic acid. **Chemical Communications (London)**, v. 11, p. 1578, 1968.

[218] Jones, J. H. The cativa process for the manufacture of acetic acid. **Platinum Metals Review**, v. 44, p. 94–105, 2000.

[219] Sunley, G. J. and Watson, D. J. High productivity methanol carbonylation catalysis using iridium. the cativatm process for the manufacture of acetic acid. **Catalysis Today**, v. 58, p. 293–307, 2000.

[220] Martín-Espejo, J. L.; Gandara-Loe, J.; Odriozola, J. A.; Reina, T. R. and Pastor-Pérez, L. Sustainable routes for acetic acid production: Traditional processes vs a low-carbon, biogas-based strategy. **Science of the Total Environment**, v. 840, 9 2022.

[221] Agreda, V. H. and Zoeller, J. **Acetic acid and its derivatives**: MARCEL DEKKER, 1993.

[222] Kent, J. A. **Kent and riegel's handbook of industrial chemistry and biotechnology**: Springer US, 2007.

[223] Weissermel, K. and Arpe, H. J. **Industrial organic chemistry**. 4 ed: Wiley-VCH, 2003. 491 p.

[224] Suzuki, T.; Yoshikawa, H.; Abe, K. and Sano, K. No. **Wo94/22803**, 1994.

[225] Jr, J. H. M.; Kaiser, S. W. and O'connor, G. L. No. **Acetic acid from ethane, ethylene and oxygen**, 1988.

[226] Borchert, H.; Dingerdissen, U. and Weiguny, J. No. **Process for the selective preparation of acetic acid using a molybdenum, palladium, and rhenium catalyst**, 2000.

[227] Borchert, H.; Dingerdissen, U. and Roesky, R. No. **Method for producing acetic acid in a reactor cascade**, 1998.

[228] Kawako, F.; Shima, K. and Yoshikazu, N. No. **Process for producing acetic acid**, 1997.

[229] Volkov, S.; Kosmambetova, G.; Kharkova, L.; Shvets, O.; Yanko, O.; Gritsenko, V. and Strizhak, P. Catalytic perfomance of rhodium chalcogen halides and rhodium chalcogenides over silica supports in methane oxidative carbonylation. **Journal of Natural Gas Chemistry**, v. 18, p. 399–406, 2009.

[230] Qian, Q.; Zhang, J.; Cui, M. and Han, B. Synthesis of acetic acid via methanol hydrocarboxylation with co2 and h2. **Nature Communications**, v. 7, p. 11481, 2016.

[231] Li, J.; Wang, L.; Cao, Y.; Zhang, C.; He, P. and Li, H. Recent advances on the reduction of co2 to important c2 + oxygenated chemicals and fuels. **Chinese Journal of Chemical Engineering**, v. 26, p. 2266–2279, 2018.

[232] Dutra, M.; Schmal, M. and Guardani, R. Syntheses and characterization of zinc oxide nanoparticles on graphene sheets: Adsorption-reaction in situ drifts of methane and co2. **Catalysis Letters**, v. 148, p. 3413–3430, 2018.

[233] Bell, A. T.; Mukhopadhyay, S.; Zerella, M.; Sunley, J. G.; Gaemers, S. and Muskett, M. J. No. **Process for production of acetyl anhydrides and optionally acetic acid from methane and carbon dioxide**, BP Chemicals Ltd University of California, 2005.

[234] Freund, H.-J.; WAMBACH, J.; Seiferth, O. and Dillmann, B. No. **Method of manufacturing acetic acid**, 1995.

[235] Wilcox, E. M.; Roberts, G. W. and Spivey, J. J. Direct catalytic formation of acetic acid from co2and methane. **Catalysis Today**, v. 88, p. 83–90, 2003.

[236] Havran, V.; Duduković, M. P. and Lo, C. S. Conversion of methane and carbon dioxide to higher value products. **Industrial and Engineering Chemistry Research**, v. 50, p. 7089–7100, 2011.

[237] Ding, Y. H.; Huang, W. and Wang, Y. G. Direct synthesis of acetic acid from ch4 and co2 by a step-wise route over pd/sio2 and rh/sio2 catalysts. **Fuel Processing Technology**, v. 88, p. 319–324, 2007.

[238] Huang, W.; Zhang, C.; Yin, L. and Xie, K. Direct synthesis of acetic acid from ch 4 and co 2 in the presence of o 2 over a v 2 o 5 -pdcl 2 / al 2 o 3 catalyst. **Journal of Natual Gas Chemistry**, v. 13, p. 113–115, 2004.

[239] Spivey, J. J.; Wilcox, E. M. and Roberts, G. W. Direct utilization of carbon dioxide in chemical synthesis: Vinyl acetate via methane carboxylation. **Catalysis Communications**, v. 9, p. 685–689, 2008.

[240] Rabie, A. M.; Betiha, M. A. and Park, S. E. Direct synthesis of acetic acid by simultaneous co-activation of methane and co2 over cu-exchanged zsm-5 catalysts. **Applied Catalysis B: Environmental**, v. 215, p. 50–59, 2017.

[241] Montejo-Valencia, B. D.; Pagán-Torres, Y. J.; Martínez-Iñesta, M. M. and Curet-Arana, M. C. Density functional theory (dft) study to unravel the catalytic properties of m-exchanged mfi, (m = be, co, cu, mg, mn, zn) for the conversion of methane and carbon dioxide to acetic acid. **ACS Catalysis**, v. 7, p. 6719–6728, 2017.

[242] Ahmad, W.; Koley, P.; Dwivedi, S.; Shrotri, A. and Tanksale, A. Aqueous phase conversion of co 2 into acetic acid over thermally transformed mil-88b. 2021.

[243] Li, C.; Zhao, X.; Wang, A.; Huber, G. W. and Zhang, T. Catalytic transformation of lignin for the production of chemicals and fuels. **Chemical Reviews**, v. 115, p. 11559–11624, 2015.

[244] Jia, C.; Gao, J.; Dai, Y.; Zhang, J. and Yang, Y. The thermodynamics analysis and experimental validation for complicated systems in co2hydrogenation process. **Journal of Energy Chemistry**, v. 25, p. 1027–1037, 2016.

[245] Thonemann, N. and Pizzol, M. Consequential life cycle assessment of carbon capture and utilization technologies within the chemical industry. **Energy and Environmental Science**, v. 12, p. 2253–2263, 7 2019.

[246] Li, D.; Rohani, V.; Fabry, F.; Ramaswamy, A. P.; Sennour, M. and Fulcheri, L. Direct conversion of co2 and ch4 into liquid chemicals by plasma-catalysis. **Applied Catalysis B: Environmental**, v. 261, 2 2020.

[247] Alcantara, M. L.; Pacheco, K. A.; Bresciani, A. E. and Alves, R. M. B. Thermodynamic analysis of carbon dioxide conversion reactions. case studies: Formic acid and acetic acid synthesis. **Industrial and Engineering Chemistry Research**, v. 60, p. 9246–9258, 6 2021.

[248] Linnhoff, B. and of Chemical Engineers (Great Britain), I. **A user guide on process integration for the efficient use of energy**: Institution of Chemical Engineers, 1982.

[249] Douglas, J. M. **Conceptual design of chemical processes**: McGraw-Hill, 1988.

[250] Wu, W.; Yenkie, K. and Maravelias, C. T. A superstructure-based framework for bio-separation network synthesis. **Computers and Chemical Engineering**, v. 96, p. 1–17, 2017.

[251] Szargut, J.; Morris, D. R. and Steward, F. R. **Exergy analysis of thermal, chemical, and metallurgical processes**: Hemisphere Publishing,New York, NY, 1987.

[252] Wilcox, E.; Gogate, M.; Spivey, J. and Roberts, G. **Direct synthesis of acetic acid from methane and carbon dioxide**. v. 136: Elsevier Masson SAS, 2001. 259-264 p.

[253] Richardson, J. F.; Harker, J. H. and Backhurst, J. R. **Coulson & richardson's chemical engineering**. v. 2: Butterworth-Heinemann London, 2002.

[254] Smith, W. R. and Missen, R. W. **Chemical reaction equilibrium analysis: theory and algorithms**: Wiley New York, 1982. 136 p.

[255] Noble, B. **Applied linear algebra**: Prentice-Hall, 1988.

[256] Missen, R. W. and Smith, W. R. The permanganate-peroxide reaction: Illustration of a stoichiometric restriction. **Journal of Chemical Education**, v. 67, p. 876–877, 1990.

[257] Abdelouahed, L.; Authier, O.; Mauviel, G.; Corriou, J. P.; Verdier, G. and Dufour, A. Detailed modeling of biomass gasification in dual fluidized bed reactors under aspen plus. **Energy & Fuels**, v. 26, p. 3840–3855, 6 2012.

[258] Castier, M.; Rasmussen, P. and Fredenslund, A. Calculation of simultaneous chemical and phase equilibria in nonideal systems. **Chemical Engineering Science**, v. 44, p. 237–248, 1 1989.

[259] Michelsen, M. Calculation of multiphase equilibrium. **Computers & Chemical Engineering**, v. 18, p. 545–550, 7 1994.

[260] Bolat, P. and Thiel, C. Hydrogen supply chain architecture for bottom-up energy systems models. part 2: Techno-economic inputs for hydrogen production pathways. **International Journal of Hydrogen Energy**, v. 39, p. 8898–8925, 6 2014.

[261] Barnicki, S. D. and Fair, J. R. Separation system synthesis: a knowledge-based approach. 2. gas/vapor mixtures. **Industrial & Engineering Chemistry Research**, v. 31, p. 1679–1694, 7 1992.

[262] Barnicki, S. D. and Fair, J. R. Separation system synthesis: a knowledge-based approach. 1. liquid mixture separations. **Industrial & Engineering Chemistry Research**, v. 29, p. 421–432, 3 1990.

[263] Douglas, J. M. Synthesis of separation system flowsheels. **AIChE Journal**, v. 41, p. 2522–2536, 1995.

[264] Dimian, A. C.; Bildea, C. S. and Kiss, A. A. Chapter 9 - synthesis of separation systems. v. 35: Elsevier, 2014. p. 345–395.

[265] Ghasem, N. Chapter 14 - polymeric membranes for co2 separation: Woodhead Publishing, 2020. p. 311–329.

[266] Pettersen, T. and Lien, K. A new robust design model for gas separating membrane modules, based on analogy with counter-current heat exchangers. **Computers & Chemical Engineering**, v. 18, p. 427–439, 5 1994.

[267] Gassner, M.; Baciocchi, R.; Maréchal, F. and Mazzotti, M. Integrated design of a gas separation system for the upgrade of crude sng with membranes. **Chemical Engineering and Processing: Process Intensification**, v. 48, p. 1391–1404, 2009.

[268] Morosanu, E. A.; Saldivia, A.; Antonini, M. and Bensaid, S. Process modeling of an innovative power to lng demonstration plant. **Energy and Fuels**, v. 32, p. 8868–8879, 2018.

[269] Nguyen, T. V. and de Oliveira Júnior, S. System evaluation of offshore platforms with gas liquefaction processes. **Energy**, v. 144, p. 594–606, 2018.

[270] Abetz, V.; Brinkmann, T.; Dijkstra, M.; Ebert, K.; Fritsch, D.; Ohlrogge, K.; Paul, D.; Peinemann, K. V.; Nunes, S. P.; Scharnagl, N. and Schossig, M. Developments in membrane research: From material via process design to industrial application. **Advanced Engineering Materials**, v. 8, p. 328–358, 2006.

[271] Hayden, J. G. and O'Connell, J. P. A generalized method for predicting second virial coefficients. **Industrial and Engineering Chemistry Process Design and Development**, v. 14, p. 209–216, 1975.

[272] BP. Glacial acetic acid, food grade specification. 2011. Https://www.bp.com/content/dam/bp/business-sites/en/global/bp-petrochemicals/documents/acetyls-americas/sales-specification-acetic-acid-food-grade.pdf.

[273] Celanese. Sales specification. 2016. Https://www.celanese.com/-/media/Intermediate Chemistry/Files/Sales Specifications/Sales_Specification-Acetic_Acid-Global.pdf.

[274] Feyzi, V. and Beheshti, M. Exergy analysis and optimization of reactive distillation column in acetic acid production process. **Chemical Engineering and Processing: Process Intensification**, v. 120, p. 161–172, 2017.

[275] Budiman, A. W.; Nam, J. S.; Park, J. H.; Mukti, R. I.; Chang, T. S.; Bae, J. W. and Choi, M. J. Review of acetic acid synthesis from various feedstocks through different catalytic processes. **Catalysis Surveys from Asia**, v. 20, p. 173–193, 9 2016.

[276] Haynes, A. Acetic acid synthesis by catalytic carbonylation of methanol: Springer Berlin Heidelberg, 2006. p. 179–205.

[277] Pilavachi, P. A.; Schenk, M.; Perez-Cisneros, E. and Gani, R. Modeling and simulation of reactive distillation operations. **Industrial and Engineering Chemistry Research**, v. 36, p. 3188–3197, 1997.

[278] Lee, E. J. and Kim, Y. H. Energy saving in acetic acid process using an azeotropic distillation column with a side stripper. **Chemical Engineering Communications**, v. 205, p. 1311–1322, 2018.

[279] Chen, Y. F. and Yang, J. H. Simulation and optimization on the process of acetic acid dehydration via extraction combined with azeotropic distillation. **Advanced Materials Research**, v. 548, p. 349–354, 2012.

[280] ling Li, K.; lung Chien, I. and liang Chen, C. Design and optimization of acetic acid dehydration processes. **5th International Symposium on Advance Control of Industrial Processes**, p. 126–131, 2014.

[281] Servel, C.; Roizard, D.; Favre, E. and Horbez, D. Improved energy efficiency of a hybrid pervaporation/distillation process for acetic acid production: Identification of target membrane performances by simulation. **Industrial and Engineering Chemistry Research**, v. 53, p. 7768–7779, 2014.

[282] Harvianto, G. R.; Kang, K. J. and Lee, M. Process design and optimization of an acetic acid recovery system in terephthalic acid production via hybrid extraction-distillation using a novel mixed solvent. **Industrial and Engineering Chemistry Research**, v. 56, p. 2168–2176, 2017.

[283] Kiss, A. A.; Pragt, J. J.; Vos, H. J.; Bargeman, G. and de Groot, M. T. Novel efficient process for methanol synthesis by co2 hydrogenation. **Chemical Engineering Journal**, v. 284, p. 260–269, 1 2016.

[284] Linde. Process plants | linde engineering. 2022. Https://www.linde-engineering.com/en/process-plants/index.html.

[285] S&PGlobal. Methanol production via toyo process. 12 2011. Https://www.spglobal.com/commodityinsights/en/ci/products/chemical-technology-pep-reviews-methanol-production-via-toyo-2011.html.

[286] Bansode, A. and Urakawa, A. Towards full one-pass conversion of carbon dioxide to methanol and methanol-derived products. **Journal of Catalysis**, v. 309, p. 66–70, 2014.

[287] Olah, G. A.; Goeppert, A.; Czaun, M.; Mathew, T.; May, R. B. and Prakash, G. K. Single step bi-reforming and oxidative bi-reforming of methane (natural gas) with steam and carbon dioxide to metgas (co-2h<inf>2</inf>) for methanol synthesis: Self-sufficient effective and exclusive oxygenation of methane to methanol with oxygen. **Journal of the American Chemical Society**, v. 137, p. 8720–8729, 2015.

[288] Santos, B. A.; Loureiro, J. M.; Ribeiro, A. M.; Rodrigues, A. E. and Cunha, A. F. Methanol production by bi-reforming. **Canadian Journal of Chemical Engineering**, v. 93, p. 510–526, 2015.

[289] Ng, K. S.; Zhang, N. and Sadhukhan, J. A graphical co2emission treatment intensity assessment for energy and economic analyses of integrated decarbonised production systems. **Computers and Chemical Engineering**, v. 45, p. 1–14, 2012.

[290] Song, C. and Pan, W. Tri-reforming of methane: A novel concept for catalytic production of industrially useful synthesis gas with desired h2/co ratios. **Catalysis Today**, v. 98, p. 463–484, 2004.

[291] Meunier, N.; Chauvy, R.; Mouhoubi, S.; Thomas, D. and Weireld, G. D. Alternative production of methanol from industrial co2. **Renewable Energy**, v. 146, p. 1192–1203, 2020.

[292] International, C. R. **Recycling co2 to produce methanol**: https://www.carbonrecycling.is/co2-methanol.

[293] Nizami, M.; Slamet and Purwanto, W. W. Solar pv based power-to-methanol via direct co2hydrogenation and h2o electrolysis: Techno-economic and environmental assessment. **Journal of CO2 Utilization**, v. 65, 11 2022.

[294] Basini, L. E.; Furesi, F.; Baumgärtl, M.; Mondelli, N. and Pauletto, G. Co2 capture and utilization (ccu) by integrating water electrolysis, electrified reverse water gas shift (e-rwgs) and methanol synthesis. **Journal of Cleaner Production**, v. 377, 12 2022.

[295] Yousaf, M.; Mahmood, A.; Elkamel, A.; Rizwan, M. and Zaman, M. Techno-economic analysis of integrated hydrogen and methanol production process by co2 hydrogenation. **International Journal of Greenhouse Gas Control**, v. 115, 3 2022.

[296] Cordero-Lanzac, T.; Ramirez, A.; Navajas, A.; Gevers, L.; Brunialti, S.; Gandía, L. M.; Aguayo, A. T.; Sarathy, S. M. and Gascon, J. A techno-economic and life cycle assessment for the production of green methanol from co2: catalyst and process bottlenecks. **Journal of Energy Chemistry**, v. 68, p. 255–266, 5 2022.

[297] de Oliveira Campos, B. L.; John, K.; Beeskow, P.; Delgado, K. H.; Pitter, S.; Dahmen, N. and Sauer, J. A detailed process and techno-economic analysis of methanol synthesis from h2 and co2 with intermediate condensation steps. **Processes**, v. 10, 8 2022.

[298] Thomas, G.; Feng, B.; Veeraragavan, A.; Cleary, M. J. and Drinnan, N. Emissions from dme combustion in diesel engines and their implications on meeting future emission norms: A review. **Fuel Processing Technology**, v. 119, p. 286–304, 3 2014.

[299] Im-orb, K. and Piroonlerkgul, P. Sustainability analysis of the bio-dimethyl ether (bio-dme) production via integrated biomass gasification and direct dme synthesis process. **Renewable Energy**, v. 208, p. 324–330, 5 2023.

[300] Prabowo, B.; Yan, M.; Syamsiro, M.; Setyobudi, R. H. and Biddinika, M. K. State of the art of global dimethyl ether production and it's potentional application in indonesia. **Proceedings of the Pakistan Academy of Sciences: Part B**, v. 54, p. 29–39, 2017.

[301] Falco, M. D. Dimethyl ether (dme) production - oil&gas portal. 2022. Https://www.oil-gasportal.com/dimethyl-ether-dme-production-2/.

[302] MULLER, M. and BSCH, U. H. Dimethyl ether. **Ullmanns Encyclopedia of Industrial chemistry**, v. 11, p. 305–308, 2012.

[303] Schakel, W.; Oreggioni, G.; Singh, B.; Strømman, A. and Ramírez, A. Assessing the techno-environmental performance of co2 utilization via dry reforming of methane for the production of dimethyl ether. **Journal of CO2 Utilization**, v. 16, p. 138–149, 2016.

[304] Dias, R. F.; Souza, P. H. G.; Menezes, D. Q. F.; Silva, S. A.; Prata, D. M. and Fluminense, U. F. Análise comparativa do ecoindicador de emissão de co 2 para a indústria de dimetil Éter. 2016.

[305] Mevawala, C.; Jiang, Y. and Bhattacharyya, D. Plant-wide modeling and analysis of the shale gas to dimethyl ether (dme) process via direct and indirect synthesis routes. **Applied Energy**, v. 204, p. 163–180, 2017.

[306] Michailos, S.; Mccord, S.; Sick, V.; Stokes, G. and Styring, P. Dimethyl ether synthesis via captured co2 hydrogenation within the power to liquids concept : A techno-economic assessment. **Energy Conversion and Management**, v. 184, p. 262–276, 2019.

[307] Farooqui, A.; Di, F.; Bose, A.; Ferrero, D.; Llorca, J. and Santarelli, M. Techno-economic and exergy analysis of polygeneration plant for power and dme production with the integration of chemical looping co 2 / h 2 o splitting. **Energy Conversion and Management**, v. 186, p. 200–219, 2019.

[308] Fernández-dacosta, C.; Shen, L.; Schakel, W.; Ramirez, A. and Kramer, G. J. Potential and challenges of low-carbon energy options : Comparative assessment of alternative fuels for the transport sector. **Applied Energy**, v. 236, p. 590–606, 2019.

[309] Tomatis, M.; Mahmud, A.; Afzal, M. T.; Mareta, S.; Wu, T.; He, J. and He, T. Utilization of co2 in renewable dme fuel production : A life cycle analysis (lca) -based case study in china. **Fuel**, v. 254, p. 115627, 2019.

[310] Graaf, G. H.; Stamhuis, E. J. and Beenackers, A. A. Kinetics of low-pressure methanol synthesis. **Chemical Engineering Science**, v. 43, p. 3185–3195, 1988.

[311] Bussche, K. M. V. and Froment, G. F. A steady-state kinetic model for methanol synthesis and the water gas shift reaction on a commercial cu/zno/al2o3 catalyst. **Journal of Catalysis**, v. 161, p. 1–10, 1996.

[312] Mignard, D. and Pritchard, C. On the use of electrolytic hydrogen from variable renewable energies for the enhanced conversion of biomass to fuels. **Chemical Engineering Research and Design**, v. 86, p. 473–487, 2008.

[313] Mota, C. J.; Monteiro, R. S.; Maia, E. B.; Pimentel, A. F.; Miranda, J. L.; Alves, R. M. and Coutinho, P. L. Carbon dioxide as a feedstock for the chemical industry. production of green methanol. **Revista Virtual de Quimica**, v. 6, p. 44–59, 2014.

[314] Amann, J. M. Study of co2 capture processes in power plants. 2007. Http://inis.iaea.org/search/search.aspx?orig_q=RN:39075154.

[315] Berčič, G. and Levec, J. Catalytic dehydration of methanol to dimethyl ether. kinetic investigation and reactor simulation. **Industrial and Engineering Chemistry Research**, v. 32, p. 2478–2484, 1993.

[316] Berčič, G. and Levee, J. Intrinsic and global reaction rate of methanol dehydration over y-al2o3 pellets. **Industrial and Engineering Chemistry Research**, v. 31, p. 1035–1040, 1992.

[317] Diep, B. T. and Wainwright, M. S. Thermodynamic equilibrium constants for the methanol-dimethyl ether-water system. **Journal of Chemical and Engineering Data**, v. 32, p. 330–333, 1987.

[318] Scott, J. A. and Adams, T. A. Biomass-gas-and-nuclear-to-liquids (bgntl) processes part i: Model development and simulation. **Canadian Journal of Chemical Engineering**, v. 96, p. 1853–1871, 2018.

[319] ISO. Iso 16861:2015 - petroleum products — fuels (class f) — specifications of dimethyl ether (dme). 2015. Https://www.iso.org/standard/57835.html.

[320] Éverton Simões Van-Dal and Bouallou, C. Design and simulation of a methanol production plant from co2 hydrogenation. **Journal of Cleaner Production**, v. 57, p. 38–45, 2013.

[321] Samiee, L. and GhasemiKafrudi, E. Assessment of different kinetic models of carbon dioxide transformation to methanol via hydrogenation, over a cu/zno/al2o3 catalyst. **Reaction Kinetics, Mechanisms and Catalysis**, v. 133, p. 801–823, 8 2021.

[322] Raoof, F.; Taghizadeh, M.; Eliassi, A. and Yaripour, F. Effects of temperature and feed composition on catalytic dehydration of methanol to dimethyl ether over y-alumina. **Fuel**, v. 87, p. 2967–2971, 10 2008.

[323] Dowling, A. W. and Biegler, L. T. A framework for efficient large scale equation-oriented flowsheet optimization. **Computers and Chemical Engineering**, v. 72, p. 3–20, 2015.

[324] Mencarelli, L.; Chen, Q.; Pagot, A. and Grossmann, I. E. A review on superstructure optimization approaches in process system engineering. **Computers and Chemical Engineering**, v. 136, p. 106808, 2020.

[325] Hirschfeld, L.; Swanson, K.; Yang, K.; Barzilay, R. and Coley, C. W. Uncertainty quantification using neural networks for molecular property prediction. **Journal of Chemical Information and Modeling**, v. 60, p. 3770–3780, 8 2020.

[326] Garona, H. A.; Cavalcanti, F. M.; de Abreu, T. F.; Schmal, M. and Alves, R. M. B. Evaluation of fischer-tropsch synthesis to light olefins over co- and fe-based catalysts using artificial neural network. **Journal of Cleaner Production**, v. 321, p. 129003, 2021.

[327] Cavalcanti, F. M.; Kozonoe, C. E.; Pacheco, K. A. and de Brito Alves, R. M. Application of artificial neural networks to chemical and process engineering. **Deep Learning Applications**, p. Ch. 9, 2021.

[328] Zhang, S.; Bi, K. and Qiu, T. Bidirectional recurrent neural network-based chemical process fault diagnosis. **Industrial & Engineering Chemistry Research**, v. 59, p. 824–834, 1 2020.

[329] Wu, Z.; Rincon, D. and Christofides, P. D. Process structure-based recurrent neural network modeling for model predictive control of nonlinear processes. **Journal of Process Control**, v. 89, p. 74–84, 2020.

[330] Khezri, V.; Yasari, E.; Panahi, M. and Khosravi, A. Hybrid artificial neural network–genetic algorithm-based technique to optimize a steady-state gas-to-liquids plant. **Industrial & Engineering Chemistry Research**, v. 59, p. 8674–8687, 5 2020.

[331] jian Wang, Y.; Ren, Y. M. and guang Li, H. Symbolic multivariable hierarchical clustering based convolutional neural networks with applications in industrial process operating trend predictions. **Industrial & Engineering Chemistry Research**, v. 59, p. 15133–15145, 8 2020.

[332] Alves, R. and Nascimento, C. Neural network based approach applied to for modeling and optimization an industrial isoprene unit production. **AIChE Annual Meeting, Conference Proceedings**, p. 7663–7682, 2004.

[333] Hang, P.; Zhou, L. and Liu, G. Thermodynamics-based neural network and the optimization of ethylbenzene production process. **Journal of Cleaner Production**, v. 296, p. 126615, 2021.

[334] Savage, T.; Almeida-Trasvina, H. F.; del Río-Chanona, E. A.; Smith, R. and Zhang, D. An adaptive data-driven modelling and optimization framework for complex chemical process design. **Computer Aided Chemical Engineering**, v. 48, p. 73–78, 2020.

[335] Henao, C. A. and Maravelias, C. T. Surrogate-based superstructure optimization framework. **AIChE Journal**, v. 57, p. 1216–1232, 2011.

[336] Leperi, K. T.; Yancy-Caballero, D.; Snurr, R. Q. and You, F. 110th anniversary: Surrogate models based on artificial neural networks to simulate and optimize pressure swing adsorption cycles for co2 capture. **Industrial and Engineering Chemistry Research**, v. 58, p. 18241–18252, 2019.

[337] Zapf, F. and Wallek, T. Case-study of a flowsheet simulation using deep-learning process models for multi-objective optimization of petrochemical production plants. **Computers and Chemical Engineering**, v. 162, 6 2022.

[338] Li, X. and Kraslawski, A. Conceptual process synthesis: Past and current trends. **Chemical Engineering and Processing: Process Intensification**, v. 43, p. 583–594, 2004.

[339] Montastruc, L.; Belletante, S.; Pagot, A.; Negny, S. and Raynal, L. From conceptual design to process design optimization: A review on flowsheet synthesis. **Oil and Gas Science and Technology**, v. 74, 2019.

[340] McKay, M. D.; Beckman, R. J. and Conover, W. J. A comparison of three methods for selecting values of input variables in the analysis of output from a computer code. **Technometrics**, v. 42, p. 55–61, 1979.

[341] Ye, K. Q. Orthogonal column latin hypercubes and their application in computer experiments. **Journal of the American Statistical Association**, v. 93, p. 1430–1439, 1998.

[342] Towler, G. and Sinnott, R. **Chemical engineering design: Principles, practice and economics of plant and process design**. 2 ed: Butterworth-Heinemann, 2013. 1265 p.

[343] Turton, R.; Bailie, R. C.; Whiting, W. B.; Shaeiwitz, J. A. and Bhattacharyya, D. **Analysis, synthesis and design of chemical processes**. 4 ed: Prentice Hall, 2012.

[344] Gurney, K. **An introduction to neural networks**: CRC press, 1997.

[345] Müller, B.; Reinhardt, J. and Strickland, M. T. **Neural networks: An introduction**: Springer Berlin Heidelberg, 2012.

[346] Liu, B.; Wei, Y.; Zhang, Y. and Yang, Q. Deep neural networks for high dimension, low sample size data. **IJCAI International Joint Conference on Artificial Intelligence**, v. 0, p. 2287–2293, 2017.

[347] Goodfellow, I.; Bengio, Y.; Courville, A. and Bengio, Y. **Deep learning**. v. 1: MIT press Cambridge, 2016.

[348] Piotrowski, A. P.; Napiorkowski, J. J. and Piotrowska, A. E. Impact of deep learning-based dropout on shallow neural networks applied to stream temperature modelling. **Earth-Science Reviews**, v. 201, p. 103076, 2020.

[349] Ramachandran, P.; Zoph, B. and Le, Q. V. Swish: A self-gated activation function. **arXiv:1710.05941**, 2017.

[350] Gu, J.; Lu, S.; Shi, F.; Wang, X. and You, X. Economic and environmental evaluation of heat-integrated pressure-swing distillation by multiobjective optimization. 2022.

[351] Zhao, X. and You, F. **Sustainable process design and synthesis for hdpe recycling**. v. 50: Elsevier Masson SAS, 2021. 31-36 p.

[352] Tang, J.; Kang, L. and Liu, Y. Design and optimization of a clean ammonia synthesis system based on biomass gasification coupled with a ca–cu chemical loop. **Industrial & Engineering Chemistry Research**, 2022.

[353] Shen, F.; Zhao, L.; Du, W.; Zhong, W.; Peng, X. and Qian, F. Data-driven stochastic robust optimization for industrial energy system considering renewable energy penetration. **ACS Sustainable Chemistry and Engineering**, v. 10, p. 3690–3703, 2022.

[354] Kianinia, M. and Abdoli, S. M. The design and optimization of extractive distillation for separating the acetone/ n-heptane binary azeotrope mixture. **ACS Omega**, v. 6, p. 22447–22453, 2021.

[355] Chia, D. N.; Duanmu, F. and Sorensen, E. **Optimal design of distillation columns using a combined optimisation approach**. v. 50: Elsevier Masson SAS, 2021. 153-158 p.

[356] Parhi, S. S.; Pramanik, A.; Rangaiah, G. P. and Jana, A. K. Evolutionary algorithm based multiobjective optimization of vapor recompressed batch extractive distillation: Assessing economic potential and environmental impact. **Industrial and Engineering Chemistry Research**, v. 59, p. 5032–5046, 3 2020.

[357] Smith, R. M. **Chemical process: Design and integration**: Wiley, 2005. 712 p.

[358] Christopher, C. C. E.; Dutta, A.; Farooq, S. and Karimi, I. A. Process synthesis and optimization of propylene/propane separation using vapor recompression and self-heat recuperation. **Industrial and Engineering Chemistry Research**, v. 56, p. 14557–14564, 2017.

[359] Navarro-Amorós, M. A.; Ruiz-Femenia, R. and Caballero, J. A. Integration of modular process simulators under the generalized disjunctive programming framework for the structural flowsheet optimization. **Computers and Chemical Engineering**, v. 67, p. 13–25, 2014.

[360] EPA. Greenhouse gas reporting program (ghgrp) | us epa. 2021. Https://www.epa.gov/ghgreporting.

[361] Grimstad, B. and Andersson, H. Relu networks as surrogate models in mixed-integer linear programs. **Computers and Chemical Engineering**, v. 131, p. 106580, 2019.

[362] Marler, R. T. and Arora, J. S. Survey of multi-objective optimization methods for engineering. **Structural and Multidisciplinary Optimization**, v. 26, p. 369–395, 4 2004.

[363] Srinivasan, K.; Garg, A.; Chen, B. Y.; Chang, C. T.; Cherukuri, A. K. and Christopher, J. P. P. Application of artificial neural networks for optimizing operating conditions of a chemical process. **2018 IEEE International Conference on Consumer Electronics-Taiwan, ICCE-TW 2018**, p. 31–32, 2018.

[364] Li, L.; Jamieson, K.; DeSalvo, G.; Rostamizadeh, A. and Talwalkar, A. Hyperband: A novel bandit-based approach to hyperparameter optimization. **Journal of Machine Learning Research**, v. 18, n. 185, p. 1–52, 2018.

[365] Lastusilta, T.; Bussieck, M. R. and Westerlund, T. Comparison of some high-performance minlp solvers. **Chemical engineering transactions**, v. 11, p. 125–130, 2007.

[366] Kronqvist, J.; Bernal, D. E.; Lundell, A. and Grossmann, I. E. A review and comparison of solvers for convex minlp. **Optimization and Engineering**, v. 20, p. 397–455, 2019.

[367] METHANEX. Methanex. 2022. Https://www.methanex.com/.

[368] IEA. Global average levelised cost of hydrogen production by energy source and technology, 2019 and 2050 - charts - data & statistics - iea. 2022. Https://www.iea.org/data-and-statistics/charts/global-average-levelised-cost-of-hydrogen-production-by-energy-source-and-technology-2019-and-2050.

[369] Hansen, J.; Pryor, J. D. C. and Citizens, J. I. Carbon pricing leadership report 2021/22. **Jessica Lam (Microsoft)**, 2022.

[370] Skorikova, G.; Saric, M.; Sluijter, S. N.; van Kampen, J.; Sánchez-Martínez, C. and Boon, J. The techno-economic benefit of sorption enhancement: Evaluation of sorption-enhanced dimethyl ether synthesis for co2 utilization. **Frontiers in Chemical Engineering**, v. 2, 12 2020.

[371] Zondervan, E.; Nawaz, M.; de Haan, A. B.; Woodley, J. M. and Gani, R. Optimal design of a multi-product biorefinery system. **Computers & Chemical Engineering**, v. 35, p. 1752–1766, 2011.

[372] Chakkingal, A.; Janssens, P.; Poissonnier, J.; Virginie, M.; Khodakov, A. Y. and Thybaut, J. W. Multi-output machine learning models for kinetic data evaluation : A fischer–tropsch synthesis case study. **Chemical Engineering Journal**, v. 446, p. 137186, 2022.

[373] SciFinder. Scifinder a cas solution - commercial sources. 2018. Http://scifinder.cas.org.

[374] PRODCOM. European commission: Eurostat - production statistics. 2017. Https://ec.europa.eu/eurostat/web/prodcom/data/excel-files-nace-rev.2.

[375] ICIS. Europe butac prices stable, mixed pressures from feedstocks. 2018. Https://www.icis.com/explore/resources/news/2018/10/01/10262983/europe-butac-prices-stable-mixed-pressures-from-feedstocks/?redirect=english.

[376] ICIS. Europe butac prices stable, oxea force majeure ongoing. 2018. Https://www.icis.com/explore/resources/news/2018/12/03/10289630/europe-butac-prices-stable-oxea-force-majeure-ongoing/.

[377] ICIS. Acetic acid production and manufacturing process - icis explore. Https://www.icis.com/explore/resources/news/2007/10/31/9074780/acetic-acid-production-and-manufacturing-process/.

[378] ICIS. Outlook '17: China po declines to hasten in 2h on additional capacity - icis explore. 2018. Https://www.icis.com/explore/resources/news/2017/01/06/10067648/outlook-17-china-po-declines-to-hasten-in-2h-on-additional-capacity/.

[379] ICIS. Propylene oxide - asia - prices, news and market analysis. 2018. Https://www.icis.com/explore/commodities/chemicals/propylene-oxide/asia/.

[380] Bank, W. European union natural gas import price. 2018. Https://ycharts.com/indicators/europe_natural_gas_price.

[381] ICIS. International urea prices start recovery on indian tender announcement. 2019. Https://www.icis.com/explore/resources/news/2019/01/11/10305409/international-urea-prices-start-recovery-on-indian-tender-announcement/.

[382] Methanex. Methanex european posted contract price methanex asian posted contract price (mepcp) (apcp) methanex monthly average regional posted contract price history (mndrp) methanex non-discounted reference price. 2018. Https://www.methanex.com/sites/default/files/methanol-price/MxAvgPrice_Mar 29

[383] ICIS. Us october ethylene contracts settle down 7.4 2018. Https://www.icis.com/explore/resources/news/2018/11/02/10277089/us-october-ethylene-contracts-settle-down-7-4-on-feedstocks/.

[384] System, H.-F. Independent report to the dutch government - h2-fuel.nl. 2018. Http://www.h2-fuel.nl/en/h2fuel_pdf/independent-report-dutch-government/.

[385] Office, F. C. T. Progress in hydrogen and fuel cells. 2017. Https://www.energy.gov/sites/prod/files/2017/10/f37/fcto-progress-fact-sheet-august-2017.pdf.

[386] Commission, C. E. California energy commission california air resources board joint agency staff report on assembly bill 8: Assessment of time and cost needed to attain 100 hydrogen refueling stations in california. 2015.

[387] ICIS. Europe fuel ethanol prices stable with little activity in 2019. 2019. Https://www.icis.com/explore/resources/news/2019/01/02/10301215/europe-fuel-ethanol-prices-stable-with-little-activity-in-2019/.

[388] ICIS. European fuel ethanol prices ascend to 20-month high. 2018. Https://www.icis.com/explore/resources/news/2018/12/06/10291741/european-fuel-ethanol-prices-ascend-to-20-month-high/.

[389] ICIS. International ammonia prices remain soft on oversupply and weak demand. 2019. Https://www.icis.com/explore/resources/news/2019/03/08/10330310/international-ammonia-prices-remain-soft-on-oversupply-and-weak-demand/.

[390] Qi, W.; Sathre, R.; III, W. R. M. and Shehabi, A. Unit price scaling trends for chemical products. p. 17, 2015.

Appendix A

List of Compounds Studied in the Thermodynamic Property Estimation

Table A.1 shows the chemical species studied in this work, along with their internal identification (ID), there are also other information as IUPAC Name, CAS Number (it is a unique numerical identifier assigned by the Chemical Abstracts Service to every chemical substance described in the open scientific literature), chemical class and the location of a 2D representation of the molecule (Figures A.1 to A.10).

Table A.1: Dataset of molecules assessed.

ID	Name	CAS	Chemical Class[a]	Figure
1	Formic acid	64-18-6	CRBAC	A.1A
2	Acetic acid	64-19-7	CRBAC	A.1B
3	Propionic Acid	79-09-4	CRBAC	A.1C
4	Acrylic acid	79-10-7	CRBAC	A.1D
5	Formylformic Acid	298-12-4	CRBAC	A.1E
6	Methacrylic Acid	79-41-4	CRBAC	A.1F
7	Oxalic Acid	144-62-7	CRBAC	A.1G
8	Benzoic Acid	65-85-0	ACRBA	A.1H
9	p-Salicylic acid	99-96-7	ACRBA	A.1I
10	Salicylic acid	69-72-7	ACRBA	A.1J
11	3-Phenylpropynoic acid	637-44-5	ACRBA	A.1K
12	9H-Fluorene-9-carboxylic acid	1989-33-9	ACRBA	A.1L
13	1,3-Indenedicarboxylic acid	82947-33-9	ACRBA	A.1M
14	2-formylbutanoic acid	4442-98-2	CARBX	A.2A
15	3-Oxo-pentanedioic acid	542-05-2	CARBX	A.2B
16	5-Methyl-3-oxohexanoic acid	131991-42-9	CARBX	A.2C
17	2-Hydroxybenzoylformic acid	17392-16-4	CARBX	A.2D
18	2-Oxo-1,3-cyclohexanedicarboxylic acid	22775-31-1	CARBX	A.2E
19	Indanone-2-carboxylic acid	6742-29-6	CARBX	A.2F
20	2-Carboxy-α-tetralone	62952-26-5	CARBX	A.2G
21	4-Hydroxy-4-phenyl-2-butynoic acid	62952-24-3	CARBX	A.2H
22	2-Carboxycyclohexanone	18709-01-8	CARBX	A.2I
23	3-Oxo-3-phenylpropanoic acid	614-20-0	CARBX	A.2J
24	4-Chlorobenzoylacetic acid	17589-68-3	CARBX	A.2K
25	p-Bromobenzoylacetic acid	64929-35-7	CARBX	A.2L
26	p-Methylbenzoylacetic acid	13422-78-1	CARBX	A.2M
27	p-Methoxybenzoylacetic acid	13422-77-0	CARBX	A.2N
28	3-Ethenyl-2-methyl-cyclopentane-carboxylic acid	108451-44-1	CRBAC	A.3A
29	3-Ethenyl-2-methylene-cyclopentane-carboxylic acid	108451-43-0	CRBAC	A.3B

Continued on next page...

Table A.1 (continued)

ID	Name	CAS	Chemical Class[a]	Figure
30	(Z)-6-methyl-2-(propan-2-ylidene)hepta-4,6-dienoic acid	134226-09-8	CRBAC	A.3C
31	3-Hexenedioic acid	29311-53-3	CRBAC	A.3D
32	(Z)-5-methyl-2-(propan-2-ylidene)hepta-4,6-dienoic acid	134226-08-7	CRBAC	A.3E
33	Bis(methallyl) carbonate	64057-79-0	CRBAC	A.3F
34	Diallyl carbonate	15022-08-9	CRBAC	A.3G
35	Dibenzyl carbonate	3459-92-5	CRBAC	A.3H
36	Acetaldehyde	75-07-0	ALDEH	A.4A
37	Formaldehyde	50-00-0	ALDEH	A.4B
38	Methanol	67-56-1	ALCOH	A.4C
39	Propanol	71-23-8	ALCOH	A.4D
40	Methane	74-82-8	ALKAN	A.4E
41	Styrol	100-42-5	BENZD	A.4F
42	Dimethyl ether	115-10-6	ETHER	A.4G
43	Ethylene Oxide	75-21-8	EPOXI	A.4H
44	Acetone	67-64-1	KETON	A.4I
45	Ethylene carbonate	96-49-1	CARBN	A.4J
46	Propylene carbonate	108-32-7	CARBN	A.4K
47	Dimethyl Carbonate	616-38-6	CARBN	A.4L
48	Diethyl Carbonate	105-58-8	CARBN	A.4M
49	Methyl Carbamate	598-55-0	AMIDS	A.5A
50	Urethane	51-79-6	AMIDS	A.5B
51	Butyl carbamate	592-35-8	AMIDS	A.5C
52	Ethyl N-(cyclohexylmethyl)carbamate	500912-98-1	AMIDS	A.5D
53	Methyl N-Phenylcarbamate	2603-10-3	AMIDS	A.5E
54	O-Ethyl N-phenylcarbamate	101-99-5	AMIDS	A.5F
55	Methyl benzylcarbamate	5817-70-9	AMIDS	A.5G
56	Ethyl Benzylcarbamate	2621-78-5	AMIDS	A.5H
57	2-Oxazolidone	497-25-6	AMIDS	A.5I
58	4-Methyl-2-oxazolidone	16112-59-7	AMIDS	A.5J
59	(4S)-(-)-4-Isopropyl-2-oxazolidone	17016-83-0	AMIDS	A.5K
60	(4R)-4-Phenyl-1,3-oxazolidin-2-one	90319-52-1	AMIDS	A.5L
61	5-Phenyl-1,3-oxazolidin-2-one	7693-77-8	AMIDS	A.5M
62	(-)-4-(Phenylmethyl)-2-oxazolidinone	102029-44-7	AMIDS	A.5N
63	N-Methyl-2-oxazolidone	19836-78-3	AMIDS	A.5O
64	Diphenyl-5,6,7,7a-tetrahydropyrrolo[1,2-c]oxazol-3(1H)-one	160424-29-3	AMIDS	A.5P
65	2-Oxo-1,3-dioxane	2453-03-4	HETEO	A.6A
66	3-Hydroxypropylene carbonate	931-40-8	HETEO	A.6B
67	4,4-Dimethyl-1,3-dioxolan-2-one	4437-69-8	HETEO	A.6C
68	4-Ethyl-1,3-dioxolan-2-one	4437-85-8	HETEO	A.6D
69	4,4-Dimethyl-5-methylene-1,3-dioxolan-2-one	4437-80-3	HETEO	A.6E
70	n-Butylethylene carbonate	66675-43-2	HETEO	A.6F
71	4-Ethenyl-1,3-dioxolan-2-one	4427-96-7	HETEO	A.6G
72	Hexahydro-1,3-benzodioxol-2-one	4389-22-4	HETEO	A.6H
73	4-Methylene-1,3-dioxaspiro[4.5]decan-2-one	92474-80-1	HETEO	A.6I
74	4-Phenyl-1,3-dioxolan-2-one	4427-92-3	HETEO	A.6J
75	4-Hydroxycoumarin	1076-38-6	HETEO	A.7A
76	4-Hydroxy-3-methylcoumarin	15074-17-6	HETEO	A.7B
77	8-Methyl-4-hydroxycoumarin	24631-83-2	HETEO	A.7C
78	3,6-Dimethyl-4-hydroxycoumarin	118157-94-1	HETEO	A.7D
79	7-Methyl-4-hydroxycoumarin	18692-77-8	HETEO	A.7E

Continued on next page...

Table A.1 (continued)

ID	Name	CAS	Chemical Class[a]	Figure
80	3-Ethyl-4-hydroxycoumarin	21315-28-6	HETEO	A.7F
81	3-Phenyl-4-hydroxycoumarin	1786-05-6	HETEO	A.7G
82	7-Methoxy-4-hydroxycoumarin	17575-15-4	HETEO	A.7H
83	Methyl isocyanate	624-83-9	ISOCA	A.8A
84	n-Hexyl isocyanate	2525-62-4	ISOCA	A.8B
85	n-Butyl isocyanate	111-36-4	ISOCA	A.8C
86	Isopropyl Isocyanate	1795-48-8	ISOCA	A.8D
87	t-Butylisocyanate	1609-86-5	ISOCA	A.8E
88	Cyclohexyl isocyanate	3173-53-3	ISOCA	A.8F
89	Isocyanatobenzene	103-71-9	ISOCA	A.8G
90	p-Tolyl isocyanate	622-58-2	ISOCA	A.8H
91	4-Methyl-2(5H)-furanone	6124-79-4	LACTN	A.9A
92	1(3H)-Isobenzofuranone	87-41-2	LACTN	A.9B
93	7-Methoxy-3H-isobenzofuran-1-one	28281-58-5	LACTN	A.9C
94	6,7-Dimethoxyphthalide	569-31-3	LACTN	A.9D
95	5,7-Dimethoxyphthalide	3465-69-8	LACTN	A.9E
96	Furo[3,4-e]-1,3-benzodioxol-8(6H)-one	4741-65-5	LACTN	A.9F
97	4-Hydroxy-6-methyl-2H-pyran-2-one	675-10-5	LACTN	A.9G
98	4-Hydroxy-5,6-dimethyl-2H-pyran-2-one	50405-45-3	LACTN	A.9H
99	4,6-Dimethyl-2-pyrone	675-09-2	LACTN	A.9I
100	Tetraethyl-2-pyrone	67530-99-8	LACTN	A.9J
101	Tetrapropyl-2-pyranone	77664-31-4	LACTN	A.9K
102	4,6-Dibutyl-2-pyrone	65095-32-1	LACTN	A.9L
103	4-Hydroxy-6-phenylpyran-2-one	5526-38-5	LACTN	A.9M
104	1,4-Diethyl-5,6,7,8-tetrahydro-3H-2-benzopyran-3-one	111395-92-7	LACTN	A.9N
105	Urea	57-13-6	UREAD	A.10A
106	N,N'-Dipropylurea	623-95-0	UREAD	A.10B
107	N,N'-Dibutylurea	1792-17-2	UREAD	A.10C
108	N,N'-Dihexylurea	2763-88-4	UREAD	A.10D
109	1,3-Diisopropylurea	4128-37-4	UREAD	A.10E
110	N,N'-Di-sec-butylurea	869-79-4	UREAD	A.10F
111	N,N'-Diisobutylurea	1189-23-7	UREAD	A.10G
112	1,3-Diallylurea	1801-72-5	UREAD	A.10H
113	1,3-Bis(2-methoxyethyl)urea	6849-92-9	UREAD	A.10I
114	N,N'-Dicyclohexylurea	2387-23-7	UREAD	A.10J
115	1,3-Diphenylurea	102-07-8	UREAD	A.10K
116	N,N'-Dibenzylurea	1466-67-7	UREAD	A.10L
117	N,N'-Bis(benzhydryl)urea	6744-64-5	UREAD	A.10M
118	Tetrahydro-2-pyrimidone	1852-17-1	UREAD	A.10N
119	3,4-Dihydro-1H-quinazolin-2-one	66655-67-2	UREAD	A.10O
120	2-Imidazolidinone	120-93-4	UREAD	A.10P
121	4-Methyl-2-imidazolidinone	6531-31-3	UREAD	A.10Q
122	Hexahydro-2-benzimidazolinone	1123-97-3	UREAD	A.10R

[a]The chemical class representation are described as: CRBAC - Carboxylic Acid, ACRBA - Aromatic Carboxylic Acid, ALDEH - Aldehyde, ALCOH - Alcohol, ALKAN - Alkane, BENZD - Benzene derivative, ETHER - Ether, EPOXI - Epoxide, KETON - Ketone, CARBN - Carbonate, AMIDS - Amides and carbamate, HETEO - Heterocycles with oxygen, ISOCA - Isocyanate, LACTN - Lactone, UREAD - Urea Derivative and CARBX - Carboxylic acids with additional oxygen function.

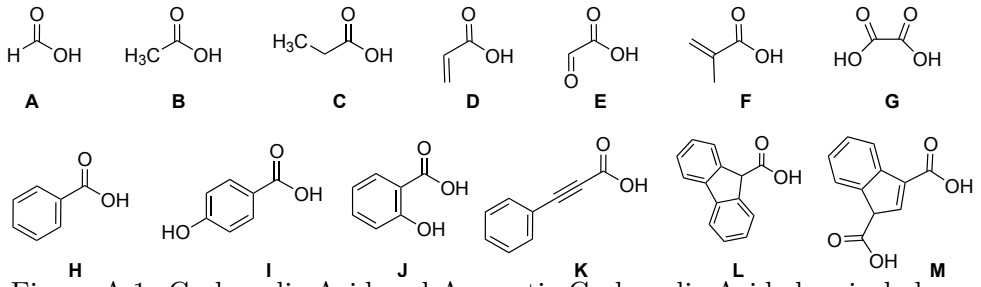

Figure A.1: Carboxylic Acid and Aromatic Carboxylic Acid chemical class.

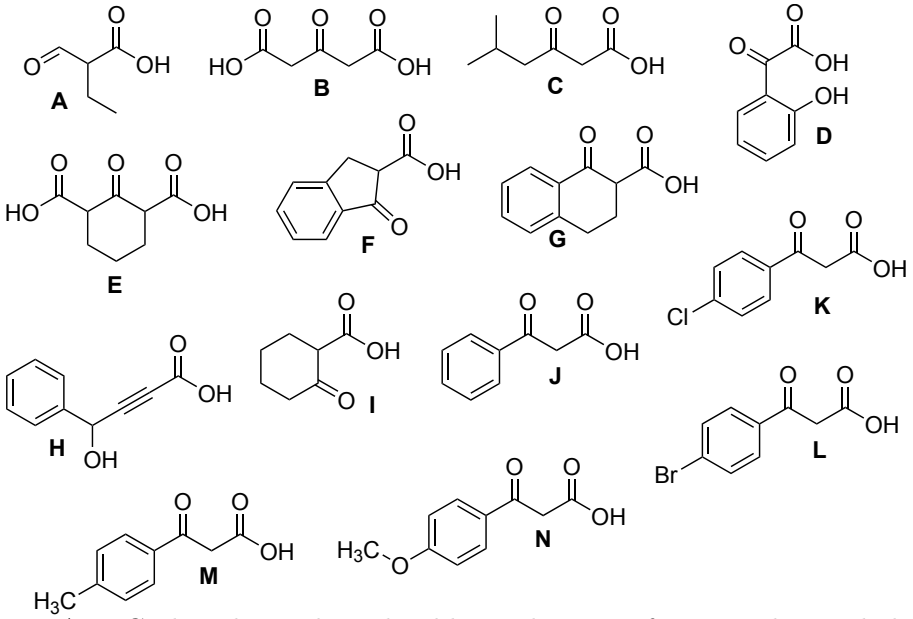

Figure A.2: Carboxylic acids with additional oxygen function chemical class.

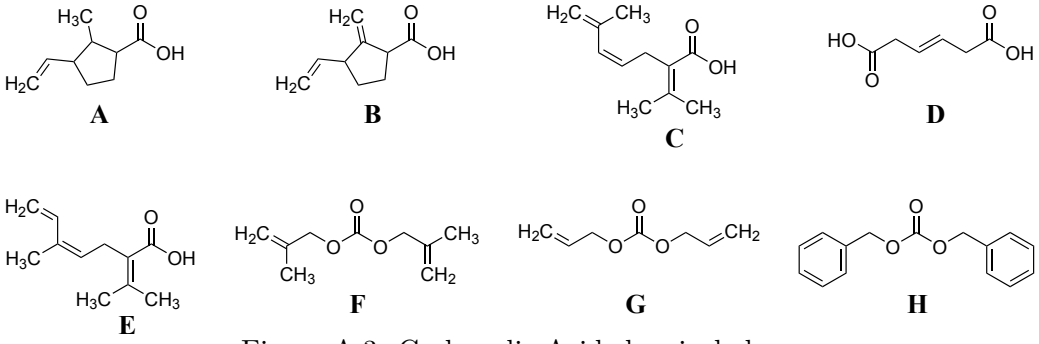

Figure A.3: Carboxylic Acid chemical class.

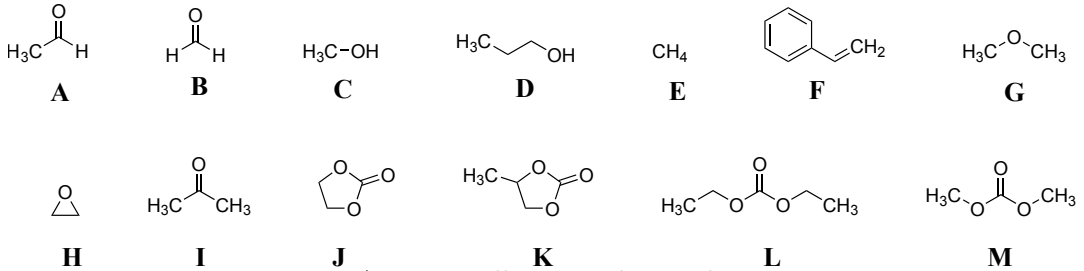

Figure A.4: Miscellaneous chemical species.

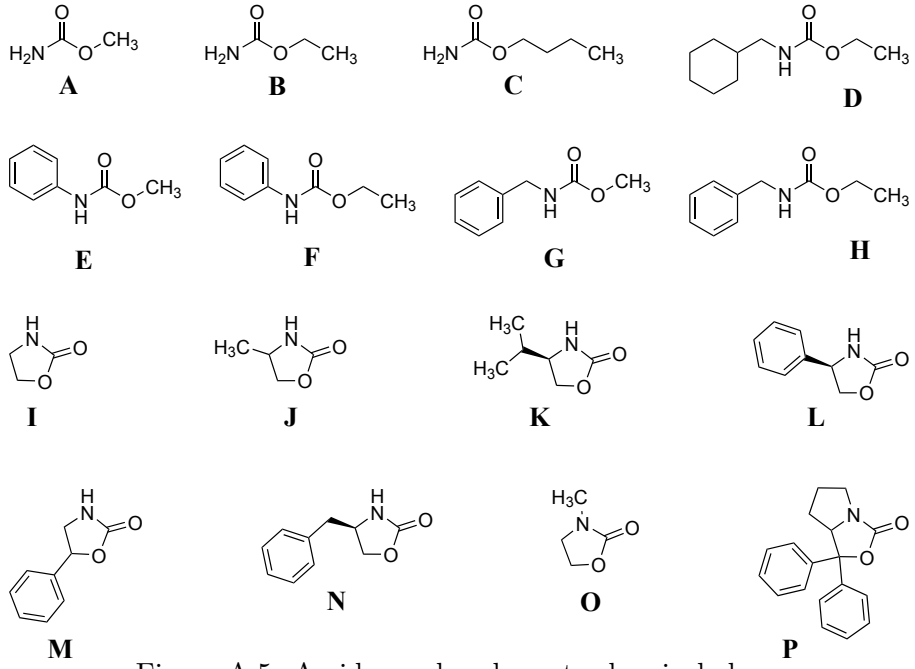

Figure A.5: Amides and carbamate chemical class.

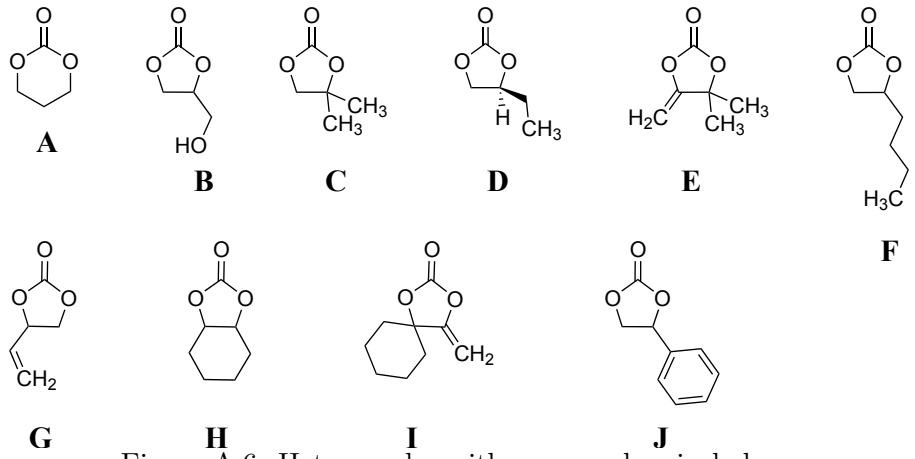

Figure A.6: Heterocycles with oxygen chemical class.

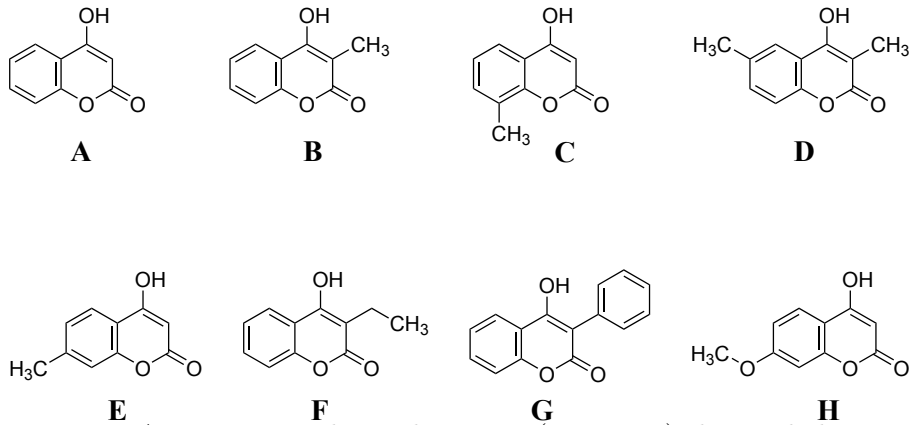

Figure A.7: Heterocycles with oxygen (coumarin) chemical class.

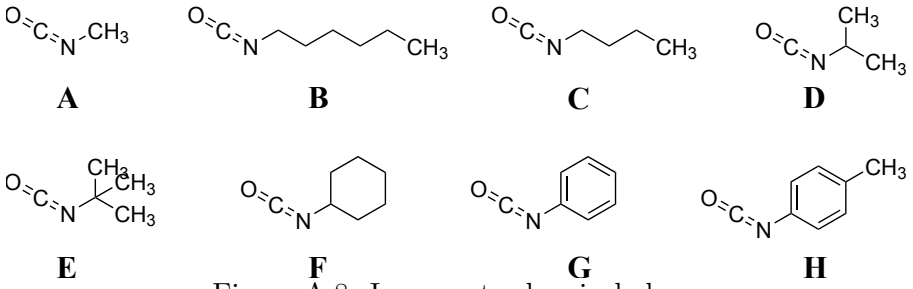

Figure A.8: Isocyanate chemical class.

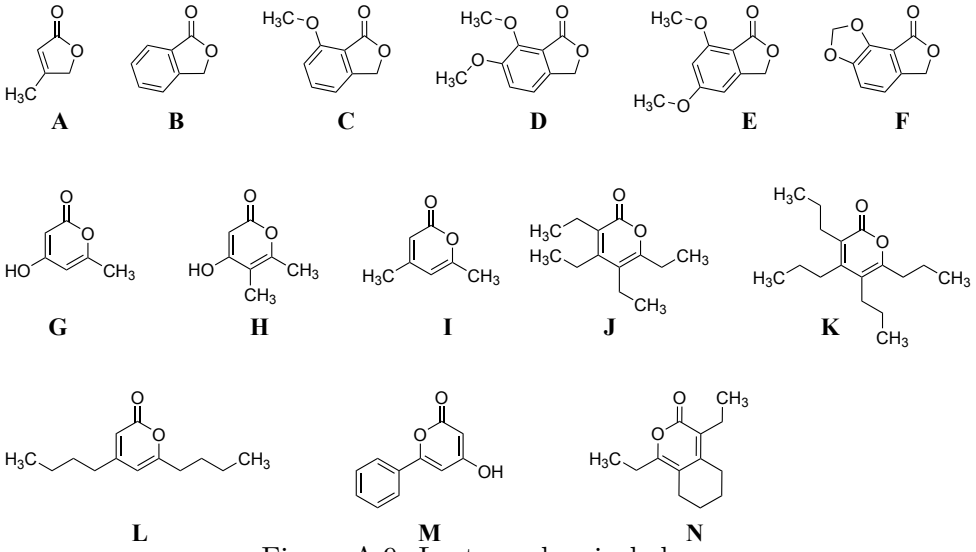

Figure A.9: Lactone chemical class.

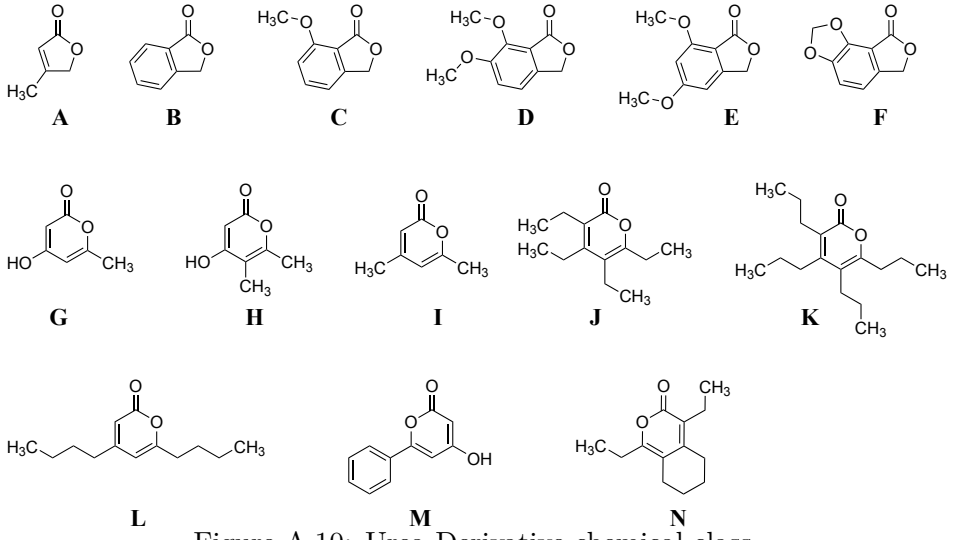

Figure A.10: Urea Derivative chemical class.

Appendix B

Performance Matrix for the First Screening

Table B.1 presents the performance matrix for the first screening.

Table B.1: Performance matrix for the First Screening.

Alternatives	Criteria		
	ΔG_f^o (kcal/mol)	ΔH_{rxn}^o (kcal/mol)	Sci. Rel. (–)
Methanol	-66.06	-11.84	100
Methane	-27.66	-39.44	100
Urea	-70.77	1.91	100
Ethylene carbonate	-139.45	-15.11	90
Propylene carbonate	-151.29	-16.44	90
Dimethyl Carbonate	-150.99	-4.10	90
Dimethyl ether	-64.17	-29.27	80
Salicylic acid	-133.92	-0.22	90
p-Salicylic acid	-132.86	2.49	90
Formic acid	-98.77	3.57	90
Formaldehyde	-41.12	10.28	100
Styrol	11.99	38.31	90
Oxalic Acid	-182.10	17.25	90
Formylformic Acid	-127.98	27.49	80
Acetaldehyde	-60.14	14.14	90
Acetone	-76.62	20.23	100
Acetic acid	-116.34	8.60	100
Benzoic Acid	-85.32	4.08	90
Propanol	-84.75	-37.24	90
Acrylic acid	-97.38	3.90	90
Methacrylic Acid	-109.09	2.39	90
Ethylene Oxide	-28.55	42.51	90
Propionic Acid	-122.90	-28.42	90
Diethyl Carbonate	-171.96	-4.30	80
3-Oxo-3-phenylpropanoic acid	-136.83	9.40	50
p-Methylbenzoylacetic acid	-148.23	10.75	30

Continued on next page...

Table B.1 (continued)

Alternatives	Criteria		
	ΔG_f^o (kcal/mol)	ΔH_{rxn}^o (kcal/mol)	Sci. Rel. (–)
4-Chlorobenzoylacetic acid	-144.61	10.86	30
p-Bromobenzoylacetic acid	-132.95	11.78	30
p-Methoxybenzoylacetic acid	-180.81	6.73	40
Indanone-2-carboxylic acid	-128.70	2.73	20
2-Hydroxybenzoylformic acid	-161.67	28.66	20
2-Carboxy-α-tetralone	-139.66	8.85	20
5-Methyl-3-oxohexanoic acid	-187.69	9.89	10
3-Oxo-pentanedioic acid	-254.39	16.32	60
2-Oxo-1,3-cyclohexanedicarboxylic acid	-256.76	17.88	10
2-Carboxycyclohexanone	-171.43	5.14	40
4-Hydroxy-4-phenyl-2-butynoic acid	-77.25	16.05	10
2-formylbutanoic acid	-160.78	10.29	10
1,3-Indenedicarboxylic acid	-155.63	-64.85	10
9H-Fluorene-9-carboxylic acid	-68.72	7.68	50
3-Phenylpropynoic acid	-30.52	19.70	60
4-Hydroxycoumarin	-110.98	18.70	80
7-Methyl-4-hydroxycoumarin	-124.07	24.58	40
8-Methyl-4-hydroxycoumarin	-122.40	17.90	40
4-Hydroxy-3-methylcoumarin	-120.40	15.81	30
3-Ethyl-4-hydroxycoumarin	-130.46	12.99	20
3-Phenyl-4-hydroxycoumarin	-97.12	13.76	40
7-Methoxy-4-hydroxycoumarin	-156.42	19.57	40
3,6-Dimethyl-4-hydroxycoumarin	-133.97	15.43	10
4,6-Dibutyl-2-pyrone	-145.41	-68.19	10
Tetraethyl-2-pyrone	-147.54	-63.39	10
Tetrapropyl-2-pyranone	-177.91	-63.99	10
4,6-Dimethyl-2-pyrone	-101.36	-68.34	40
4-Hydroxy-6-methyl-2H-pyran-2-one	-137.20	17.84	60
4-Hydroxy-5,6-dimethyl-2H-pyran-2-one	-146.44	10.97	20
4-Hydroxy-6-phenylpyran-2-one	-107.00	19.80	40
1,4-Diethyl-5,6,7,8-tetrahydro-3H-2-benzopyran-3-one	-132.73	-62.35	10
1(3H)-Isobenzofuranone	-72.03	12.06	70
7-Methoxy-3H-isobenzofuran-1-one	-117.33	12.90	30
6,7-Dimethoxyphthalide	-156.13	14.03	40
5,7-Dimethoxyphthalide	-161.98	14.18	30
Furo[3,4-e]-1,3-benzodioxol-8(6H)-one	-134.99	16.25	20
4-Methyl-2(5H)-furanone	-92.36	-21.75	40
3-Ethenyl-2-methyl-cyclopentane-carboxylic acid	-122.55	-48.19	10
3-Ethenyl-2-methylene-cyclopentane-carboxylic acid	-100.29	-25.98	10

Continued on next page...

Table B.1 (continued)

Alternatives	Criteria		
	ΔG_f^o (kcal/mol)	ΔH_{rxn}^o (kcal/mol)	Sci. Rel. (–)
(Z)-5-methyl-2-(propan-2-ylidene)hepta-4,6-dienoic acid	-120.33	-23.57	10
(Z)-6-methyl-2-(propan-2-ylidene)hepta-4,6-dienoic acid	-117.96	-19.97	10
Diallyl carbonate	-123.37	3.90	50
Dibenzyl carbonate	-113.62	8.43	50
Bis(methallyl) carbonate	-147.88	11.77	20
3-Hexenedioic acid	-200.32	-6.89	40
4-Ethyl-1,3-dioxolan-2-one	-158.72	-18.62	60
n-Butylethylene carbonate	-173.42	-12.91	50
4-Phenyl-1,3-dioxolan-2-one	-122.99	-11.98	60
3-Hydroxypropylene carbonate	-190.08	-10.89	60
4,4-Dimethyl-1,3-dioxolan-2-one	-162.56	-12.98	40
4-Ethenyl-1,3-dioxolan-2-one	-128.26	-12.51	60
Hexahydro-1,3-benzodioxol-2-one	-150.65	-1.03	50
2-Oxo-1,3-dioxane	-146.35	-9.34	60
4,4-Dimethyl-5-methylene-1,3-dioxolan-2-one	-144.22	-17.37	40
4-Methylene-1,3-dioxaspiro[4.5]decan-2-one	-150.97	-17.08	30
N,N'-Bis(benzhydryl)urea	-0.78	-8.12	20
N,N'-Dicyclohexylurea	-127.66	-2.65	60
1,3-Diphenylurea	-27.98	2.38	60
N,N'-Dibenzylurea	-37.50	-4.80	50
1,3-Diisopropylurea	-114.59	-3.77	40
N,N'-Dipropylurea	-109.84	-4.63	40
N,N'-Dibutylurea	-124.45	-4.49	50
N,N'-Diisobutylurea	-125.47	-3.48	30
N,N'-Di-sec-butylurea	-128.64	-31.08	20
N,N'-Dihexylurea	-153.06	22.73	40
1,3-Diallylurea	-49.52	-8.81	40
1,3-Bis(2-methoxyethyl)urea	-173.93	-11.71	10
2-Imidazolidinone	-60.27	-2.49	70
4-Methyl-2-imidazolidinone	-71.16	2.19	40
Tetrahydro-2-pyrimidone	-70.84	-6.97	50
Hexahydro-2-benzimidazolinone	-78.56	0.26	20
3,4-Dihydro-1H-quinazolin-2-one	-45.87	3.67	20
(-)-4-(Phenylmethyl)-2-oxazolidinone	-93.07	4.43	60
(4R)-4-Phenyl-1,3-oxazolidin-2-one	-84.24	5.79	50
(4S)-(-)-4-Isopropyl-2-oxazolidone	-126.76	2.43	60
5-Phenyl-1,3-oxazolidin-2-one	-84.89	5.67	40
N-Methyl-2-oxazolidone	-105.13	6.10	50
2-Oxazolidone	-101.72	3.60	60

Continued on next page...

Table B.1 (continued)

Alternatives	Criteria		
	ΔG_f^o (kcal/mol)	ΔH_{rxn}^o (kcal/mol)	Sci. Rel. (–)
Diphenyl-5,6,7,7a-tetrahydropyrrolo[1,2-c]oxazol-3(1H)-one	-71.66	7.44	10
4-Methyl-2-oxazolidone	-111.97	-19.23	40
Urethane	-125.46	-4.08	80
Methyl Carbamate	-114.88	-6.33	60
Butyl carbamate	-140.36	2.68	50
Methyl benzylcarbamate	-99.59	-3.94	40
Ethyl Benzylcarbamate	-110.26	-3.97	40
Ethyl N-(cyclohexylmethyl)carbamate	-159.53	-5.53	10
Methyl N-Phenylcarbamate	-93.86	0.19	60
O-Ethyl N-phenylcarbamate	-104.61	0.10	60
Isocyanatobenzene	-20.69	78.30	80
Isopropyl Isocyanate	-63.88	74.96	70
n-Butyl isocyanate	-69.01	74.37	70
t-Butylisocyanate	-72.51	77.38	70
Cyclohexyl isocyanate	-70.91	75.15	70
n-Hexyl isocyanate	-83.98	88.56	60
Methyl isocyanate	-44.68	85.31	80
p-Tolyl isocyanate	-33.98	76.05	70

Appendix C

Results Detailed for the First Screening

Table C.1 shows the final results for the first screening.

Table C.1: Final Results for the First Screening.

Product	Score	Classification
Propionic Acid	0.7845	1
Propanol	0.7841	2
Methane	0.7761	3
Propylene carbonate	0.7637	4
Ethylene carbonate	0.7553	5
Methanol	0.7402	6
Dimethyl Carbonate	0.7276	7
Dimethyl ether	0.714	8
Salicylic acid	0.7111	9
Urea	0.7089	10
Acetic acid	0.7074	11
p-Salicylic acid	0.7032	12
Methacrylic Acid	0.6956	13
Diethyl Carbonate	0.6923	14
Formic acid	0.6889	15
Acrylic acid	0.6875	16
Benzoic Acid	0.6828	17
Formaldehyde	0.6784	18
Urethane	0.6777	19
Oxalic Acid	0.6747	20
Acetone	0.6667	21
Acetaldehyde	0.6488	22
4-Hydroxycoumarin	0.6133	23
4-Ethyl-1,3-dioxolan-2-one	0.6088	24
2-Imidazolidinone	0.5998	25
3-Hydroxypropylene carbonate	0.5988	26
Formylformic Acid	0.5956	27
4-Ethenyl-1,3-dioxolan-2-one	0.5864	28
2-Oxo-1,3-dioxane	0.584	29
4-Phenyl-1,3-dioxolan-2-one	0.5837	30

Continued on next page...

Table C.1 (continued)

Product	Score	Classification
Ethylene Oxide	0.5755	31
Styrol	0.5738	32
1(3H)-Isobenzofuranone	0.5682	33
Methyl Carbamate	0.568	34
4,6-Dimethyl-2-pyrone	0.5678	35
N,N'-Dicyclohexylurea	0.5628	36
(4S)-(-)-4-Isopropyl-2-oxazolidone	0.5501	37
O-Ethyl N-phenylcarbamate	0.5495	38
3-Oxo-pentanedioic acid	0.5476	39
Methyl N-Phenylcarbamate	0.5463	40
2-Oxazolidone	0.5402	41
n-Butylethylene carbonate	0.5386	42
(-)-4-(Phenylmethyl)-2-oxazolidinone	0.5358	43
1,3-Diphenylurea	0.5222	44
4-Hydroxy-6-methyl-2H-pyran-2-one	0.5151	45
N,N'-Dibutylurea	0.5062	46
Hexahydro-1,3-benzodioxol-2-one	0.5049	47
Tetrahydro-2-pyrimidone	0.4978	48
Butyl carbamate	0.4931	49
Diallyl carbonate	0.4855	50
4,4-Dimethyl-5-methylene-1,3-dioxolan-2-one	0.4847	51
N,N'-Dibenzylurea	0.484	52
3-Phenylpropynoic acid	0.4823	53
4-Methyl-2(5H)-furanone	0.4819	54
4-Methyl-2-oxazolidone	0.4809	55
4,4-Dimethyl-1,3-dioxolan-2-one	0.4794	56
3-Oxo-3-phenylpropanoic acid	0.4757	57
3-Hexenedioic acid	0.4752	58
N-Methyl-2-oxazolidone	0.4752	59
Dibenzyl carbonate	0.4717	60
(4R)-4-Phenyl-1,3-oxazolidin-2-one	0.4704	61
Isocyanatobenzene	0.4702	62
Methyl isocyanate	0.4641	63
4,6-Dibutyl-2-pyrone	0.4621	64
9H-Fluorene-9-carboxylic acid	0.4617	65
Tetrapropyl-2-pyranone	0.4608	66
1,3-Indenedicarboxylic acid	0.4586	67
Tetraethyl-2-pyrone	0.4551	68
1,4-Diethyl-5,6,7,8-tetrahydro-3H-2-benzopyran-3-one	0.4512	69
N,N'-Dipropylurea	0.4458	70
1,3-Diisopropylurea	0.4449	71
Ethyl Benzylcarbamate	0.4443	72

Continued on next page...

Table C.1 (continued)

Product	Score	Classification
Methyl benzylcarbamate	0.4414	73
1,3-Diallylurea	0.4414	74
2-Carboxycyclohexanone	0.4387	75
p-Methoxybenzoylacetic acid	0.4376	76
n-Butyl isocyanate	0.4375	77
Cyclohexyl isocyanate	0.4366	78
4-Methylene-1,3-dioxaspiro[4.5]decan-2-one	0.4365	79
Isopropyl Isocyanate	0.4356	80
t-Butylisocyanate	0.4336	81
p-Tolyl isocyanate	0.4285	82
3-Ethenyl-2-methyl-cyclopentane-carboxylic acid	0.4255	83
N,N'-Di-sec-butylurea	0.4229	84
4-Methyl-2-imidazolidinone	0.4189	85
5-Phenyl-1,3-oxazolidin-2-one	0.4135	86
6,7-Dimethoxyphthalide	0.4123	87
7-Methoxy-4-hydroxycoumarin	0.3987	88
N,N'-Diisobutylurea	0.3971	89
3-Phenyl-4-hydroxycoumarin	0.3959	90
8-Methyl-4-hydroxycoumarin	0.3924	91
N,N'-Dihexylurea	0.3898	92
4-Hydroxy-6-phenylpyran-2-one	0.3831	93
3-Ethenyl-2-methylene-cyclopentane-carboxylic acid	0.377	94
7-Methyl-4-hydroxycoumarin	0.3761	95
(Z)-5-methyl-2-(propan-2-ylidene)hepta-4,6-dienoic acid	0.3756	96
n-Hexyl isocyanate	0.3677	97
p-Methylbenzoylacetic acid	0.3674	98
(Z)-6-methyl-2-(propan-2-ylidene)hepta-4,6-dienoic acid	0.3672	99
4-Chlorobenzoylacetic acid	0.3659	100
5,7-Dimethoxyphthalide	0.3631	101
1,3-Bis(2-methoxyethyl)urea	0.3617	102
p-Bromobenzoylacetic acid	0.3599	103
7-Methoxy-3H-isobenzofuran-1-one	0.3522	104
4-Hydroxy-3-methylcoumarin	0.3454	105
N,N'-Bis(benzhydryl)urea	0.345	106
Ethyl N-(cyclohexylmethyl)carbamate	0.3438	107
Indanone-2-carboxylic acid	0.3424	108
Hexahydro-2-benzimidazolinone	0.3361	109
2-Carboxy-α-tetralone	0.3297	110
4-Hydroxy-5,6-dimethyl-2H-pyran-2-one	0.3262	111
Bis(methallyl) carbonate	0.3246	112
2-Oxo-1,3-cyclohexanedicarboxylic acid	0.3243	113
3,4-Dihydro-1H-quinazolin-2-one	0.32	114

Continued on next page...

Table C.1 (continued)

Product	Score	Classification
5-Methyl-3-oxohexanoic acid	0.3162	115
3-Ethyl-4-hydroxycoumarin	0.3157	116
Furo[3,4-e]-1,3-benzodioxol-8(6H)-one	0.3084	117
2-formylbutanoic acid	0.3062	118
Diphenyl-5,6,7,7a-tetrahydropyrrolo[1,2-c]oxazol-3(1H)-one	0.2889	119
2-Hydroxybenzoylformic acid	0.2857	120
3,6-Dimethyl-4-hydroxycoumarin	0.2844	121
4-Hydroxy-4-phenyl-2-butynoic acid	0.2662	122

Appendix D

Price Estimation

D.1 Introduction

Traditionally, the prices of chemicals are available through market reports, considering the assumption that the chemical is a commodity. Even though the database is extensive, it does not include some of the chemicals used in this assessment, hence a method to estimate the chemical prices is needed.

Hart *et al.* [190] develop a technique to estimate the price of chemicals manufactured in small quantities using data price from laboratory catalogs. This method is particularly useful because it does not require prior knowledge of the prices or volume of production for a particular chemical.

The prices for several chemicals can be retrieved from SciFinder Commercial Sources [373], informations about technical grade, purity level and the producer company are included.

D.2 Methods

The price estimation was based on the conceptual framework proposed by Hart *et al.* [190].

Prior to undertaking the analysis, data collection for the laboratory prices was performed using the SciFinder database [373]. Data were collected during the time window from November - December 2018.

The first step in this process was to develop a price P-quantity Q correlation, as presented in Equation D.2.1.

$$P = a \cdot Q^b \tag{D.2.1}$$

rewriting in logarithmic form,

$$\log P = \log a + b \cdot \log Q \tag{D.2.2}$$

where P stands for the unit price (US$/kg), Q is the quantity (g). Individual values of the intercept a and the slope b were regressed for each of the chemicals.

The volumetric quantities (if that was the case) was converted to mass quantities [48]. Prices for multi-packages were not included to avoid additional packaging costs.

After the linear regression fitted for every chemical, bulk amount values (Q_B) were calculated, it took into account bulk prices (P_B) for the aforementioned chemical, according to Equation D.2.3.

$$Q_B = 10^{\frac{logP_B - loga}{b}} \tag{D.2.3}$$

A weighted-average value for the bulk amount was calculated using Equation D.2.4

$$Q_{B,avg} = \frac{\sum |r_i| \cdot Q_{B,i}}{\sum |r_i|} \qquad i = 1, 2, \cdots, N \tag{D.2.4}$$

where N is the number of chemicals and $|r_i|$ is the absolute value of the correlation coefficient for the chemical i, used as weighting factor.

Commodity chemicals were excluded in the generation of the correlation, they are presented as comparison in Table D.2.

The final stage of the method is to use the average bulk amount to estimate the price for other chemicals, according to Equation D.2.5.

$$P_B = a \cdot (Q_{B,avg})^b \tag{D.2.5}$$

D.3 Results and Discussions

The results of the regression fit for propionic acid are set out in Figure D.1, it illustrates the procedure used for all the chemicals.

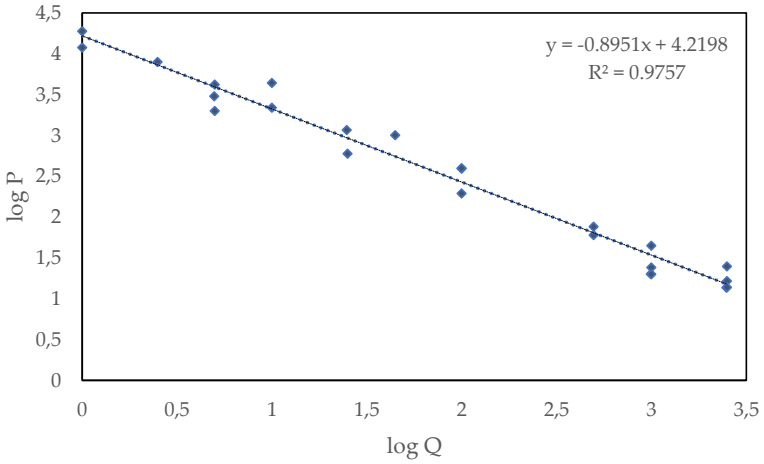

Figure D.1: Regression Fit for Propionic Acid.

The price-quantity data was plotted in log-log coordinates; moreover a least- squares regression fit yield in a slope of -0.8951 and a intercept of 4.2198 ($a = 16.5891$). The correlation (r^2) was 0.9757, indicating a excellent fit between data and the estimated function.

The prices per unit of product decreases monotonically with the increasing purchase amount. Similar behaviour was observed by Hart *et al.* [190], emphasizing a requirement of at least four data points are needed for the correlation.

Table D.1 presents the summary of the values of the intercept $log(a)$ and slope b for each one of the chemicals.

Table D.1: Price Correlations of Laboratory Prices for 6 Chemicals.

Chemical Name	Intercept [log(a)]	Slope [b]	Abs. Correl. Coef. $\lvert r_i \rvert$	$b \cdot \lvert r_i \rvert$	Bulk Price [P_B]	Ref.	Bulk Amount [Q_B (kg)]	$\lvert r_i \rvert \cdot Q_B$
Propionic Acid	4.2198	-0.8951	0.988	-0.873	3.51	[374]	12.74	12.58
Oxalic Acid	3.9523	-0.6811	0.958	-0.652	2.67	[374]	150.42	144.04
Salicylic acid	3.5477	-0.5439	0.923	-0.502	4.69	[374]	194.04	179.00
Acetic acid	3.5733	-0.6071	0.961	-0.583	0.95	[375, 376]	838.24	805.46
Acrylic acid	4.5978	-0.8776	0.955	-0.838	2.25	[377]	68.79	65.68
Propylene oxide	4.6070	-0.9443	0.974	-0.920	1.02	[378, 379]	58.83	57.30
Weighted Average		**-0.7587**					**219.55**	

The slope values for all the chemicals were negative, indicating a reduction of the unit purchase price with the increase in the amount purchased. The absolute correlation coefficients are superior than 0.92, representing good agreement.

As discussed in the Section D.2, some chemical commodities were excluded [190]. Table D.2.

Table D.2: Prices of selected chemical commodities.

Chemical Name	Price (US$/kg)	Ref.
Methane	0.34	[380]
Urea	0.30	[381]
Acetone	1.23	[374]
Methanol	0.48	[382]
Ethylene	0.65	[383]
Ethylene Oxide	0.80	[374]
Hydrogen	6.00	[384–386]
Phenol	1.95	[374]
Ethanol	0.67	[387, 388]
Ammonia	0.33	[389]
Propene	0.71	[374]
Benzene	0.76	[374]

The value of the average weighted slope was -0.7587, very close to that reported by Hart *et al.* [190], that find a value of -0.7518.

Qi, Sathre, III and Shehabi [390] also proposed a method to estimate prices of chemicals from lab-scale prices. In their work the authors divided the group of products into categories, for the organic compounds they obtained a value of -0.67 (in their case, the median was used rather than the weighted average).

From Table D.1 the bulk amounts varies from 12 to 838 kg, the weighted average of bulk amount was 219.55 kg, therefore this value was used to calulate the estimated price of chemical, using Equation D.2.5. Table D.3 shows the results obtained for the group of 14 another chemicals.

Table D.3: Estimations of Bulk Prices of 13 Chemicals from Laboratory-scale Prices.

Chemical Name	Intercept	Slope	Correl.	b.|r|	Bulk Price [PB] (US$/kg)		
	[log(a)]	[b]	|r|		Estimated	Published	Ref.
Propylene carbonate	4.1176	-0.8021	0.947	-0.759	0.68		
Propanol	4.6655	-0.8457	0.946	-0.800	1.41	1.45	[374]
Ethylene carbonate	3.5766	-0.5428	0.918	-0.498	4.76		
Dimethyl Carbonate	4.1325	-0.6212	0.902	-0.560	6.52		
Diethyl Carbonate	3.8679	-0.6403	0.945	-0.605	2.80		
p-Salicylic acid	3.6144	-0.5311	0.983	-0.522	5.99		
Methacrylic Acid	3.7563	-0.6428	0.973	-0.625	2.10	1.77	[374]
Dimethyl ether	4.5654	-0.7034	0.955	-0.672	6.43		
Formic acid	4.4254	-0.8533	0.955	-0.815	0.74		
Urethane	4.0074	-0.6086	0.914	-0.556	5.71		
Benzoic Acid	3.7000	-0.5826	0.960	-0.559	3.87	3.48	[374]
Formaldehyde	3.8564	-0.6976	0.919	-0.641	1.35		
Acetaldehyde	4.7757	-0.8134	0.951	-0.773	2.70		

In order to test the correlation and the average bulk amount achieved using the method, the estimated prices were compared with some published data. Among the chemical with published price, propanol showed the smallest difference, 2.95%, followed by benzoic acid, 10%, while methacrilic acid showed a absolute deviation of 0.33 US$/kg.

D.4 Conclusions

The method of linear regression of log- log relations was able to estimate the price of chemicals. The lab-scale prices along with bulk prices were employed to calculate the weighted average bulk amount. It was, then, used to estimate the prices of chemicals which did not present historical data or even demand consumption.

The outcome correlation can help to address more robust techno-economic modelling of technologies. However, the interpretation and use to other systems must be evaluated case by case.

Appendix E

Methanol Kinetic Model Rearranged for Aspen Plus

The final values for all the parameters are described in Table E.1.

Table E.1: Methanol Kinetic Model Rearranged for Aspen Plus

Parameter	Constant	Value
kA	A	-29.894
	B	4.811.162
kB	A	8.147
	B	0.000
kC	A	-6.452
	B	2.068.439
kD	A	-34.951
	B	14.928.915
kE	A	4.804
	B	-11.797.450
kF	A	17.520
	B	-2.248.564
kG	A	0.131
	B	-7.024.191

Table E.2: Aspen Plus implementation of the Methanol synthesis kinetics model.

R1 (CO2 + 3H2 -> CH3OH + H2O)	
kinetic factor	k= 1
	E = 0
	driving force expressions
term 1	
conc. exponents for reactants:	CO2 = 1 ; H2 = 1
conc. exponents for products:	CH3OH = 0 ; H2O = 0
coefficients:	A = -29.866 ; B = 4810.895
term 2	
conc. exponents for reactants:	CO2 = 0 ; H2 = -2
conc. exponents for products:	CH3OH = 1 ; H2O = 1
coefficients:	A = 17.549 ; B = -2248.831
	adsorption expression
adsorption term exponent	3
concentration exponent:	
term 1:	CO2 = 0 ; H2 = 0 ; H2O = 0 ; CO = 0
term 2:	CO2 = 0 ; H2 = -1 ; H2O = 1 ; CO = 0
term 3:	CO2 = 0 ; H2 = 0.5 ; H2O = 0 ; CO = 0
term 4:	CO2 = 0 ; H2 = 0 ; H2O = 1 ; CO = 0
adsorption constants:	
term 1:	A = 0 ; B = 0 ; C = 0 ; D = 0
term 2:	A = 8.147 ; B = 0 ; C = 0 ; D = 0
term 3:	A = -6.452 ; B = 2068.324 ; C = 0 ; D = 0
term 4:	A = -34.951 ; B = 14928.085 ; C = 0 ; D = 0
R2 (CO2 + H2 -> CO + H2O)	
kinetic factor	k= 1
	E = 0
	driving force expressions
term 1	
conc. exponents for reactants:	CO2 = 1 ; H2 = 0
conc. exponents for products:	CO = 0 ; H2O = 0
coefficients:	A = 4,804 ; B = -11796.794
term 2	
conc. exponents for reactants:	CO2 = 0 ; H2 = -1
conc. exponents for products:	CO = 1 ; H2O = 1
coefficients:	A = 0.132 ; B = -7023.536
	adsorption expression
adsorption term exponent	1
concentration exponent:	
term 1:	CO2 = 0 ; H2 = 0 ; H2O = 0 ; CO = 0
term 2:	CO2 = 0 ; H2 = -1 ; H2O = 1 ; CO = 0
term 3:	CO2 = 0 ; H2 = 0.5 ; H2O = 0 ; CO = 0
term 4:	CO2 = 0 ; H2 = 0 ; H2O = 1 ; CO = 0
adsorption constants:	
term 1:	A = 0 ; B = 0 ; C = 0 ; D = 0
term 2:	A = 8.147 ; B = 0 ; C = 0 ; D = 0
term 3:	A = -6.452 ; B = 2068.324 ; C = 0 ; D = 0
term 4:	A = -34.951 ; B = 14928.085 ; C = 0 ; D = 0

Appendix F

DME Kinetic Model Rearranged for Aspen Plus

To calculate the input parameters for Aspen for the kinetic term, the original parameters from Berčič and Levec [315] were used. Eq.F.0.1, rearrange the terms.

$$\begin{aligned} k_{\mathrm{DME}} &= k_H K^2_{\mathrm{CH3OH}} \\ k_{\mathrm{DME}} &= \left(5.35 \times 10^{13}\ e^{-17280/T}\right) \cdot \left(5.39 \times 10^{-4}\ e^{8487/T}\right)^2 \\ k_{\mathrm{DME}} &= 1.554\,29 \times 10^{7}\ e^{-306/T} \end{aligned} \tag{F.0.1}$$

However, the kinetic term, in Aspen Plus, is expressed as $k^n exp(-E/RT)$. The exponential factor is represented as (E/RT), where E is the activation energy, T is the temperature and R is the universal gas constant. It is crucial to consider this conversion factor. In this particular case, the value of 607.62 cal/mol or 2544 kJ/kmol is utilized for Aspen Plus calculations.

The adsorption expression is represented by Eq. F.0.2.

$$\left(1 + 2\sqrt{K_{\mathrm{CH3OH}} C_{\mathrm{CH3OH}}} + K_{\mathrm{H2O}} C_{\mathrm{H2O}}\right)^4 \tag{F.0.2}$$

The first term is 1, the second term can be rearranged as Eq. F.0.3 (and logarithm in Eq. F.0.4).

$$\begin{aligned} K_{\mathrm{Term\ 2}} &= 2 \cdot \sqrt{K_{\mathrm{CH3OH}}} \\ K_{\mathrm{Term\ 2}} &= 2 \cdot \sqrt{5.39 \times 10^{-4}\ e^{8487/T}} \\ K_{\mathrm{Term\ 2}} &= 0.0464327\ e^{4243.5/T} \end{aligned} \tag{F.0.3}$$

$$ln(K_{\mathrm{Term\ 2}}) = -3.069751327 + \frac{4243.5}{T} \tag{F.0.4}$$

The term 3 is described in logarithm form in Eq. F.0.5

$$ln(K_{\mathrm{Term\ 3}}) = -2.468639677 + \frac{5070}{T} \tag{F.0.5}$$

The thermodynamic equilibrium constant parameters ($K_{eq,MeOHdeh}$) were obtained from Diep [317] as described in Eq. F.0.6.

$$ln(K_{eq,MeOHdeh}) = \frac{2835.2}{T} + 1.675 \cdot ln(T) - 2.39 \times 10^{-4} \cdot T - 0.21 \times 10^{-6} \cdot T^2 - 13.36 \quad \text{(F.0.6)}$$

Table F.1 present the implementation in Aspen Plus.

Table F.1: Aspen Plus implementation of the DME synthesis kinetics model.

R1 (2CH3OH -> CH3OCH3 + H2O)	
kinetic factor	k= 15542873.5
	E = 2544
	driving force expressions
term 1	
conc. exponents for reactants:	CH3OH = 2
conc. exponents for products:	DME = 0 ; H2O = 0
coefficients:	A = 0 ; B = 0 ; C = 0 ; D = 0
term 2	
conc. exponents for reactants:	CH3OH = 0
conc. exponents for products:	DME = 1 ; H2O = 1
coefficients:	A = 13.36 ; B = -2835.2 ; C = -1.675 ; D = 0.000239
	adsorption expression
adsorption term exponent	4
concentration exponent:	
term 1:	CH3OH = 0 ; H2O = 0
term 2:	CH3OH = 0.5 ; H2O = 0
term 3:	CH3OH = 0 ; H2O = 1
adsorption constants:	
term 1:	A = 0 ; B = 0 ; C = 0 ; D = 0
term 2:	A = -3.06975 ; B = 4243.5 ; C = 0 ; D = 0
term 3:	A = -2.46864 ; B = 5070 ; C = 0 ; D = 0

Appendix G

Detailed Information for the Neural Networks - ANN1

Detailed process flowsheet

In this section the detailed process flowsheet is described. The Figure G.1 depicts the region of the process flowsheet from where the neural network will be generated.

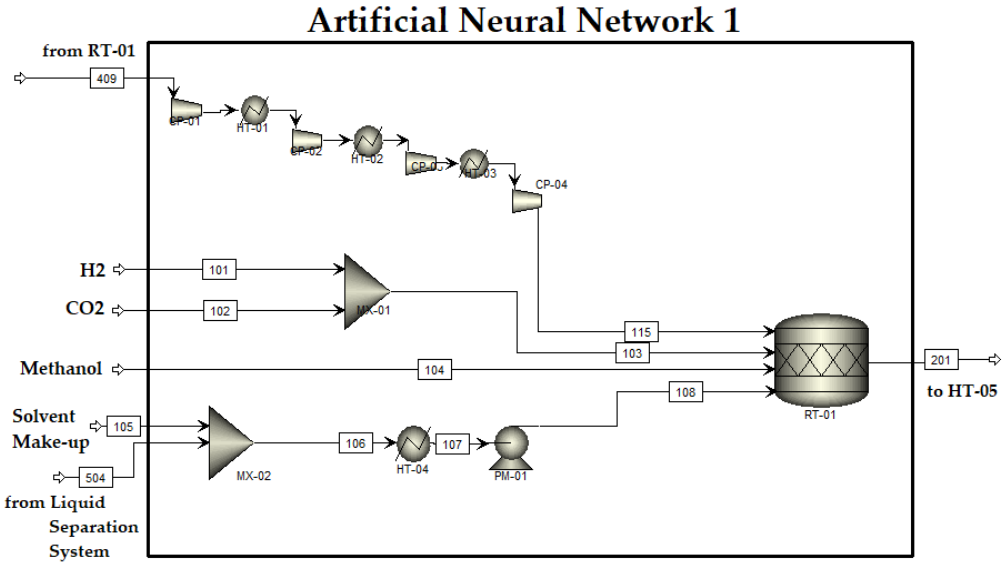

Figure G.1: Feed Conditioning and Reaction System as a neural network - Acetic Acid.

The considered variables are the flows of the stream 412 (for the following chemical compounds: hydrogen, carbon dioxide and methane), the temperature of the stream 412, the stream 504 (for the following chemical compounds: acetic acid and solvent), the temperature of the stream 504, the temperature of the heat exchanger HT-03 and the temperature of the reactor.

The collected output variables are the total capital cost, utility usage (water and electric), utility $CO_{2,equivalent}$ usage and conversion of R1 and R2.

Neural Network Architecture

The Figure G.2 translates the feed conditioning and reaction system section of the acetic acid process (Figure G.1) into a neural network. There are 10 input variables and 7 output variables.

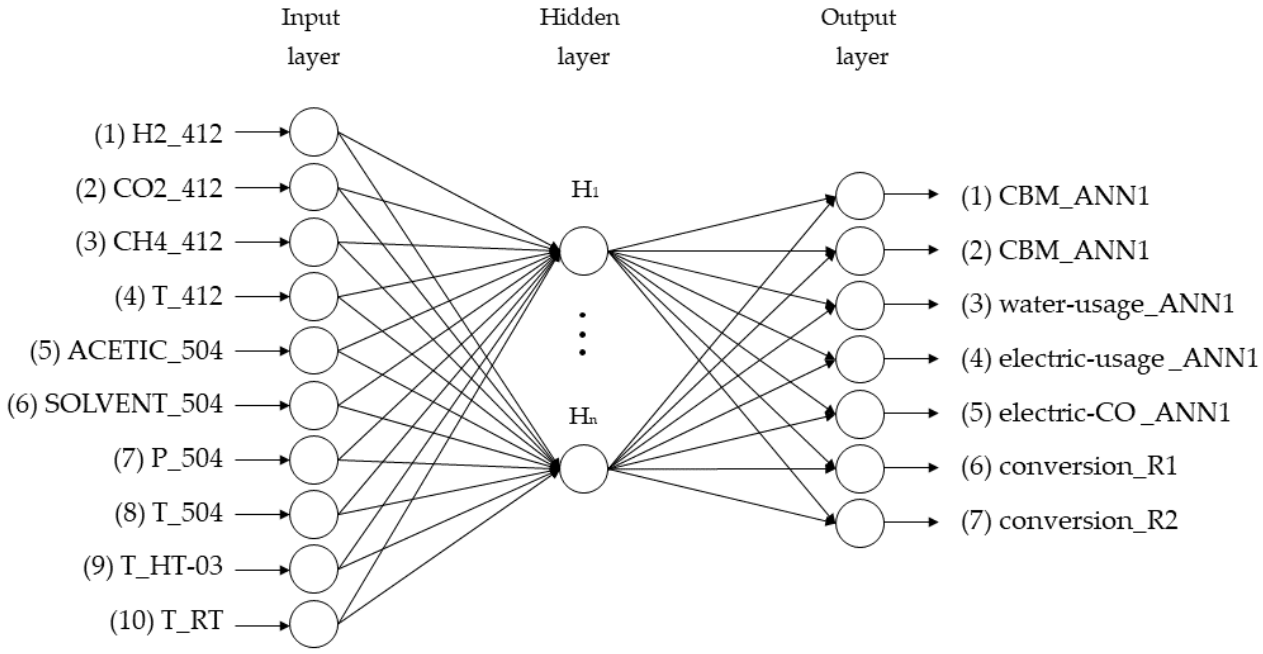

Figure G.2: Detailed architecture for acetic acid ANN1.

It is a feed forward neural network with only one hidden layer, the number of neurons is defined in the hyperparameter tuning.

Limits of the input variables

The Table G.1 presents the values used as upper and lower bonds for the data collection and neural network generation.

The Figure G.3 presents the distribution of the input parameters using the Latin hipercube sampling method.

Table G.1: Limits of the inout variables for acetic acid ANN1.

Variable	Stream/ Unit	lower	upper	Unit
H2_412	412	1200	1500	kmol/h
CO2_412	412	900	1200	kmol/h
CH4_412	412	2	20	kmol/h
T_412	412	15	30	kmol/h
ACETIC_504	504	0.6	0.7	kmol/h
SOLVENT_504	504	780	781.725	kmol/h
P	504	1	3	bar
T	504	215	230	oC
T	HT-03	70	130	oC
T	RT-01	170	190	oC

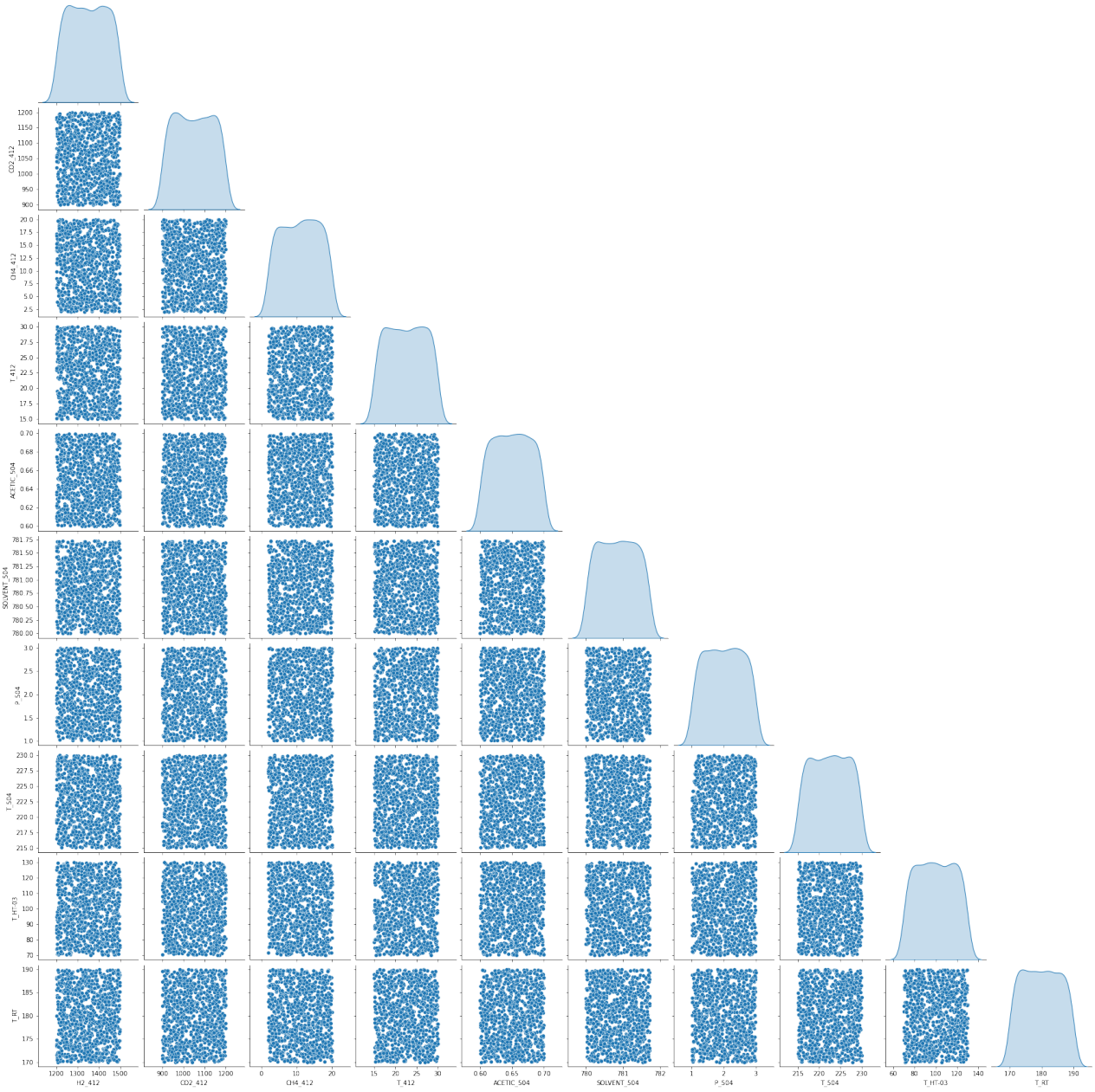

Figure G.3: Input variable distribution for the acetic acid ANN1.

It is possible to verify that the distribution is uniform in each variable assessed.

The Figure G.4 presents the distribution of the output variables.

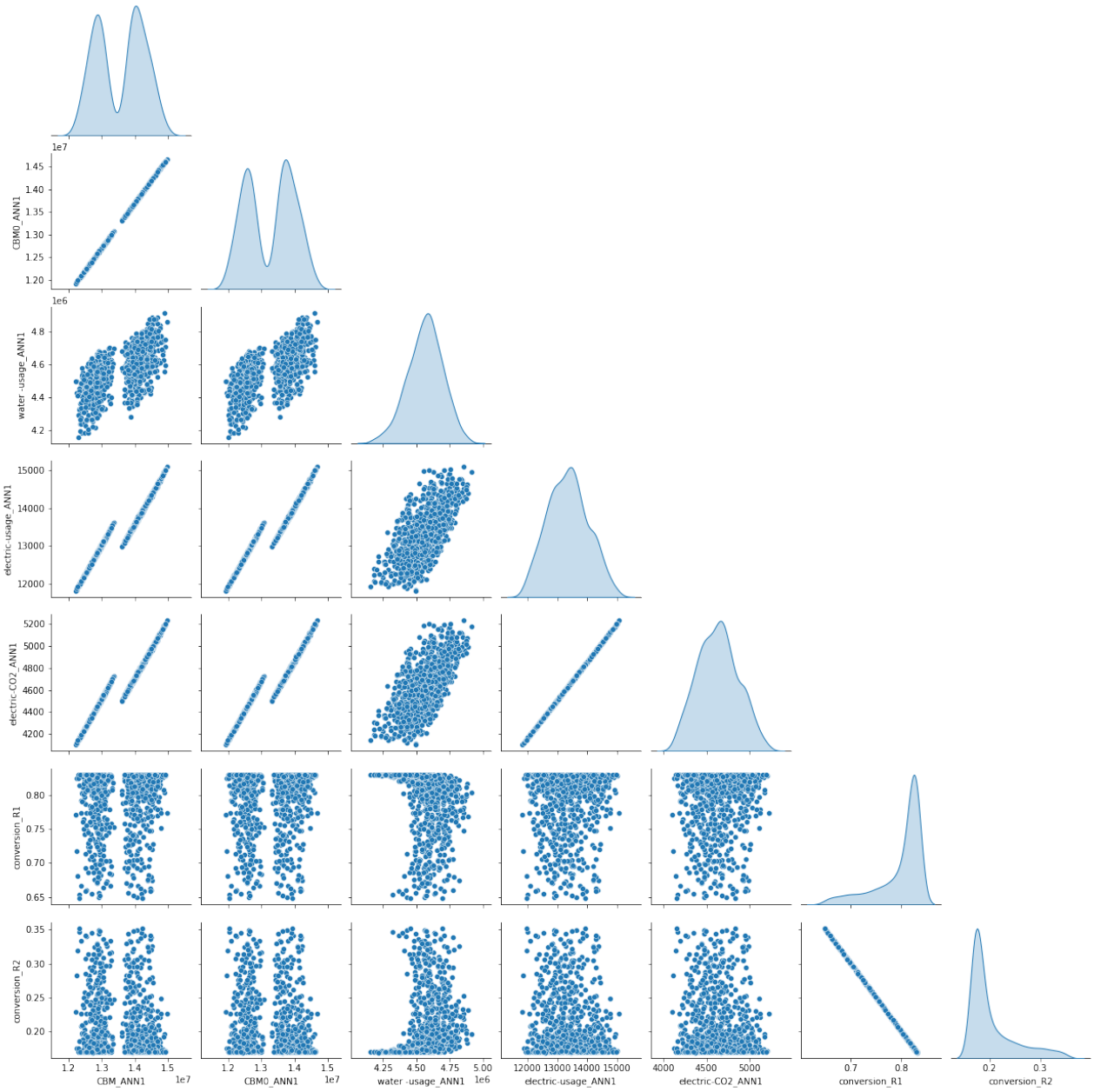

Figure G.4: Output variable distribution.

Hyperparameter Tuning

The Figure G.5 presents hyperparameter tunning for the Artificial Neural Network 1.

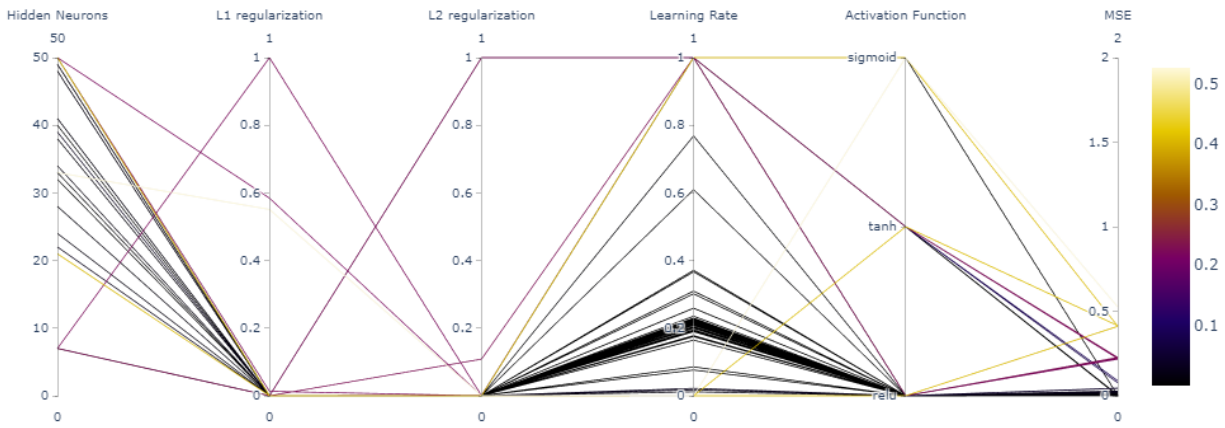

Figure G.5: Hyperparameter Tunning for ANN1.

The hyperparameter exploration has finished, revealing that the ideal configuration consists of a hidden densely-connected layer with 32 units, a learning rate of 0.1 for the optimizer, and relu as the activation function. Additionally, the regularization values are l1 = 1e-07 and l2 = 3.6573e-5, with an epsilon of 0.01.

Predicted vs. Observed

Figure G.6 depicts the comparison between the predicted values (from the best model, after the tunning) with the observed values (from phenomenological simulation).

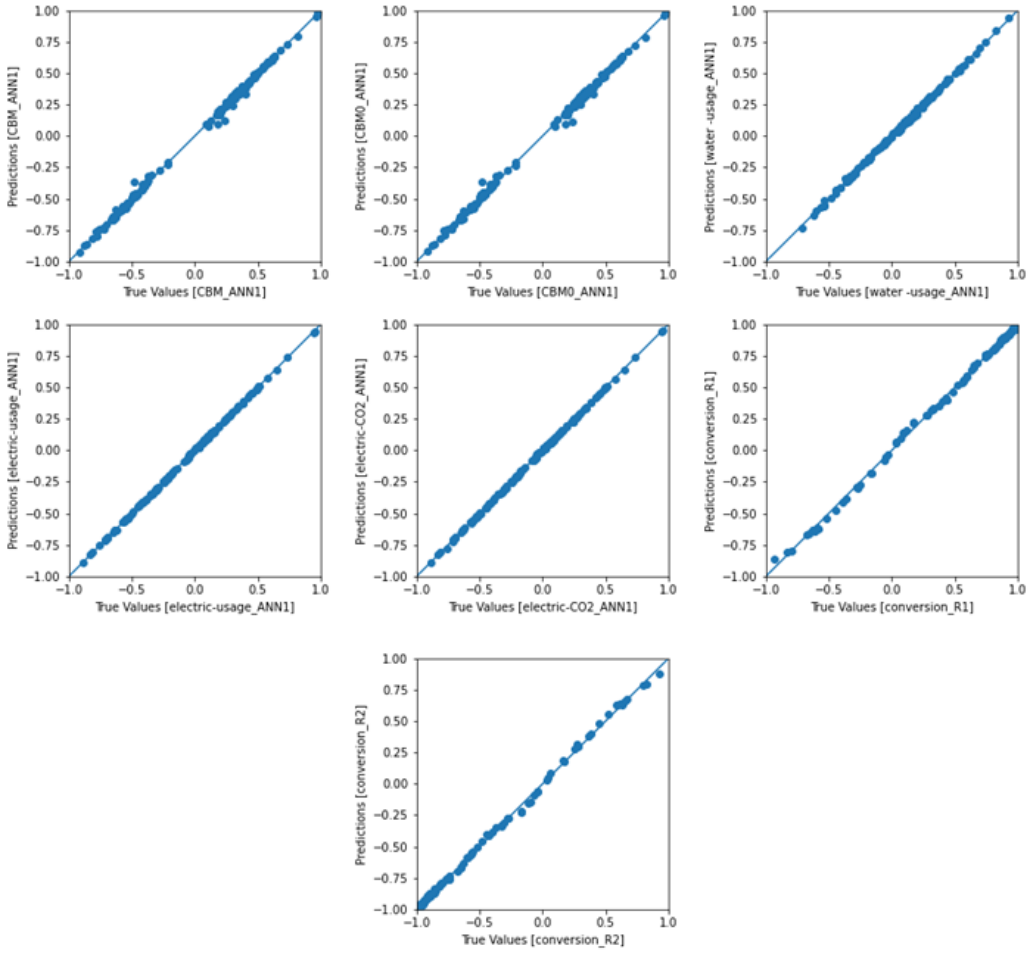

Figure G.6: Predicted Values vs. Observed Values for ANN1.

Base Case Comparison

Table G.2 compares phenomenological simulation with neural network results for the base case.

Table G.2: Comparison the Phenomenological Simulation with Neural Network Results for the Base Case.

Variables	Phenomenological Simulation	Neural Network
H2_412	1397.544062	1397.544062
CO2_412	1077.049209	1077.049209
CH4_412	3.289895384	3.289895384
T_412	20	20
ACETIC_504	0.625257141	0.625257141
SOLVENT_504	780.9928888	780.9928888
P_504	1.110316117	1.110316117
T_504	228.8005623	228.8005623
T_HT-03	90	90
T_RT	180	180
CBM_ANN1	14035977.88	13999945
CBM0_ANN1	13745911.51	13722542
water -usage_ANN1	4912361.718	4685660.5
electric-usage_ANN1	13631.03594	13652.48242
electric-CO2_ANN1	4728.648282	4740.450684
conversion_R1	0.819670146	0.818215668
conversion_R2	0.180279854	0.181538984

Appendix H

Detailed Information for the Neural Networks - Acetic Acid ANN2

Detailed process flowsheet

In this section the detailed process flowsheet is described. The Figure H.1 depicts the region of the process flowsheet from where the neural network will be constructed.

It contains a heater (HT-05), a valve (VL-01) and a flash drum (FL-01) as unit operations, one input stream (201) and two output streams (303 and 304).

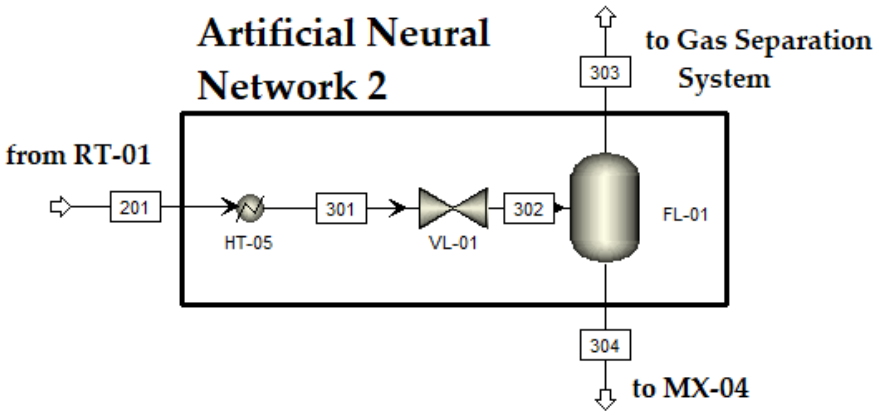

Figure H.1: Detailed process flowsheet for gas liquid split.

The considered variables are the flows of the input stream (for the following chemical compounds: hydrogen, carbon dioxide, acetic acid, water and methane), the temperature of the input stream, the temperature of the heat exchanger, the pressure in the valve, and temperature and pressure of the flash drum.

The collected output variables are the mole flows, pressure and temperature of stream 303, pressure and temperature of stream 304, total capital cost, utility usage (water and low pressure steam) and utility $CO_{2,equivalent}$ usage.

Neural Network Architecture

The Figure H.2 translates the gas-liquid split section of the acetic acid process (Figure H.1) into a neural network. There are 10 input variables and 29 output variables.

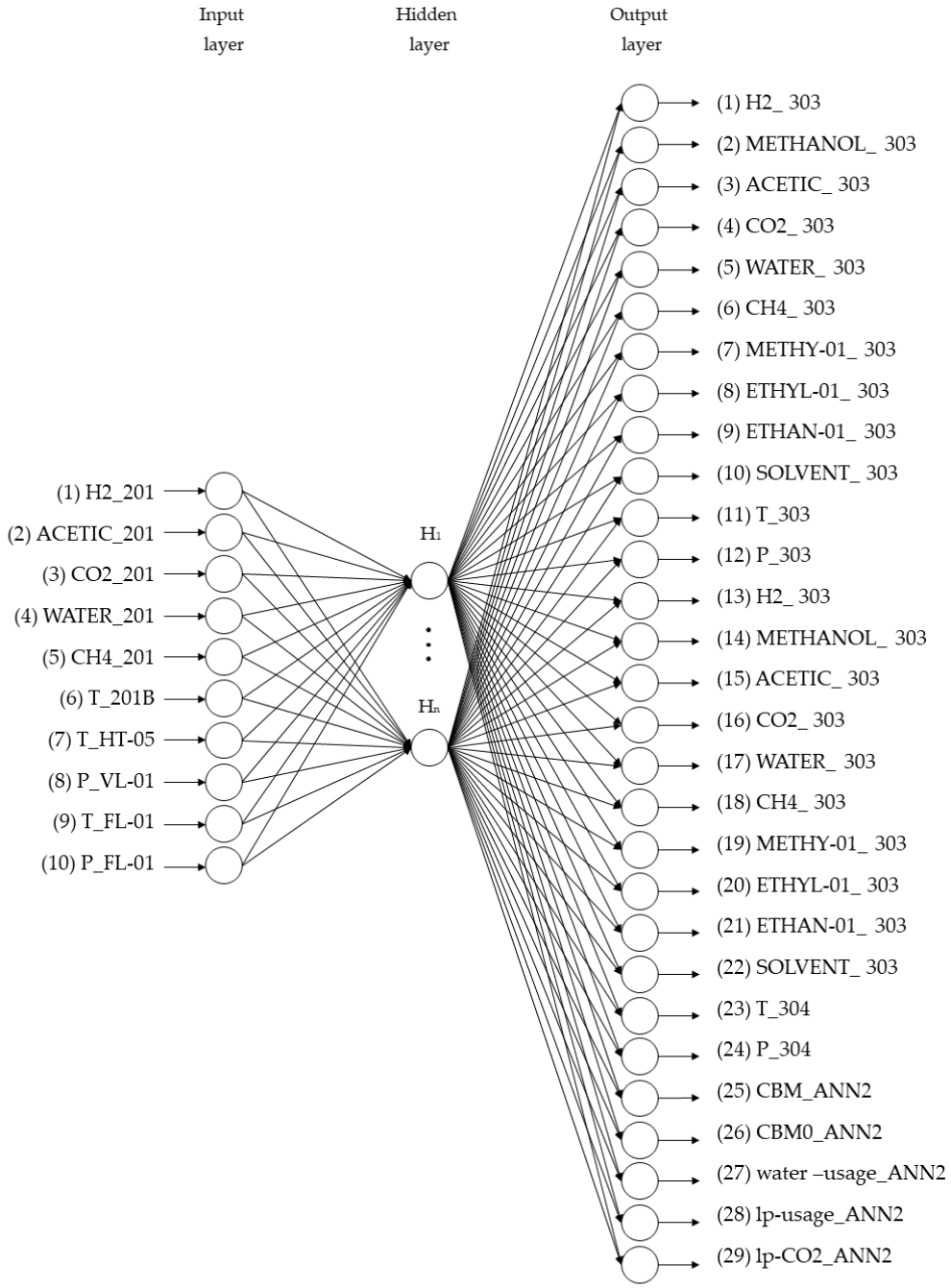

Figure H.2: Detailed architecture for acetic acid ANN2.

It is a feed forward neural network with only one hidden layer, the number of neurons is defined in the hyperparameter tuning.

Limits of the input variables

The Table H.1 presents the values used as upper and lower bonds for the data collection and neural network generation.

Table H.1: Input variable limits for the acetic acid ANN2.

Variable	Stream/ Unit	lower	upper	Unit
H2	201	1430	1560	kmol/h
ACETIC	201	330	425	kmol/h
CO2	201	1300	1430	kmol/h
WATER	201	380	460	kmol/h
CH4	201	55	140	kmol/h
T_201B	201	170	190	oC
T_HT-05	HT-05	60	120	oC
P_VL-01	VL-01	5	20	bar
T_FL-01	FL-01	30	60	oC
P_FL-01	FL-01	0,25	1	percentage

The Figure H.3 presents the distribution of the input parameters using the Latin hipercube sampling method.

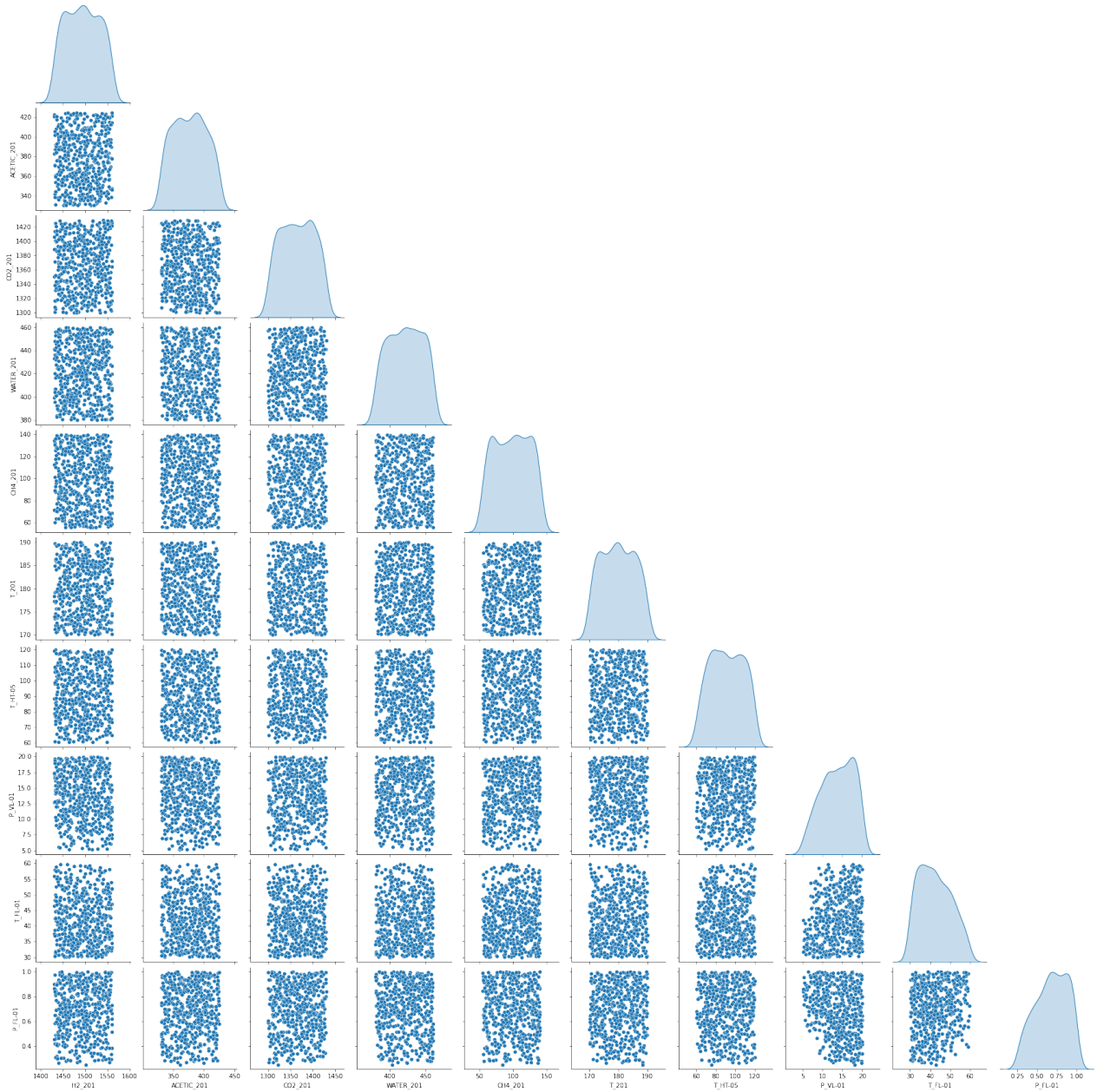

Figure H.3: Input variable distribution for the acetic acid ANN2.

It is possible to verify that the distribution is uniform in each variable assessed.

The Figure H.4 presents the distribution of the output variables.

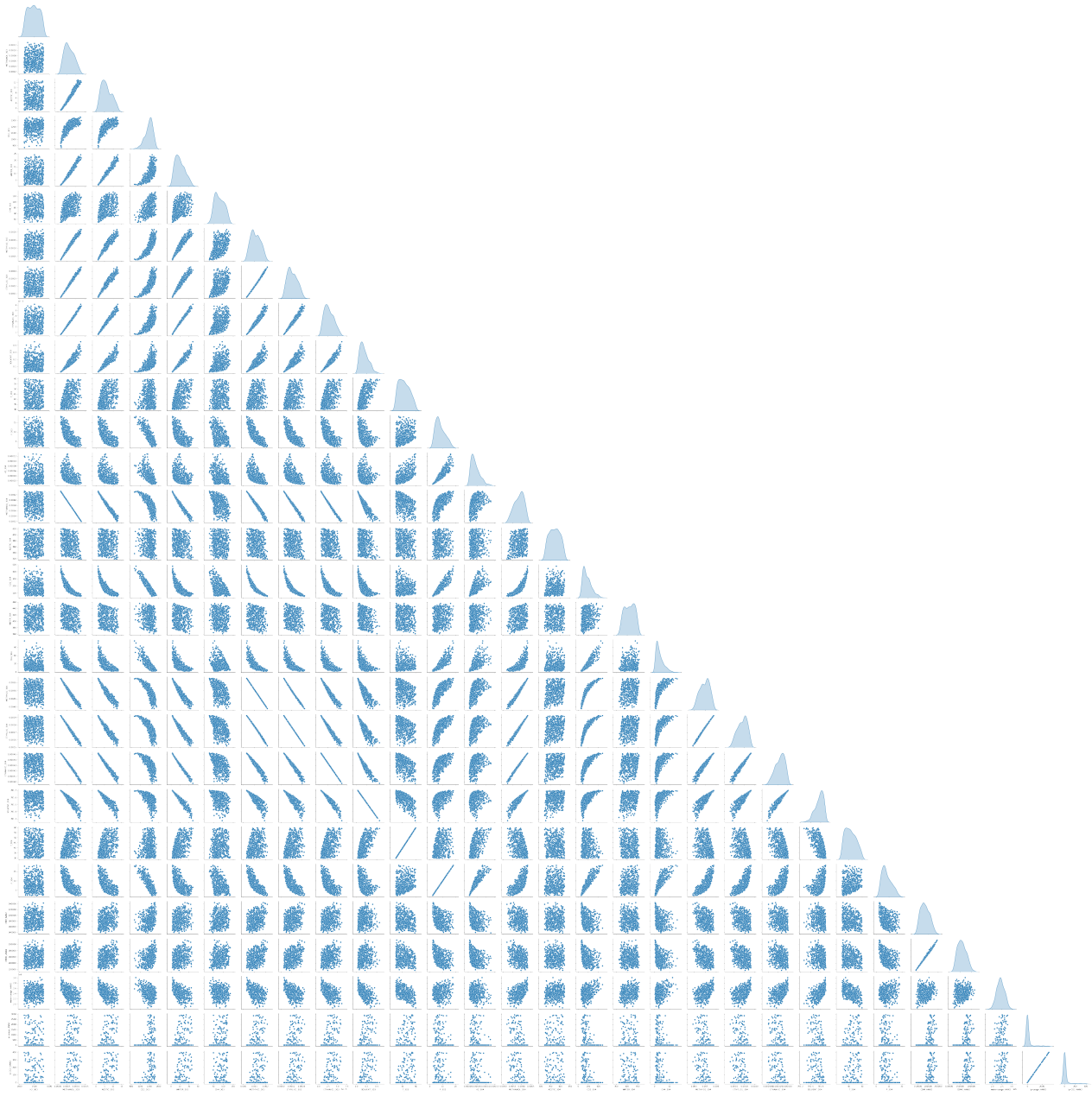

Figure H.4: Output variable distribution.

Hyperparameter Tuning

The Figure H.5 presents hyperparameter tunning for the Artificial Neural Network 2.

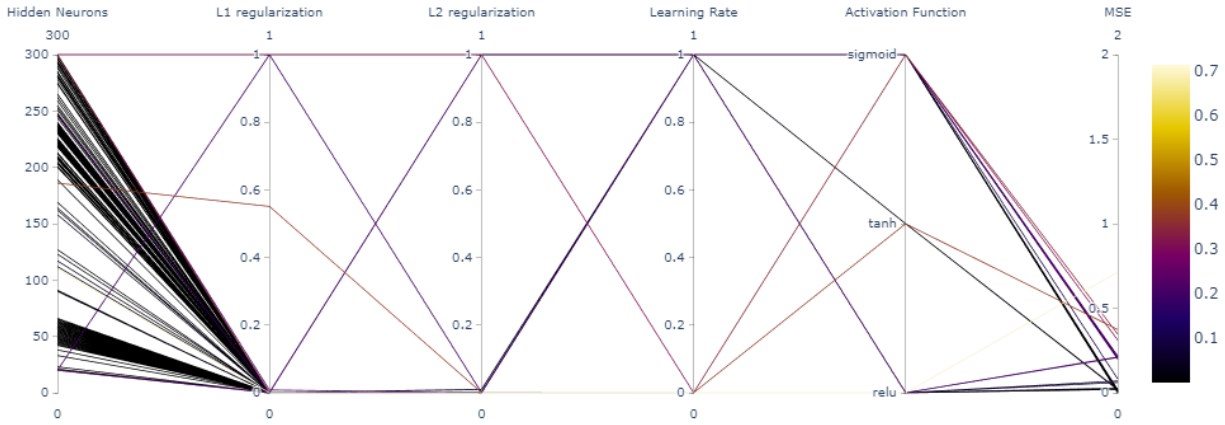

Figure H.5: Hyperparameter Tunning for ANN2.

The hyperparameter exploration has finished, revealing that the ideal configuration consists of a hidden densely-connected layer with 47 units, a learning rate of 1.0 for the optimizer adam, and relu as the activation function. Additionally, the regularization values are l1 = 4.4937432101e-05 and l2 = 1.573098799380131e-08, with an mse of 0.000866918824613.

Predicted vs. Observed

Figure H.6 and Figure H.7 depicts the comparison between the predicted values (from the best model, after the tunning) with the observed values (from phenomenological simulation).

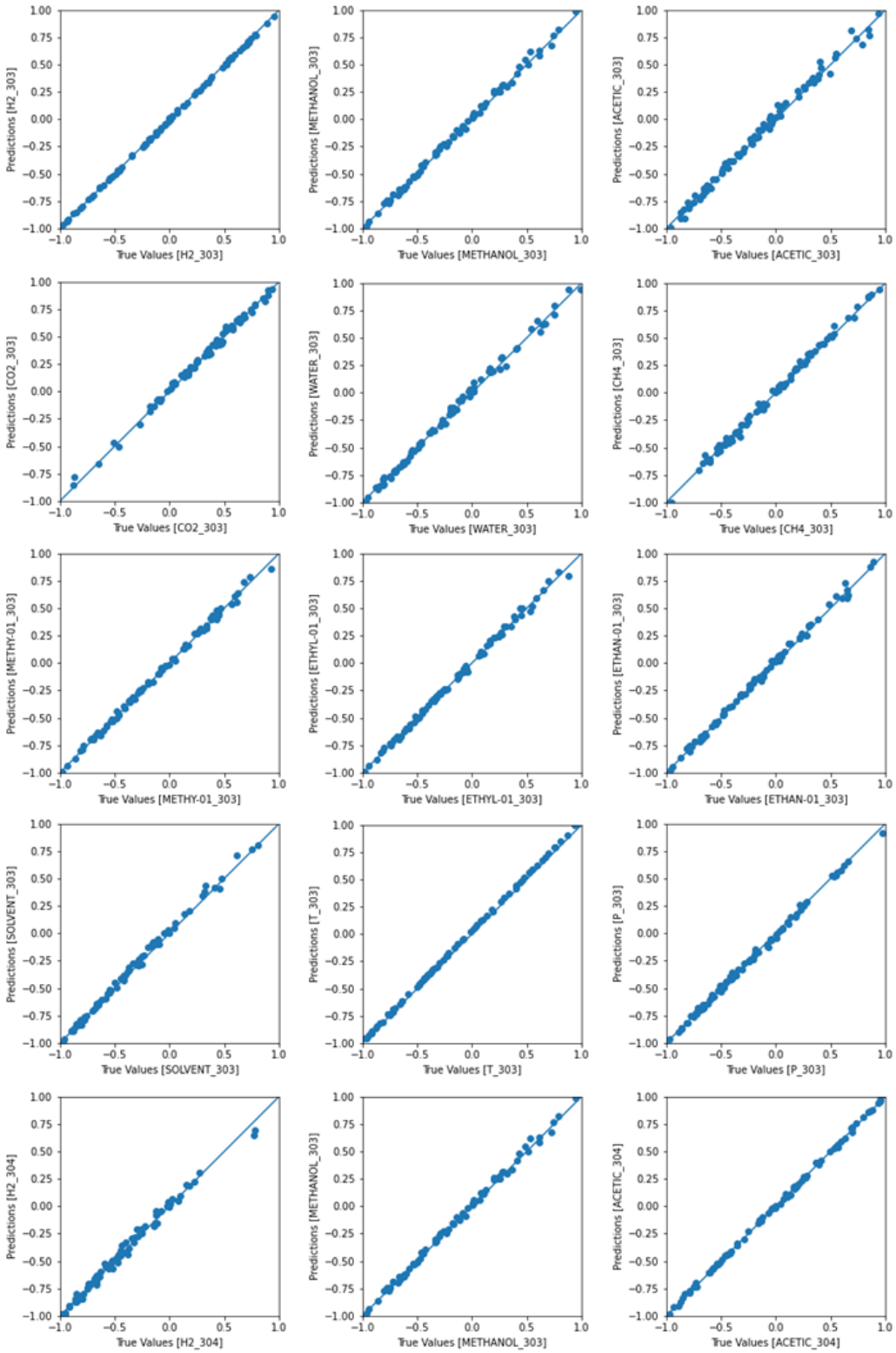

Figure H.6: Predicted Values vs. Observed Values for ANN2.

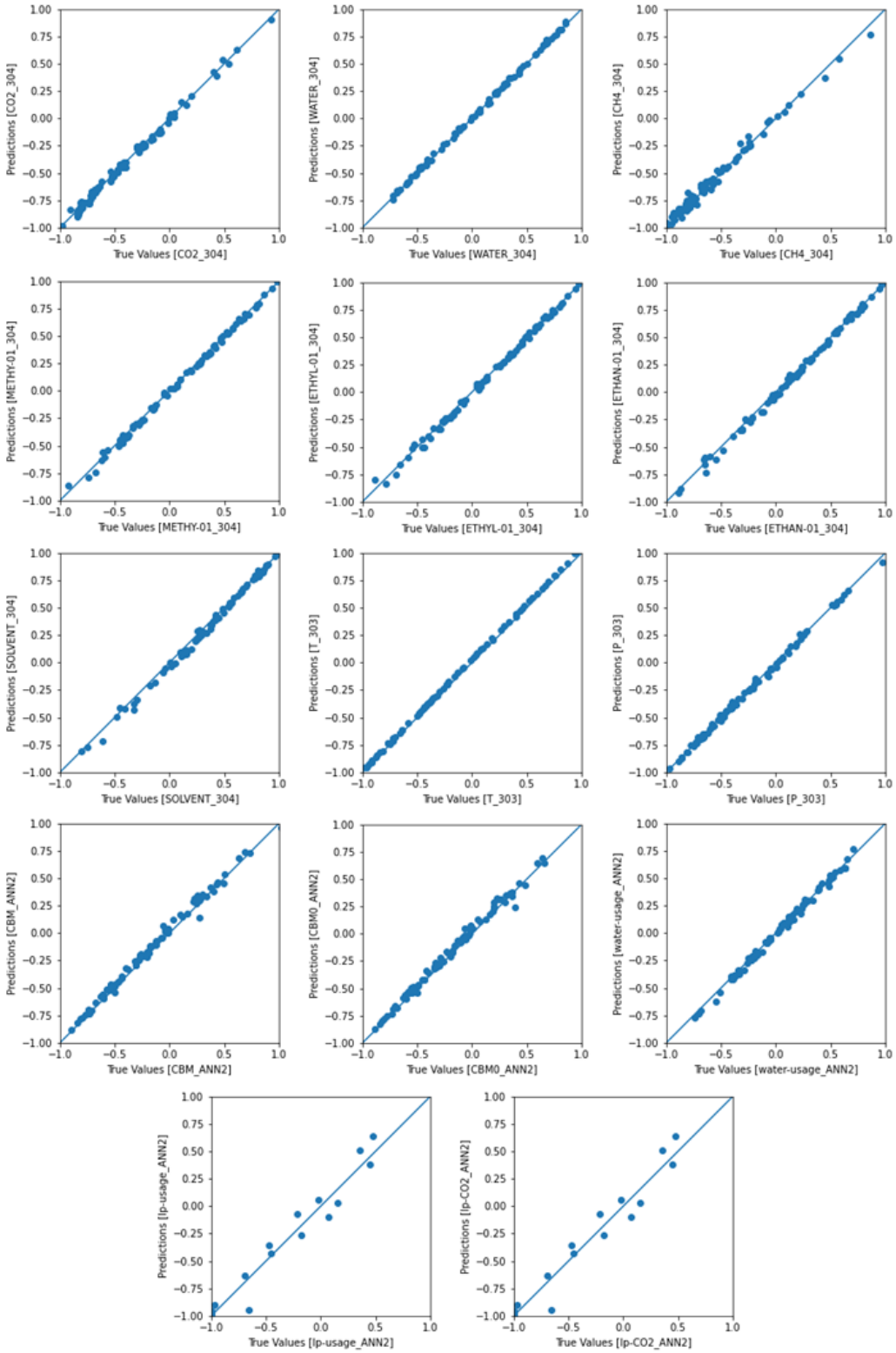

Figure H.7: Predicted Values vs. Observed Values for ANN2.

Base Case Comparison

Table H.2 compares phenomenological simulation with neural network results for the base case.

Table H.2: Comparison the Phenomenological Simulation with Neural Network Results for the Base Case.

Variables	Phenomenological Simulation	Neural Network
H2_201	1441.769507	1441.769507
ACETIC_201	418.1641359	418.1641359
CO2_201	1309.894407	1309.894407
WATER_201	448.1578517	448.1578517
CH4_201	64.50962684	64.50962684
T_201	180	180
T_HT-05	70	70
P_VL-01	5	5
T_FL-01	38	38
P_FL-01	0.83451	0.83451
H2_303	1441.76949	1439.817261
METHANOL_303	0.000953446	0.00092953
ACETIC_303	10.6804583	9.947603226
CO2_303	1231.56207	1234.075928
WATER_303	16.8412244	15.84536839
CH4_303	61.3020035	61.57397461
METHY-01_303	0.001728819	0.001695596
ETHYL-01_303	0.000353742	0.000344966
ETHAN-01_303	4.13431E-05	4.01281E-05
SOLVENT_303	0.204986894	0.197103575
T_303	38	38.367733
P_303	3.17255	3.081218243
H2_304	1.22215E-05	1.3784E-05
METHANOL_304	0.005541053	0.005564956
ACETIC_304	407.483678	409.4006042
CO2_304	78.3323379	77.84811401
WATER_304	431.316627	433.7226563
CH4_304	3.20762338	2.835086346
METHY-01_304	0.004332714	0.004365999
ETHYL-01_304	0.001624321	0.001633096
ETHAN-01_304	0.000417092	0.000418307
SOLVENT_304	781.520013	781.5278931
T_304	38	38.36842346
P_304	3.17255	3.080977917
CBM_ANN2	230970.4081	232663.4219
CBM0_ANN2	200023.7969	201206.0156
water-usage_ANN2	2426919.9	2406522.5
lp-usage_ANN2	439.797741	203.548111
lp-CO2_ANN2	60.1742717	27.87847137

Appendix I

Detailed Information for the Neural Networks - Acetic Acid ANN3

Detailed process flowsheet

In this section the detailed process flowsheet is described. The Figure I.1 depicts the region of the process flowsheet from where the neural network will be constructed.

It contains only a mixer (MX-04), two input stream (304 and 407) and one output streams (501).

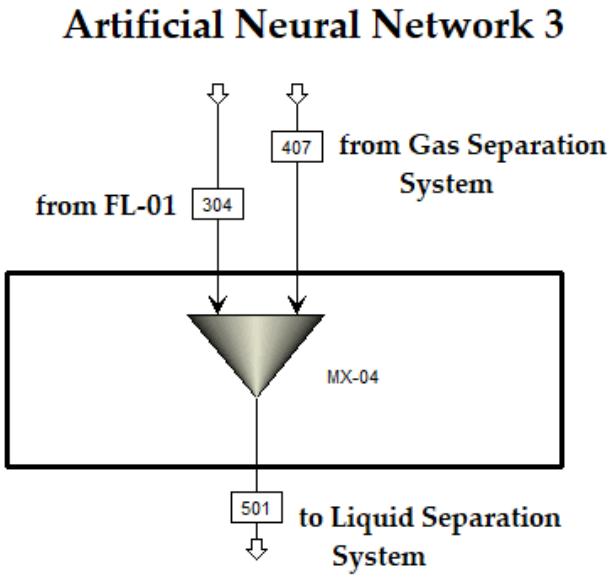

Figure I.1: Detailed process flowsheet for mixer.

The considered variables are the flows of the input stream with temperature and pressure.

The collected output variables are the mole flows, pressure and temperature of stream 501.

Neural Network Architecture

The Figure I.2 translates the mizing of streams section of the acetic acid process into a neural network. There are 24 input variables and 12 output variables.

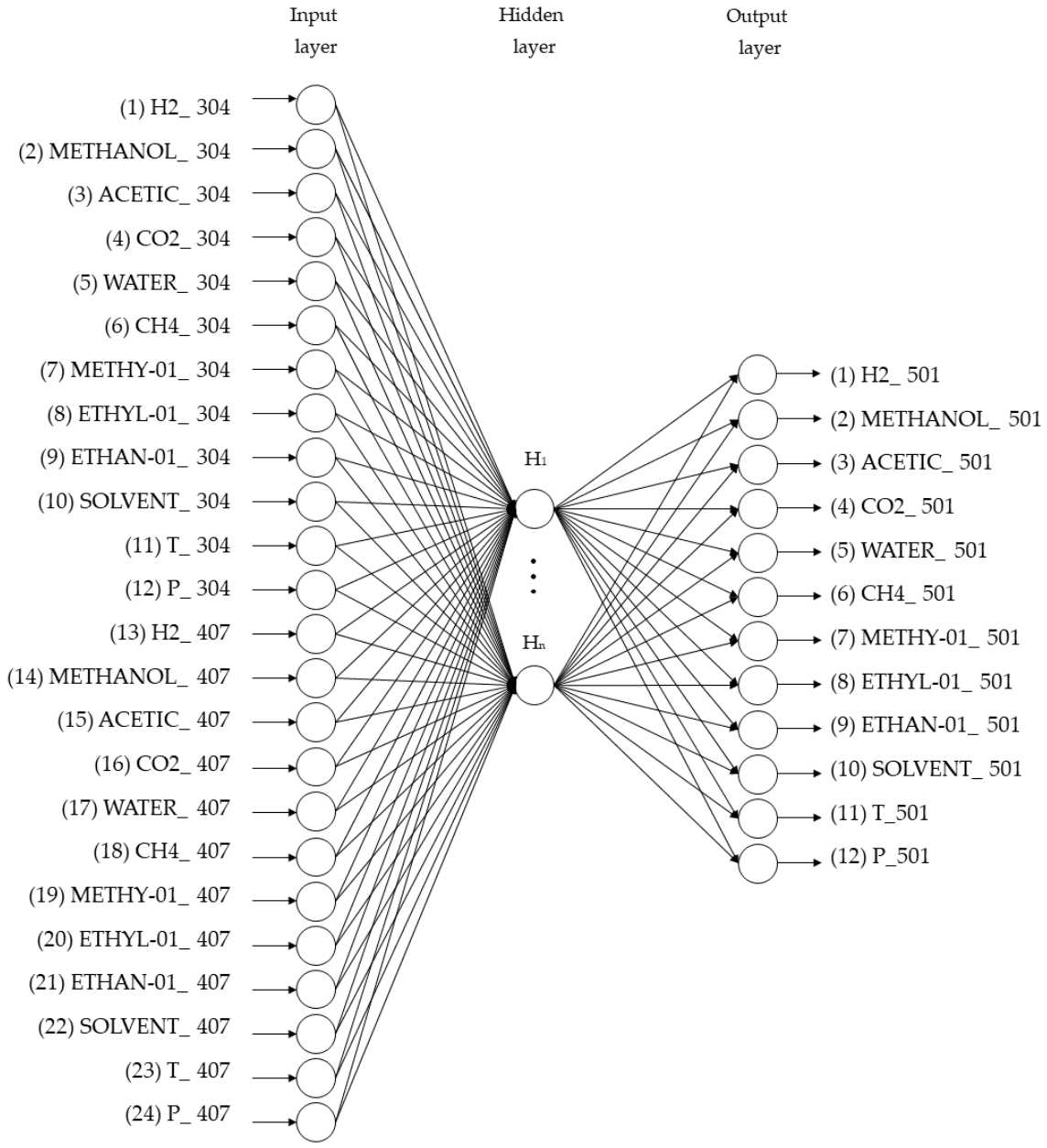

Figure I.2: Detailed architecture for acetic acid ANN3.

It is a feed forward neural network with only one hidden layer, the number of neurons is defined in the hyperparameter tuning.

Limits of the input variables

The Table I.1 presents the values used as upper and lower bonds for the data collection and neural network generation.

Table I.1: Limits of input variables for acetic acid ANN3.

Variable	Stream/Unit	lower	upper	Unit
H2	304	3.00E-06	0.0001	kmol/h
METHANOL	304	0.002	0.0065	kmol/h
ACETIC	304	300.00	418.00	kmol/h
CO2	304	10.00	280.00	kmol/h
WATER	304	290.00	460.00	kmol/h
CH4	304	0.3	35.00	kmol/h
METHY-01	304	0.001	0.0058	kmol/h
ETHYL-01	304	0.0006	0.002	kmol/h
ETHAN-01	304	0.0002	0.0005	kmol/h
SOLVENT	304	777.00	781.7	kmol/h
T	304	30.00	60.00	oC
P	304	0.7	15.00	bar
H2	407	1.00E-06	3.00E-06	kmol/h
METHANOL	407	0.001	0.003	kmol/h
ACETIC	407	8.00	20.00	kmol/h
CO2	407	20.00	40.00	kmol/h
WATER	407	10.00	25.00	kmol/h
CH4	407	2.00	15.00	kmol/h
METHY-01	407	0.001	0.0058	kmol/h
ETHYL-01	407	0.0006	0.002	kmol/h
ETHAN-01	407	0.0001	0.0004	kmol/h
SOLVENT	407	0.1	0.5	kmol/h
T	407	15.00	30.00	oC
P	407	5.00	30.00	bar

The Figure I.3 presents the distribution of the input parameters using the Latin hipercube sampling method.

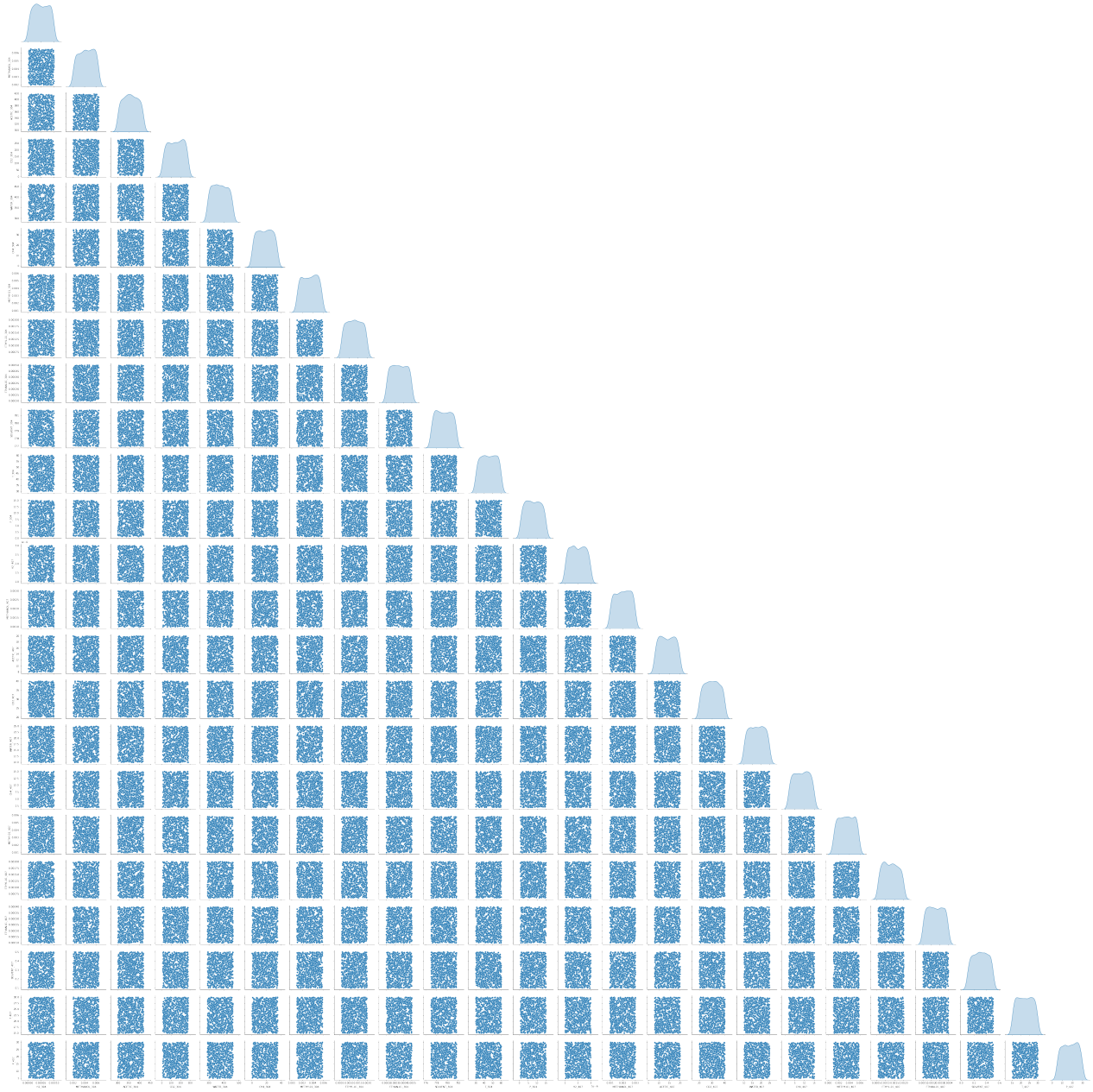

Figure I.3: Distribution of inputs for acetic acid ANN3.

It is possible to verify that the distribution is uniform in each variable assessed.

The Figure I.4 depicts the distribution of the inputs.

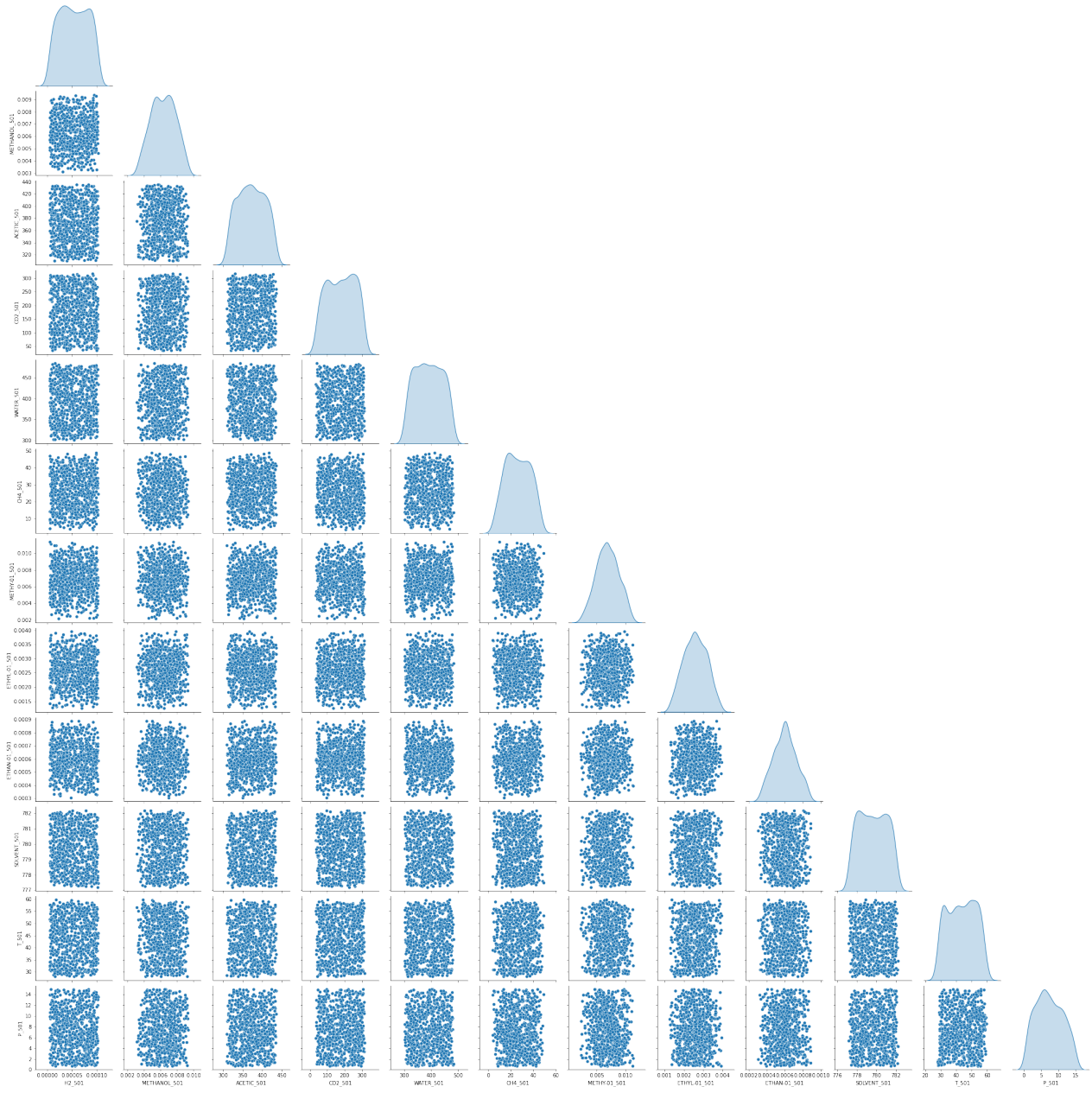

Figure I.4: Distribution of output for acetic acid ANN3.

Hyperparameter Tuning

The Figure I.5 presents hyperparameter tunning for the Artificial Neural Network 3.

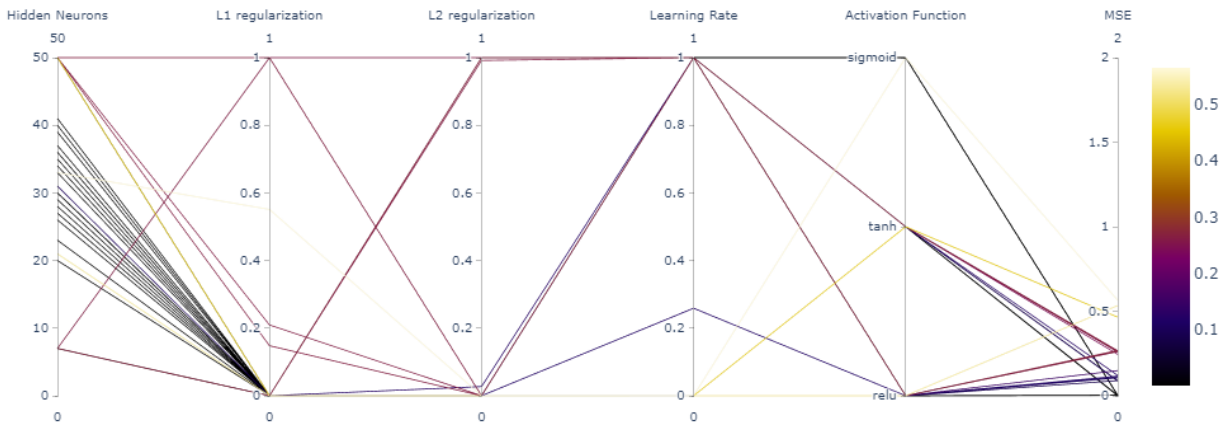

Figure I.5: Hyperparameter Tunning for ANN3.

The hyperparameter exploration has finished, revealing that the ideal configuration consists of a hidden densely-connected layer with 27 units, a learning rate of 1.0 for the optimizer adam, and relu as the activation function. Additionally, the regularization values are l1 = 2.3429131032e-06 and l2 = 1e-08, with an mse of 0.000222015165491.

Predicted vs. Observed

Figure I.6 depicts the comparison between the predicted values (from the best model, after the tunning) with the observed values (from phenomenological simulation).

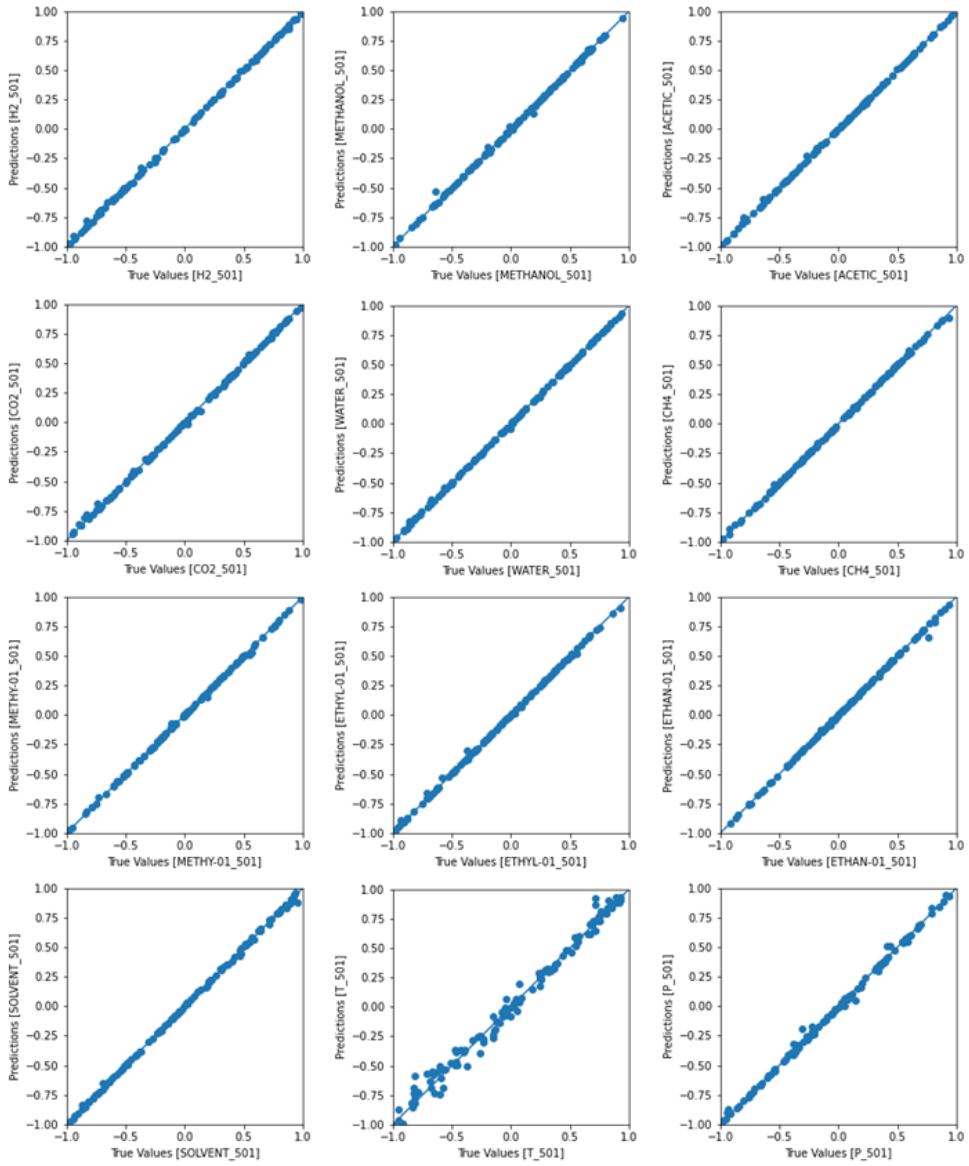

Figure I.6: Predicted Values vs. Observed Values for ANN3.

Base Case Comparison

Table I.2 compares phenomenological simulation with neural network results for the base case.

Table I.2: Comparison the Phenomenological Simulation with Neural Network Results for the Base Case.

Variables	Phenomenological Simulation	Neural Network
H2_304	1.22215E-05	1.22215E-05
METHANOL_304	0.005541053	0.005541053
ACETIC_304	407.4836823	407.4836823
CO2_304	78.33235798	78.33235798
WATER_304	431.316634	431.316634
CH4_304	3.207625162	3.207625162
METHY-01_304	0.004398659	0.004398659
ETHYL-01_304	0.001624321	0.001624321
ETHAN-01_304	0.000417092	0.000417092
SOLVENT_304	781.5205867	781.5205867
T_304	38	38
P_304	3.17255	3.17255
H2_407	1.25817E-06	1.25817E-06
METHANOL_407	0.001488769	0.001488769
ACETIC_407	10.13028894	10.13028894
CO2_407	32.76892445	32.76892445
WATER_407	17.07701118	17.07701118
CH4_407	7.873478421	7.873478421
METHY-01_407	0.002469235	0.002469235
ETHYL-01_407	0.0009044	0.0009044
ETHAN-01_407	0.00011227	0.00011227
SOLVENT_407	0.204854353	0.204854353
T_407	20	20
P_407	25	25
H2_501	1.34797E-05	1.3558E-05
METHANOL_501	0.007029822	0.00703337
ACETIC_501	417.613971	417.5280762
CO2_501	111.101282	111.6036224
WATER_501	448.393645	448.4588623
CH4_501	11.0811036	11.11147308
METHY-01_501	0.006867894	0.006863201
ETHYL-01_501	0.002528721	0.002523979
ETHAN-01_501	0.000529362	0.000529013
SOLVENT_501	781.725441	781.7136841
T_501	36.3883558	36.13733673
P_501	3.17255	3.134570122

Appendix J

Detailed Information for the Neural Networks - Acetic Acid ANN4a

Detailed process flowsheet

In this section the detailed process flowsheet is described. The Figure J.1 depicts the region of the process flowsheet from where the neural network will be constructed.

It contains a heat exchanger (HT-09), one input stream (501), one column (CL-01) and two output streams (503 and 504).

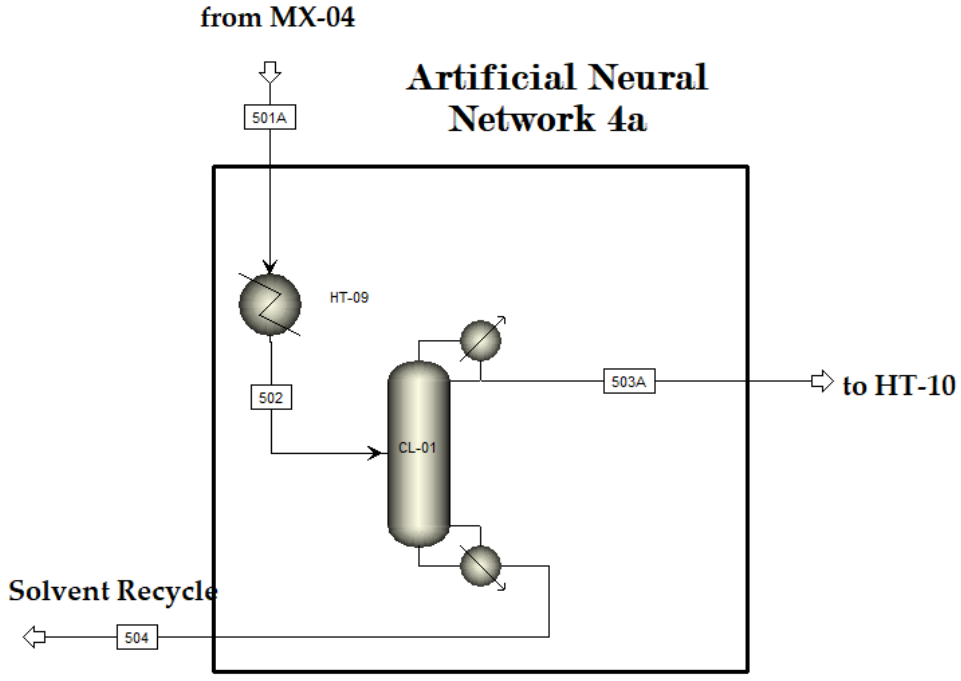

Figure J.1: Detailed process flowsheet for Liquid Separation System - CL-01.

The considered variables are the flows of the input stream with temperature and pressure, the temperature of the heat exchanger, the reflux ratio, the distilate to feed and feed stage.

The collected output variables are the mole flows, pressure and temperature of stream 503 and 504, the utilities, total capital cost and $CO_{2,eq}$.

Neural Network Architecture

The Figure J.2 translates the mizing of streams section of the acetic acid process into a neural network. There are 16 input variables and 11 output variables.

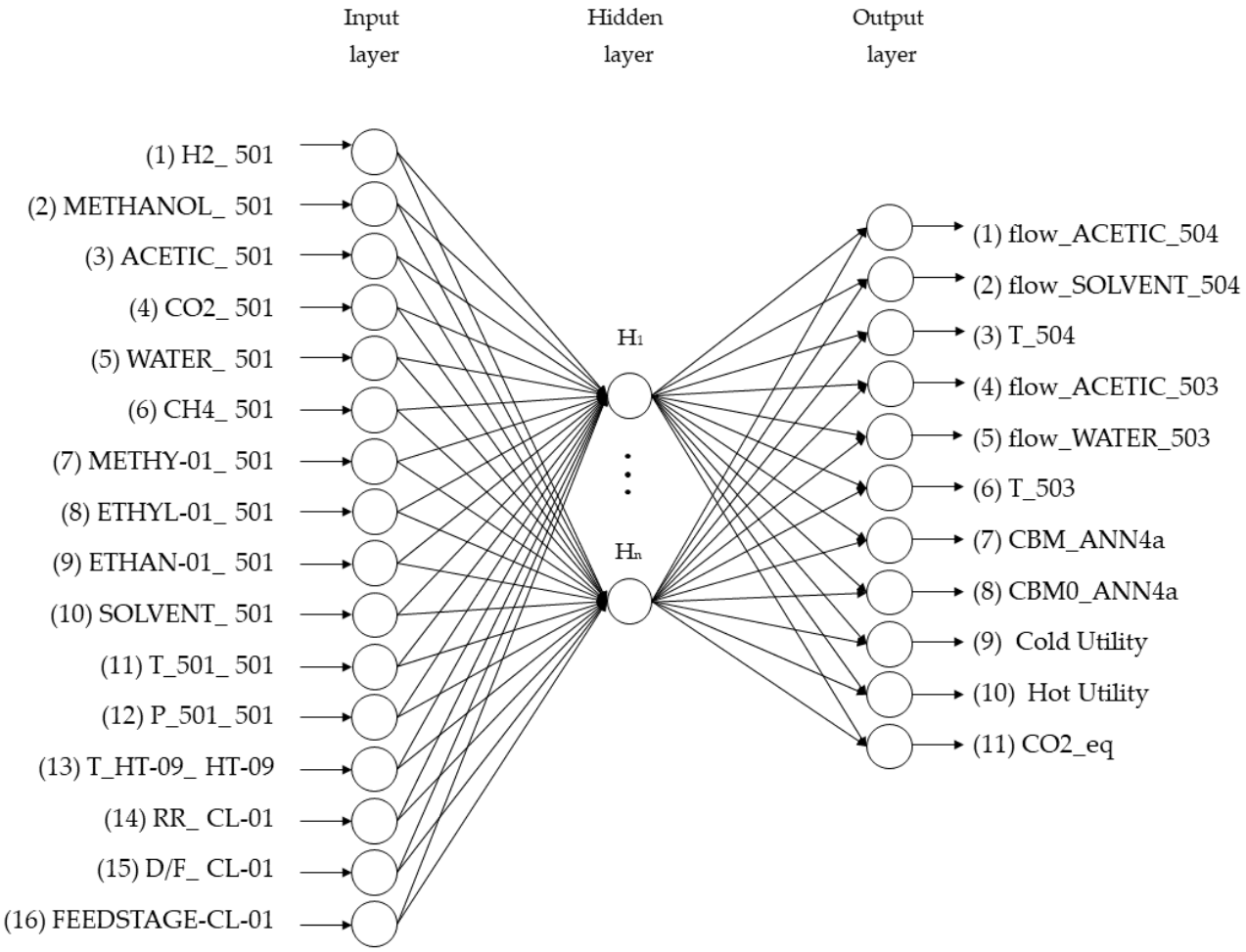

Figure J.2: Detailed architecture for acetic acid ANN4a.

It is a feed forward neural network with only one hidden layer, the number of neurons is defined in the hyperparameter tuning.

Limits of the input variables

The Table J.1 presents the values used as upper and lower bonds for the data collection and neural network generation.

Table J.1: Limits of input variables for acetic acid ANN4a.

Variable	Stream/Unit	lower	upper	Unit
H2	501	6.7E-06	9.8E-05	kmol/h
METHANOL	501	3.0E-03	1.0E-02	kmol/h
ACETIC	501	400	430	kmol/h
CO2	501	70	308	kmol/h
WATER	501	350	480	kmol/h
CH4	501	3.5	48	kmol/h
METHY-01	501	2.1E-03	9.9E-03	kmol/h
ETHYL-01	501	1.1E-03	3.9E-03	kmol/h
ETHAN-01	501	3.0E-04	9.0E-04	kmol/h
SOLVENT	501	775.32	782.11	kmol/h
T_501	501	28.83	54.56	oC
P_501	501	1.1	3.96	bar
T_HT-09	HT-09	35	50	oC
RR	CL-01	0.03	3.00	
D/F	CL-01	0.43	0.56	
FEEDSTAGE	CL-01	0.38	0.8	

The Figure J.3 presents the distribution of the input parameters using the Latin hipercube sampling method.

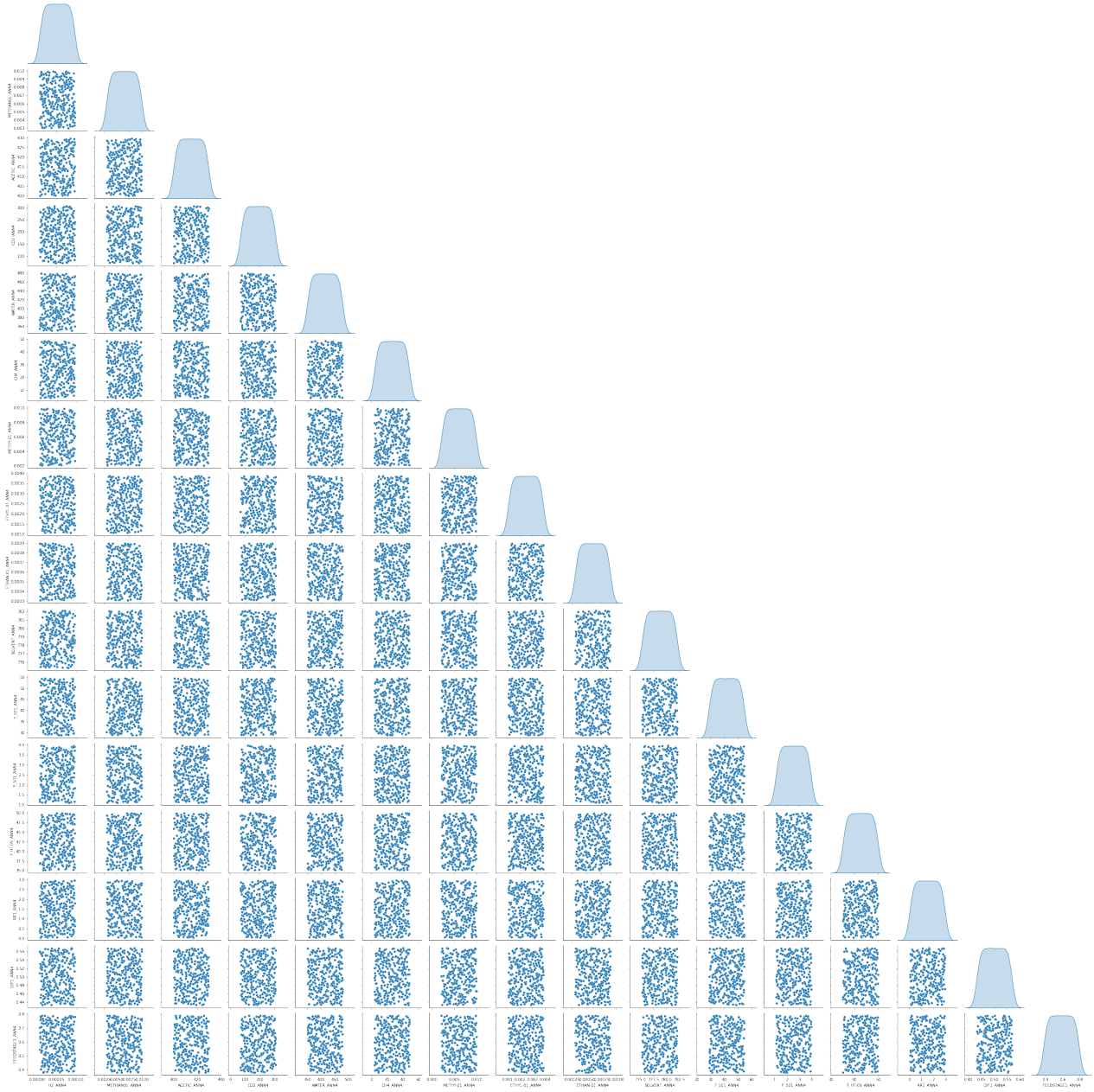

Figure J.3: Distribution of inputs for acetic acid ANN4a.

It is possible to verify that the distribution is uniform in each variable assessed.

The Figure J.4 depicts the distribution of the inputs.

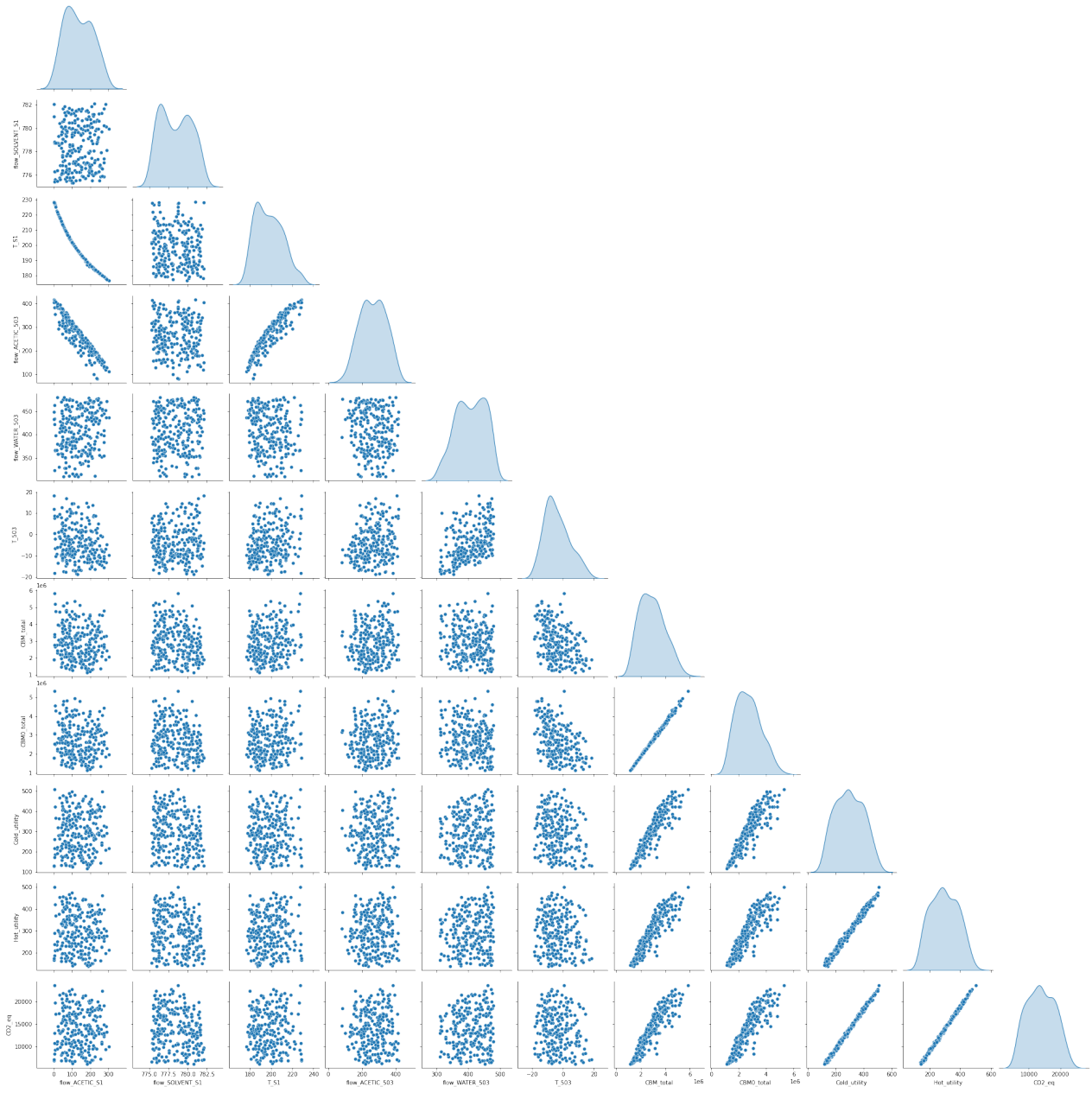

Figure J.4: Distribution of output for acetic acid ANN4a.

Hyperparameter Tuning

The Figure J.5 presents hyperparameter tunning for the Artificial Neural Network 4a.

Figure J.5: Hyperparameter Tunning for ANN4a.

The hyperparameter exploration has finished, revealing that the ideal configuration consists of a hidden densely-connected layer with 15 units, a learning rate of 0.0129137565760207 for the optimizer adam, and relu as the activation function. Additionally, the regularization values are l1 = 5.6750051062e-06 and l2 = 2.3167246344713836e-08, with an mse of 0.0051949534099549.

Predicted vs. Observed

Figure J.6 depicts the comparison between the predicted values (from the best model, after the tunning) with the observed values (from phenomenological simulation).

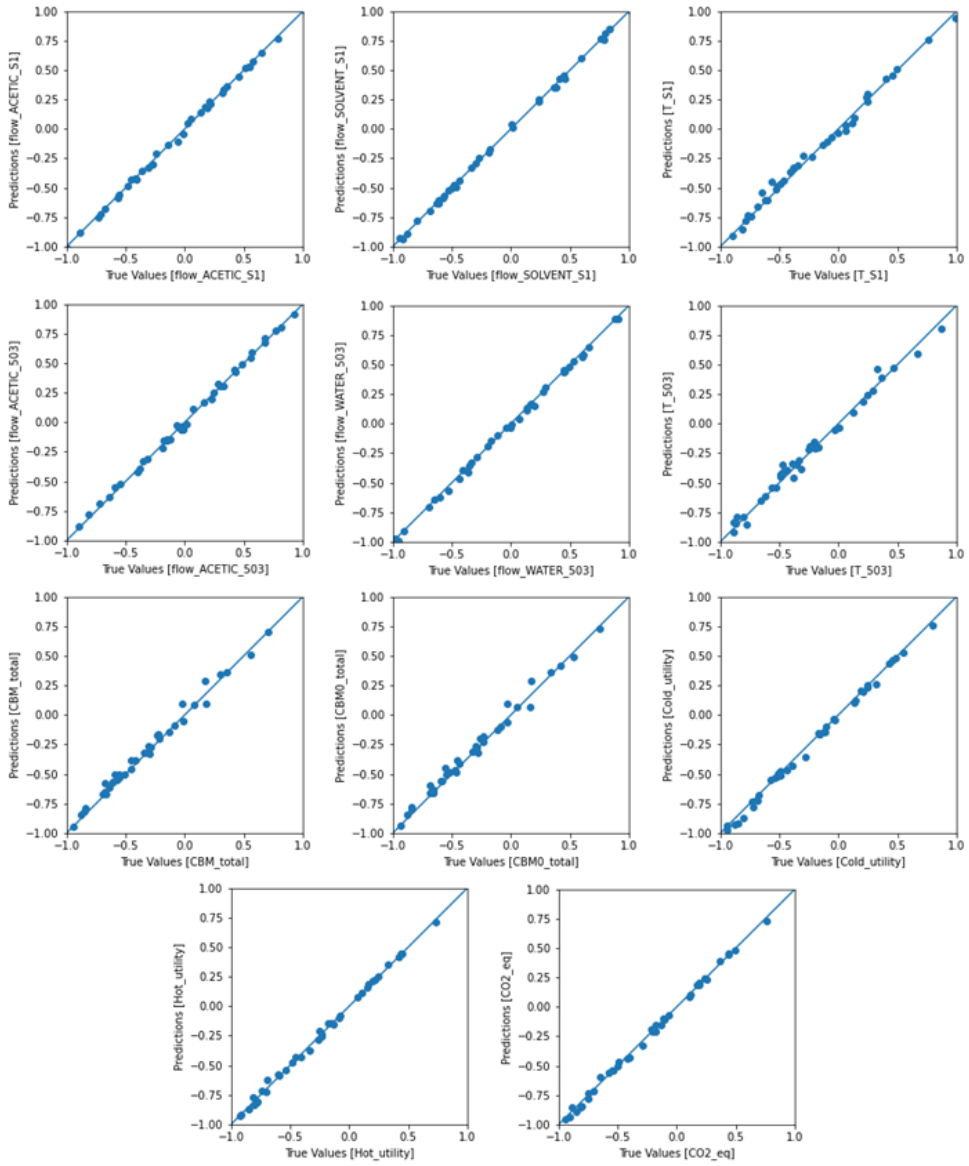

Figure J.6: Predicted Values vs. Observed Values for ANN4a.

Base Case Comparison

Table J.2 compares phenomenological simulation with neural network results for the base case.

Table J.2: Comparison the Phenomenological Simulation with Neural Network Results for the Base Case.

Variables	Phenomenological Simulation	Neural Network
H2_ANN4	0.0000135	0.0000135
METHANOL_ANN4	0.007029822	0.007029822
ACETIC_ANN4	417.6139712	417.6139712
CO2_ANN4	111.1012824	111.1012824
WATER_ANN4	448.3936452	448.3936452
CH4_ANN4	11.08110358	11.08110358
METHY-01_ANN4	0.006867894	0.006867894
ETHYL-01_ANN4	0.002528721	0.002528721
ETHAN-01_ANN4	0.000529362	0.000529362
SOLVENT_ANN4	781.725441	781.725441
T_501_ANN4	36.38835597	36.38835597
P_501_ANN4	3.17255	3.17255
T_HT-09_ANN4	38	38
RR1_ANN4	0.091854716	0.091854716
D/F1_ANN4	0.558390927	0.558390927
FEEDSTAGE1_ANN4	0.411764706	0.411764706
flow_ACETIC_S1	0.625257183	0.751201153
flow_SOLVENT_S1	780.992917	781.7676392
T_S1	228.800562	227.6748962
flow_ACETIC_503	416.988714	416.0863037
flow_WATER_503	448.393608	448.0773926
T_503	12.0736217	11.22586727
CBM_total	1915561.985	2177807.5
CBM0_total	1792995.501	2002897.125
Cold_utility	126.7732076	137.1387177
Hot_utility	166.3901831	177.0614014
CO2_eq	6966.993473	7508.929199

Appendix K

Detailed Information for the Neural Networks - Acetic Acid ANN4b

Detailed process flowsheet

In this section the detailed process flowsheet is described. The Figure K.1 depicts the region of the process flowsheet from where the neural network will be constructed.

It contains a heat exchanger (HT-10), one input stream (503), two columnd (CL-02 ans CL-03) and three output streams (506, 508 and 509).

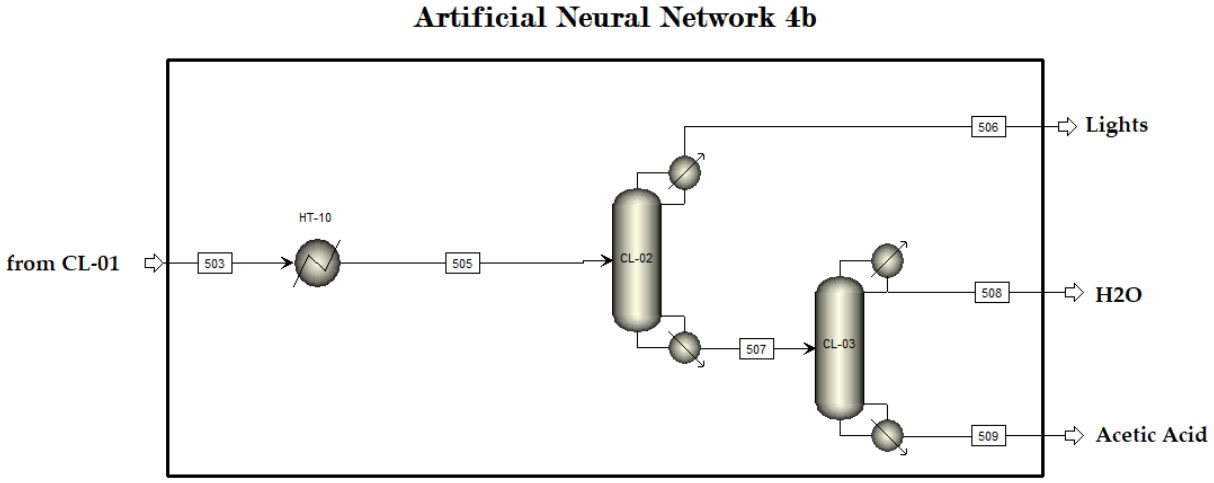

Figure K.1: Detailed process flowsheet for Liquid Separation System - CL-01.

The considered variables are the flows of the input stream with temperature and pressure, the temperature of the heat exchanger, the reflux ratio, the distilate to feed and feed stage.

The collected output variables are the mole flows, and purity of stream 508 and 509, the utilities, total capital cost and $CO_{2,eq}$.

Neural Network Architecture

The Figure K.2 translates a part of the liquid separation system section of the acetic acid process into a neural network. There are 18 input variables and 8 output variables.

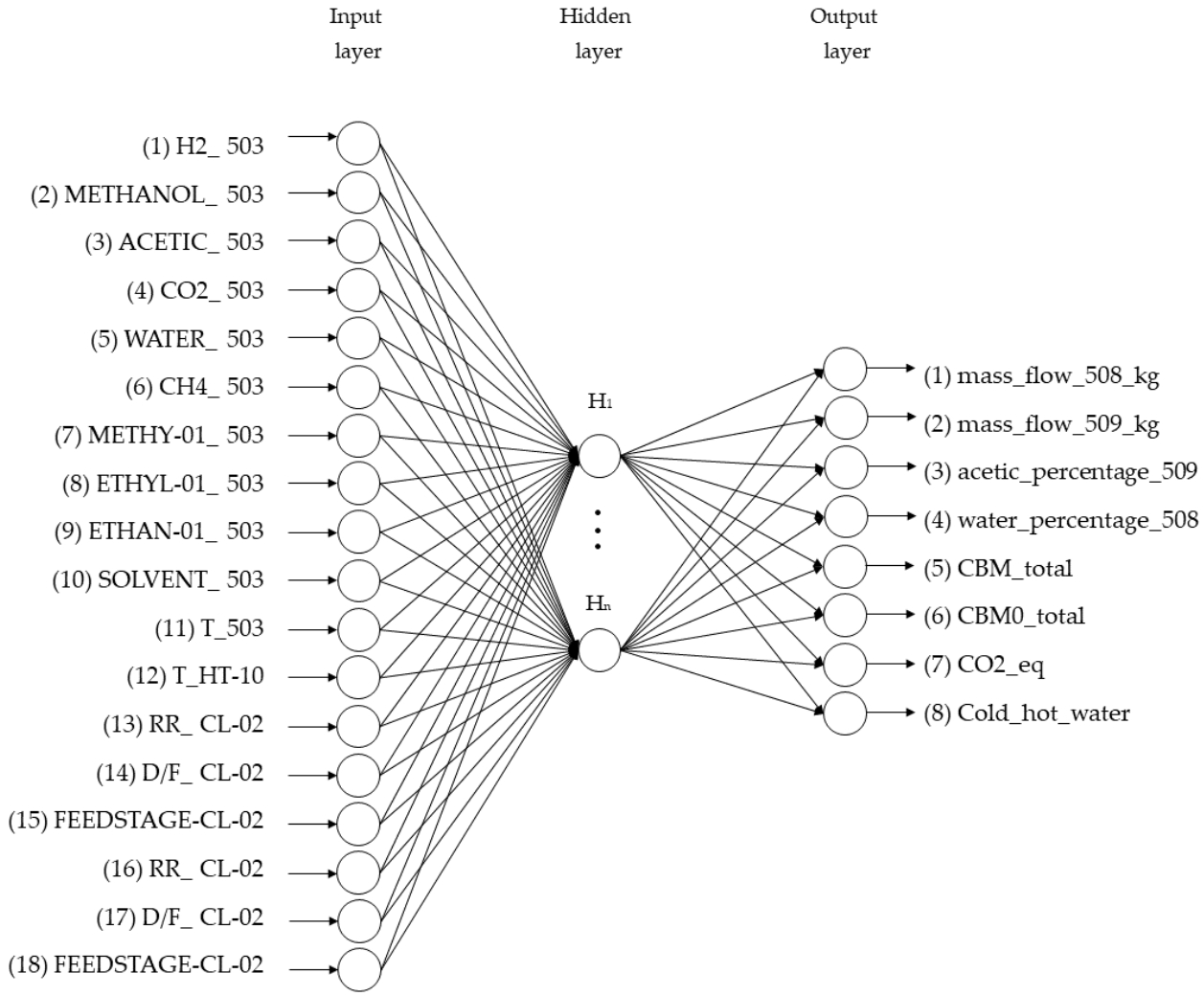

Figure K.2: Detailed architecture for acetic acid ANN4b.

It is a feed forward neural network with only one hidden layer, the number of neurons is defined in the hyperparameter tuning.

Limits of the input variables

The Table K.1 presents the values used as upper and lower bonds for the data collection and neural network generation.

Table K.1: Limits of input variables for acetic acid ANN4b.

Variable	Stream/Unit	lower	upper	Unit
H2	503	7.22E-06	9.74E-05	kmol/h
METHANOL	503	0.003057	0.009951	kmol/h
ACETIC	503	385	439.5135	kmol/h
CO2	503	70.89092	305.0215	kmol/h
WATER	503	311.5689	478.8353	kmol/h
CH4	503	3.651608	48.57961	kmol/h
METHY-01	503	0.002074	0.009892	kmol/h
ETHYL-01	503	0.001068	0.003866	kmol/h
ETHAN-01	503	0.000309	0.000887	kmol/h
SOLVENT	503	0.001114	0.734	kmol/h
T_503	503	-18.5038	18.00174	oC
T_HT-10	HT-10	35	50	oC
RR	CL-02	0.66	5	–
D/F	CL-02	0.1	0.2	–
FEEDSTAGE	CL-02	0.4	0.75	–
RR	CL-03	3	15	–
D/F	CL-03	0.2	0.67	–
FEEDSTAGE	CL-03	0.4	0.8	–

The Figure K.3 presents the distribution of the input parameters using the Latin hipercube sampling method.

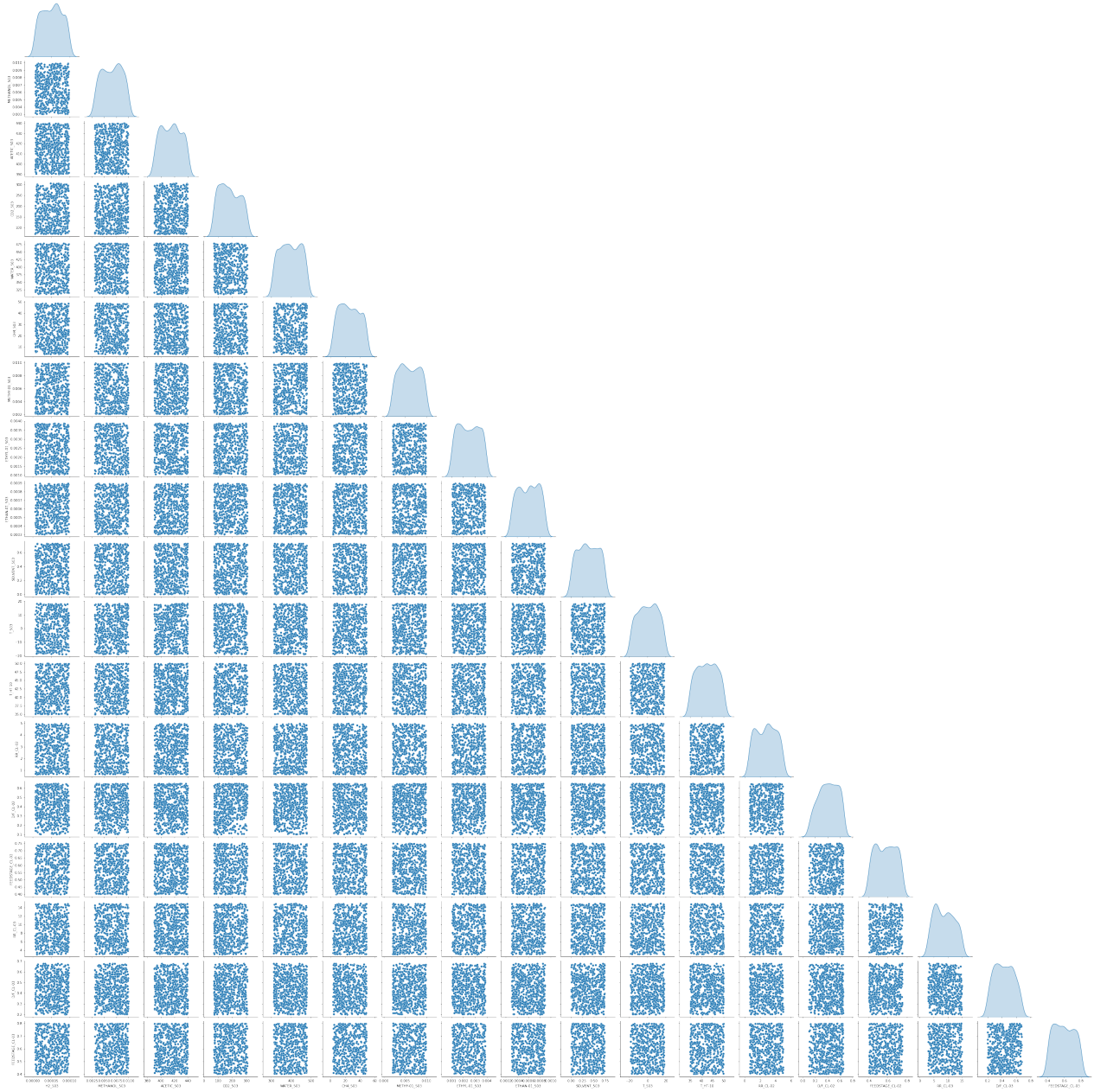

Figure K.3: Distribution of inputs for acetic acid ANN4b.

It is possible to verify that the distribution is uniform in each variable assessed.

The Figure K.4 depicts the distribution of the inputs.

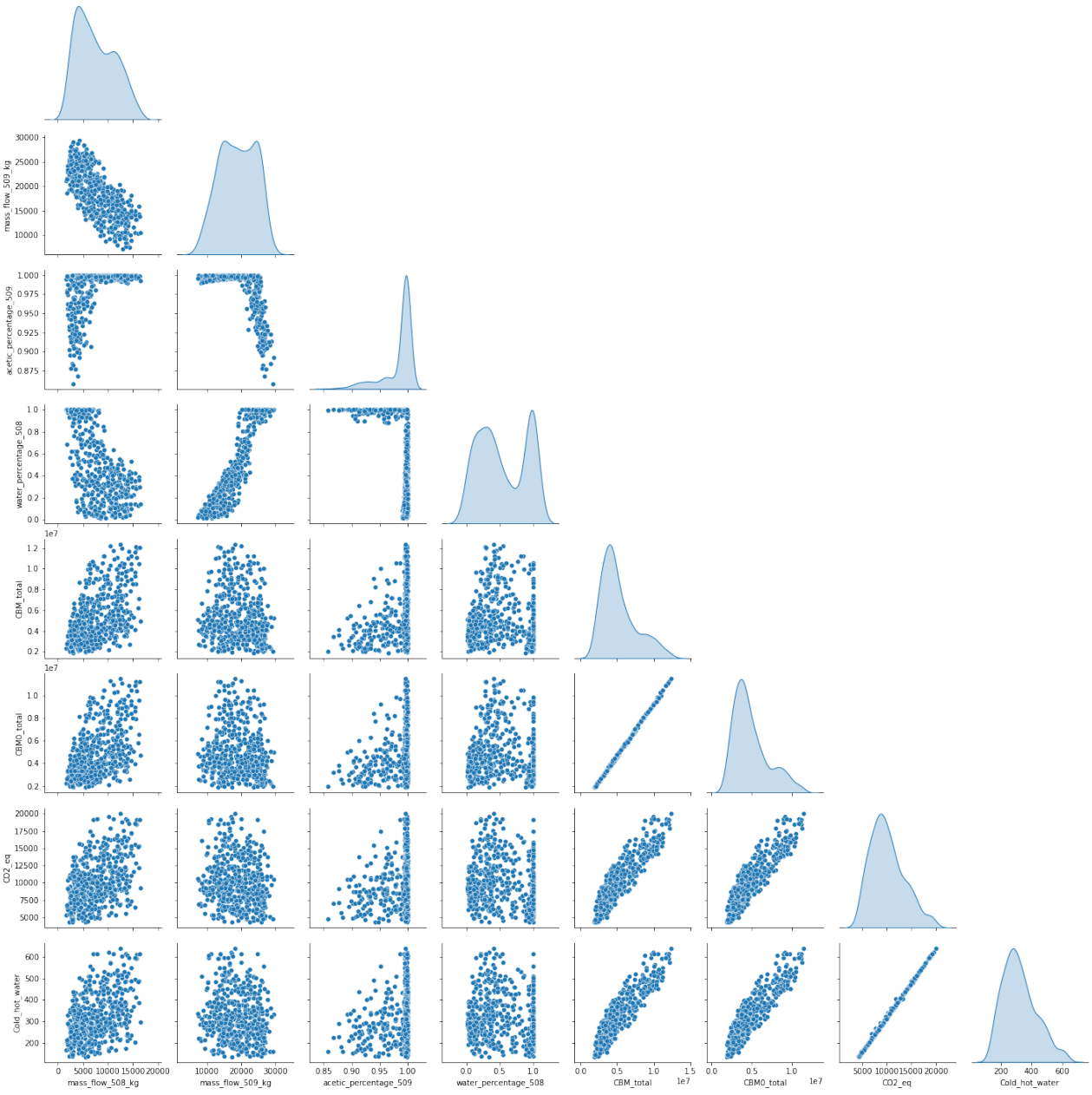

Figure K.4: Distribution of output for acetic acid ANN4b.

Hyperparameter Tuning

The Figure K.5 presents hyperparameter tunning for the Artificial Neural Network 4a.

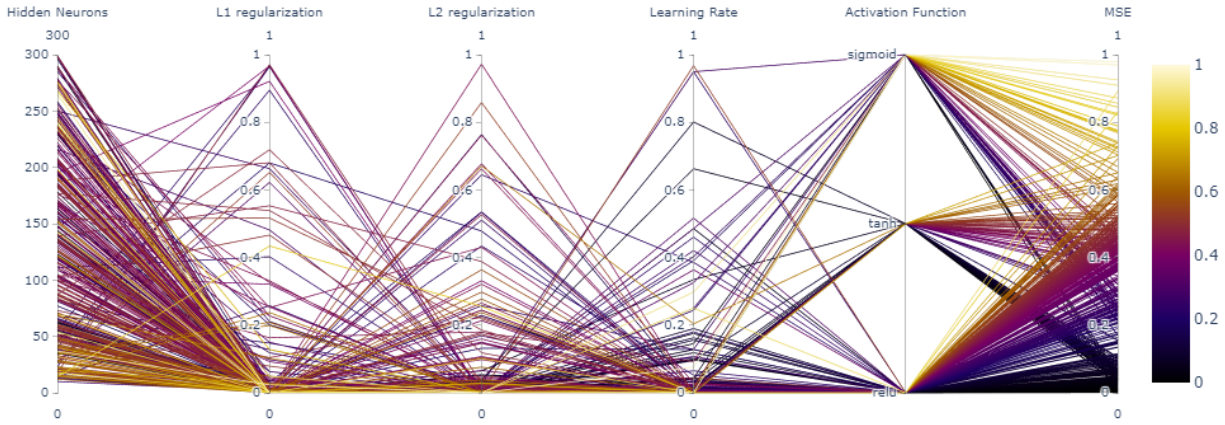

Figure K.5: Hyperparameter Tunning for ANN4b.

The hyperparameter exploration has finished, revealing that the ideal configuration consists of a hidden densely-connected layer with 134 units, a learning rate of 0.485563523295023 for the optimizer adam, and relu as the activation function. Additionally, the regularization values are l1 = 4.993578654868367e-08 and l2 = 0.0001202674364624, with an mse of 0.0007859788602218.

Predicted vs. Observed

Figure K.6 depicts the comparison between the predicted values (from the best model, after the tunning) with the observed values (from phenomenological simulation).

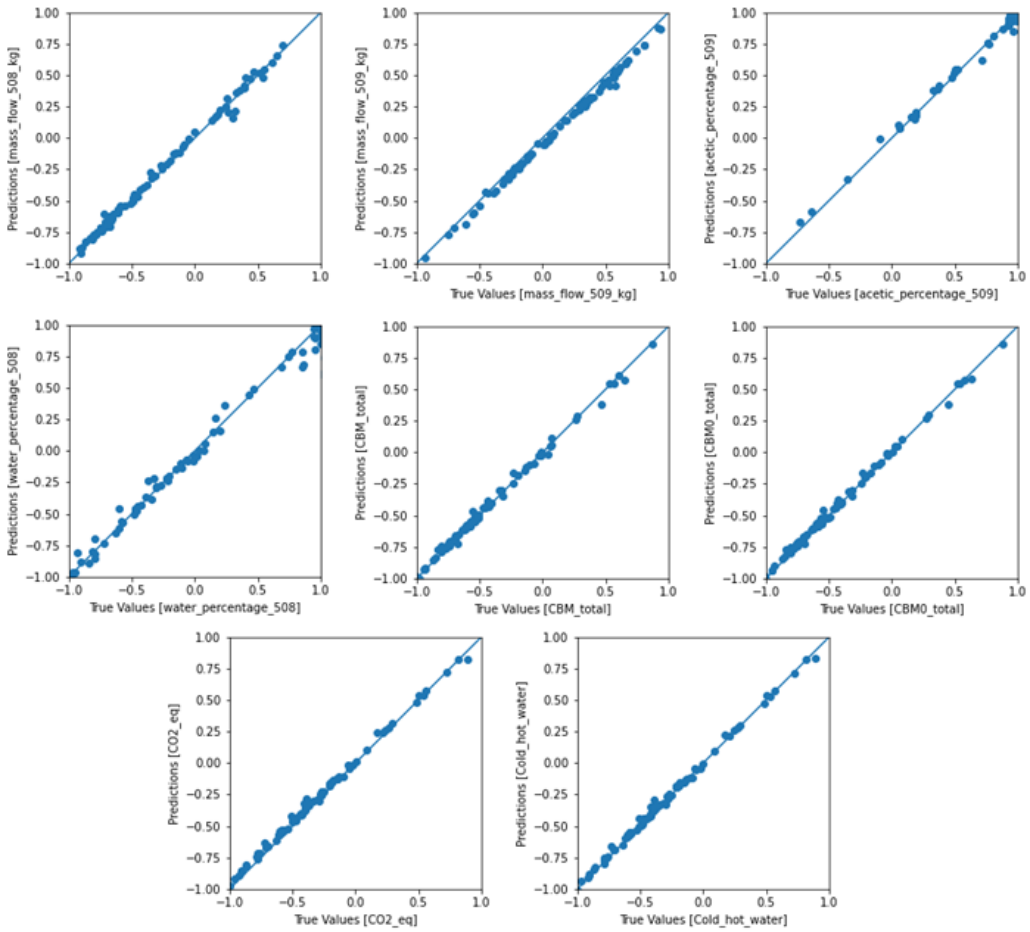

Figure K.6: Predicted Values vs. Observed Values for ANN4b.

Base Case Comparison

Table K.2 compares phenomenological simulation with neural network results for the base case.

Table K.2: Comparison the Phenomenological Simulation with Neural Network Results for the Base Case.

Variables	Phenomenological Simulation	Neural Network
H2_503	1.34797E-05	1.34797E-05
METHANOL_503	0.007029822	0.007029822
ACETIC_503	416.9887141	416.9887141
CO2_503	111.1012824	111.1012824
WATER_503	448.3936077	448.3936077
CH4_503	11.08110358	11.08110358
METHY-01_503	0.006867894	0.006867894
ETHYL-01_503	0.002528721	0.002528721
ETHAN-01_503	0.000529362	0.000529362
SOLVENT_503	0.732523548	0.732523548
T_503	12.07362527	12.07362527
T_HT-10	38	38
RR_CL-02	2.38270768	2.38270768
D/F_CL-02	0.124004396	0.124004396
FEEDSTAGE_CL-02	0.666666667	0.666666667
RR_CL-03	5.81529718	5.81529718
D/F_CL-03	0.517075136	0.517075136
FEEDSTAGE_CL-03	0.575	0.575
mass_flow_508_kg	8101.49	9022.21
mass_flow_509_kg	25092.25	23522.35
acetic_percentage_509	0.996	0.984
water_percentage_508	0.994	0.914
CBM_total	6675877	6588430
CBM0_total	6136092	6115064
CO2_eq	10219	9490
Cold_hot_water	339.025	300.454

Appendix L

Detailed Information for the Neural Networks - Acetic Acid ANN5

Detailed process flowsheet

In this section the detailed process flowsheet is described. The Figure L.1 depicts the region of the process flowsheet from where the neural network will be constructed. It contains 3 heat exchangers, 2 valves, a flash drum and a membrane module.

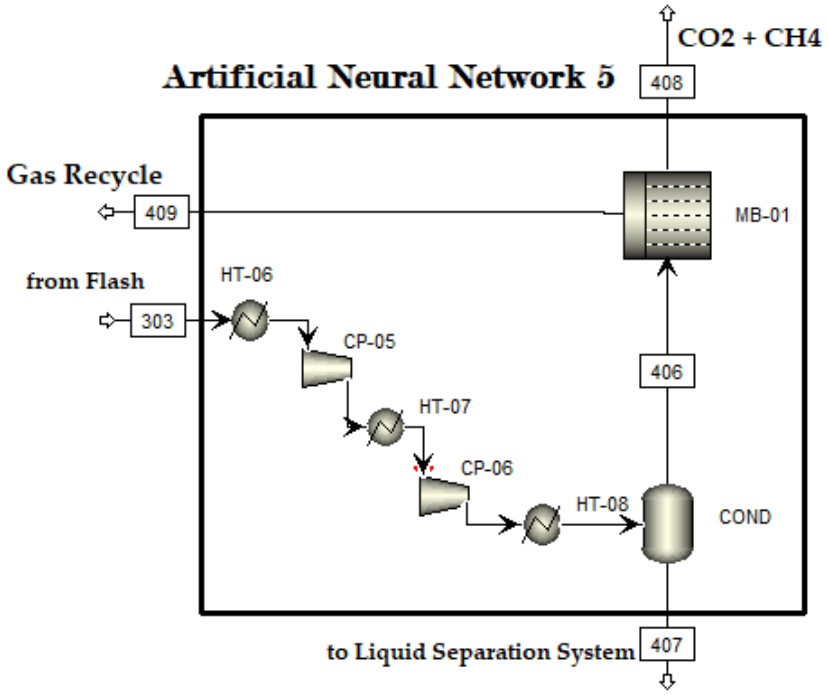

Figure L.1: Detailed process flowsheet for gas separation system.

The considered variables are the flows of the input stream, the temperature and pressure, the temperature of the heat exchangers and the membrane area.

The collected output variables are the mole flows, pressure and temperature of streams 407 and 412, total capital cost, utility usage and utility $CO_{2,equivalent}$ usage.

Neural Network Architecture

The Figure L.2 translates the gas separation system section of the acetic acid process (Figure L.1) into a neural network. There are 16 input variables and 22 output variables.

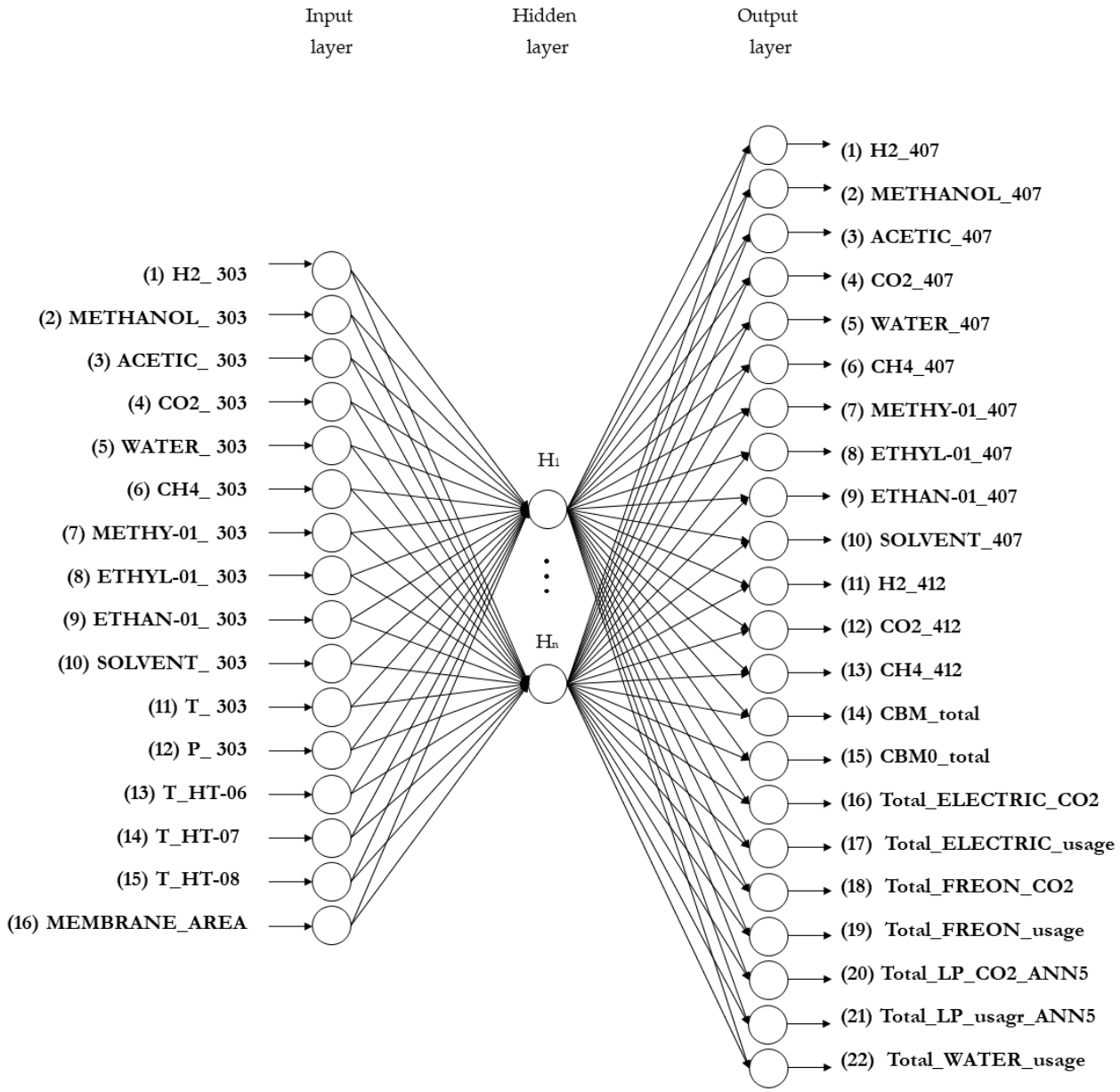

Figure L.2: Detailed architecture for acetic acid ANN5.

It is a feed forward neural network with only one hidden layer, the number of neurons is defined in the hyperparameter tuning.

Limits of the input variables

The Table L.1 presents the values used as upper and lower bonds for the data collection and neural network generation.

Table L.1: Limits of the input variables for acetic acid ANN5.

Variable	Stream/Unit	lower	upper	Unit
H2	303	1216	1815	kmol/h
METHANOL	303	1.62E-04	1.31E-03	kmol/h
ACETIC	303	1.31	12.69	kmol/h
CO2	303	868	1420	kmol/h
WATER	303	1.53	21.73	kmol/h
CH4	303	29.84	135.27	kmol/h
METHY-01	303	3.13E-04	2.15E-03	kmol/h
ETHYL-01	303	5.32E-05	4.63E-04	kmol/h
ETHAN-01	303	6.11E-06	6.16E-05	kmol/h
SOLVENT	303	2.83E-02	4.53E-01	kmol/h
T_303	303	29	60	oC
P_303	303	2	8	bar
T_HT-06	HT-06	20	48	oC
T_HT-07	HT-07	38	57	oC
T_HT-08	HT-08	16	24	oC
MEMBRANE_AREA	MB-01	3000	8000	m2

The Figure L.3 presents the distribution of the input parameters using the Latin hipercube sampling method.

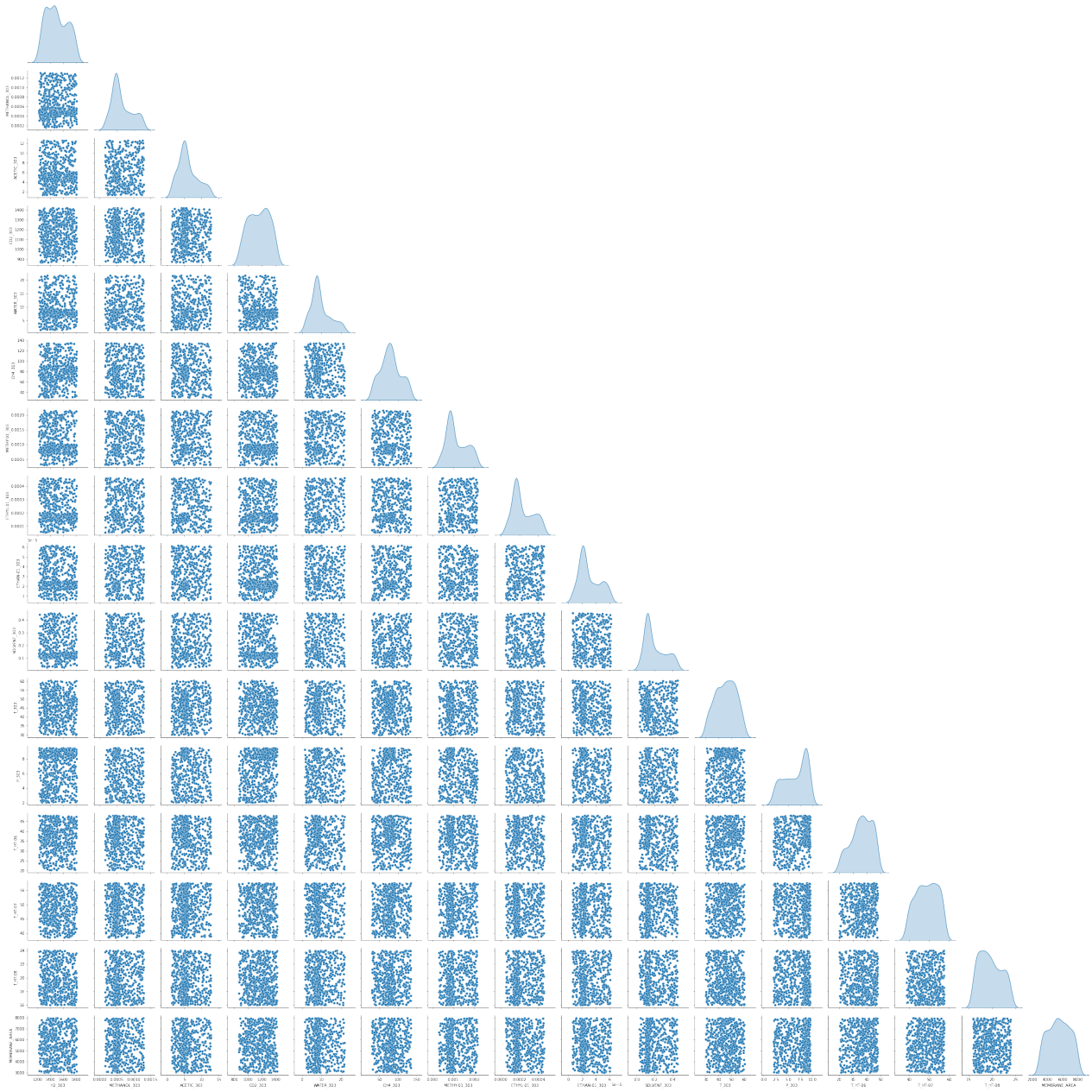

Figure L.3: Distribution of inputs for acetic acid ANN5.

It is possible to verify that the distribution is uniform in each variable assessed.

The Figure L.4 presents the distribution of the output variables.

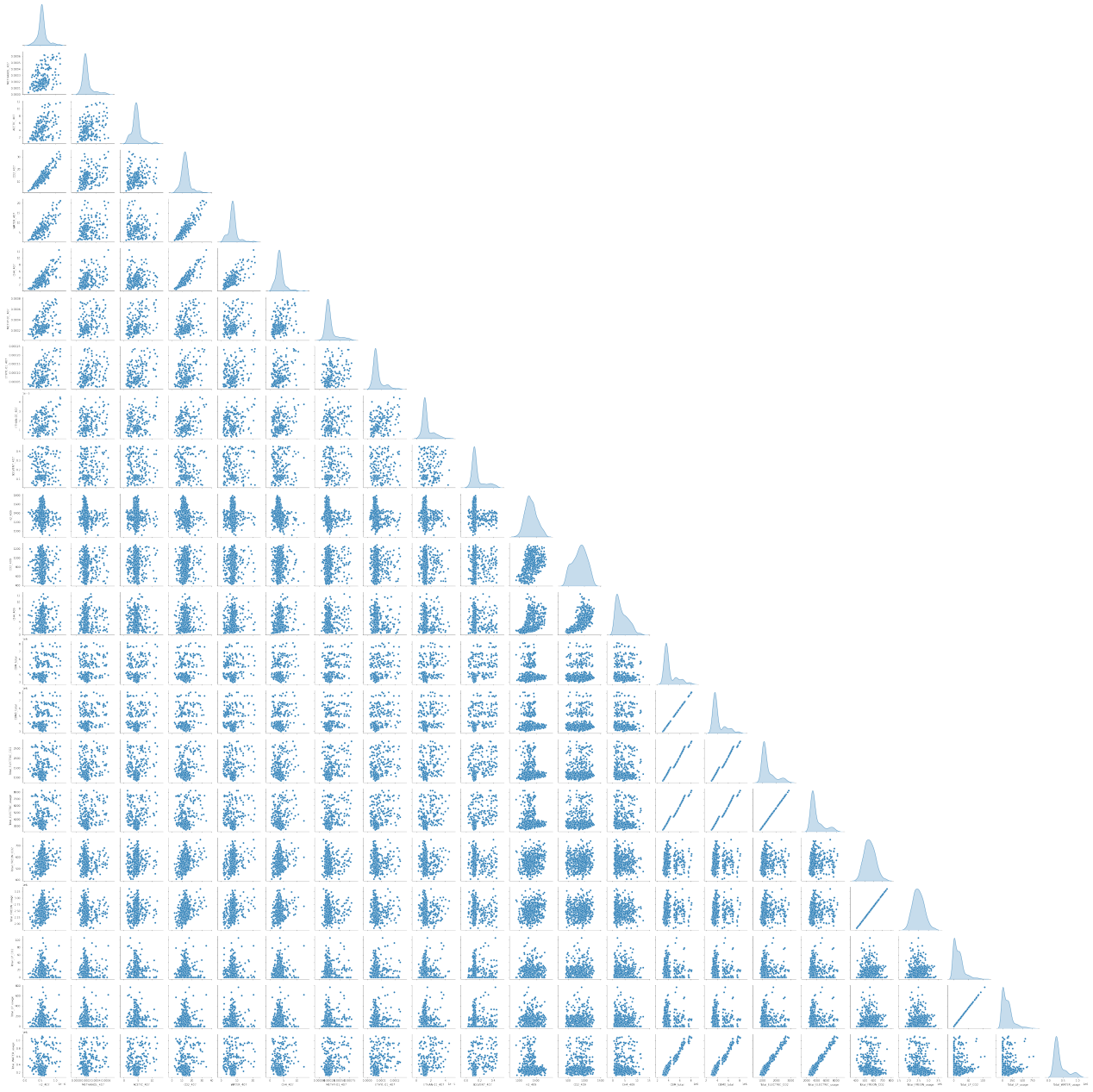

Figure L.4: Distribution of output for acetic acid ANN5.

Hyperparameter Tuning

The Figure L.5 presents hyperparameter tunning for the Artificial Neural Network 5.

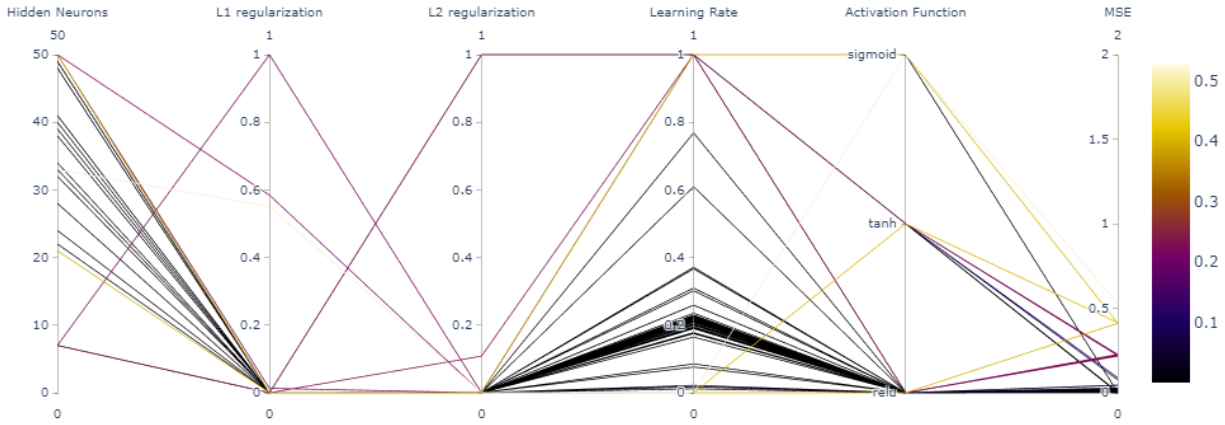

Figure L.5: Hyperparameter Tunning for ANN5.

The hyperparameter exploration has finished, revealing that the ideal configuration consists of a hidden densely-connected layer with 47 units, a learning rate of 1.0 for the optimizer adam, and relu as the activation function. Additionally, the regularization values are l1 = 0.0001896187501971 and l2 = 9.2722367699e-05, with an mse of 0.0100764269009232.

Predicted vs. Observed

Figure L.6 and Figure L.7 depict the comparison between the predicted values (from the best model, after the tunning) with the observed values (from phenomenological simulation).

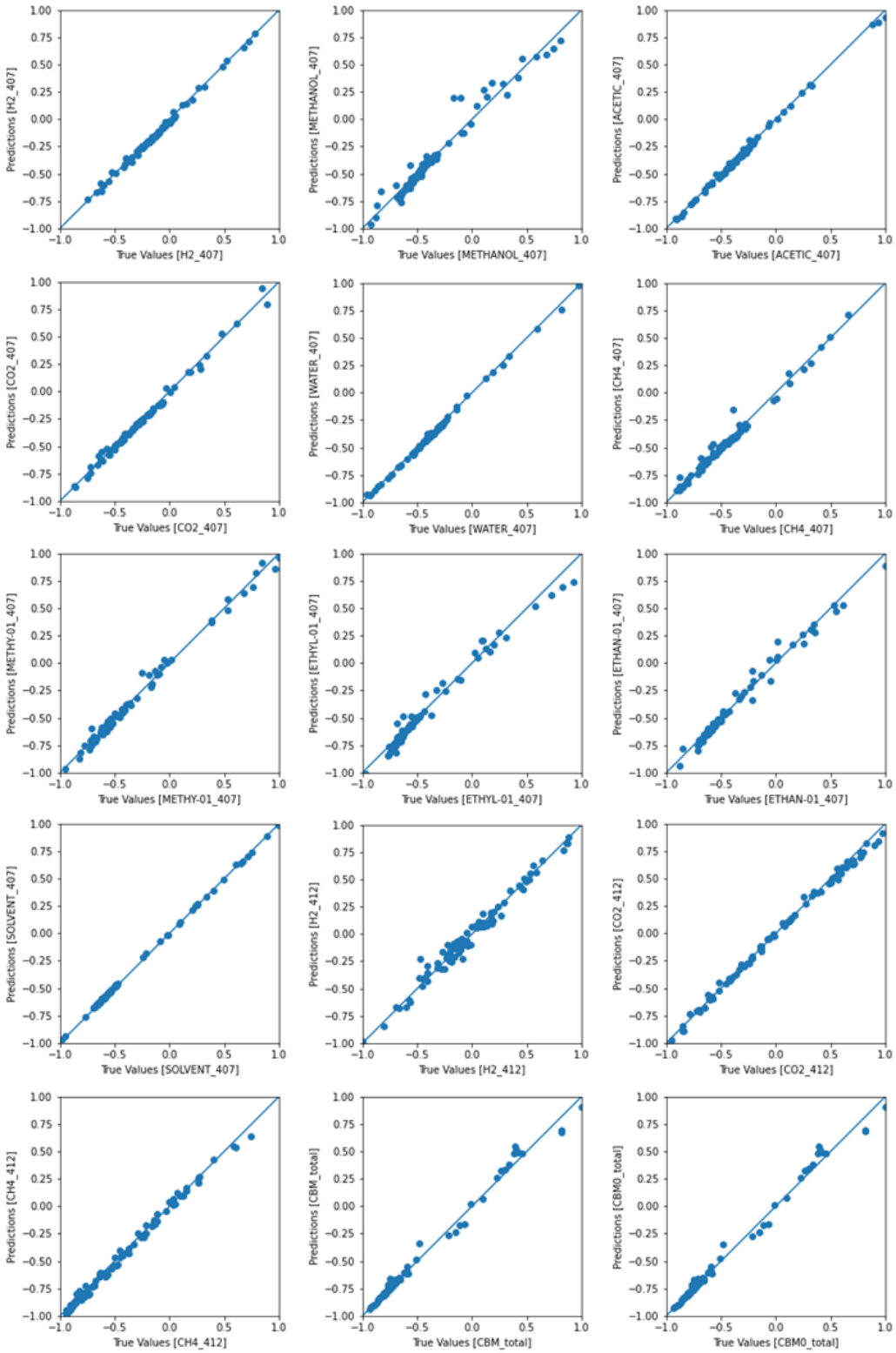

Figure L.6: Predicted Values vs. Observed Values for ANN5.

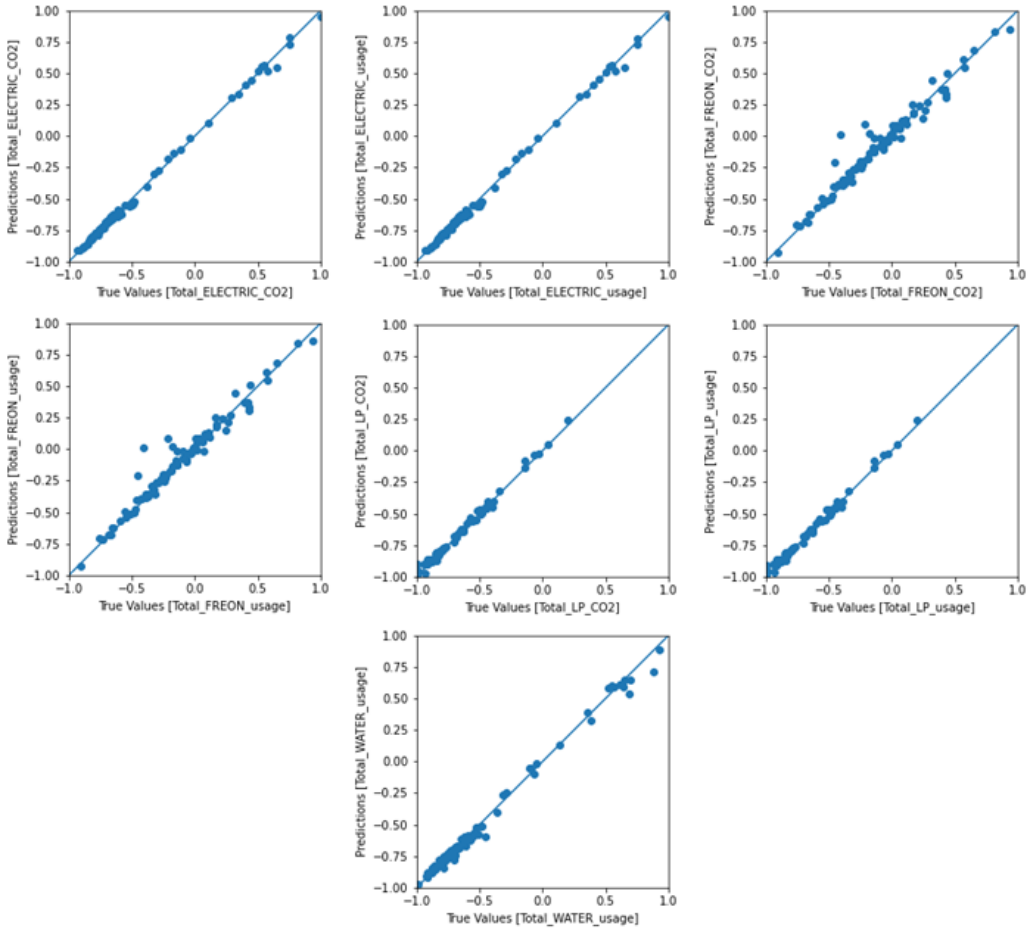

Figure L.7: Predicted Values vs. Observed Values for ANN5.

Base Case Comparison

Table L.2 compares phenomenological simulation with neural network results for the base case.

Table L.2: Comparison the Phenomenological Simulation with Neural Network Results for the Base Case.

Variables	Phenomenological Simulation	Neural Network
H2_303	1441.769495	1441.769495
METHANOL_303	0.000953446	0.000953446
ACETIC_303	10.68045355	10.68045355
CO2_303	1231.562049	1231.562049
WATER_303	16.84121775	16.84121775
CH4_303	61.30200167	61.30200167
METHY-01_303	0.001755131	0.001755131
ETHYL-01_303	0.000353742	0.000353742
ETHAN-01_303	4.13431E-05	0.000041343
SOLVENT_303	0.204986968	0.204986968
T_303	38	38
P_303	3.17255	3.17255
T_HT-06	40	40
T_HT-07	48	48
T_HT-08	20	20
MEMBRANE_AREA	6000	6000
H2_407	1.21572E-06	1.2062E-06
METHANOL_407	0.000544152	0.000538171
ACETIC_407	9.93660152	9.751560211
CO2_407	29.364979	29.27304649
WATER_407	16.4131625	16.20596504
CH4_407	6.51549703	6.982434273
METHY-01_407	0.000750407	0.000725992
ETHYL-01_407	0.000195744	0.000181512
ETHAN-01_407	3.05454E-05	3.14296E-05
SOLVENT_407	0.204852983	0.209995553
H2_412	1400.552134	1395.817993
CO2_412	1021.123289	1009.228271
CH4_412	3.413289115	3.312969923
CBM_total	6483280.382	6757367
CBM0_total	6475647.603	6770259
Total_ELECTRIC_CO2	2343.697669	2372.252686
Total_ELECTRIC_usage	6756.05908	6799.539551
Total_FREON_CO2	560.576017	568.8803101
Total_FREON_usage	2507499.65	2547068.5
Total_LP_CO2	12.143	16.65307808
Total_LP_usage	88.7502662	117.5222626
Total_WATER_usage	887359.585	873163.125

Appendix M

Publications

The publications from this work are described below.

Journal Publication

1. **Pacheco, Kelvin A.**, Bresciani, Antonio E., Alves, Rita M. B. (2023) Process Design and Simulation of Acetic Acid Production from Carbon Dioxide. *Journal of CO_2 Utilization*, UNDER FINAL REVISION.

2. Alcantara, Murilo L., **Pacheco, Kelvin A.**, Bresciani, Antonio E., Alves, Rita M. B. (2021) Thermodynamic Analysis of Carbon Dioxide Conversion Reactions. Case Studies: Formic Acid and Acetic Acid Synthesis. *Industrial & Engineering Chemistry Research*, v 60, 25, p 9246–9258, `https://doi.org/10.1021/acs.iecr.1c00989`

3. **Pacheco, Kelvin A.**, Bresciani, Antonio E., Alves, Rita M. B. (2021) Multi criteria decision analysis for screening carbon dioxide conversion products. *Journal of CO_2 Utilization*, v 43, p 101391, `https://doi.org/10.1016/j.jcou.2020.101391`

4. **Pacheco, Kelvin A.**, Bresciani, Antonio E., Nascimento, Cláudio A. O., Alves, Rita M. B. (2020) Assessment of property estimation methods for the thermodynamics of carbon dioxide-based products. *Energy Conversion and Management*, v 211, p 112756, `https://doi.org/10.1016/j.enconman.2020.112756`.

5. **Pacheco, Kelvin A.**, Bresciani, Antonio E., Nascimento, Cláudio A. O., Alves, Rita M. B. (2019) Assessment of the Brazilian Market for Products by Carbon Dioxide Conversion. *Front. Energy Res.*, 07 August 2019. `https://doi.org/10.3389/fenrg.2019.00075`

Book Chapter

6. Cavalcanti, Fabio M., Kozonoe, Camila E., **Pacheco, Kelvin A.**, Alves, Rita M. B. 2021. Application of Artificial Neural Networks to Chemical and Process Engineering. In Book: *Artificial Neural Networks and Deep Learning - Applications and Perspective*, Editor Pier Luigi Mazzeo. doi: 10.5772/intechopen.96641.

Conference Proceedings

7. Garona, Higor, **Pacheco, Kelvin A.**, Silva, Lucas, Schmal, Martin, Giudici, Reinaldo, Alves, Rita M. B. A. Machine learning methods applied to CO2 and CO conversion into carbonaceous products through Fischer Tropsch Synthesis. *3rd Latin American Conference on Sustainable Development of Energy Water and Environmental Systems*. Sao Paulo, Brazil. July 24-28, 2022.

8. Isabel. M., **Pacheco, Kelvin A.**, Alves, Rita M. B., Evaluation of a Post Combustion Co_2 Capture Process Through Modeling And Simulation. In: *Anais do 23° Congresso Brasileiro de Engenharia Química*. Gramado, Rio Grande do Sul, Brazil. September, 2021.

9. Carvalho, Kaccnny. M., **Pacheco, Kelvin A.**, Alves, Rita M. B., Kulay, Luis. A. Environmental performance analysis for an alternative route for synthesis of Acetic Acid. *15th Conference on Sustainable Development of Energy, Water and Environment Systems - SDEWES Conference*. Cologne, Germany. October, 2020.

10. **Pacheco, Kelvin A.**, Bresciani, Antonio E, Nascimento, Cláudio A. O., Alves, Rita M. B. 2020 CO_2-based Acetic Acid Production Assessment. *Computer Aided Chemical Engineering*. Volume 48, Pages 1027-1032. `https://doi.org/10.1016/B978-0-12-823377-1.50172-5`

11. **Pacheco, Kelvin A.**, Bresciani, Antônio E., Nascimento, Cláudio A. O., Alves, Rita M. B., Evaluation of acetic acid production from CO_2 through thermodynamic equilibrium calculations. *I Congresso Brasileiro em Engenharia de Sistemas em Processos (PSE-BR 2019)*. Rio de Janeiro, Brazil. May, 2019.

12. **Pacheco, Kelvin A.**, Bresciani, Antonio E, Nascimento, Cláudio A. O., Alves, Rita M. B., Thermodynamics of carbon dioxide related compounds. *14th Conference on Sustainable Development of Energy, Water and Environment Systems - SDEWES Conference*. Dubrovnik. October, 2019.

13. **Pacheco, K. A.**; Bresciani, A. E.; Nascimento, C. A. O.; Alves, R. M. B. Opportunities Identification for CCU in Brazil. In *4º Congresso Brasileiro de CO_2 na indústria de petróleo, gás e biocombustíveis*. Rio de Janeiro, RJ - Brazil, 28-29 June 2018.

14. **Pacheco, K. A.**; Reis, A. C.; Nascimento, C. A. O.; Alves, R. M. B. Assessment of the Brazilian Market for Products by conversion of CO_2 from thermal power plants. In *16^{th} International Conference on Carbon Dioxide Utilization - ICCDU*. Rio de Janeiro, RJ - Brazil, 27-30 August 2018.

15. **Pacheco, K. A.**; Reis, A. C.; Bresciani, A. E.; Alves, R. M. B.; Nascimento, C. A. O. Potential Products from CO_2 Utilization. In *3^{rd} Sustainable Gas Research and Innovation*. São Paulo, SP - Brazil, 25-26 September 2018.

16. Reis, A. C.; **Pacheco, K. A.**; Nascimento, C. A. O.; Alves, R. M. B. Brazilian Market Forecast for Carbon Dioxide Utilization. In *13^{th} Conference on Sustainable Development of Energy, water and environment systems - SDEWES*. Palermo, Italy, 30 September - 04 October 2018.